

# Sheffield Hallam University

*Validation and uncertainty of inverse dynamics analysis applied to high acceleration movements.*

DOMONE, Sarah Katherine.

Available from the Sheffield Hallam University Research Archive (SHURA) at:

<http://shura.shu.ac.uk/23508/>

## A Sheffield Hallam University thesis

This thesis is protected by copyright which belongs to the author.

The content must not be changed in any way or sold commercially in any format or medium without the formal permission of the author.

When referring to this work, full bibliographic details including the author, title, awarding institution and date of the thesis must be given.

Please visit <http://shura.shu.ac.uk/23508/> and <http://shura.shu.ac.uk/information.html> for further details about copyright and re-use permissions.

LEARNING CENTRE  
COLLEGIATE CRESCENT  
SHEFFIELD S10 2BP

102 040 855 3



ProQuest Number: 10760405

All rights reserved

INFORMATION TO ALL USERS

The quality of this reproduction is dependent upon the quality of the copy submitted.

In the unlikely event that the author did not send a complete manuscript and there are missing pages, these will be noted. Also, if material had to be removed, a note will indicate the deletion.



ProQuest 10760405

Published by ProQuest LLC (2018). Copyright of the Dissertation is held by the Author.

All rights reserved.

This work is protected against unauthorized copying under Title 17, United States Code  
Microform Edition © ProQuest LLC.

ProQuest LLC.  
789 East Eisenhower Parkway  
P.O. Box 1346  
Ann Arbor, MI 48106 – 1346

**Validation and uncertainty of inverse  
dynamics analysis applied to high acceleration  
movements**

Sarah Katherine Domone

A thesis submitted in partial fulfilment of the  
requirements of Sheffield Hallam University for the  
degree of Doctor of Philosophy

April 2014

## Abstract

This thesis is motivated by the lack of knowledge of the uncertainty in the estimation of joint forces and moments derived through inverse dynamics analysis. Previous studies have shown uncertainty bounds can be substantial during slow, simple movements such as gait or lifting however little is known about the uncertainty in inverse dynamics solutions applied to high acceleration, open chain, complex tasks. A three dimensional full body model was used to provide a mechanical basis for evaluating joint forces and moments during the golf swing. Eight male skilled golfers were used; kinematic data was recorded using the Polhemus LIBERTY, an electromagnetic tracker system, using 12 sensors attached to the body with a specially designed jacket. Force plates were used to measure ground reaction forces.

Validation of the derived joint forces and moments is problematic since no 'gold standard' is available for comparison. A comparison of the measured with the estimated ground reaction forces, as well as a comparison of the moments at the T8/T9 intervertebral joint that results from bottom up and top down mechanical analysis provided an initial measure of validity. The high acceleration, complex nature of the golf swing resulted in a reduced validity compared to previous studies concerned with lifting, fast trunk rotations and slow speed golf swings. The residuals between the measured and predicted GRF were greatest during the downswing. Similarly, the residuals between the joint reaction forces and moments at the upper trunk joint measured using a top down and bottom up mechanical analysis were greatest during the downswing, exemplified by an increase in joint moment RMS differences of 30.9 Nm, 24.4 Nm and 25.2 Nm for lateral bending, axial rotation and flexion-extension respectively. It was shown that for open chain movements, through periods of high acceleration, inverse dynamics solutions can be subject to errors which have the capacity to significantly affect the interpretation of resultant joint moments depending on whether a top down or bottom up mechanical analysis is used. Top down-bottom up comparisons do not account for two sources of error; the joint centre location and the anatomical coordinate system of the joint where the two models meet. A further drawback associated with these validation methods is that nothing can be learnt about the individual sources of error and how they contribute to the total residual error.

A consideration of how errors in measured variables propagate through inverse dynamics equations to produce uncertainties associated with the result was necessary. To analyse this, the Taylor Series Method for error propagation was used. Inaccuracies in body segment parameters, kinematics and external force measurement were determined experimentally. Soft tissue artefact and joint centre location errors were extracted from the literature. Inaccuracies in variables were assumed to be random and uncorrelated and results were representative of the upper bound uncertainty. Uncertainty in joint moment estimations was greatest for downswing where segments were moving with the greatest acceleration. The magnitude of the uncertainty was substantial and ranged from 6-339% of the peak joint moment magnitude. Inaccuracies in proximal moment arms and centre of mass accelerations had the most influence on the joint moment uncertainty and this uncertainty had the capability to alter the timing of peak joint moments by as much as 560ms. The results were critical to the interpretation of inverse dynamics derived joint forces and moments for high acceleration, open chain motions.

## **Acknowledgements**

First and foremost I would like to thank my supervisors Dr Jon Wheat, Dr Simon Choppin and Nick Hamilton for their guidance throughout this research.

Thank you to Golphysics Ltd who sponsored this PhD and who hold the intellectual property rights of aspects of the lab system and inverse dynamics model utilised in this thesis. I would like to acknowledge the work of Tom Outram a fellow PhD student with whom the data collection was carried out and also for his help in recruiting participants. Additional thanks to Dr Derek Marriott and Dr Carl Birkinshaw for their work in developing the infrastructure used to access the golf swing database.

And finally, my thanks are also due to all members of the Centre for Sports Engineering Research group at Sheffield Hallam whom have helped and supported me throughout the duration of this project.

# Table of Contents

Abstract .....	i
Acknowledgements.....	ii
List of figures.....	viii
List of tables .....	xii
1. Introduction .....	1
2. Literature Review.....	4
2.1. Introduction, Scope and Structure.....	4
2.2. Biomechanics, Kinematics and Kinetics .....	4
2.3. Applied Inverse Dynamics.....	7
2.3.1. Sports Applications .....	8
2.3.2. The Golf Swing .....	11
2.3.3. Discussion.....	15
2.4. Assumptions and Sources of Error in Inverse Dynamics Solutions.....	15
2.4.1. The rigid body assumption.....	16
2.4.2. Joint constraints.....	16
2.4.3. Body Segment Parameters.....	17
2.4.4. Joint centre location .....	18
2.4.5. Kinematic measurements .....	19
2.4.6. External force measurement .....	20
2.4.7. Closed kinematic chain indeterminacy .....	20
2.4.8. Filtering of non-stationary signals.....	21
2.4.9. Discussion.....	22
2.5. Methods of Validation .....	22
2.5.1. Top Down/Bottom Up Joint Force and Moment Comparison.....	23
2.5.2. Predicted GRF vs. Measured GRF.....	26
2.5.3. External Measurement Devices .....	27
2.6. Sensitivity Analyses .....	28
2.7. Uncertainty Analyses .....	33

2.7.1.	Taylor Series Method .....	34
2.7.2.	Monte Carlo Method .....	37
2.8.	Summaries .....	40
2.9.	Conclusion.....	42
2.10.	Aims and Objectives.....	43
2.11.	Contribution to knowledge .....	43
3.	Data Collection Methods and Procedures .....	44
3.1.	Golphysics Ltd laboratory set-up and data analysis methods .....	44
3.1.1.	Experimental set-up.....	44
3.1.2.	Global Coordinate System definition .....	45
3.1.3.	Pre Testing Procedures .....	46
3.1.4.	Experimental Protocol .....	47
3.1.5.	Golphysics geometric model for the calculation of Body Segment Parameters	50
3.1.6.	Joint Centre Locations.....	55
3.1.7.	Joint coordinate system definition .....	58
3.1.8.	Data analysis .....	60
3.1.9.	Calculation of derivatives.....	61
3.1.10.	Calculation of the transformation matrix .....	62
3.1.11.	Inverse Dynamics Calculations.....	63
3.1.12.	Special cases.....	66
3.1.13.	Model indeterminacy.....	68
3.1.14.	Calculation sequence .....	68
3.2.	Sample.....	69
3.3.	Filtering .....	70
4.	Validation of Inverse Dynamics Solutions.....	73
4.1.	Introduction .....	73
4.2.	Method .....	75
4.2.1.	Data Analysis.....	75
4.3.	Results.....	76

4.3.1.	Measured compared to predicted GRF.....	76
4.3.2.	Top down vs. bottom up calculated joint reaction forces and moments at the T8/T9 joint.....	80
4.4.	Discussion.....	84
4.5.	Conclusion.....	89
5.	Quantification of Inaccuracy Magnitudes.....	91
5.1.	Identification of inaccuracies.....	91
5.1.1.	Sources of Inaccuracy .....	95
5.2.	Body Segment Parameter Inaccuracy.....	95
5.2.1.	Introduction .....	95
5.2.2.	Methods.....	97
5.2.3.	Results.....	99
5.2.4.	Discussion.....	101
5.2.5.	Conclusion.....	105
5.3.	Force Plate Measurement Inaccuracy .....	108
5.3.1.	Introduction .....	108
5.3.2.	Method.....	109
5.3.3.	Results.....	113
5.3.4.	Discussion.....	114
5.3.5.	Conclusion.....	116
5.4.	Kinematic Measurement Inaccuracy .....	116
5.4.1.	Introduction .....	116
5.4.2.	Methods.....	118
5.4.3.	Results.....	122
5.4.4.	Discussion.....	127
5.4.5.	Conclusion.....	129
5.5.	Soft Tissue Artefact and Joint Centre Location Inaccuracy: A literature review .....	130
5.5.1.	Introduction .....	130
5.5.2.	Soft Tissue Artefact .....	131

5.5.3.	Methods.....	131
5.5.4.	Results.....	132
5.5.5.	Discussion.....	141
5.5.6.	Conclusion.....	146
5.5.7.	Joint Centre Location .....	147
5.5.8.	Methods.....	148
5.5.9.	Results.....	150
5.5.10.	Discussion.....	154
5.5.11.	Conclusion.....	155
5.6.	Noise in derivatives obtained from kinematic measurement data .....	156
5.6.1.	Sensor measurement noise .....	157
5.6.2.	Soft Tissue Artefact .....	160
6.	Taylor Series Uncertainty Analysis.....	162
6.1.	Introduction .....	162
6.2.	Methods.....	165
6.2.1.	Taylor Series Method for Propagation of Uncertainty .....	165
6.2.2.	Quantification of inaccuracies in input parameters .....	167
6.2.3.	Data Analysis.....	168
6.3.	Results.....	169
6.4.	Discussion.....	181
6.5.	Conclusion.....	187
7.	Summary, conclusion and future research .....	188
7.1.	Future research.....	195
7.2.	Conclusion.....	197
	Bibliography.....	198
	APPENDIX A: Body segment parameters equations .....	1
	APPENDIX B: Force platform calculations.....	5
	APPENDIX C: Force plate and force transducer calibration .....	7
	Static force plate calibration.....	7

Transducer calibration .....	8
APPENDIX D: Calculation of the combined standard uncertainty using numerical methods ....	10
APPENDIX E: Complete list of inaccuracy values for sets 1, 2 and 3.....	15
APPENDIX F: Uncertainty results tables for inaccuracy sets 2 and 3.....	21
APPENDIX G: Uncertainty figures for inaccuracy sets 2 and 3.....	29
APPENDIX H: Top five most influential parameters tables.....	30
APPENDIX I: BSP Inaccuracy Study - Participant Information Sheet.....	33
APPENDIX J BSP Inaccuracy Study - Ethics Form.....	35
APPENDIX K: BSP Inaccuracy Study - Risk Assessment form .....	43
APPENDIX L: Golf Swing Data Collection - Participant Information Sheet.....	47
APPENDIX M: Golf Swing Data Collection - Ethics Form .....	49
APPENDIX N: Golf Swing Data Collection - Risk Assessment Form.....	57
APPENDIX O: Table of Assumptions.....	59

## List of figures

Figure 1 Golf swing laboratory set up .....	44
Figure 2 Sensor attachment locations.....	48
Figure 3 Geometric Model, ellipsoids outlined in red, stadium solids outlined in blue.....	50
Figure 4 Geometric model segmentation planes for the arms, trunk and legs .....	51
Figure 5 Segment length definition; the width and depth of the segment at each boundary level were defined using four digitised points shown as red crosses. Segment length was defined as the distance between the two virtual centre markers. ....	52
Figure 6 Left: stadium solid dimensions, Right: Stadium solid cross section .....	52
Figure 7 Semi ellipsoid and elliptical solid parameters .....	53
Figure 8 Joint centre markers and virtual centres for the shank; L1 and M1 are the lateral and medial femoral epicondyles respectively used to define the proximal joint centre V1. L2 and M2 are the lateral and medial malleoli respectively used to define the distal joint centre V2 .....	57
Figure 9 Hip joint centre definition (Bell et al., 1989); PW = pelvis width = the distance between the right and left anterior superior iliac spine (ASIS). ....	57
Figure 10 Shoulder joint centre definition (Schmidt et al., 1999) (shoulder illustration from <a href="http://www.shoulderdoc.co.uk/article.asp?section=3&amp;article=1">http://www.shoulderdoc.co.uk/article.asp?section=3&amp;article=1</a> ) .....	58
Figure 11 Local coordinate system definition within a rigid body. $p1, p2$ and $p3$ are three non-collinear points with known coordinates. Vectors $r1, r3, r4$ are mutually orthogonal which when divided by their own length become mutually orthogonal unit vectors or the local coordinate axes $x, y, z$ .....	59
Figure 12 Golphysics linked segment model of the body, locations of joints and segment centre of mass (COM) are shown. Left: Full body linked segment model in the anatomical position adopted during participant calibration. The local coordinate system directions for each segment located at the origin of each segment are shown as well as the joint positions. Right: full boy linked segment model in a golf stance. ....	60
Figure 13 Graph to describe the three point forward difference method.....	61
Figure 14 Free body diagram of the foot showing the force and moments acting at the centre of mass. ....	64
Figure 15 Free body diagram of the shank.....	66
Figure 16 Pelvis free body diagram of joint moment and joint reaction force calculations .....	67
Figure 17 Free body diagram of the club segment. No external forces or moments were assumed to act on the club segment, where $d$ = distance from the centre of mass to the hand grip, $m$ =club mass, $g$ = acceleration due to gravity, $jrf$ = joint reaction force, $jm$ = joint moment.....	68
Figure 18 Golphysics linked segment model calculation sequence indicated by arrows. Two recursive strategies were used beginning at the feet and the hands and meeting at the T8/T9 intervertebral joint. ....	69
Figure 19 Wavelet de-noising process .....	72
Figure 20 Wavelet De-Noising (WDN) applied to club segment angular acceleration in the Y direction for an exemplar swing trial. WDN is compared to a Butterworth filter (BWF) (cutoff frequency 12Hz) and raw angular acceleration data.....	72

Figure 21 A representative example of the time series of the measured (solid line) and predicted (---) ground reaction force comparisons. Swing begins at take-away and ends 3 frames before impact. The vertical dotted line indicates top of backswing.....	78
Figure 22 A typical example of the time series of the top down (---) and bottom up (solid line) joint reaction force comparisons at the T8/T9 joint. Swing begins at take-away and ends 3 frames before impact. The vertical dotted line indicates top of backswing.....	81
Figure 23 A typical example of the time series of the top down (---) and bottom up (solid line) joint moment comparisons at the T8/T9. Swing begins at take-away and ends 3 frames before impact. The vertical dotted line indicates top of backswing.....	82
Figure 24 Flow chart of parameters used in the in the computation of the proximal net joint reaction force using inverse dynamics. BSP = body segment parameters; COM = centre of mass; GRF = ground reaction forces; JRF = joint reaction force; FPCS = force plate coordinate system; LCS = local coordinate system; GCS = global coordinate system. Pink boxes indicate input parameters which were included in the uncertainty analysis. ....	93
Figure 25 Flow chart of parameters used in the in the computation of the proximal net joint moment using inverse dynamics. BSP= body segment parameters; COM = centre of mass; GRF = ground reaction force; JRF = joint reaction force; CS = coordinate system; GCS = global coordinate system; FPCS = force plate coordinate system; LCS = local coordinate system. Pink boxes indicate input parameters which were included in the uncertainty analysis.....	94
Figure 26 The three participants marked up in preparation for the laser scan, left to right: mesomorph- endomorph, balanced mesomorph, balanced ectomorph .....	98
Figure 27 Upper arm segment (ME); segmentation planes of the upper arm defined by anatomical landmarks; Right: scanned upper arm in dark grey with transparent elliptical solid overlaid aligned at the origin along the longitudinal axis. ....	104
Figure 28 Left: Thigh (ME), solid thigh scanned segment and transparent stacked elliptical solids aligned at origin along the longitudinal axis. Right: Forearm (ME), solid forearm scanned segment and transparent stacked elliptical solids aligned at the origin along the longitudinal axis.....	104
Figure 29 Instrumented pole showing static trial set up with 'TIP' and 'TOP' markers shown. These were removed during dynamic trials. ....	110
Figure 30 Experimental apparatus used for quantification of force plate measurement error. (Left) Instrumented pole used for application and dynamic point loads with marker set during measurement trials. (Right) A grid was laid on plate surface to apply forces at known positions. The crosses represent each of the 77 measurement locations which were spaced 5cm apart.....	111
Figure 31 Vectors of mean centre of pressure errors (blue arrows) for each grid position on each force plate showing position of transducers in platforms outlines in black .....	114
Figure 32 Lab set-up showing position of transmitter (source box) in relation to force plates.....	118
Figure 33 Polhemus sensors. Positions of the electrical centre and local coordinate system of sensors are shown.....	119
Figure 34 Test pole and brackets upon which sensors were mounted during testing. ....	119

Figure 35 Grid positions for testing. The test pole is shown in the first grid position, there were sixteen grid positions in total which covered a test volume which had dimensions of 100x250x200cm along the x, y and z directions respectively. .... 120

Figure 36 Histograms of variance for dynamic trials associated with the measurement of relative distance (left) and orientation (right) of two sensors for the Polhemus Liberty system ..... 123

Figure 37 Histogram of variance associated with the measurement of distance between sensors for a) 65cm b) 145cm c) 225cm above the force plates for dynamic trials ..... 125

Figure 38 Histogram of variance associated with the measurement of orientation between sensors for a) 65 cm b) 145 cm c) 225 cm above the force plates for dynamic trials..... 125

Figure 39 Variance in distance between the two sensors as a function of distance from the transmitter for (a,b) static and (c) dynamic trials. Plot (b) for static trials is a zoomed in version of plot (a); exclusion of outliers highlighted the trend that variance increased with distance from the transmitter. .... 126

Figure 40 Variance in relative orientation of the two sensors as a function of distance from the transmitter for static (a, b) and dynamic (c) trials. Plot (b) for static trials is a zoomed in version of plot (a); exclusion of outliers highlighted the trend that variance increased with distance from the transmitter. .... 126

Figure 41 Schematic diagram of a Polhemus sensor ..... 131

Figure 42 Representative example of method used to calculate signal bandwidth. (Left) Club COM displacement in the y direction. (Right) Cumulative power spectrum of COM displacement of club, 99% of the signal is contained within 6.2 Hz. .... 159

Figure 43 Time varying joint moment estimates (thick black line) and  $\pm U_1$ ,  $\pm U_2$ ,  $\pm U_3$  confidence limits (thin grey, dotted grey and double grey lines respectively) derived using set 1, 2 and 3 inaccuracy values respectively. Joint moments are presented in the local coordinate system of the distal segment. Vertical dotted line indicates top of backswing event. Joints are ordered distal to proximal. From left to right plots represent lateral-bending, axial rotation and flexion-extension moments respectively. Swing begins at takeaway and ends three frames before impact. .... 169

Figure 44 Time varying joint moment estimates (thick black line) and  $\pm U_1$ ,  $\pm U_2$ ,  $\pm U_3$  confidence limits (thin grey, dotted grey and double grey lines respectively) derived using set 1, 2 and 3 inaccuracy values respectively. Joint moments are presented in the local coordinate system of the distal segment. Vertical dotted line indicates top of backswing event. Joints are ordered distal to proximal. From left to right plots represent lateral-bending, axial rotation and flexion-extension moments respectively. Swing begins at takeaway and ends three frames before impact. .... 170

Figure 45 Time varying joint moment estimates (thick black line) and  $\pm U_1$ ,  $\pm U_2$ ,  $\pm U_3$  confidence limits (thin grey, dotted grey and double grey lines respectively) derived using set 1, 2 and 3 inaccuracy values respectively. Joint moments are presented in the local coordinate system of the distal segment. Vertical dotted line indicates top of backswing event. Joints are ordered distal to proximal. From left to right plots represent lateral-bending, axial rotation and flexion-extension moments respectively. Swing begins at takeaway and ends three frames before impact. .... 171

Figure 46 Time varying joint moment estimates (thick black line) and  $\pm U_1$ ,  $\pm U_2$ ,  $\pm U_3$  confidence limits (thin grey, dotted grey and double grey lines respectively) derived using set 1, 2 and 3 inaccuracy values

respectively. Joint moments are presented in the local coordinate system of the distal segment. Vertical dotted line indicates top of backswing event. Joints are ordered distal to proximal. From left to right plots represent lateral-bending, axial rotation and flexion-extension moments respectively. Swing begins at takeaway and ends three frames before impact. .... 172

Figure 47 Bottom up joint moment uncertainties based on set 1 inaccuracy values, moments are presented in the local coordinate system of the distal segment. Moments were normalised with respect to the body weight and height of each participant before being averaged across all trials and participants for each 1% of the swing duration. Vertical dotted line indicates top of backswing event, swing begins at takeaway and ends three frames before impact. .... 175

Figure 48 Top down joint moment uncertainties based on set 1 inaccuracy values. Moments are presented in the local coordinate system of the distal segment. Moments were normalised with respect to the body weight and height of each participant before being averaged across all trials and participants for each 1% of the swing duration. Vertical dotted line indicates top of backswing event, swing begins at takeaway and ends three frames before impact. .... 175

Figure 49 Ground reaction force profiles in global coordinate system normalised by body weight for comparison to uncertainty profiles. Mean GRFs of all participants are presented. Vertical dotted line indicates top of backswing event, swing begins at takeaway and ends three frames before impact. .... 175

Figure 54 The relative magnitude of inaccuracy sets 1, 2 and 3. The magnitude of inaccuracies for sets 1 and 2 are presented as percentages of set 3. For parameters with direction or segment specific inaccuracies, mean inaccuracy values are presented. .... 181

Figure 55 Example of main contributors to uncertainty in joint moments (normalised by height and weight) using set 1 inaccuracy values. (Left) at the upper trunk joint using the top down model and (right) at the lower trunk joint using the bottom up model. U: uncertainty; PA: proximal moment arm; DA: distal moment arm. .... 183

Figure 56 Semi ellipsoid geometric solid ..... 1

Figure 57 Elliptical solid geometric shape ..... 2

Figure 58 Stadium solid ..... 2

Figure 59 KISTLER coordinate system ..... 6

Figure 60 Force plate calibration data ..... 8

Figure 61 Front plate transducer calibration data ..... 8

Figure 62 Back plate transducer calibration data ..... 9

Figure 63 Set 2 uncertainty at each joint ..... 29

Figure 64 Set 3 uncertainty at each joint ..... 29

## List of tables

Table 1 Segment densities applied to segments for calculation of body segment parameters (Dempster, 1955) .....	54
Table 2 Anatomical placement of markers which made up the geometric model .....	54
Table 3 Joint centre definitions used by geometric model .....	56
Table 4 Participant details .....	70
Table 5 Mean measured and predicted GRF and the difference between measured and predicted GRF averaged across all participants and trials. ....	79
Table 6 Peak measured and predicted GRF and the difference between measured and predicted GRF averaged across all participants and trials. ....	79
Table 7 RMS differences and Pearson correlation coefficients between measured and predicted GRF ...	79
Table 8 Mean joint reaction forces and moments for the top down and bottom up models and the difference between top down and bottom up models averaged across all participants and trials. ....	83
Table 9 Absolute peak joint reaction forces and moments for the top down and bottom up models and the difference between top down and bottom up models averaged across all participants and trials. ...	83
Table 10 RMS differences and Pearson correlation coefficients between top down and bottom up joint reaction forces and joint moments at the T8/T9 joint. RMS differences are in Newtons and newton metres for forces and moments respectively. ....	84
Table 11 Absolute peak segment angular acceleration differences in the global coordinate system during the backswing and downswing. Peak angular accelerations were averaged across all swings and participants. ....	85
Table 12 Methods of error quantification for input parameters .....	95
Table 13 Somatotype classification of the three participants using the Heath Carter method (1967) ....	97
Table 14 Error in segment mass estimates for the three participants .....	99
Table 15 Error in longitudinal centre of mass (COM) estimates for the three participants .....	100
Table 16 Error in antero-posterior centre of mass (COM) estimates for the three participants .....	100
Table 17 Error in medio-lateral centre of mass (COM) estimates for the three participants .....	100
Table 18 Error in moment of inertia ( $I_{ap}$ ) estimates about the antero-posterior axis for the three participants .....	100
Table 19 Error in moment of inertia ( $I_{long}$ ) estimates about the longitudinal axis for the three participants .....	100
Table 20 Error in moment of inertia ( $I_{ml}$ ) estimates about the medio-lateral axis for the three participants .....	101
Table 21 Three sets of inaccuracies (Set 1: minimum error, set 2: mean error, set 3: maximum error) for body segment parameters including mass, centre of mass and moment of inertia .....	106
Table 22 Mean absolute errors for force and centre of pressure measurements .....	113
Table 23 Mean COP absolute error for both plates showing distance away from plate centre, all measurements are in cm .....	114
Table 24 Inaccuracy sets for force and centre of pressure measurements .....	116

Table 25 Variance associated with the measurement of distance and orientation between two sensors for the Polhemus Liberty system .....	123
Table 26 Variance associated with the measurement of distance and orientation between sensors for the Polhemus Liberty system in relation to vertical distance from the force plates for static trials .....	124
Table 27 Variance associated with the measurement of distance and orientation between sensors for the Polhemus Liberty system in relation to vertical distance from the force plates for dynamic trials ..	124
Table 28 Variance in the relative position of two sensors for dynamic trials with and without mapping. ....	127
Table 29 Three sets of inaccuracies (Set 1: minimum, Set 2: mean, Set3: maximum) of position and orientation variance for the Polhemus Liberty system based on mapped dynamic measurements.....	129
Table 30 Data extraction table from reviewed articles which quantified STA .....	134
Table 31 Direct results obtained from reviewed articles .....	136
Table 32 Indirect results obtained from reviewed articles. STA artefact was quantified as either the effect of STA on joint angles and segment translations or the relative motion between the bone embedded coordinate system and the marker defined coordinate system.....	136
Table 33 Movement speed and range of movement reported for reviewed articles.....	137
Table 34 Similarity form used in literature review, questions were scored out of 3 .....	138
Table 35 Similarity analysis results from reviewed articles.....	138
Table 36 Inaccuracy sets for proximal and distal moment arms and kinematics caused by STA.....	147
Table 37 Joint centre definitions used by geometric model to define each joint centre .....	147
Table 38 Data extraction table from reviewed articles which quantified joint centre location error .....	149
Table 39 Reported joint centre error for studies identified in the literature review .....	150
Table 40 Inaccuracy sets (mm) for proximal and distal moment arms caused by error in joint centre location.....	156
Table 41 Three sets of inaccuracies (Set 1: minimum, Set 2: mean, Set3: maximum) of position and orientation variance for the Polhemus Liberty system based on mapped dynamic measurements.....	158
Table 42 Minimal noise variance in COG linear and angular velocity and acceleration calculated from the equations of Lanshammar (1980) .....	160
Table 43 Minimal noise variance in linear and angular velocity and acceleration due to STA calculated from the equations of Lanshammar (1980) .....	161
Table 44 Inaccuracy sets for kinematic measurements. These were the sum of errors quantified for motion marker noise and STA. ....	168
Table 45 Uncertainty analysis results for set 1 inaccuracy values for the upper body joints .....	176
Table 46 Uncertainty analysis results for set 1 inaccuracy values for the lower body joints.....	177
Table 47 Uncertainty analysis results for set 2 and 3 inaccuracy values for the upper body joints .....	178
Table 48 Uncertainty analysis results for set 2 and 3 inaccuracy values for the lower body joints.....	179
Table 49 Effect of uncertainty on the timing of absolute peak joint moments .....	180
Table 50 Calibrated sensitivity coefficients for each plate.....	5
Table 51 Force parameter calculations .....	5
Table 52 Static vertical force comparison: KISTLER plates vs. known static weights.....	7

Table 53 Mean joint moment estimates and uncertainty estimates for three sets of perturbations for top down model. Results represent the mean of all participants and swings. Moments have been normalised by body weight and height.....	21
Table 54 Mean joint moment estimates and uncertainty estimates for three sets of perturbations for bottom up model. Results represent the mean of all participants and swings. Moments have been normalised by body weight and height.....	22
Table 55 Maximum joint moment estimates and uncertainty estimates for three sets of perturbations for top down model. Results represent the mean of all participants and swings. Moments have been normalised by body weight and height.....	23
Table 56 Maximum joint moment estimates and uncertainty estimates for three sets of perturbations for bottom up model. Results represent the mean of all participants and swings. Moments have been normalised by body weight and height.....	24
Table 57 Percentage contribution relative to peak JM for three sets of perturbations for top down model .....	25
Table 58 Percentage contribution relative to peak JM for three sets of perturbations for bottom up model .....	26
Table 59 Effect of uncertainty on the timing of peak joint moments for the top down model.....	27
Table 60 Effect of uncertainty on the timing of peak joint moments for the bottom up model .....	28
Table 61 Top five most influential parameters that contributed to the total uncertainty at the upper trunk joint.....	30
Table 62 Top five most influential parameters that contributed to the total uncertainty at the mid trunk joint .....	31

## 1. Introduction

Biomechanical models of living systems used to describe and predict mechanical behaviour are becoming increasingly complex with the advancement in computational tools (Anderson et al., 2007). This has led to rapid increases in knowledge within the research field. However, critical to this advance in model complexity is the adequate verification and validation of such computational biomechanics. Verification and validation is important for peer acceptance of studies and their conclusions (Henninger et al., 2010). It is the process by which evidence is generated and credibility established that the model yields results with sufficient accuracy for the intended use of the model. To achieve this, the mathematical equations governing the model must be implemented correctly, the model should be an accurate representation of the underlying physics of the problem and an assessment of the error or uncertainty should be accounted for in the model predictions (Anderson et al., 2007).

Inverse dynamics is a method used to calculate forces and moments based on the kinematics and inertial characteristics of a body. Joint forces and moments provide a valuable tool for the analysis of human movement (Winter, 1980). In a sporting context, the use of joint forces and moments to improve performance and reduce the risk of injury is well established (Bahamonde and Knudson, 2003; Consiglieri and Pires, 2009; Elliott et al., 2003; Ferdinands et al., 2009; Greene et al., 2009; Iino and Kojima, 2011; Nunome et al., 2006). Error in inverse dynamics solutions can come from a large number of assumptions made during the modelling process and these are compounded by the iterative nature of inverse dynamics calculations using the Newton-Euler approach which cause error to propagate through the kinematic chain (Challis and Kerwin, 1996; Riemer et al., 2008). Within the field of sports biomechanics, often inverse dynamics is applied without concern for the validity of the model output (Akutagawa and Kojima, 2005; Bahamonde and Knudson, 2003; Elliott et al., 2003; Ferdinands et al., 2009; Fleisig et al., 2006; Gatt et al., 1998; Nunome et al., 2002). This is especially concerning since previous research suggests that for applications involving high acceleration, open chain movements, the validity of inverse dynamics solutions is reduced (Pearsall and Costigan, 1999). Without knowledge of validity or uncertainty in

---

solutions the conclusions drawn using any analysis technique will be of little value (Challis and Kerwin, 1996; Coleman and Steele, 2009).

In this thesis, a study of the validity and uncertainty involved in the estimation of joint forces and moments via an inverse dynamics analysis is carried out. The golf swing was used to provide a mechanical basis for this analysis. The primary goal of a golf drive is to maximise the distance the ball travels whilst maintaining accuracy (Hume et al., 2005). The golf swing is a complex, high acceleration activity, involving the interaction of many segments in a coordinated pattern. It is therefore a complex and challenging motion to model.

The remainder of this thesis consists of 6 further chapters and is structured as below;

**Chapter 2** reviews the current literature relating to the application and validation of inverse dynamics analysis. Applied inverse dynamics is discussed with a particular focus on the golf swing. The latter part of the literature review relates to the validation of inverse dynamics solutions and methods which have been used to analyse the uncertainty in joint moments in the wider field of biomechanics. It shows that only a small number of previous studies have recognised the importance of validation and uncertainty in inverse dynamics solutions. To conclude this chapter the aims and objectives of this thesis are presented.

**Chapter 3** presents the methodology of the thesis. This chapter describes methods which were developed by Golphysics Ltd, these included; data collection and three dimensional motion analysis procedures, the development of a 3D rigid dynamic model of the golf swing and the implementation of inverse dynamics methods to calculate joint moments and forces. Details on sample selection and filtering methods are also included here.

**Chapter 4** implements the methods presented in the literature review to validate the joint force and moment predictions using the over-determined nature of inverse dynamics calculations. It presents and discusses the validity of inverse dynamics applied to the golf swing in relation to previous research concerned with slower, less-complex tasks. The limitations of such validation techniques in the absence of a "gold standard" measurement are discussed.

**Chapter 5** is concerned with the quantification of inaccuracy in input parameters. Experiments to quantify inaccuracies in external force measurement, kinematics and body segment parameters were carried out. Sources of inaccuracy which were not possible to quantify through experiments were synthesised from existing research by means of an in-depth literature review.

**Chapter 6** is an uncertainty analysis of joint moments. The inaccuracies in input parameters quantified in chapter 5 are utilised here. It presents and discusses the uncertainty in joint moment estimations for each joint of the rigid dynamics model, determines which joints experience the greatest uncertainty relative to the magnitude of joint moments and which input parameters were the most influential to the uncertainty.

**Chapter 7** is the conclusion of the thesis. It summarises and discusses the results of the thesis and their importance and applicability. Future research directions are also discussed.

Publications associated with this thesis are;

Outram, T. A., Domone, S. and Wheat, J., 2012. The reliability of trunk segment inertial parameter estimates made from geometric models. In: 30<sup>th</sup> Annual Conference of Biomechanics in Sports, Melbourne, Australia, 2 - 6 July 2012.

Domone, S., Wheat, J., Choppin, S., Hamilton, N and Heller, B., 2012. Wavelet based de-noising of non-stationary kinematic signals. In: 30<sup>th</sup> Annual Conference of Biomechanics in Sports, Melbourne, Australia, 2 - 6 July 2012.

Outram, T., Domone, S., Hart, J and Wheat, J., 2012. The use of geometric shapes in estimating the geometry of body segments. *Journal of Sports Sciences*, pg 24-25.

---

## 2. Literature Review

### 2.1. Introduction, Scope and Structure

This thesis is concerned with the application of inverse dynamics to high acceleration complex movements and the uncertainty involved in the estimation of joint forces and moments. This literature review begins with an introduction to inverse dynamics in the wider context of the biomechanics of human movement. A review of the applications of inverse dynamics with a focus on high acceleration movements and the way in which results have been interpreted and used is followed by a description of the assumptions and possible sources of error involved in inverse dynamics solutions. This brief discussion is included to provide a basic understanding of the potential for error in input parameters used to derive joint forces and moments. A detailed review of the techniques that have been used to validate inverse dynamics solutions is presented and the limitations of such techniques are highlighted. The final section of this literature review looks in detail at the types of uncertainty analysis that have been used both in regard to inverse dynamics and also in the wider field of human movement biomechanics. The case is made for an in depth validation and uncertainty analysis of joint moments and forces derived through inverse dynamics for complex, high acceleration movements forming the main body of this thesis.

### 2.2. Biomechanics, Kinematics and Kinetics

Biomechanics applies the principles of mechanics to the structure, functioning or movement of a living system (Hatze, 1974). The improvement of performance and the reduction and treatment of injury are two main areas of biomechanical research applied to human movement (Hoffman, 2009). Kinematics and kinetics are branches of biomechanics concerned with the description of movement and the causes of movement respectively (Robertson et al., 2004).

A kinematic analysis provides a complete description of the motion of a body. This includes a description and quantification of the linear and angular positions of the body and its time derivatives without concern for the causes of motion (Robertson et al., 2004). The quantitative description of a body is defined in a Cartesian Coordinate System within which frames of reference are established such as the global coordinate system and the local coordinate system of a segment necessary for three dimensional

analyses. Typically imaging or motion capture systems are used to record the motion of markers fixed to the moving participant and the coordinates are processed to obtain kinematic variables that describe segmental or joint movements. Alternative methods include measuring acceleration directly using accelerometers or the use of electrogoniometers to measure joint angles electronically. Kinematic variables can be used to understand motion characteristics of movements, compare motion of different individuals or to show intervention effects; for example kinematics have been used to investigate segmental sequencing in throwing and striking skills (Putnam, 1993), differences in first and second serves in tennis (Chow et al., 2003), the effect of foot orthotics during walking and running (Eng and Pierrynowski, 1994) and the effect of training on golf driver kinematics (Fletcher and Hartwell, 2004). The accurate quantification of kinematics is not only important for kinematic studies but also studies that use kinematics for subsequent kinetic analysis such as inverse dynamics (Robertson et al., 2004).

Kinetics is the study of the causes of motion (Zatsiorsky, 2002). In biomechanics this relates to the forces and moments that result from muscle contractions which produce segmental movement and movement of the body as a whole (Robertson et al., 2004). External forces can be measured directly using transducers such as force plates, pressure distribution sensors or isokinetic devices. In cycling, instrumented pedals were used to measure forces applied during different cycling conditions (Caldwell et al., 1998), and in golf force plates were used to identify weight transfer styles (Ball and Best, 2007). Internal force measurement can be used to determine the forces acting on individual ligaments, tendons and joints; for example Buckle transducers were used to measure in vivo Achilles tendon loading during jumping (Fukashiro et al., 1995). Such internal measurement devices are mounted directly to tendons or ligaments. The highly invasive nature of these measurement techniques has limited their use in human studies (Robertson et al., 2004). Musculo-skeletal modelling can be used as a less-invasive alternative.

Inverse and forward dynamics are two types of analytical techniques that can be used in situations not directly amenable to measurement techniques (Robertson et al., 2004). A forward dynamics analysis predicts movement from joint forces and moments. Forward dynamics models use optimal control techniques to determine the

forces and moments required to accomplish a task. These optimal control techniques can be defined as the movement pattern that minimises muscular effort or reduces risk of injury. For example McLean et al. (2008) used forward dynamics to determine muscular control strategies that reduced the risk of anterior cruciate ligament (ACL) injury during dynamic sports postures. Due to the complex nature of muscle recruitment patterns, the modelling of such mechanisms is based on assumptions of optimality; this can restrict the validity of the methodology to relatively slow and simple motions such as gait. The same degree of optimality cannot necessarily be expected to hold for other types of highly dynamic complex motions such as the golf swing (Robertson et al., 2004).

Inverse dynamics derives net joint force and net joint moments of force from a combination of measured kinematics, segment inertial parameters and measured external forces. Inverse dynamics is unable to quantify the individual forces in specific anatomical structures. These include muscle and ligament forces, bone to bone forces and forces from the skin, bursa and joint capsule (Robertson et al., 2004). The forces acting across a joint form an indeterminate system where there are more unknowns than equations. To reduce the number of unknowns, each force is resolved to its equivalent force and moment at the segment's endpoint. Therefore a single *net* force and *net* moment of force is produced. This is the summed effect of all the internal forces and moments of force acting across a joint and represents the total forces and moments required to create motion. These net forces and moments are mathematical concepts that cannot be measured directly. Net forces and moments can be calculated using four different inverse dynamics methods based on; 1) vectors and Euler angles, 2) wrenches and quaternions, 3) homogeneous matrices or 4) generalised coordinates and forces (Dumas et al., 2007). The four methods differ in the way the kinematics and dynamics are calculated, however the joint force and moment computations are theoretically equivalent (Dumas et al., 2007).

Segments are assumed to be rigid bodies with a fixed mass, centre of mass and inertia. The inertial properties of the body segments can be estimated using regression equations, geometric models or scanning techniques. Using Newton's second law of motion, the net joint reaction forces are determined from the linear acceleration and mass of the segment. Net joint moments are calculated from segment moments of

inertia, angular acceleration, angular velocity, and segment centre of mass position. Calculations begin at the most proximal or terminal segment, such as the foot or hand, where external forces are known or can be analytically determined. For example during the stance phase of gait, ground reaction forces can be measured using a force plate or during the swing phase of gait the external forces are theoretically assumed to be zero. Newton's third law dictates that the net joint reaction forces and moments acting at the distal end of a segment are equal in magnitude and opposite in sign to those acting on the proximal end of the adjacent segment. Calculations proceed proximally up the kinematic chain. This process is termed the linked-segment or iterative Newton-Euler method (Robertson et al., 2004). In addition to net joint forces and moments, the results from an inverse dynamics analysis can be used to compute work, segment power and joint power.

### **2.3. Applied Inverse Dynamics**

Joint moments have been described as "one of the most valuable biomechanical variables in the analysis of human movement" (Winter, 1980). Here an overview of the way in which inverse dynamics derived net joint forces and moments have been used in the analysis of human movement is provided. This section is focussed on sporting applications and in particular those which involve high accelerations. Golf swing inverse dynamics analysis is investigated in detail since this is the exemplar movement used in this thesis which is representative of a complex, high acceleration activity.

Inverse dynamics is frequently used in gait analysis studies. The experimental set up for such tasks generally comprises a motion analysis system for kinematic measurement and force plates for measurement of external forces and moments at the feet during the stance phase. External forces and moments at the foot during the swing phase are assumed to be zero. Model complexity varies between studies with the majority opting for lower body models consisting of two or three rigid links. Sagittal plane inverse dynamics gait studies have been used for rehabilitation to aid treatment, therapy and prostheses choice (Andriacchi et al., 1980; Cappozzo et al., 1975; Hale, 1990; Stanic et al., 1977; Wahrenberg et al., 1978). Hale et al. (1990) modelled the lower leg as a rigid two link system to determine the effect of varying prosthetic shank mass in above knee amputee gait. Crowninshield et al. (1978) used

hip joint forces and moments to inform the design and development of hip implants. Such two dimensional models have been shown to be adequate; inter-individual variation in joint moment patterns during the stance phase of gait was observed for both 2D and 3D models (Alkjaer et al., 2001). Conversely, three dimensional models have been shown to be essential for specific studies. Apkarian et al. (1989) highlighted the importance of three dimensional gait models for pathological gait analysis where treatment of a condition such as cerebral palsy is directed at decreasing rotational abnormalities. Likewise, Zabala et al. (2012) found the three components of external moment at the knee were important for a comprehensive understanding of the differences between healthy control knees and ACL reconstruction knees.

Three dimensional analysis has been shown to be essential in studies concerned with back loading where asymmetric lifting movements are associated with an increased risk of lower back disorders (Cunningham and Kelsey, 1984; Marras and Granata, 1995). The forces and moments at the L5/S1 joint have been the focus of a substantial amount of research due to the high incidence of back injury in industrial workers involved in Manual Materials Handling (Freivalds et al., 1984). Gagnon et al. (1993) reported that pivoting during lifting was a good way to minimise complex trunk loading and Kromodihardjo and Mital (1986) found that asymmetric lifting tasks, lifting boxes without handles and lifting more bulky boxes produced the largest stress on the lumbar spine.

### **2.3.1. Sports Applications**

Net joint forces and moments derived through inverse dynamics are often used in a sporting context as an objective criterion to assess performance. They have also been used to gain an insight into potential for injury and how this risk can be reduced. Consiglieri and Pires (2009) found in ergometer rowing that a lower initial handle position decreased upper body joint moments and therefore risk of injury. Greene et al. (2009) used an instrumented handle and foot stretcher to measure force generation for input into a full body model during elite male ergometer rowing. Joint moments were multiplied by angular velocity to calculate power, a commonly used performance indicator in rowing. Rowers with shorter lower legs were exposed to greater spinal moments which could predispose these rowers to overuse injuries (Greene et al., 2009). Both studies assumed two dimensional movements in the sagittal plane. This

was deemed suitable for the controlled and constrained motion of the participant imposed by the ergometer. A three dimensional asymmetric model would be more appropriate for applications involving rowing in water where the rower would be subjected to multidimensional loads (Consiglieri and Pires, 2009).

More complex movements that involve fast moving segments, highly skilled coordination patterns, and are asymmetric in nature provide a greater modelling challenge. Nevertheless this is an increasing area of interest and more and more research is concerned with the joint moment histories during high acceleration, complex motions in sports such as tennis (Bahamonde and Knudson, 2003; Elliott et al., 2003; Kawasaki et al., 2005), football (Nunome et al., 2002), golf (Gatt et al., 1998; Neal and Wilson, 1985; Nesbit and Serrano, 2005; Tsujiuchi et al., 2002; Vaughan, 1981), cricket (Ferdinands et al., 2009) and baseball (Fleisig et al., 2006; Sabick, 2004).

Kawasaki et al. (2005) investigated the kinetics of the body during one and two handed backhands in tennis. Lower lumbar net joint forces and moments during the swing were determined using inverse dynamics. Two force plates measured the ground reaction forces (GRF) at the feet whilst high speed cameras recorded the three dimensional kinematics. Body segment parameters (BSP) of the lower extremities were determined using regression equations. It was reported that, compared to double handed strokes, one handed backhands reduced maximal moments imposed on the lower spine. Bahamonde and Knudson (2003) compared the joint forces and moments of the upper extremities during both square and open stance tennis forehand groundstrokes. Peak shoulder internal rotation moments and wrist flexion moments were significantly greater in the square stance than the open stance technique. Peak moments at the shoulder and elbow had the potential for the development of overuse injuries and strength imbalances (Bahamonde and Knudson, 2003). Previous kinematic studies had failed to show significant trends in ball rebound velocity advantages between styles. Elliot et al. (2003) used inverse dynamics to investigate the effect of deep knee bend in the backswing phase of the tennis serve on joint loading in the upper extremities. Players with greater knee flexion produced lower joint loading at the shoulder indicating knee flexion should be encouraged during the backswing. In table tennis, Iino and Kojima (2011) compared upper limb kinetics of intermediate and advanced players during top spin forehands. Advanced

---

players exerted significantly larger internal rotation shoulder torque and were able to transfer mechanical energy from the trunk to upper arm at a higher rate than less skilled players. These results provided information important for performance improvement (Iino and Kojima, 2011). Nunome et al. (2002) investigated the kinetics of kicking in football using a three link three dimensional model consisting of the thigh, shank and foot. External hip rotation torque was dominant in the side-foot kick and higher in magnitude than with an instep kick. Identification of the main mechanics involved in both types of kick was used to improve coaching techniques. In these studies it was noted that inverse dynamics analysis provided an insight that kinematic analysis alone could not (Bahamonde and Knudson, 2003; Elliott et al., 2003; Iino and Kojima, 2011; Nunome et al., 2002).

The high incidence of shoulder and elbow injuries sustained by baseball pitchers, particularly at collegiate level, has led to considerable interest in injury prevention. Fleisig et al. (2006) calculated wrist, elbow and shoulder kinetics of collegiate pitchers who threw balls using four different types of pitching style. Previous kinematic studies had indicated that breaking pitches were more stressful than fast ball pitches however the kinetic analysis showed that no pitching technique was potentially more dangerous (Fleisig et al., 2006). Sabick et al. (2004) used inverse dynamics to investigate humeral torque during baseball pitching. It was shown that peak humeral torque occurred at the point of maximum shoulder external rotation. Spontaneous humeral fracture, a well-known phenomenon, was likely to occur at this time. Increased elbow extension at stride foot contact produced lower peak moments so this was recommended to reduce the likelihood of injury. Based on a large sample of elite players, Fleisig et al. (1995) identified maximal arm loading patterns during pitching. Maximum internal rotation torque at the shoulder occurred during arm cocking and the maximum compressive force occurred during arm acceleration. These findings supported the belief that overuse injuries of the shoulder occurred during these phases. The maximum elbow moment was produced at the instant of maximum shoulder internal rotation moment which was related to elbow injury. The authors suggested this information would be useful for orthopaedic surgeons to better understand mechanisms of overuse injury in order to optimise treatment (Fleisig et al., 1995).

Fast bowling in cricket has been the subject of inverse dynamics analysis for the prediction of spinal loads, the causal mechanism for lumbar injury (Ferdinands et al., 2009). Kinematic studies had previously shown large shoulder rotation was associated with this type of injury (Elliott, 2000; Portus et al., 2004). The three dimensional kinematics of 21 fast bowlers were recorded and a 15 segment full body model was developed. Two force plates were used to measure GRF of each foot during stance phases. Power calculations were used to determine whether actuation was active or controlled. Dynamic loading patterns were cyclic in nature and a complex activation pattern was found. Injury was most likely to occur when the spine was positioned near its end range of motion (Ferdinands et al., 2009).

### 2.3.2. The Golf Swing

The following subsection reviews the literature related to the kinetic analysis of the golf swing. Particular attention is paid to the golf swing as it is used in this thesis as a sports movement representative of a high acceleration motion, involving the whole body. The golf swing has been described as one of the most difficult biomechanical motions in sport to execute (Nesbit, 2005). A better understanding of the mechanics would help the golfer, the coach and equipment manufacturers (Nesbit, 2005). A summary of both forward and inverse dynamics analysis applied to the golf swing follows to illustrate how modelling techniques and golf swing analysis have evolved over the past few decades. Some of the difficulties involved in modelling such a complex movement are also highlighted.

Two dimensional models have been used to further the understanding of a number of factors influencing golf performance. Simplifications and assumptions have varied between studies depending on the individual aims and objectives. The ground-breaking work by Cochran and Stobbs (1968) was among the first to explore basic mechanics and optimal coordination patterns of the swing using a simple double pendulum model. A rigid upper link was used to represent the arms of the golfer and a rigid lower link represented the club, both of which rotated about a fixed hub located in the upper part of the chest. The model was validated against real swings and many other studies have used their approach for both inverse dynamics analyses and forward dynamics simulations. Budney and Bellow (1982) used inverse dynamics to predict joint torques using a double pendulum model driven by real kinematic data.

Other two segment models have considered optimal wrist release patterns (Jorgensen, 1970), effects of club length, backswing range and club head mass on swing speed (Reyes and Mittendorf, 1998) and swing 'efficiency' (White, 2006). Forward dynamics simulation studies have used both simplified torque functions applied at the fixed hub and wrist (Chen et al., 2007; Jorgensen, 1970; Milne and Davis, 1992; Miura, 2001) as well as more complex torque profiles derived through optimization algorithms (Pickering, 1998; Pickering and Vickers, 1999). A limited number of double pendulum models have included hub movement; such studies have found that this swing characteristic can significantly increase the kinetic energy of the club head at impact (Jorgensen, 1970; Miura, 2001). Shaft deflection has been included in several two dimensional simulation studies (Iwatsubo et al., 2002; Milne and Davis, 1992; Suzuki et al., 2006; Tsujiuchi et al., 2002).

Tsujiuchi et al. (2002) composed a three segment model with a flexible shaft that was able to estimate shoulder torques in addition to the wrist and the elbow torques applied during the downswing. The magnitude of the forward bending of the shaft at impact was dependent on the torque pattern applied by the player. Other three segment models have investigated optimum control (Campbell and Reid, 1985; Kaneko and Sato, 2000), wrist release patterns, power sequencing and equipment testing (Sprigings and Mackenzie, 2002; Sprigings and Neal, 2001). Iwatsubo et al. (2002) compared a two link model with a four link model which included elbow and shoulder joints in addition to wrist and neck joints of the two link model. Inverse dynamics was used to compare the derived joint torques and it was concluded that the more complex four link model was more accurate in determining the skill level of golfers.

The development of three dimensional swing models that consider the movement of the whole body are potentially more realistic but can be considerably more complex than two dimensional models (Betzler et al., 2008). Some three dimensional studies have used partial models of the lower or upper extremities (Gatt et al., 1998; Neal and Wilson, 1985; Tsujiuchi et al., 2002; Tsunoda, 2004; Vaughan, 1981). An early example by Vaughan (1981) analysed the forces and moments applied by four golfers to a rigid model of the club using inverse dynamics. It was found that players did not swing the club in one static plane, yet confirmed the conclusions of previous two dimensional studies that a negative moment was applied to the club just before impact resulting in

acceleration of the club head. More recently Tsunoda et al. (2004) used a more complex model consisting of two rigid links representing the left upper arm and forearm and a flexible shaft. To deal with the complexity of the model, multibody kinetic software was used to run the inverse dynamics simulation. Shaft strain measurements were used to validate the model output which over predicted strain just before impact; this was thought to be due to the rigid link between the hand and club which neglected any possible dampening caused by the hands. Gatt et al. (1998) used a lower body model to calculate the three dimensional knee moments during the golf swing to determine the influence of shoe type and skill on peak knee joint loads. The research was intended to assess the risk of knee injury or re-injury for those in rehabilitation after surgery. Results indicated that the downswing was the most stressful stage of the swing however shoe type and skill did not influence knee loading patterns. It was therefore suggested that shoe and skill level need not be a concern in deciding the time to return to golf after injury.

Research attempting to model the whole body's motion during the swing has been limited perhaps due to the increased difficulty in deriving and solving the equations motion (Nesbit, 2005). Most studies have opted to use multibody software and a combination of inverse and forward dynamics simulations to obtain joint forces and moments. A multibody system is used to model the dynamic behaviour of interconnected bodies (De Jalon and Bayo, 2011). Multibody software refers to commercial computer packages that are used to solve problems in multibody system analysis. An additional complexity is introduced by the indeterminacy caused by the club handle, arms and shoulders forming a closed kinematic chain (Vaughan et al., 1982a). McGuan (1996) used multi-body software to show the effect of shaft stiffness variations on club head velocity. The kinematics of a single player were recorded and used to drive the inverse dynamics model. A flexible shaft was included in the model, the stiffness of which was varied during simulations. No information was provided on how the model was validated. Stewart and Haigh (n.d.) used a three dimensional full body model to examine the relationship between hip moments and club head angular velocity. A full body model was described; however, hip moments alone were presented. Club head angular velocity at impact and maximum hip moments showed significant correlation supporting anecdotal evidence of the importance of hip moments in achieving maximum driving distance.

Nesbit (2005) used multibody software to develop a three dimensional, 15 segment, full body model. This was coupled to a flexible shaft model of the club. Regression equations were used to estimate body segment parameters. Kinematic data was used to drive the model simulations which output kinematics and kinetics. The feet were constrained using a ground surface model; a spring damper system was used to simulate contact between the feet and the floor. A torque control function based on the measured ground reaction forces was used to force the feet in contact with the ground. Verification of the model output was achieved in three steps; firstly the simulated joint motions were compared to kinematic data. Secondly, static and inverse dynamic test cases were applied to the model and the joint forces and moments were compared to analytical results. Lastly, dynamic tests involved applying harmonic motions to individual segments. How well the derived forces and moments were able to represent the actual loads was not considered. Validation was achieved by comparing ground reaction forces predicted by the model to the force plate measured ground reaction forces. Only vertical ground reaction forces were compared. Additionally, kinematic and kinetic model outputs for the club were compared to published data. A large sample of 84 males and 1 female were analysed, however the swing kinetics of just four participants were examined. The mechanics of the club in terms of linear and angular force and torques applied by the wrist were discussed in detail. Total work and power for each player were presented however no information on individual joint forces and moments were provided for the rest of the body. In a later paper by the same author the development of the model was described in more detail (Nesbit, 2007). The indeterminacy caused by the hands and club forming a closed loop was addressed directly; the load was distributed equally between both arms though no justification for this decision was made. The same five validation tests described above were used. An additional test was used to validate the forward dynamics simulation; model predicted joint torques were used to drive the model to see if the motion matched the original swing kinematics. This resulted in unpredictable results and simulation failure.

Kenny et al. (2006) developed a 19 segment musculoskeletal computer model and ran a simulation of a single golfer swinging three clubs of differing lengths. The primary objective of the paper was model validation. Both forward and inverse dynamic simulations were performed. Kinetic output of the model was validated by comparing

grip force measurements from previous studies; "reasonable" agreement was found. Inverse dynamics simulations were run in order to capture joint angles whilst passive training muscles learnt lengthening and shortening patterns. Forward dynamics was then applied to calculate joint moments. No data on joint forces or moments was presented.

Three dimensional, full body models go some way into overcoming some of the limitations of two dimensional analyses, however validation of the kinetic output of these models is lacking. In the majority of swing models the right arm of the player was ignored or both arms were considered as one segment. In the two examples of full body models discussed, only Nesbit et al. (2007) considered the closed loop problem, choosing to distribute the load equally between the arms although seemingly no attempt was made to validate this assumption.

### **2.3.3. Discussion**

Inverse dynamics has been applied to a wide variety of sporting movements ranging from simple planar lifting to more complex sporting movements such as the tennis serve and the golf swing. Joint forces and moments have been used for injury prevention, rehabilitation, prosthetic design, the development of coaching techniques and performance improvement. Such kinetic analyses have provided a more complete picture of mechanics, often discovering things that were not apparent from the kinematics alone. The complexity of models varied depending on a study's objectives; partial models consisting of only a few segments and constraining movement to two dimensions are simplifications that have been used most often. Three dimensional studies are becoming increasingly important for the realistic representation of complex movement patterns like the golf swing (Neal and Wilson, 1985; Vaughan, 1981). However, much of the research concerning golf swing kinetics and other high acceleration movements has been lacking in terms of validation and uncertainty of the derived joint forces and moments.

## **2.4. Assumptions and Sources of Error in Inverse Dynamics**

### **Solutions**

This section will briefly discuss some of the assumptions and potential sources of error that can affect joint forces and moments calculated using inverse dynamics analysis.

For a summary of the assumptions made in the calculation of joint moments using inverse dynamics analysis see APPENDIX O: Table of Assumptions, pg. 59.

#### 2.4.1. The rigid body assumption

Inverse dynamics simplifies complex anatomical structures to a set of solvable equations that indirectly quantify the net effect of internal forces and moments acting across joints necessary to create motion (Robertson et al., 2004). Segments are represented as rigid bodies with a fixed mass, centre of mass and inertia. Rigid bodies have no moving parts and cannot be deformed. The assumption of rigidity simplifies the dynamical analysis considerably and is based on the idea that deformations that do take place are small in comparison to the overall movements of the segment (Vaughan et al., 1982a). However, inertial characteristics can change during movement due to the displacement of internal organs and muscles (Zatsiorsky, 2002). It has been shown that during the impact phase of a drop landing, the soft tissue in each segment of the body moved relative to bony parts and wobbled in a complex damped manner (Gruber et al., 1998). Movements involving high accelerations and impulsive loadings are especially susceptible to these errors (Hatze, 2002; Pain and Challis, 2006). For controlled impact experiments, the mean magnitude of soft tissue motion for the shank and thigh were  $1.8 \pm 0.2$ cm and  $3.2 \pm 0.9$ cm respectively (Pain and Challis, 2006). This corresponded to a 50% decrease in joint forces and moments for a wobbling mass model during drop landing simulations compared to a rigid model. Particular body segments such as the trunk and the feet are particularly susceptible to this type of error (Zatsiorsky, 2002). For example the foot can bend at the metatarsal-phalangeal joint however it is commonly modelled as one segment (Robertson et al., 2004). Similarly, the trunk is a series of rigid bodies interconnected by many vertebrae as well as the pelvis and scapulae (Robertson et al., 2004).

#### 2.4.2. Joint constraints

In an inverse dynamics model, segments are linked together into a kinematic chain using joints with 1-6 degrees of freedom. The number of segments and the joint constraints determine the total number of degrees of freedom the model has. These ideal revolute joints do not dissipate any energy due to friction or deformation which can be caused by passive resistance to motion (Zatsiorsky, 2002). Revolute joints also

---

assume pure rotation about a fixed joint axis when movement can be more complex, for example the shoulder joint can translate significantly (Zatsiorsky, 2002).

### 2.4.3. Body Segment Parameters

Body Segment Parameters (BSP) refer to the mass, centre of mass and moments of inertia of a segment which are assumed to be fixed during inverse dynamics analysis. Segmentation is used to divide the body so that it can be approximately represented as a multilink chain. This can only be achieved with limited accuracy; the human body is continuous with muscles, ligaments and other soft tissues crossing over body parts making segmentation subject to judgement (Zatsiorsky, 2002). Segmentation methods vary from study to study. Methods used to determine BSP include regression equations, scanning methods and geometric modelling techniques. Regression equations assume that segmental mass distribution is similar among members of a particular population. These parameters should be selected from a population that closely matches the subject (Zatsiorsky, 2002). Despite providing the fastest method for BSP estimation, regression equations do not account for individual body morphology differences and have been shown to provide the least accurate BSP estimates (Durkin and Dowling, 2003). Medical imaging techniques such as Magnetic Resonance Imaging (MRI), gamma ray scanning, Dual-Energy X-ray Absorptiometry (DEXA) and Computed Tomography Imaging (CTI) enable the most accurate BSP estimates to be made directly from live participants (Durkin et al., 2002). However due to financial costs, ethical issues (e.g. radiation), inaccessibility and the need for highly trained operators it is generally not practical for investigators to use these techniques.

Geometric modelling techniques are used to derive subject specific BSP and hence overcome some of the drawbacks associated with regression methods (Yeadon and Morlock, 1989). Geometric models make two primary assumptions; the volume and shape of the segment can be accurately modelled using a series of geometric shapes and the density of a segment is uniform throughout. Wicke and Dumas (2010) found that adopting a uniform density function produced only minor errors in the inertial estimates for the trunk. The greatest errors were due to inaccuracies in the volume function (Wicke and Dumas, 2010). The literature also suggests that some segments are more difficult to model than others. The trunk appears to be particularly difficult; in studies where segmentation was consistent and the sample was homogenous, the

mass of the trunk relative to the whole body mass varied from 35.8% - 48.0% (Pearsall and Reid, 1994). Furthermore the mass of the abdominal region where body fat is most readily accumulated ranged in the literature from 10.4%-21.6% of relative body mass (Zatsiorsky, 2002).

A further issue with BSP estimates is the reliability and accuracy of palpation of anatomical landmarks. Palpation is a method of examination used to determine the location of a specific anatomical landmark. In order to build participant specific geometric models and define segment coordinate systems, a large number of anthropometric measurements must be taken at segment boundary levels. Any errors in palpation will contribute to errors in BSP estimation. Segment volume estimates have been shown to be sensitive to width and depth measurements taken at segment boundary levels (Yeadon, 1990). Standardization of measurement techniques is claimed to be the best way to improve the reliability of static palpation (Domholdt, 2000; Fritz and Wainner, 2001). The accuracy of palpation may be reduced in people who are obese or muscular because of the increased difficulty in accurately locating bony points through the skin (Clarke, 1972; Giles and Taylor, 1981).

#### **2.4.4. Joint centre location**

Inverse dynamics calculations assume that the lines of action of joint reaction forces pass through joint centres. There are a huge number of different methods that have been used to define various joint centre locations for biomechanics applications. These include regression equations, 2D and 3D offsets (Anglin and Wyss, 2000; Schmidt et al., 1999) and functional methods. Functional methods include the mean helical screw axis (Churchill et al., 1998) and constraint based approaches such as that used by O'Brien et al. (2000) which locates the joint centre location as the point that moves the least between two adjacent body segments during functional movements. The accuracy with which these methods can estimate joint centre locations can be dependent on the marker location, anthropometric measurements and regression uncertainty. Since joint centre definitions often rely on palpation of anatomical landmarks the accuracy and reliability with which these can be located are also factors to be considered. Joint centre location error will effect body segment parameter estimation in addition to the length of moment arms of joint reaction forces.

#### 2.4.5. Kinematic measurements

There are issues associated with the non-invasive measurement of skeletal kinematics. The instantaneous positions of markers or sensors placed on the surface of the skin are tracked using motion capture systems and *in vivo* kinematics are reconstructed. Soft tissue artefact (STA) is the movement of skin markers or sensors relative to the underlying bone (Leardini et al., 2005). STA has been shown to be task specific (Akbarshahi et al., 2010), participant specific (Reinschmidt, Bogert, Nigg, et al., 1997) and location specific (Schache et al., 2008). Studies attempting to characterise STA have been contradictory; several have reported consistent patterns of STA between subjects (Akbarshahi et al., 2010; Benoit et al., 2006; Garling et al., 2007; Shultz et al., 2011), others have reported consistent patterns only within participants (Andersen et al., 2010; Manal et al., 2003) and others have reported no consistent pattern whatsoever (Kuo et al., 2011). STA can affect the calculation of segment angles, kinematic variables such as segment linear and angular acceleration, as well as joint centre location and segment centre of mass location.

Instrumental errors arising from the finite precision limits of the motion measurement system can be systematic or random in nature. Systematic errors using stereo photogrammetry techniques depend on the size of the field and the position of the marker within it (Gazzani, 1993). Random error due to electronic noise, marker flickering, digitisation, marker image shape distortion at high velocities, obscured images or merging of markers can be reduced with various data smoothing techniques. Electromagnetic tracking systems can suffer from distortion caused by metal or conductive materials and equipment near the emitter or receiver (Kindratenko, 2000). Whilst instrumental errors can be minimised they are always present and this error can propagate unpredictably to the estimation of segment kinematics (Chiari et al., 2005). Position and orientation data collected using motion capture systems are numerically differentiated to give the first and second order derivatives needed for calculation of forces and moments. The process of differentiation amplifies noise (Lanshammer, 1982) and will therefore affect the accuracy with which segment acceleration and velocity can be measured.

#### 2.4.6. External force measurement

Many inverse dynamics studies use external force measurement devices such as force plates or instrumented equipment to measure grip forces. For example, Larivière and Gagnon (1999a) used force plates and a dynamometric box to measure force data at the feet and hands respectively during lifting tasks. The measurement of external forces can contain error in both force magnitudes and centre of pressure location (Lewis et al., 2007). In addition there may be discrepancy in the registration between the global coordinate system and external force measurement device coordinate system since these are independent measurement systems (Kim et al., 2006; McCaw and DeVita, 1995; Robertson et al., 2004). The accuracy of the parameters measured by force plates are affected by calibration which is often done *in situ*. These errors will affect joint forces and moments at the most distal end of the kinematic chain which will propagate up the chain potentially causing larger errors at the more distal joints (Riemer et al., 2008).

#### 2.4.7. Closed kinematic chain indeterminacy

The assumption that there are sufficient independent equations to determine the unknown forces is implicit to inverse dynamics analysis (Vaughan et al., 1982a). However this is not always the case; for example in the golf swing indeterminacy is caused by the club handle, arms and shoulders forming a closed kinematic chain. A similar situation occurs in baseball batting and the double support phase in gait. In gait, this problem has been overcome by using two force plates to measure the forces of each foot independently (Alkjaer et al., 2001). Other studies have attempted to calculate force plate parameters using only the kinematic data with optimisation algorithms (Pillet et al., 2010; Ren et al., 2008). In golf swing analysis Nesbit (2005) considered the closed loop problem, choosing to distribute the load equally between the arms although seemingly no attempt was made to validate this assumption. For this type of application the solution requires the addition of force transducers in the grip to provide the extra information required. This is a technically difficult solution but has been attempted in baseball (Koike et al., 2004) and golf (Koike et al., 2006) using strain gauge instrumented grips. Similarly in golf flexible pressure arrays have been used (Broker and Ramey, 2007) and have indicated that forces applied by the left hand during the swing are dominant over forces applied by the right hand. The conversion of these pressure distributions and/or grip strains to data which could be

---

used as input to an inverse dynamics analysis to solve the indeterminacy problem is not trivial and has yet to be achieved in the literature.

#### 2.4.8. Filtering of non-stationary signals

In some applications, such as golf, tennis or baseball, impact is implicit in the movement being analysed. Impact is of interest since a relationship between impact and chronic sports injuries have been suggested (Collins and Whittle, 1989; James et al., 2003). These non-stationary signals have a frequency content that varies with time. Raw displacement-time data are often differentiated in order to calculate velocity and acceleration. Differentiation preferentially amplifies high frequency components so that low level, high frequency noise present in the displacement signal dominates higher order derivatives (Wood, 1982). Digital filtering techniques, such as the Butterworth filter, can isolate the frequency content of the signal; however they cannot determine when these components occurred in time. Sharp, high frequency components, such as those caused by impacts, are often over-smoothed (Lavanon and Dapena, 1998). In kicking in football, this has been shown to result in an underestimation of segmental acceleration in the joint moment calculations just before and during the impact phase (Nunome et al., 2002). During tennis forehands, the deceleration of the racket and arm produced by impact appeared to start before the impact itself and systematic errors in the kinematics were produced in the last frames before impact (Knudson and Bahamonde, 2001).

To avoid such problems, extrapolation procedures have been used to make more accurate estimations of impact parameters (Knudson and Bahamonde, 2001; Lavanon and Dapena, 1998). The most appropriate extrapolation technique has been shown to be dependent on the specific kinematic variable of interest (Giakas and Baltzopoulos, 1997; Knudson and Bahamonde, 2001). Extrapolation procedures are limited by the requirement of a precise knowledge of the time of impact which can be difficult. Furthermore, no post impact data can be processed. Time-frequency filtering methods such as Wavelet De-Noising (WDN) (Donoho and Johnstone, 1995) and the Wigner distribution (Giakas et al., 2000) have the ability to localise the frequency components of a signal. WDN has been utilised for a number of biomedical problems, including spectral analysis and noise removal of myoelectric signals (Singh and Tiwari, 2006). However, studies utilising WDN in biomechanical context have mainly dealt with

synthesised signals (Ismail and Asfour, 1999; Wachowiak et al., 2000). Issues with WDN techniques exist. 'Pseudo-Gibbs' artefacts are sometimes present after smoothing (Alonso et al., 2005; Giakas et al., 2000; Wachowiak et al., 2000). These are visible as oscillations around the true signal and are caused by singularities associated with the exact alignment between signal features and features of the mother wavelet (Coifman and Donoho, 1995). Furthermore there have been difficulties with selecting a suitable mother wavelet from an infinite family of candidates (Giakas et al., 2000; Wachowiak et al., 2000). Other time-frequency filtering techniques such as the Wigner function have shown promising results (Giakas et al., 2000; Nunome et al., 2006). However, issues with the complexity involved in devising an automatic and systematic implementation procedure and the correct choice of filter function still exist (Alonso et al., 2005).

#### 2.4.9. Discussion

Error implicit in inverse dynamics calculations comes from a variety of sources, all of which propagate to the estimation of joint moments and forces. Errors can be minimised through careful consideration of the experimental set up and data processing techniques used (i.e. filtering) however they can never be eliminated completely. The iterative nature of inverse dynamics analysis means that errors are propagated up the kinetic chain from the most distal to the most proximal segment and so the cumulative effect of these errors is of concern.

#### 2.5. Methods of Validation

Validation is defined by the American Society of Mechanical Engineers (ASME) standards committee for Verification and Validation of Computational Solid Mechanics as "the process of determining the degree to which a model is an accurate representation of the real world from the perspective of the intended use of the model" (Schwer, 2006). Validation of inverse dynamics derived joint moments and forces is problematic since in most cases comparison to a 'gold standard' or direct comparison to *in vivo* measured loads is not possible. A "gold standard" is defined as the best measure available under reasonable conditions (Versi, 1992). However, the over determined nature of inverse dynamics solutions can be exploited for this purpose. Three different validation methods of inverse dynamics models have been identified from the literature; 1) top down bottom up comparison of joint forces and

moments, 2) measured compared to predicted ground reaction forces, and 3) a comparison of forces and moments measured using external measurement devices. This section is concerned with studies which have used these methods to validate joint forces and moments derived through inverse dynamics.

### **2.5.1. Top Down/Bottom Up Joint Force and Moment Comparison**

This technique compares joint moments and forces calculated using two different recursive strategies performed on kinematic chains. The 'top down' model begins at the top of the kinematic chain, usually at the distal end of the hand segment, and proceeds proximally to the elbow, followed by the shoulder and so on. The 'bottom up' model begins at the feet and proceeds proximally up the leg. The forces and moments of the joint at which these two models meet is then over determined and the forces and moments estimated by each of the strategies can be compared. In an ideal system they will be equal in magnitude and opposite in direction. This method of validation is therefore only suitable for systems with two free ends, for example full body models, and hence the method is not universally applicable to all studies. Top down bottom up comparisons do not account for two sources of error; the joint centre location and the anatomical coordinate system of the joint where the two recursive strategies meet (Kingma, De Looze, et al., 1996). A major drawback associated with this method is that nothing can be learnt about the individual sources of error and how they contribute to the total residual error. Furthermore, a primary assumption of these validation methods is that all the error is cumulative when it is possible that errors of different origins can compensate for each other (De Looze et al., 1992); for example, the effect of pelvis segment mass error on the calculated moment at the L5/S1 joint may be cancelled out by error in a more distal segment's moment of inertia.

A large area of research is concerned with lower back injury caused by manual materials handling (MMH) in an industrial context. Inverse dynamics is frequently employed to estimate loading at the lumbo-sacral joint (L5/S1) during lifting and so the validation of such methods has been investigated (De Looze et al., 1992; Kingma, De Looze, et al., 1996; Kingma, Toussaint, et al., 1996; Larivière and Gagnon, 1999b; Plamondon et al., 1996). De Looze et al. (1992) used top down/bottom up comparisons to validate joint force and moments calculated using a two dimensional eight segment full body model applied to planar lifting tasks. More proximal joints

such as the L5/S1 and pelvis showed the greatest correlation whereas joint moments were less similar for more distal joints. Peak moments at the L5/S1 joint were 10.9% (22.8Nm) higher for the top down calculations compared to bottom up. No significant difference in joint reaction forces between the two models was found. Therefore the differences in joint moments could be attributed to errors in moment arm lengths, segment moments of inertia, angular acceleration and the partitioning of segment masses as these did not affect joint reaction force calculations. A similar two dimensional study by Kingma et al. (1996) compared residual joint forces and moments at the L5/S1 joint during lifting tasks for two sets of BSP estimates; one set derived using the regression equations of Plagenhoef (1983) and one set using the geometric model proposed by Yeadon (1990). The geometric model yielded smaller joint moment residuals suggesting that it provided better BSP estimates than regression equations, however, the type of lifting movement strongly influenced results. This method of validation has also been used for three dimensional models applied to asymmetric lifting tasks (Kingma, De Looze, et al., 1996; Larivière and Gagnon, 1999b; Larivière and Gagnon, 1998; Plamondon et al., 1996). Root Mean Square (RMS) differences for joint forces were generally between 10N and 15N and between 4Nm and 9Nm for joint moments (Plamondon et al., 1996). Maximum differences for forces and moments were 59N and 38Nm respectively (Plamondon et al., 1996). There was an increase in RMS difference for both joint forces and moments with an increase in speed of the lifting movement indicating segmental accelerations contributed to the error (Larivière and Gagnon, 1998; Plamondon et al., 1996). Larivière and Gagnon (1999a) reported that a geometric trunk model produced smaller L5/S1 extension moment errors than the proportional model and this was particularly obvious for larger participants and with the trunk in a flexed posture. When trunk segment COM was determined using trunk-line centres of gravity instead of using a straight line from the hips to the shoulders, errors in extension moments were reduced. Errors were also decreased when the trunk was divided into 3 instead of 2 segments. In these studies it was assumed that a reduction in joint force and moment residuals at the L5/S1 joint indicated a reduction in error. This assumption was considered reasonable supposing error was cumulative as calculations proceeded down the kinematic chain; however it is possible that individual sources of error could compensated for each other (De Looze et al., 1992).

Other studies have used this method of validation for gait trials (MacKinnon and Winter, 1993; Reimer et al., 2008), balance recovery movements (Robert et al., 2007), ergometer rowing (Greene et al., 2009), slow speed golf swings (Tsai, 2005) and most recently for fast and large spine movements (Iino and Kojima, 2012). Robert et al. (2007) applied this technique in order to assess the influence of different BSP estimates on the accuracy of joint moment estimates during balance recovery. Modelling the upper body as a single rigid segment instead of two was found to increase the difference in joint moments calculated between the pelvis and the thorax. The influence varied along the movement demonstrating that the arms contributed dynamically to balance recovery. Reimer et al. (2008) used the residual joint moments at each joint to validate the results of an uncertainty analysis performed using a two dimensional full body model during gait. The upper bound uncertainty of joint torques and forces was calculated using Taylor series approximation (Taylor, 1997). Error in individual input parameters used to calculate joint moments were determined and used in the uncertainty analysis. Two sets of error estimates were used. The residual was found to be bounded by the uncertainty estimated using the more conservative set of error estimates for input parameters. Therefore it was concluded that the lower set of error bounds were more realistic.

The validity of inverse dynamics joint moments for slow speed golf swings has been assessed (Tsai, 2005). Mean RMS differences in joint moments at the L5/S1 joint were 11.1 Nm, 13.2 Nm and 9.5 Nm for lateral bending, flexion-extension and axial rotation respectively. This is one of the few studies that applied this method of validation to a more complex movement, however, only "slow speed" swings were considered. This was due to the motion measurement system used not being fast enough to track the markers on the wrists, hands and club during the downswing at a normal swing speed. Therefore, it is not unexpected that RMS differences were of similar magnitude to asymmetric lifting tasks discussed previously. Iino and Kojima (2012) investigated the validity of inverse dynamics analysis applied to fast and large spine movements; maximum angles of the upper thorax achieved were comparable to professional golfers performing a drive. Three sets of BSP regression equations were used to estimate BSPs of 9 male collegiate students. Validity was assessed by comparing top down and bottom up approaches for the estimation of pelvic moments. All three tasks for all three BSP sets produced mean RMS errors of less than 10Nm for pelvis moments.

This implied that moments were as valid for fast and large trunk movements as lifting tasks using the top down approach. Peak RMS joint moment errors occurred at the maximal extended position of the trunk, expected to be the most deformed position and therefore less likely to conform to the rigid body assumption. Marker movement relative to the bone at these extended positions and when the movement was changing direction was likely to be maximal and contributed to this error. Error was extremely variable between participants with peak error varying from 5-30Nm between participants. It was concluded that this highlighted the unsuitability of the application of regression equations to certain individuals and the importance of accurate BSP estimates for joint moment validity. This was the only study which validated inverse dynamics applied to a high acceleration activity; however movements were artificial and restricted to the spine.

### **2.5.2. Predicted GRF vs. Measured GRF**

An alternative measure of validity exploits the over determined nature of a full body model at the ground end of the kinematic chain. This method requires a force measurement device at the feet and a full body model. The net GRF can be estimated by summing, over all body segments, the segment masses multiplied by the segment acceleration vector and subtracting the gravity vector (Kingma, De Looze, et al., 1996). This can then be compared to the measured GRF by summing the GRFs for both feet; the GRF cannot be separated for the feet since the two legs form an indeterminate loop during a top down analysis. This method has been described as more 'rigorous' than top down bottom up comparisons (Kingma, De Looze, et al., 1996) since two completely independent measures are being compared however this method will not be affected by errors in segment moment arm lengths (De Looze et al., 1992). The prediction of GRF includes all body segments so the reported residual may be maximised due to the accumulation of error as calculations proceed down the kinetic chain. As with the top down/bottom up comparison, no information on how individual sources of error contribute to the total residual error can be extracted using this method.

This technique has been used to validate planar models applied to standing broad jumps (Pezzack and Norman, 1981), rapid knee bends (Pezzack and Norman, 1981), planar lifting tasks (De Looze et al., 1992; Freivalds et al., 1984; Kingma, Toussaint, et

al., 1996) and three dimensional asymmetric lifting tasks (Kingma, De Looze, et al., 1996; Kromodihardjo and Mital, 1986). Pezzack and Norman (1981) used a six segment planar model to estimate joint forces during a bisymmetrical standing broad jump. The maximum residual error was 10% and 15% of the horizontal and vertical components of force respectively. Vertical ground reaction forces for a rapid knee bend also showed close agreement. Freivalds et al. (1984) used a seven link planar full body model to determine loads at the L5/S1 joint during lifting tasks. Peak predicted vertical GRF showed close agreement with measured with a difference of 9 N, however, the predicted time to reach this peak was approximately 90ms faster than measured. This was thought to be due to synchronisation errors caused by miss triggering at the start of the movement. Kromodihardjo and Mital (1986) were among the first to develop a three dimensional model for analysis of compressive and shear forces at the L5/S1 joint during lifting capable of analysing asymmetric movements. Validation via comparison of measured and predicted vertical ground reaction force reported correlations of 0.65 which were substantially higher than previous sagittal plane models which reported correlations of 0.43 (Freivalds et al., 1984). A three dimensional study by Kingma et al. (1996) reported higher correlations ( $r = 0.93$ ) for vertical ground reaction forces during lifting tasks than previous studies (Kromodihardjo and Mital, 1986). It was hypothesised this was due to a reduction in skin motion artefact by using braces for marker attachment. Furthermore, the model used by Kromodihardjo and Mital (1986) only allowed for flexion-extension movements at the elbow and knee joints. De Looze et al. (1992) used this method to compare both the vertical and horizontal components of predicted and measured GRF. This was used to assess the validity of an 8 segment sagittal plane model applied to lifting. Correlations between the measured and predicted vertical components of GRFs compared favourably to previous 2D and 3D studies with a mean difference of 0.07 N and a mean correlation of 0.88 (Freivalds et al., 1984; Kromodihardjo and Mital, 1986). The horizontal component had a low correlation ( $r = 0.32$ ) due in part to the smaller amplitude of horizontal force relative to the vertical force; this was less of a concern since it would only have a small influence on the joint moments.

### 2.5.3. External Measurement Devices

Studies have used other external measurement devices to validate inverse dynamics solutions. Andersson (1980) used a top down model to predict loads on the lumbar

spine during industrial work tasks and compared these to myoelectric activity measurements. A good agreement was found between changes in myoelectricity activity levels and lumbar load predictions. It was concluded that this was valid method of predicting lumbar spine loads in the workplace. A similar study by Freivalds et al. (1984) reported the compression forces at the L5/S1 joint predicted by inverse dynamics analysis correlated significantly with smoothed and rectified electromyograph (EMG) of the erector spinae muscles during lifting tasks.

In addition to a comparison between measured and predicted GRF, De Looze et al. (1992) compared predicted and known loads and moments at the hands during lifting. The reactive forces and moments at the wrists should equal the forces and moments required for translational and angular acceleration of the hands, therefore any residual forces (besides gravity) or moments were considered erroneous. Only small deviations from the expected zero level of residual force and moments were found and this was equivalent to 1-2% of the peak spinal moment. Pezzack and Norman (1981) compared the net reaction forces and moments at the toe during the airborne phase of a stride jump predicted by inverse dynamics to the expected zero magnitude. A 15 segment model was used and calculations began at the left toe with zero moments and forces and proceeded through all the links ending at the right toe. Large deviations of up to 96N and 155Nm were reported suggesting that these more complex models with no measured force inputs or centre of pressure values can produce large errors.

## 2.6.Sensitivity Analyses

A sensitivity analysis is concerned with the influence of input parameters on the model output. It is often useful to perform sensitivity analyses in conjunction with validation experiments. They provide a measure of how error in a specific model input impacts the simulation result, scaling the relative importance of the inputs (Henninger et al., 2010; Roache, 1998). Generally, a single model input or parameter is perturbed by an order of magnitude or multiples of the standard deviation about the mean, while holding the others constant. Unlike the validation methods discussed in the previous section, a sensitivity analysis has the ability to isolate the effects of individual parameter variations. Studies reporting the sensitivity of joint forces and moments to errors in input parameters are considered in this section.

Joint force and moment sensitivity during gait trials has been investigated for perturbations in BSP (Challis, 1996; Pearsall and Costigan, 1999; Ren et al., 2008; Silva and Ambrosio, 2004), GRF (Silva and Ambrosio, 2004), anatomical landmark coordinates (Silva and Ambrosio, 2004), knee joint centre location (Holden and Stanhope, 1998), hip joint centre location (Stagni et al., 2000), centre of pressure location (McCaw and DeVita, 1995) and digital filtering cut off frequency (Ren et al., 2008). Input parameter perturbations were in some cases based on arbitrary selected values, for example Ren et al. (2008) varied cut-off frequencies from 3 – 9Hz and segment mass, MOI and COM positions were varied by  $\pm 30\%$ . Other studies based perturbations on expected error bounds, for example Pearsall and Costigan (1999) varied the mass, centre of mass and transverse moment of inertia of the thigh and shank in isolation for 2D gait trials. Each parameter was perturbed by a maximum of  $\pm 40\%$ . This variation was representative of the variance resulting from the use of six different predictive functions to estimate BSP for the 15 participants used in the study. Stagni et al. (2000) shifted the hip joint centre in 6mm increments up to  $\pm 30\text{mm}$  in all three axes. A 30mm shift was chosen to represent the maximum reported hip joint centre location error reported in the literature using prediction equations.

Gait studies tend to consider only one or two parameters and these were perturbed in isolation of each other. Sensitivity of only the lower extremity joints were reported since lower body models were used which terminated at the hip. Studies which considered the effect of perturbations of more than one input parameter were able to identify the parameters which had the greatest effect on joint force and moment profiles. Silva and Ambrosio (2004) investigated sensitivities for each joint during the stride phase of gait. Perturbations in segment mass, digitised anatomical point coordinates and the components of the GRF for one foot were performed in isolation. Joint moments were not very sensitive to small perturbations in segment mass; a 1kg error would lead to a difference of less than 10Nm in system response. Typical digitisation errors in identifying anatomical coordinates of 0.01m produced errors of less than 0.3Nm. The most influential parameters were the external force magnitude, point of force application and precision of anatomical point positions of the segments in the kinematic chains to which these external forces were applied, i.e. the foot, shank and thigh segments during the stance phase of gait. Ren et al. (2008) investigated the sensitivity of the predicted ground reaction forces and moments to digital filtering and

body segment parameters using a three dimensional full body model during gait trials. Error was defined as the difference between the predicted ground forces and moments and those measured using force plates. In contradiction to the findings of Silva and Ambrosio (2004), Ren et al. (2008) reported segment mass variation had the largest effect on the forces; a 30% increase in torso mass led to a 71% increase in the RMS error of the vertical ground reaction force. The largest segments had the largest effect and these effects were sometimes disproportionate to the perturbations. Joint moments were particularly sensitive to COM positions which were perturbed along all three axes, unlike other studies which shifted the COM along the longitudinal axis of the segment only (Pearsall and Costigan, 1999). A 30% medial offset of the torso COM resulted in a 131% increase in RMS error of the frontal plane moment. The thorax and lumbar were modelled as a single segment and so had a relatively high mass in comparison to other segments (32% of total body mass) which may have contributed to its dominance in the results.

A comparison of the results between gait sensitivity studies is difficult; different sets of input parameters were perturbed, sometimes simultaneously or in isolation of each other and perturbation levels varied. Studies reported propagation of error up the kinematic chain (Challis, 1996; McCaw and DeVita, 1995; Pearsall and Costigan, 1999; Stagni et al., 2000) with the hip joint at the end of the chain experiencing the greatest effect of perturbations on joint moments and forces. Perturbations were shown to effect timings of joint force and moment event profiles; Stagni et al. (2000) reported hip joint centre location perturbations of 30mm in the posterior direction resulted in a delay of the flexion to extension event by 25% of stride duration. McCaw and Devita (1995) shifted the centre of pressure (COP) location in the anteroposterior direction under the support foot in the stance phase of gait. Relative transition times between flexor and extensor moments were increased or decreased on average by 7% and 13% respectively. The effect of perturbations was non-uniform throughout the different phases of gait; Van Den Bogert and Koning (1996) used simulated running data to determine the error in known joint loading as a function of cut off frequency of the low pass filter applied to the kinematics. Large errors in moments occurred during the impact phase, especially when kinematic data was filtered but force plate data were not. Pearsall and Costigan (1999) found that BSP perturbations of  $\pm 40\%$  significantly effected joint moments during the swing phase of gait. These errors could be

---

particularly concerning for open chain, high acceleration activities (Pearsall and Costigan, 1999).

The sensitivity of joint forces and moments during lifting tasks has also been the focus of a number of studies (Gagnon and Gagnon, 1992; Kingma, De Looze, et al., 1996; Kingma, Toussaint, et al., 1996; Larivière and Gagnon, 1999a; Larivière and Gagnon, 1998; Plamondon et al., 1996). In these studies, the sensitivity of the L5/S1 joint moments and forces were generally reported without any consideration of other joints. Of the lifting studies discussed in this literature review, Plamondon et al. (1996) and Larivière and Gagnon (1999a) provided the most detailed analysis, between them considering the effect of error in BSP, joint centre location, external force magnitude, centre of pressure position, orientation of the pelvis anatomical coordinate system and segment centre of mass linear acceleration. However, perturbations in joint centre location and local coordinate system orientation were limited to the L5/S1 joint and the pelvis respectively. Results related to the effect that these perturbations had on the RMS difference in joint moments at the L5/S1 joint between the top down and bottom up models. Differences in top down/bottom up model sensitivities were recognized; GRF and COP were identified as the most influential parameters for the bottom up model, whilst external force measurement, linear acceleration of the segment COM and BSP parameters were dominant in the top down models (Larivière and Gagnon, 1999a; Plamondon et al., 1996). Larivière and Gagnon (1999a) offered a more comprehensive appraisal of error magnitudes than previous studies for three dimensional lifting tasks. Error magnitudes for the pelvis joint centre location, anatomical coordinate system orientation of the pelvis, external force location and magnitude, segment mass, segment centre of mass location and segment moments of inertia were extracted from the literature. Centre of mass linear acceleration error was predicted using Lanshammar's equations (1980); these are a series of equations that predict the noise expected to remain in a signal after smoothing and differentiation. The parameters were perturbed in isolation and also the effect of perturbations of individual parameters was summed so that the relative contribution of each to joint moment error could be calculated. This study was limited to a small sample of three participants. Perturbations of the orientation of the pelvis anatomical coordinate system axes and joint centre location produced differences of 39Nm in the sagittal plane and 16Nm in the transverse plane respectively. External forces were

largest for the bottom up model so a small error in the moment arm affected joint moments to a greater extent than the top down model. A shift of 10mm in the point of application of the external force resulted in maximum absolute errors of 9Nm in the transverse plane for the bottom up model compared to absolute errors of 1Nm for the top down model.

Besides gait and lifting the sensitivity of joint moments during overarm throwing and elbow flexion against load have been considered. Challis (1996) perturbed moment of inertia values of the hand and forearm by  $\pm 5\%$  during an overarm throwing trial which had peak angular velocity of  $22.5 \text{ rads}^{-1}$ . The difference between baseline and perturbed moment profiles was not constant. Challis and Kerwin (1996) performed an in depth analysis of the magnitude of uncertainties involved in joint moment estimates applied to elbow flexion against an external load. Errors in BSP, kinematic variables and joint centre location were quantified. The noise in kinematic variables that remained after smoothing and differentiation were established using prediction equations of Lanshammar (1980). Inertial parameters were perturbed by  $\pm 1\%$  for segment mass and centre of mass, and  $\pm 5\%$ ,  $\pm 3\%$  and  $\pm 3\%$  for MOI about the x, y and z axis respectively. These errors were based on the expected effects that volume and density error from predictive equations may have on these parameters. Joint centre location was shifted by 0.01m for all three axes which reflected the expected combined error from the 3D measurement system and variation in the location of the joint centre during movement. A single female participant performed elbow flexion at maximum speed holding a 17.37kg dumbbell and inverse dynamics was used to estimate joint moments at the elbow. The geometric model consisted of two segments, with the forearm, wrist and dumbbell considered a single segment and the upper arm the second. Input variables were perturbed in isolation and in combination. Results showed that elbow joint moments were most sensitive to uncertainties in derivatives computed from kinematic data. BSP uncertainties played a lesser role due to the dominating influence of the accurately known inertial properties of the dumbbell. The influence of BSP uncertainties was expected to be higher for other activities which do not have such a dominating influence of an object with known inertial parameters. This study included the most comprehensive analysis of error magnitudes in comparison to the studies discussed in this literature review; nine parameters were perturbed and the expected magnitude of error was assessed in

---

some depth. However, this study was limited to simple elbow flexion movements, the model had only 2 segments and just a single participant was used. Furthermore, only elbow joint moment sensitivity was reported.

Other studies have investigated the sensitivity of inverse dynamics models by comparing the effects that different modelling techniques have on the joint forces and moments. Comparisons of BSP estimation methods have found that differences are most dominant during the swing phase of gait (Ganley and Powers, 2004; Rao et al., 2006), i.e. open chain, higher acceleration activities. Kingma et al. (1996) found geometric models outperformed proportional models during a back lifting task, however the reverse was true during leg lifting tasks. Pain and Challis (2006) compared a four segment wobbling mass model to a rigid body model during a simulated drop landing. Joint force and moments were up to 50% lower for the wobbling mass model compared with the rigid body model. Holden et al. (1997) simultaneously measured the kinematics of the shank using shell mounted targets and percutaneous skeletal trackers in order to assess the effect of STA on joint forces and moments during gait. Differences were most prominent during the stance phase. A similar study by Manal et al. (2002) reported that the largest effects occurred about the anteroposterior axis. Both studies concluded the magnitude of the effects were not large enough to influence the clinical interpretation of gait. These comparison studies were useful in identifying the influences of different modelling techniques on joint forces and moments. However, no definitive conclusions could be made as to the 'best' modelling method since all methods used would have contained errors and there was no 'gold standard' for comparison in these studies.

## **2.7.Uncertainty Analyses**

Uncertainty has been described as the "degree of goodness of a measurement or analytical result" (Coleman and Steele, 2009). Closely related to sensitivity analyses, uncertainty analyses can be characterised by a greater focus on the quantification of uncertainties in input parameters and propagation of uncertainty. A consideration of how uncertainties in measured variables propagate through inverse dynamics equations to produce uncertainties associated with the result is important for the interpretation of results (Riemer et al., 2008). Two common uncertainty propagation

---

analysis methods are the Taylor Series Method (TSM) (Taylor, 1997) and the Monte Carlo Method (MCM).

### 2.7.1. Taylor Series Method

TSM is a first order approximation of a Taylor Series expansion; systematic and random error in input variables are represented in absolute terms and the resulting uncertainty is calculated (Taylor, 1997). In assuming an absolute error term for each parameter, TSM excludes statistical information about the probability distribution for the input parameters (Laz and Browne, 2010). Such analyses assume the uncertainties in variables are random and uncorrelated (Challis and Kerwin, 1996), where this is not the case the uncertainty bounds predicted represent the upper bound of uncertainty (Riemer et al., 2008). Correlation coefficients can be added to Taylor series expansion equations where the exact forms of correlation between input variables are known to remove this limitation however these are often difficult to determine (Riemer et al., 2008). The TSM has the capability to incorporate inaccuracies in multiple input parameters and as such potential interaction effects are integrated. This results in a more robust analysis than sensitivity studies performed by varying parameters individually (Laz and Browne, 2010). In addition, sensitivity factors can be computed as part of the analysis and these can be used to indicate which parameters have the greatest influence on the uncertainty and to what extent (Laz and Browne, 2010).

In the field of biomechanics TSM has been applied to pose estimation for marker based tracking in virtual environments (Davis et al., 2006); isometric measuring apparatus (Wood et al., 1999), wheelchair propulsion measurement systems (Cooper et al., 1997) and measurement of weight transfer styles in golf (Ball, 2006). Cooper et al. (1997) wanted to assess the uncertainty involved in using a custom made kinetic measuring device, the "SMARTWHEEL", to measure pushrim forces and moments during wheelchair propulsion. The dependency of the biomechanical variables during wheelchair propulsion on wheelchair configuration, design of force moment sensing system, forces and moments produced by the participant and their interactions with one another made this a complex analysis. The results of this uncertainty analysis were used to determine the statistical power necessary to detect inter-subject or group variability to changes in wheelchair design. Any study looking at differences between groups or effect of interventions can only rely on variations which exceed the

uncertainty in the variable of interest (Cooper et al., 1997). Wood et al. (1999) used TSM to identify the sources of error which made the greatest contribution to the total error within an isometric measurement system. The system measured lower limb joint moments and consisted of a six axes transducer that measured isometric forces at the ankle. It was used to investigate the lower limb function in response to an electrical stimulation of the lumbosacral anterior roots of paraplegics. Improvements in the design of the system were based on the results. The analysis also provided confidence bounds which were used in the clinical interpretation of results. Oberhofer et al. (2009) used TSM to determine the uncertainty in the derivation of muscle-tendon lengths during pathological gait trials due to soft tissue artefact (STA). Errors in reference skin marker locations due to STA were assumed normally distributed and independent. Average standard deviation (SD) errors ranged from 6 - 50% of muscle tendon length and were dependant on the musculoskeletal model used. A constrained model whereby rotation but no translation was allowed at the hip, knee and ankle joint produced substantially smaller uncertainty values. This suggested such optimisation methods could be used to improve models. The quantification of STA was difficult and it was assumed the standard deviation of the STA at each segment was constant throughout the movement profile. This contradicted other studies that reported STA variance in each direction, across the gait cycle and from participant to participant. The benefit of TSM was that the STA error could be altered to reflect these findings in future studies (Oberhofer et al., 2009).

A limited number of studies have used TSM to analyse the uncertainty in inverse dynamics solutions. Andrews and Mish (1996) used Taylor Series to assess how the uncertainty in BSP measurements propagated to the uncertainty of joint moments for a single segment in fixed axis rotation. Mass, COM and MOI of the segment were given uncertainty values of  $\pm 5\%$ . Error percentages were chosen arbitrarily which limited the practicality of the study's results. The results showed that even with reasonably accurate BSP and segment accelerations that were not large, uncertainty bounds reached 12% of baseline moments. This study only looked at errors in BSPs and was limited to a single segment so there was no measure of how this uncertainty propagated up the kinematic chain. Desjardins et al. (1998) used Taylor Series to assess the uncertainty in three dimensional joint moments at the L5/S1 joint during lifting. This study chose an arbitrary 5% error applied to point of application of

external forces, BSPs, segment COM linear acceleration and COM angular velocity. Three participants performed an asymmetric lifting task at two speeds. For the lower body model, the external forces had the greatest effect on the L5/S1 joint moment output with a mean error of 5.1Nm. Segment masses had the most influence on the upper body model with a mean error of 2.9Nm. The limitations of this study included the use of arbitrary levels of uncertainty in input parameters. Furthermore, Taylor series expansion was performed for each parameter in isolation so the resulting uncertainty bounds were not representative of the error of the system as a whole, i.e. bounds were lower than would be expected. Riemer et al. (2008) analysed the upper bound error of joint moments derived using a sagittal plane full body model during gait trials. This study provided an in depth analysis of the uncertainties in joint moment inverse dynamics estimation. Input variables considered were BSPs, joint centre location, force plate measurements, motion capture system measurements, and segment angle error due to soft tissue artefact (STA). The study synthesised error magnitudes from the literature and performed experiments where necessary in order that comprehensive error estimates were made. Inaccuracies in BSP input parameters were segment specific. Two sets of inaccuracies, a lower and an upper set, were used to account for the variability of error magnitudes reported in the literature. Uncertainties in joint moments were reported to range between 6-236% of the estimated joint moment magnitudes, i.e. in some cases, the uncertainty was greater in magnitude than the estimated joint moment itself. Patterns of uncertainty did not always resemble moment profiles. Due to error propagation, the more proximal joints exhibited higher levels of uncertainty than the more distal joints. The parameters which contributed the most to the uncertainty were segment angle, which was mostly associated with skin motion artefact, and BSP. This uncertainty analysis was vital in determining the statistical power necessary to detect inter-subject or group variability and define confidence bounds important for clinical interpretation (Cooper et al., 1997; Riemer et al., 2008). Uncertainty estimates were validated through a comparison of the calculated residual of top down/bottom up analysis; the lower bound set of inaccuracies were shown to be a more realistic prediction of the uncertainty magnitude. This study demonstrated a comprehensive uncertainty analysis with consideration of a large number of error sources. A full body model was used and therefore the uncertainty patterns for every joint were investigated. However, the

---

study was restricted to gait, a relatively simple, slow velocity movement. Furthermore, movement in only two dimensions was considered. The task specific nature of such uncertainty analyses mean that different results were expected for different movements (Andrews and Mish, 1996; Riemer et al., 2008).

### 2.7.2. Monte Carlo Method

Probabilistic methods such as the Monte Carlo Method predict the likelihood of an output based on distributional characteristics associated with the inputs (Rubinstein, 1981). Each of the input parameters is represented as a distribution by randomly generating values for each variable according to its probability distribution. Individual error values are then summed and added to the "true" parameter values to obtain measured values. Results are calculated and this corresponds to running the simulation once. The sampling process is repeated until a converged value for the standard deviation of the output distribution is obtained. The distribution characterises the range of possible outcomes and their likelihood which leads to an understanding of probable outcomes (Coleman and Steele, 2009). This method is computationally expensive and can be time consuming since many thousands of trials must be performed for convergence to the correct solution (Laz and Browne, 2010). MCM is considered the 'gold standard' of probabilistic methods (Laz and Browne, 2010). The most challenging aspects of this method are defining suitable input parameter representations and the number of trials required for convergence. This section will review studies concerned with uncertainty analysis in the field of human movement biomechanics.

In the field of human movement biomechanics Monte Carlo simulations have been applied to studies concerned with structural reliability of implants, kinematics, joint mechanics, musculoskeletal modelling, and patient-specific musculo-skeletal representations. Many forward dynamics models have utilised the Monte Carlo method. Chang et al. (2000) demonstrated that the Monte Carlo method was a useful way of integrating population variability of physiological parameters into a biomechanical muscle model of the shoulder. Another study by Hughes et al. (1997) used the Monte Carlo method to assess the statistical distribution of shoulder muscle forces predicted by a planar biomechanical model during static arm elevation. Muscle moment arms were modelled as random variables with bounds dictated by data from

22 cadaver specimens. Simulation results were similar to muscle force predictions from the whole sample therefore lending confidence to the ability of the technique to analyse individual variability of rotator cuff muscle force. Valero-Cuevas et al. (2003) presented 50 musculoskeletal parameters making up a biomechanical model of the thumb as stochastic variables and used them to run Monte Carlo simulations for 5000 random repeats of the model. The kinematic description of the thumb was found to be the main contributor to the variability and uncertainty of the thumb tip moment predictions from the biomechanical model. Ackland et al. (2012) used the Monte Carlo method to quantify the effect of input parameter error on the whole body centre of mass of a three dimensional forward dynamics model during the stance phase of gait. Perturbations were applied to moment arm lengths and the architectural properties of muscles. Changes in tendon slack length contributed the most to model output and results were highly muscle specific. The Monte Carlo method was chosen for its ability to measure effects due to changes in multiple independent variables; sensitivity analyses which only consider changes in variables in isolation were not able to do this directly because of the complex relationship between a muscle's force and its contribution to the joint acceleration (Ackland et al., 2012).

The Monte Carlo method has been applied to inverse dynamics solutions during gait (Langenderfer et al., 2008; Nguyen et al., 2007; Reinbolt et al., 2007). Reinbolt et al. (2007) used the Monte Carlo method to evaluate how errors in joint parameters (axis position and orientation of body segments), inertial parameters (segment mass, COM, MOI) and kinematic noise effected inverse dynamics analysis during clinical gait trials. A three dimensional full body model was used with synthetic gait data to perform the analysis; however results were only presented for the joint moments of the left leg. Joint centre locations had a maximum error bound of  $\pm 10$ mm and inverse dynamics analyses were repeated using variations with 25%, 50%, 75% and 100% of the allowable bounds. Each joint centre value was selected from a uniform distribution of pseudo-random numbers. Error bounds for each parameter were selected based on the literature. Convergence of moment values was achieved with 5000 repeats. Errors in axis position and orientation of body segments had the largest effect on joint moment errors of the leg and the influence of these parameter variations was increased for the more proximal segments. Simultaneous variations in joint parameters and inertial parameters were similar to those due to joint parameters

alone indicating no significant interactions. Noise parameter variations related to the simulated effect of skin motion artefact; a continuous noise model was applied to the synthetic kinematic data, the amplitude of which represented the magnitude of the skin movement artefact. Variations in amplitude from 0.25 to 1cm had only a small effect on joint torque errors. The Monte Carlo method assumed parameter independence and uniform distributions so a more diverse assortment of full body models was simulated than may have occurred in reality resulting in higher error estimates (Reinbolt et al., 2007). Nguyen et al. (2007) reported that considerable variability in BSP did not translate to large variability in joint moment output during gait trials and these results therefore agreed with Reinbolt et al. (2007). Input BSP distributions were based on cadaver data from 6 studies and 12 studies on live participants; the maximum variability between cadaveric and living BSP derived data was 30%. This study concluded that propagation of BSP errors to joint moment calculations were not sufficient to influence clinical decision making.

Langenderfer et al. (2008) used a more efficient probabilistic method, the Advanced Mean Value method (AMV). The effect of uncertainty in BSP and anatomical landmark identification on joint moments and forces in the lower extremities was quantified during the stance phase of gait. The AMV is a discrete method that predicts performance at specific probability levels and locations in the gait cycle (Langenderfer et al., 2008). BSP distribution means were based on values reported in the literature; average coefficients of variation were 0.12, 0.20 and 0.08 for segment masses, moments of inertia and centre of mass ratios respectively. Distribution means for anatomical landmarks were the three dimensional coordinates of the benchmark data set and standard deviations of 2mm in each direction were assumed as this was the mid-range of reported intra-rater variability. The AMV method required 91 repeats and demonstrated excellent agreement with the MCM which required 1000 repeats. Variability in calculated forces and moments of 56-156% of the nominal values was reported. Anatomical landmark uncertainty had a greater effect on moments than BSP error whilst both segment masses and anatomical landmarks had a greater effect on joint forces. Findings were similar to Reinbolt et al. (2007) who reported joint parameters had the most significant effect over BSP. Obese or muscular participants on which anatomical landmark identification was more difficult may have even higher uncertainty since the 2mm variation used was relatively small. A better understanding

of joint loading variability was achieved which was important in improving clinical diagnoses.

To conclude, the Monte Carlo method has the ability to comprehensively generate the cumulative distribution function and probability density function which characterises the range of possible outcomes and their likelihood. However, a major drawback associated with the implementation of the method is that great computational effort is required for any general case. This may be the reason why studies which have used MCM for error propagation of inverse dynamics analysis have only considered a small number of input parameter inaccuracies in comparison to other studies which have used Taylor Series approximation (Riemer et al., 2008). To improve computational efficiency, some modified MC methods have been proposed; these include the importance sampling method (Kahn, 1956; Rubinstein, 1981), Latin hypercube sampling method (Walker, 1986), the shooting Monte Carlo approach (Brown and Sepulveda, 1997) and the directional simulation (Ditlevsen et al., 1987). However, even using these modifications, the Monte Carlo method is largely not affordable in the design of complex systems (Du and Chen, 2001).

## 2.8. Summaries

Validation is the process of evaluating the degree to which a model accurately represents the real world whilst fulfilling its intended purpose (Schwer, 2006).

Validation of inverse dynamics solutions is challenging since in most cases comparison to a 'gold standard' is not possible. The over determined nature of inverse dynamics solutions have been exploited for this purpose. Three different methods of validation of inverse dynamics models have been identified from the literature;

1. Top down bottom up comparison of joint forces and moments
2. Measured compared to predicted ground reaction forces
3. Comparison of forces and moments measured using external measurement devices

In general, studies report good agreement between measured and predicted parameters using these validation procedures and recommend the use of inverse dynamics analysis. The majority of studies discussed were concerned with lifting tasks due to the high incidence of lower back injury during manual lifting tasks in the

---

workplace (Larvière and Gagnon, 1998). Other studies were concerned with validation of slow tasks such as gait. Only one study attempted to validate inverse dynamics applied to high acceleration activities (Iino and Kojima, 2012) however movements were artificial and complexity of movement was restricted. Results were specific to the type of movement analysed, the speed at which the movement was performed, the measurement system and segmental models used (Plamondon et al., 1996). A major drawback associated with these validation methods is that nothing can be learnt about the individual sources of error and how they contribute to the total residual error. Furthermore, a primary assumption of these validation methods is that error is cumulative when it is possible that errors of different origins can compensate for each other (De Looze et al., 1992).

Sensitivity analyses are often performed in conjunction with validation experiments to determine how error in model inputs impact the simulation result, scaling the relative importance of the inputs (Henninger et al., 2010; Roache, 1998). A single model input or parameter is varied by an order of magnitude, while holding the others constant. In this way, the effects of individual parameter variations can be isolated. Sensitivity analyses applied to inverse dynamics solutions have most frequently investigated the effect of perturbations in body segment parameters, joint centre locations and external force measurement. Studies related to gait and lifting were the most common with only two studies relating to other movements found. The types of tasks considered in the literature were low velocity and relatively simple. No study considered more complex high acceleration movements such as the golf swing which has been the subject of inverse dynamics analysis in the past. It was shown that results were task specific with only subtle differences in movements changing the outcome (Kingma, Toussaint, et al., 1996). Furthermore it was hypothesised that the effects of errors in input parameters would be most apparent during open chain, high acceleration activities (Pearsall and Costigan, 1999) however there were no studies which had directly investigated this.

Closely related to sensitivity analyses, uncertainty analyses can be characterised by a greater focus on the quantification of inaccuracies in input parameters and propagation of uncertainty. Two common uncertainty propagation analysis methods are the Taylor Series Method (TSM) (Taylor, 1997) and the Monte Carlo Method

(MCM). The Taylor Series method assumes that inaccuracies in variables are random and uncorrelated (Challis and Kerwin, 1996). This assumption means the results were representative of the upper bound uncertainty (Riemer et al., 2008). The Monte Carlo method is a probabilistic analysis technique which includes the distributional characteristics of input variables (Laz and Browne, 2010). MCM has been described as the 'gold standard' of probabilistic methods (Laz and Browne, 2010). In the wider field of human biomechanics uncertainty analyses have been used to evaluate the limitations of current measurement techniques, evaluate the potential improvements to measurement systems (Cooper et al., 1997; Wood et al., 1999), assess the statistical power necessary to detect inter-subject or group variability (Cooper et al., 1997; Riemer et al., 2008) and define confidence bounds important for clinical interpretation (Oberhofer et al., 2009; Riemer et al., 2008). Only gait and lifting inverse dynamics solutions have been analysed in this way and results have been concerning; in gait uncertainty bounds were reported to reach 236% of the estimated joint moment magnitude (Riemer et al., 2008), for example.

## **2.9. Conclusion**

For any model approximating a physical system, an assessment of the uncertainty of the model results is necessary to ensure they are interpreted appropriately and that conclusions are reasonable. This work is motivated by the lack of knowledge of the uncertainty in the estimation of joint moments and forces derived through inverse dynamics analysis for open chain, high acceleration movements. In the absence of a 'gold standard' measurement, validation has been achieved by exploiting the over determined nature of inverse dynamics solutions, however limitations inherent to these methods mean that nothing can be learnt about the individual sources of error and how they contribute to the total residual error. Uncertainty analyses have been recognised as an integral part of the validation process, particularly for models which are difficult to validate or cannot be validated (Anderson et al., 2007). Previous studies have indicated that the effects of errors in input parameters would be most apparent during open chain, high acceleration activities (Pearsall and Costigan, 1999), however no studies have directly investigated or quantified this. Credibility of inverse dynamics applied to high acceleration, open chain movements must be established in order that decisions can be made and information can be extracted based on model predictions.

---

The importance of recognising and accounting for error is crucial for results interpretation, applicability of the model and peer acceptance (Viceconti et al., 2005).

### **2.10. Aims and Objectives**

The aim of this thesis was to investigate the validity and uncertainty of inverse dynamics solutions applied to high acceleration movements.

There were three main objectives;

1. To validate the joint forces and moments derived using inverse dynamics analysis during the golf swing.
2. To quantify the inaccuracy in input parameters for inverse dynamics solutions. It was critical that the quantification of these inaccuracies was comprehensive and carefully considered so that the results of the uncertainty analysis were realistic.
3. To estimate the uncertainty in joint moments calculated using inverse dynamics analysis. This approach was applied to three dimensional joint moments during the golf swing.

### **2.11. Contribution to knowledge**

The uncertainty in inverse dynamics solutions is of considerable interest and importance to the biomechanics community in both in a sporting and a clinical context. However, it should be noted that elements of the inverse dynamics model and collection system are subject to commercial protections, including current protection from granted patents and future potential protection from pending patents. Although the outcome of this thesis was resolved in relation to the specific case of the golf swing, such information could provide a basis for interpretation and analysis of a range of high acceleration activities. This work also demonstrates a methodology of performing such an analysis. The impact of this work is crucial in the interpretation of joint moments and may have implications to the results of previous studies which have used inverse dynamics to inform performance improvement or injury prevention during high acceleration movements.

### 3. Data Collection Methods and Procedures

#### 3.1. Golphysics Ltd laboratory set-up and data analysis methods

This section details the data collection methods and data analysis procedures developed by Golphysics Ltd for use in a golf analysis laboratory. These methods and procedures are used throughout this thesis.

##### 3.1.1. Experimental set-up

Swing trials were performed in a biomechanics laboratory at Sheffield Hallam University. Figure 1 shows a schematic of the laboratory set up.

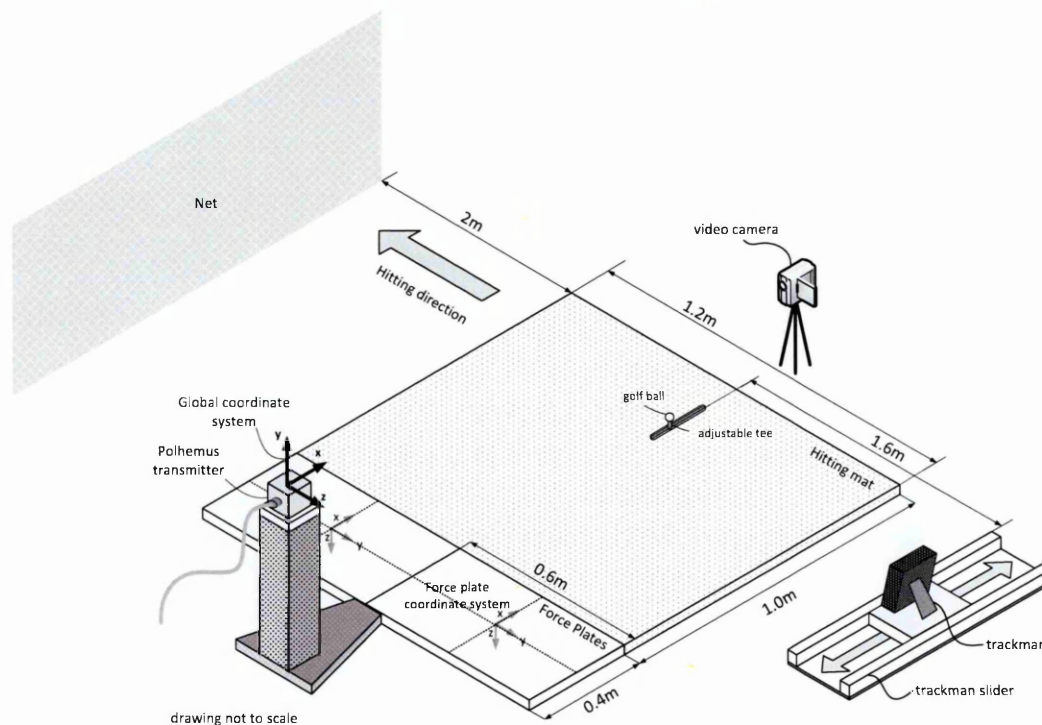


Figure 1 Golf swing laboratory set up

During testing, participants stood with each foot on an individual force plate (KISTLER type 9128C, Kistler Instrumente AG, Winterthur, Switzerland) mounted flush the laboratory floor according to the manufacturer's specifications. Two 50 mm thick plastic blocks with the same foot print as the force plates (40 x 60 cm) were bolted firmly onto the surface of the force plates to provide a suitable height and surface to stand on during swing trials. Each force plate had four transducers, which measured the three orthogonal components of the resultant force and the three components of the generated moment acting on the platform. The force plates collected data at a rate of 960 Hz. The point of application of the force and the couple acting on the

platform were calculated from the measured force and moment components (see APPENDIX B: Force platform calculations for details). The Polhemus Liberty system (Polhemus Inc., Colchester, VT, USA) was used to track the kinematics of the body segments and club using 13 sensors at a rate of 240 Hz. The tracking system consisted of a magnetic field transmitter and sensor couple. The position and orientation of each sensor was determined through a comparison of the strength of received signal to the strength of the emitted pulse. The transmitter was housed in a custom made plastic stand that was rigid and remained in position for the entire data collection. The stand was located directly behind the force plates as shown in figure 1. This ensured that the participant and therefore the sensors attached to the participant were positioned within the optimal volume limits of the system as specified by the manufacturer (Polhemus Inc., Colchester, VT, USA). The club was instrumented with an accelerometer attached to the club head for impact detection. The accelerometer and force plates collected data at 960 Hz which was down sampled to 240 Hz by taking the mean of 4 data points. The pulse signal from the Polhemus was connected to the analogue input and used as a trigger to synchronize the two data streams. Balls were hit into a large net positioned  $\approx 2.5$  m from the tee position. Ball flight characteristics were measured using a Trackman radar unit (Trackman A/S, Vedbæk, Denmark) positioned 1.6 m behind the tee position as specified by the manufacturer. Trackman provided club head speed at impact, ball speed, and ball flight characteristics such as total distance which were used to rate the quality of the shot. A video camera was used to film all swing trials in order to provide an additional quality check and reference footage.

### **3.1.2. Global Coordinate System definition**

The laboratory global reference system was a conventional three orthogonal axes system. The origin was located at the electrical centre of the Polhemus transmitter box as shown in figure 1. The Z axis pointed in the direction of the net, and therefore in the hitting direction. The Y axis was the vertical axis. The cross product of the Z axis direction and the Y axis direction, defined the direction of the X axis. For a player standing in the anatomical position so that the anterior-posterior axis was the Z axis, the X axis was parallel to a horizontal axis in the frontal plane. Therefore, the Z-Y plane represented the plane of ball progression (sagittal plane), the X-Y plane the frontal plane and the Z-X plane the transverse plane. The force platform coordinate system

was orientated differently to the global coordinate system so ground reaction forces and centre of pressure locations were transformed to the global reference system for inverse dynamics calculations.

### 3.1.3. Pre Testing Procedures

#### 3.1.3.1. *Polhemus and force plate coordinate system alignment*

The laboratory coordinate system (Polhemus) was calibrated to the kinetic coordinate system (KISTLER) as follows; a template with the position of three non-collinear points marked onto it was placed in a known position on the surface of the back force plate. A single Polhemus sensor was fixed to one end of a machined rigid plastic pole. The distance from the electrical centre of the sensor to the pointed tip of the opposite end of the pole was measured using a milling machine to  $\pm 0.1\text{mm}$ . The tip of the pole was pressed onto each marked point whilst the pole was held vertically. The position of the sensor and therefore the tip via a translation in Polhemus space was recorded simultaneously. Knowing the position of the points in both coordinate systems allowed for a transformation matrix to be calculated for conversion of force plate measurements to the global coordinate system.

#### 3.1.3.2. *Mapping*

Mapping was used to correct for distortions in the magnetic field caused by metal within the test volume. Correction of the measurement errors can be achieved through experimentally established dependencies between the true receiver position/orientation and that reported by the tracking system (Kindratenko and Bennett, 2000). These mapping techniques are based on the assumption that the transmitter's position is fixed and the surrounding metal does not move. To correct for distortions an algorithm was used based on global scattered data interpolation (Zachmann, 1997). A radial basis function was used for the interpolation and approximation of scattered data. To create the map, a bespoke plastic pole was built which had 10 Polhemus sensors placed along it. The Polhemus sensor furthest from the floor and therefore assumed to be unaffected by distortion from force plates, was used as a reference to predict the locations of all 9 other sensors. The pole was moved around the test volume through 117 positions. The true location of sensors 1-9 were tracked using a 12 camera motion analysis system (Motion Analysis Corporation, Santa

Rosa, CA, USA) operating at 200 Hz. Residual errors were calculated and used to train the radial basis function in Matlab (Chirokov, 2006).

#### 3.1.4. Experimental Protocol

Before data collection, each participant was provided with a Participant Information Sheet (see appendix, pg. 47) and required fill in a pre-screening questionnaire and to sign an informed consent form. Participants were given a verbal explanation of the data collection protocol and given the chance to ask questions. After height and weight were measured, each participant was given the opportunity to perform their standard warm up routine. Prior to sensor attachment any metallic objects which could cause distortion to the magnetic field such as watches or belts were removed. 13 Polhemus sensors were used to track the movement of the body and club during swing trials. Sensor attachment methods were designed to minimise skin motion artefact and limit the potential for sensors slipping during swing trials (figure 2). To ensure that the jacket fitted correctly, participants were asked to wear only a t-shirt on the upper body. The jacket held two upper arm sensors and thorax and lumbar sensors. Further sensors were placed on the thighs, shanks and pelvis which were attached over lightweight loose fitting trousers. All sensors were secured firmly in place using elasticated non slip straps. Additional sensors were secured to the head via a plastic clip attached to the cap provided and the hands via golf gloves that were also provided. The participant was then given an opportunity to perform practice swings with the sensors on and was able to adjust sensor and cable positions so that they were comfortable. Participants wore their preferred shoes provided any spikes were soft. A sensor was attached to the club using a bespoke plastic bracket and any loose cables were tucked away. The clothing also facilitated accurate identification of anatomical landmarks during participant calibration.



Figure 2 Sensor attachment locations

#### 3.1.4.1. Model Calibration

With the sensors secured in place, the locations of 79 anatomical landmarks on the body were recorded using a digital stylus, the output of which was recorded directly by the Polhemus system in relation to the local coordinate system of the relevant sensor. The geometric model of the body was built up in this way in order that body segment parameters and joint centre locations could be estimated. Calibration took approximately 6 minutes. For calibration of the lower half of the body, participants were asked to stand on a wooden step to lift sensors away from possible distortion of the electromagnetic field caused by metal that might be in the floor. During calibration participants were stood in the anatomical position with feet shoulder width apart, arms straight and hands in fists with backs of each thumb facing forward.

Calibration was carried out by one of two trained examiners who had received specialist training in palpation of the required anatomical landmarks. After calibration, participants were instructed not to adjust or move any sensors as this would affect the accuracy of subsequent measurements and analysis.

#### 3.1.4.2. *Collection of swing trials*

Participants were required to hit 10 shots with a driver and 5 shots each with a 5 and 9 iron (PING G15 Driver, I15 5iron, I15 9iron respectively). All clubs had a regular graphite shaft and were of regular length and standard lie angle. Graphite shafts were used rather than steel shafts to minimise the distortion to electromagnetic field. To control the effect of fatigue the order in which clubs were presented were randomly assigned. Sufficient practice trials were allowed to ensure participants were familiar with each club. For iron shots the ball was hit directly off the hitting mat. For driver shots the ball was placed on an adjustable height rubber tee, the position of which was adjusted to suit the individual player. After each shot the force plates were reset to minimise the effects of piezoelectric drift. Testing continued until participants were satisfied that 20 good swings were recorded. Trackman was used as an independent measure of swing quality by comparing club head speed and carry distance to expected ranges.

The kinematic and force data were fed into custom written software for analysis. The software accepted displacement and orientation data from the Polhemus system and analogue input from the force plates and accelerometer. Polhemus provided the raw displacement coordinates of each sensor ( $X, Y, Z$ ) and orientation data in unit quaternions ( $w, x, y, z$ ) in the global coordinate system. For a unit quaternion ( $x, y, w, z$ ) the corresponding rotation matrix  $M$  was defined as;

$$M = \begin{pmatrix} 1 - 2y^2 - 2z^2 & 2xy + 2wz & 2xz - 2wy \\ 2xy - 2wx & 1 - 2x^2 - 2z^2 & 2yz + 2wx \\ 2xz + 2wy & 2yz - 2wx & 1 - 2x^2 - 2y^2 \end{pmatrix}$$

Equation 3.1

#### 3.1.4.3. *Swing Event Definition*

The backswing began at take-away (TA) and ended at top of backswing (TOB) whilst the downswing began at TOB and ended at impact. Swing events TA and TOB were defined using kinematic algorithms based on the resultant club head velocity. Working

backwards in time from impact, TOB was defined as the frame at which the resultant velocity of the club head fell below a pre-defined velocity threshold of 50 cm/s. TA was similarly defined as the frame before TOB at which this threshold was crossed. The threshold was chosen through trial and error and visual inspection of swings.

### 3.1.5. Golphysics geometric model for the calculation of Body Segment Parameters

The Golphysics geometric model consisted of 16 segments that were assumed to be rigid bodies. Each segment was composed of a number of sub segments or geometric solids so that in total the model was composed of 28 solids. The model was made up of three distinct classes of solids: truncated cones, stadium solids and semi-ellipsoids. The stadium solid was introduced by Yeadon (Yeadon, 1990) as a more accurate way of representing the torso segments than the use of a series of stacked elliptical disks. Standard formulae from Yeadon (1990) and presented by Kwon (1998) were used to calculate the mass, centre of mass location and principle moments of inertia for the three solids and these are presented in the appendix (APPENDIX A: Body segment parameters equations).

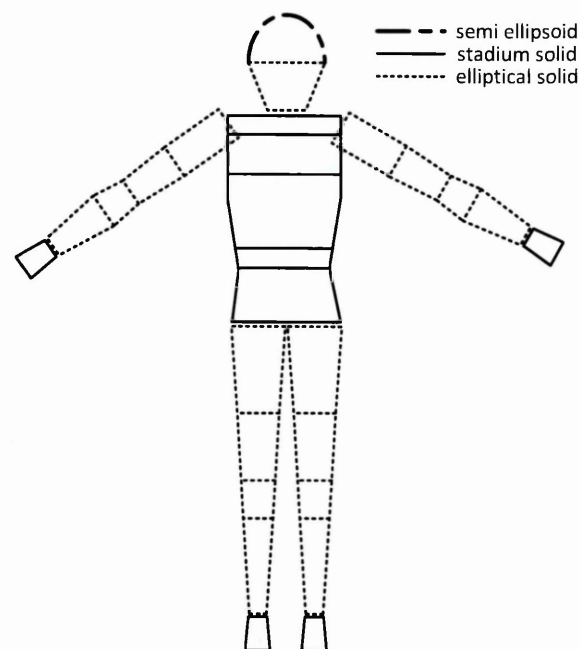


Figure 3 Geometric Model, ellipsoids outlined in red, stadium solids outlined in blue

Body segments were sectioned into solids by planes perpendicular to the longitudinal axis of the segments (figure 3). The trunk was sectioned into 6 stadium solids. The left and right arms were each made up of 5 solids as were the left and right legs. The head

was modelled using a semi-ellipsoid of circular cross section. It was assumed that the solids comprising a segment had coincident longitudinal axes. The model had symmetrical inertia values so that body segment parameters calculated for the right limbs were also used for the left limbs. This reduced the number of anatomical landmarks which had to be identified and therefore reduced the time required for calibration (Yeadon, 1990).

### 3.1.5.1. Measurements

Using the Polhemus Liberty system (Polhemus Inc., Colchester, VT, USA) the positions of the anatomical landmarks listed in table 2 were digitised using a digital stylus so that their positions were saved with respect to the relevant segment's sensor. At each boundary level the width and depth of the segment was calculated using four digitised points. The boundary levels used are shown in figure 4. The length of each solid was calculated by creating a virtual marker between the two width markers at both the proximal and distal ends of the segment. The length of the segment was defined as the total distance between the two virtual markers (figure 5).

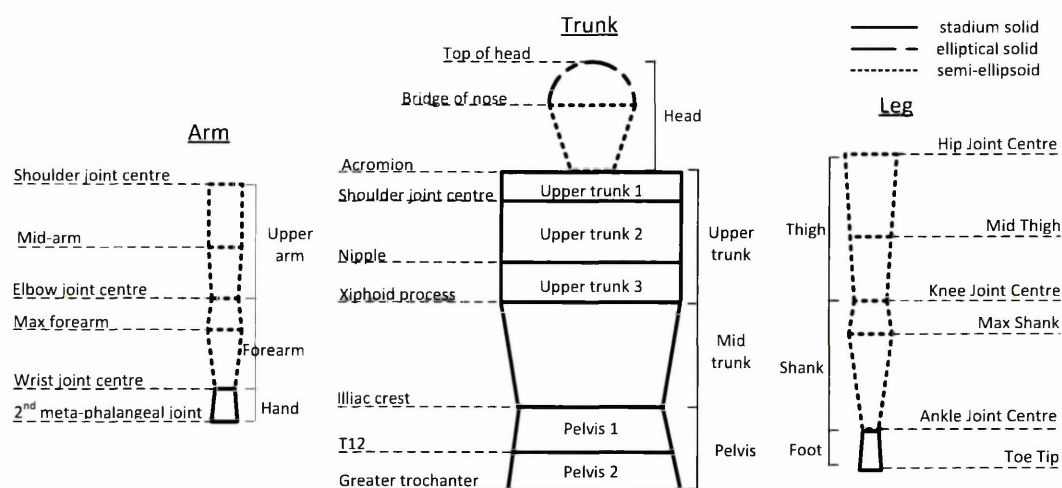


Figure 4 Geometric model segmentation planes for the arms, trunk and legs

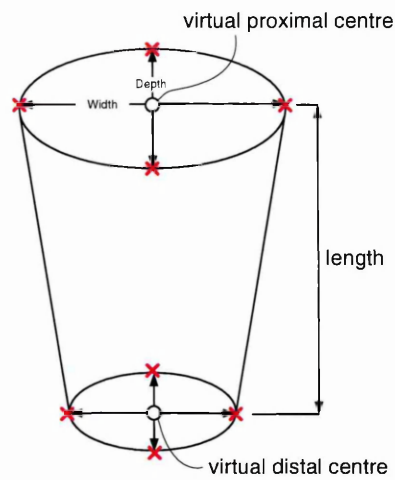


Figure 5 Segment length definition; the width and depth of the segment at each boundary level were defined using four digitised points shown as red crosses. Segment length was defined as the distance between the two virtual centre markers.

To calculate BSP for a stadium solid body the dimensions  $a$  and  $r$  (figure 6) were required at each boundary level. These were calculated from the width and depth according to Yeadon (1990); the stadium was defined as a rectangle of width  $2a$  and depth  $2r$  with an adjoining semi-circle of radius  $r$  at each end of its width;

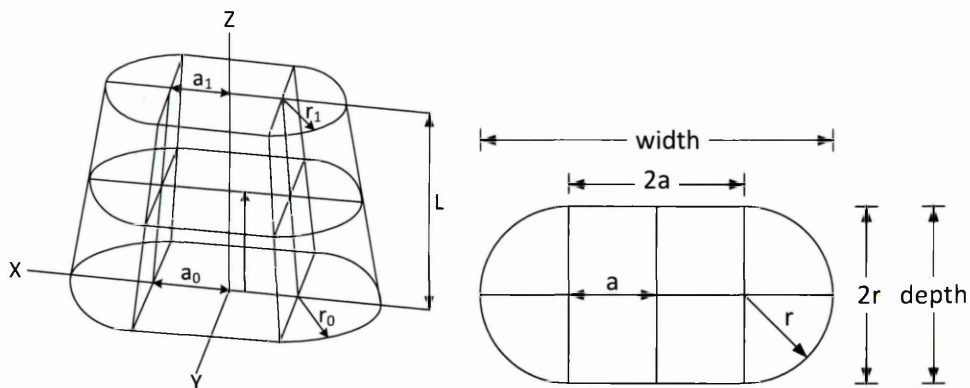


Figure 6 Left: stadium solid dimensions, Right: Stadium solid cross section

Given the dimensions of the stadium rectangle above  $r$  and  $a$  were calculated as follows;

$$\text{depth} = 2r$$

Equation 3.2

$$\text{width} = 2a + 2r$$

Equation 3.3

Rearranging equation 3.2 and equation 3.3;

$$r = \frac{\text{depth}}{2}$$

Equation 3.4

$$a = \frac{(\text{width} - 2r)}{2}$$

Equation 3.5

For elliptical solids and semi-ellipsoids the width and depth were used directly to calculate parameters  $a$  and  $b$  (figure 7);

$$a = \frac{\text{depth}}{2}$$

Equation 3.6

$$b = \frac{\text{width}}{2}$$

Equation 3.7

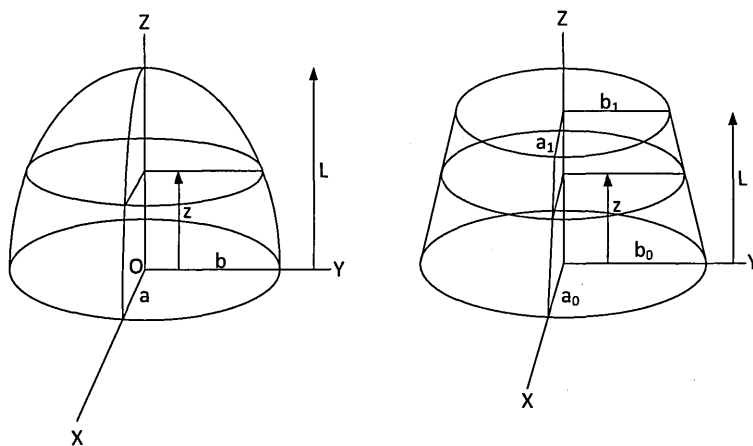


Figure 7 Semi ellipsoid and elliptical solid parameters

The assumption of symmetry for inertial parameters meant that a reduced number of points were digitised for the left leg and arm; only the lateral and medial points at each segment boundary level were required to locate joint centres with respect to the relevant sensor. A total of 79 anatomical landmarks were digitised (table 2) which took approximately 6 minutes per participant. Uniform segment densities were assigned according to Dempster (1955) (table 1).

Table 1 Segment densities applied to segments for calculation of body segment parameters (Dempster, 1955)

Segment	Density ( $kg/m^3$ )	Solid
Hand	1160	SS
Forearm	1130	ES
Upper arm	1070	ES
Head	1110	SE
Neck	1110	ES
Upper trunk 1	1040	SS
Upper trunk 2	920	SS
Upper trunk 3	920	SS
Mid trunk	1010	SS
Pelvis 1	1010	SS
Pelvis 2	1010	SS
Thigh	1050	ES
Shank	1090	ES
Foot	1100	ES

SS: Stadium solid; ES: Elliptical solid, SE: Semi-Ellipsoid

Table 2 Anatomical placement of markers which made up the geometric model

Segment	Segmentation plane	Width Markers		Depth Markers	
Head*	Proximal	Top head	-	-	-
	Distal	R Temporal mandibular	L Temporal Mandibular	Bridge of nose	Occipital tuberosity
Neck**	Proximal	R Temporal mandibular	L Temporal Mandibular	Bridge of nose	Occipital tuberosity
	Distal	-	-	Sternal Notch	T3
Upper Trunk 1	Proximal	R Acromion	L Acromion	Sternal Notch	T3
	Distal	R Shoulder Joint Centre***	L Shoulder Joint Centre	Mid Sternum	T4
Upper trunk 2	Proximal	R Shoulder Joint Centre	L Shoulder Joint Centre	Mid Sternum	T4
	Distal	Right Nipple	Left Nipple	Nipple	T6
Upper trunk 3	Proximal	Right Nipple	Left Nipple	Nipple	T6
	Distal	Right Bot Rib	Left Bot Rib	Xiphoid Process	T8
Mid trunk	Proximal	Right Bot Rib	Left Bot Rib	Xiphoid Process	T8
	Distal	Right Iliac crest	Left Iliac crest	Umbilicus	L4
Pelvis 1	Proximal	Right Iliac crest	Left Iliac crest	Umbilicus	L4
	Distal	Lat RASIS	Lat LASIS	Lower Umbilicus	Mid PSIS
Pelvis 2	Proximal	Lat RASIS	Lat LASIS	Lower Umbilicus	Mid PSIS
	Distal	Right GT	Left GT	Mid Groin Ant	Mid Groin Post
Upper Thigh	Proximal	Right GT	Left GT	Mid Groin Ant	Mid Groin Post
	Distal	Maximal thigh lateral	Maximal thigh medial	Maximal thigh anterior	Maximal thigh posterior
Lower Thigh	Proximal	Maximal thigh lateral	Maximal thigh medial	Maximal thigh anterior	Maximal thigh posterior
	Distal	Lateral femoral epicondyle	Medial femoral	Mid patella	Mid popliteal

Upper Shank	Proximal	Lateral femoral epicondyle	epicondyle Medial femoral epicondyle	Mid patella	crease Mid popliteal crease
	Distal	lat max shank	med max shank	ant max shank	post max shank
Lower Shank	Proximal	lat max shank	med max shank	ant max shank	post max shank
	Distal	lateral malleolus	med malleolus	anterior talus	post inferior fibula
Foot****	Proximal	lateral malleolus	med malleolus	anterior talus	post inferior fibula
	Distal	lateral toe	medial toe	-	-
Upper Upper Arm	Proximal	post shoulder	anterior shoulder	auxilla	acromion process
	Distal	Mid tricep	Mid tri-bi	mid bicep	deltoid insertion
Lower upper arm	Proximal	Mid tricep	Mid tri-bi	mid bicep	deltoid insertion
	Distal	lateral humeral epicondyle	medial humeral epicondyle	bicep insertion	olecranon
Upper forearm	Proximal	lateral humeral epicondyle	medial humeral epicondyle	bicep insertion	olecranon
	Distal	lateral max forearm	medial max forearm	anterior max forearm	posterior max forearm
Lower forearm	Proximal	lateral max forearm	medial max forearm	anterior max forearm	posterior max forearm
	Distal	radial styloid	ulnar styloid	mid flexor tendon	2 <sup>nd</sup> met-phalangeal joint
Hand	Proximal	radial styloid	ulnar styloid	mid flexor tendon	mid flexor tendon
	Distal	2 <sup>nd</sup> met-phalangeal joint	5 <sup>th</sup> phalangeal joint	posterior 3 <sup>rd</sup> phalanx	anterior 3 <sup>rd</sup> phalanx

\*The head was modelled as a semi-ellipsoid with circular cross section and so was completely defined with two width markers at the distal end and a single 'top head' marker to define its length.

\*\*The neck was modelled as an elliptical solid with circular cross section at its distal end so only required two markers at this boundary level.

\*\*\*Shoulder joint centre was defined by four markers at the shoulder; anterior, posterior, auxilla and acromion process.

\*\*\*\*The foot was modelled as an elliptical solid with the distal end of circular cross section.

### 3.1.6. Joint Centre Locations

For each joint of the Golphysics model a geometric centre was assumed. During calibration the location of the proximal joint centre for a particular segment was saved in the segment's sensor coordinate system. For the majority of joints, joint centre locations were estimated by calculating the position of a virtual landmark at the mid-point of two palpated points on the surface of the skin. This method made two primary assumptions; 1) the palpated points lay on the joint axis and 2) joint anatomy

was symmetrical. Table 3 lists the methods used to define the 17 joint centre locations. The hip and the shoulder joint centres were defined using regression equations, these methods are explained in more detail below (section 3.1.6.1 & 3.1.6.2).

Table 3 Joint centre definitions used buy geometric model

Joint	Joint Centre Definition
Ankle	midpoint of the lateral and medial malleoli
Knee	midpoint of the lateral and medial epicondyle
Hip	Method of Bell et al. (1989) - predictive approach
Pelvis	midpoint of the iliac crests
Mid trunk	midpoint of the right and left ribs at the height of the xiphoid process
Upper trunk	midpoint of the right and left acromion process
Shoulder	Method of Schmidt et al. (1999) - offset approach
Elbow	midpoint of medial and lateral epicondyles
Wrist	midpoint of the radial and ulnar styloids
Neck	midpoint of sternal notch and T2

The shank segment is used as a representative example of how joint centres were calculated using standard biomechanics approaches (figure 8). The following example was adapted from Robertson et al. (2004). The positions of the lateral and medial femoral epicondyles  $\vec{L}_1$  and  $\vec{M}_1$  were digitised using the stylus relative to the shank sensor coordinate system. Similarly, the position of the distal markers on the lateral and medial malleoli  $\vec{L}_2$  and  $\vec{M}_2$  were digitised. The virtual joint centre at the knee  $\vec{V}_1$  was defined as a point that was 50% of the distance from  $\vec{L}_1$  to  $\vec{M}_1$ . The ankle joint centre  $\vec{V}_2$  was similarly defined;

$$\vec{V}_1 = \vec{L}_1 + 0.5(\vec{M}_1 - \vec{L}_1)$$

Equation 3.8

$$\vec{V}_2 = \vec{L}_2 + 0.5(\vec{M}_2 - \vec{L}_2)$$

Equation 3.9

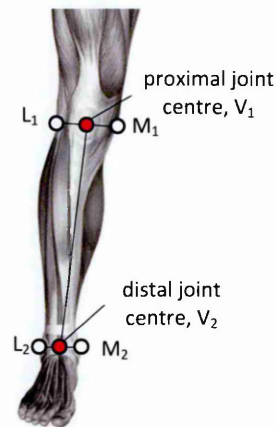


Figure 8 Joint centre markers and virtual centres for the shank; L1 and M1 are the lateral and medial femoral epicondyles respectively used to define the proximal joint centre V1. L2 and M2 are the lateral and medial malleoli respectively used to define the distal joint centre V2

### 3.1.6.1. Hip joint centre

The hip joint centres were defined using the Bell et al. (1989) method (figure 9). Hip joint centre ( $HJC$ ) was a function of pelvis width ( $PW$ ) as follows;

$$HJC_x = -0.19PW \quad HJC_y = -0.30PW \quad HJC_z = 0.36PW$$

Equation 3.10

where subscripts  $x, y, z$  were the coordinates of the right hip joint centre in the pelvis anatomical coordinate system and  $PW$  was the distance between the right and left anterior superior iliac spines (figure 9).

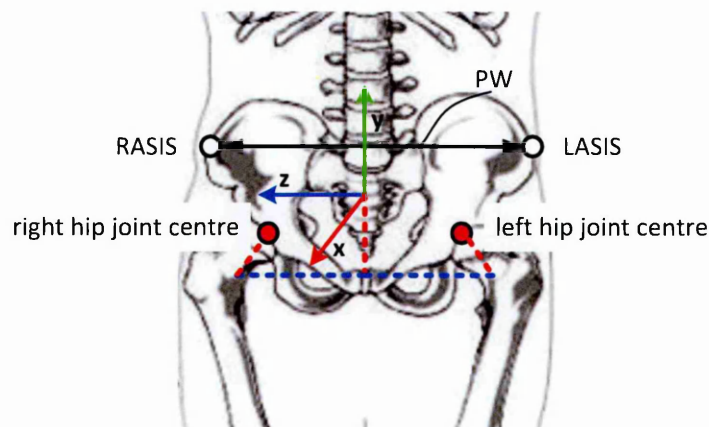


Figure 9 Hip joint centre definition (Bell et al., 1989);  $PW$  = pelvis width = the distance between the right and left anterior superior illiac spine (ASIS).

### 3.1.6.2. Shoulder joint centre

The shoulder joint centre was defined according to Schmidt et al. (1999) and was located at a position 7 cm vertically below the acromion process (figure 10).

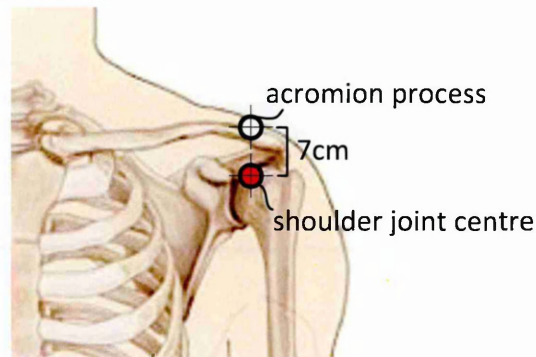


Figure 10 Shoulder joint centre definition (Schmidt et al., 1999) (shoulder illustration from <http://www.shoulderdoc.co.uk/article.asp?section=3&article=1>)

### 3.1.7. Joint coordinate system definition

Primary segments were those which had a sensor attached and therefore had a direct measure of position and orientation. Primary segments were the shanks, thighs, pelvis, mid trunk, thorax, head, upper arms and hands. Secondary segments did not have a sensor attached to them. The position and orientation of secondary segments was estimated by reconstruction of anatomical landmarks from coordinates of the points in the local coordinate system of adjacent primary segments. Therefore, a secondary segment had to be adjacent to a primary segment at both the proximal and distal end. The secondary segments were the feet, neck and forearms. The inclusion of secondary segments meant that fewer sensors were required; this was advantageous in reducing the impediment to participants and also reduced the computational load on the data collection PC.

Standard biomechanical approaches of Zatsiorsky (1998) were used to define local segment coordinate systems. The following example was adapted from that provided by Zatsiorsky (1998). To create a local coordinate system within a rigid segment, the coordinates of three non-collinear points ( $p_1, p_2, p_3$ ) must be known. The points are used to create vectors  $r_1$  and  $r_2$  (figure 11). The cross product of vectors  $r_1$  and  $r_2$  defines vector  $r_3$  and the cross product of vectors  $r_3$  and  $r_1$  defines the vector  $r_4$ . Dividing each vector by its own length creates unit vectors. The three unit vectors

$r_1, r_3, r_4$  are mutually orthogonal axes. The local coordinate system of the right shank was defined using this method as shown (figure 11);

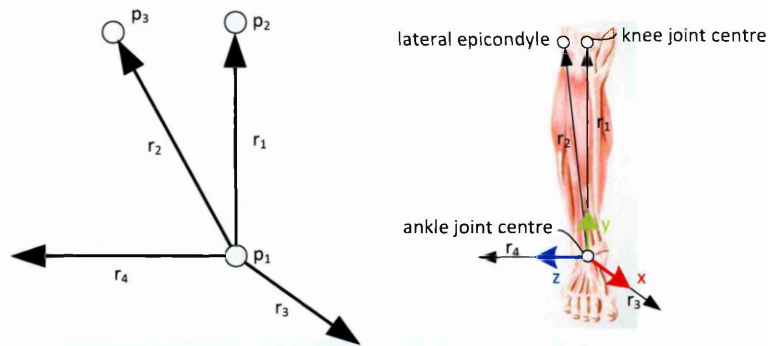


Figure 11 Local coordinate system definition within a rigid body.  $p_1, p_2$  and  $p_3$  are three non-collinear points with known coordinates. Vectors  $r_1, r_3, r_4$  are mutually orthogonal which when divided by their own length become mutually orthogonal unit vectors or the local coordinate axes  $x, y, z$ .

For all segment local coordinate systems the origin was coincident with the proximal or distal end. Local segment coordinate systems were defined such that the  $x, y$  and  $z$  axes were predominantly anterior-posterior, longitudinal and medio-lateral respectively. Segment coordinate systems were defined as follows; firstly, the  $y$  axis was defined to be coincident with the long axis of the segment. This was a unit vector coincident with a line connecting the proximal and distal joint centres of the segment. An intermediate unit vector  $q$  was then constructed that was coincident with the line connecting the joint centre at the origin end of the segment and a planar anatomical landmark at the proximal end of the segment. The  $x$  axis was defined as the cross product of  $q$  and  $y$  and the  $z$  axis was defined as the cross product of  $x$  and  $y$  unit vectors. The full body linked segment model is shown in figure 12.

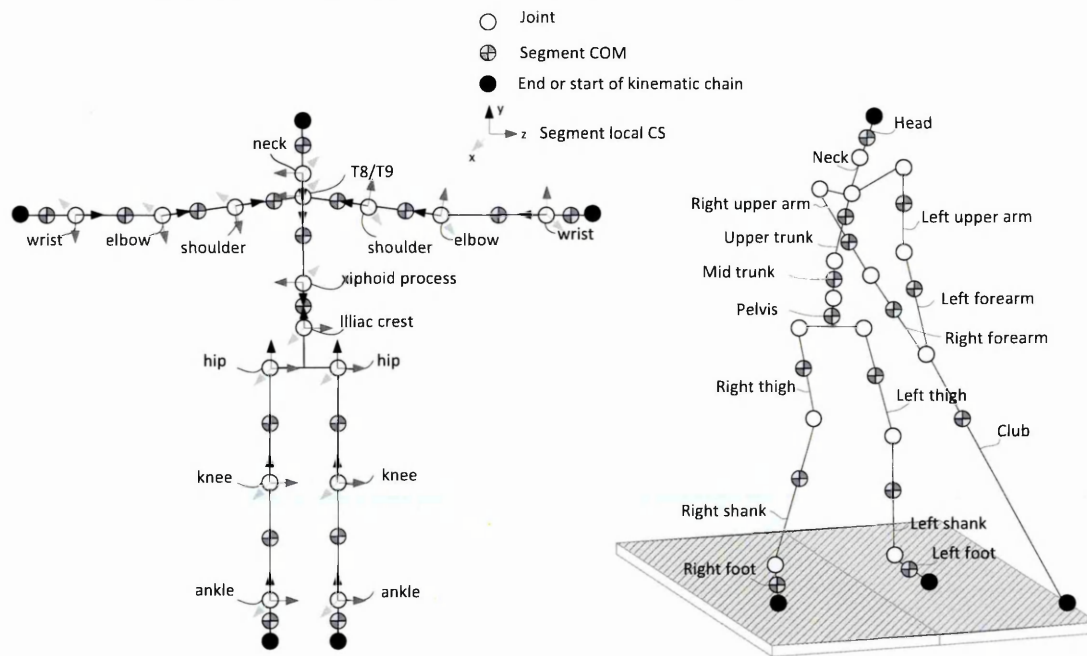


Figure 12 Golphysics linked segment model of the body, locations of joints and segment centre of mass (COM) are shown. Left: Full body linked segment model in the anatomical position adopted during participant calibration. The local coordinate system directions for each segment located at the origin of each segment are shown as well as the joint positions. Right: full body linked segment model in a golf stance.

### 3.1.7.1. The club segment

The club segment geometry and inertial parameters were based on measurements made by a non-contact laser scanner (Model Maker D100 non-contact laser scanner, Metris, Leuven, Belgium). The scanned club head was imported into Pro-Engineer (Parametric Technology Co., Waltham, MA, USA) and, given the known density of the steel club head and the scanned volume, the wall thickness of the club head was calculated assuming a constant thickness. This provided club specific mass, centre of mass and inertia parameters. The club segment was assumed to be a rigid body and position and orientation during swing trials were directly obtained from a sensor securely fixed to the shaft just below the grip (figure 2). See APPENDIX O: Table of Assumptions, pg. 59 for a summary of the assumptions made in modelling the club segment.

### 3.1.8. Data analysis

This section explains the process used to calculate the net joint reaction forces and net joint moments during the golf swing using inverse dynamics analysis. Firstly details of the calculation of derivatives are provided. This is followed by an introduction to the calculation of transformation matrices essential to the inverse dynamics process and a

description of notation conventions which will be used. The equations used to calculate the joint forces and moments via an inverse dynamics analysis are presented.

### 3.1.9. Calculation of derivatives

For inverse dynamics calculations the origin of the segment local coordinate system was translated to the segment centre of mass. For the calculation of derivatives, linear displacement was differentiated using a central difference method as follows;

$$f'x_{(i)} \approx \frac{y_{i+1} - y_{i-1}}{x_{i+1} - x_{i-1}}$$

Equation 3.11

where  $x$  is time and  $y$  is the linear displacement of the segment centre of mass and subscripts refer to the  $i$ th data point as shown in figure 13.

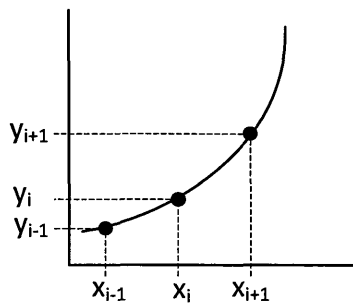


Figure 13 Graph to describe the three point forward difference method

Sensor orientation from the Polhemus Liberty System was represented as unit quaternions. A unit quaternion  $q$  is a four dimensional complex number, which consists of one real part and three imaginary parts;

$$q = w + x\hat{i} + y\hat{j} + z\hat{k}$$

Equation 3.12

which satisfies the multiplication rules (Hamilton, 1969);

$$\hat{i}^2 = \hat{j}^2 = \hat{k}^2 = -1,$$

$$\hat{i}\hat{j} = \hat{k}, \hat{j}\hat{i} = -\hat{k}$$

$$\hat{j}\hat{k} = \hat{i}, \hat{k}\hat{j} = -\hat{i}$$

$$\hat{k}\hat{i} = \hat{j}, \hat{i}\hat{k} = -\hat{j}$$

Equation 3.13

Due to the non-linearity of the unit quaternion space, quaternions could be not be differentiated using the central difference method (Hsieh et al., 1998).

Given a set of unit quaternions  $q_N = \{q_1, \dots, q_M\}$ , the discrete angular velocity  $v_i$  is given by:

$$v_i = \frac{\log(q_i^{-1}q_{i+1})}{h}$$

Equation 3.14

where  $h$  is the interval between two successive unit quaternions. Equation 3.14 provided angular velocity in three dimensional Euclidean space. Angular acceleration was calculated from angular velocity using the central difference method (equation 3.11).

### 3.1.10. Calculation of the transformation matrix

Transformation matrices were used to transform global coordinates into the local segment coordinate systems and *vice versa*. A transformation matrix is a  $4 \times 4$  matrix that allows for the position and orientation of the local coordinate system  $o - xyz$  to be described with reference to the global coordinate system  $O - XYZ$ . From Zatsiorsky (1998) translation can be described by a  $3 \times 1$  column vector  $(L_X, L_Y, L_Z)$  and rotation by a  $3 \times 3$  matrix of direction cosines. A  $1 \times 4$  row matrix with elements  $(1,0,0,0)$  is included for mathematical convenience;

$$[T] = \begin{bmatrix} 1 & 0 & 0 & 0 \\ L_X & \cos_{Xx} & \cos_{Xy} & \cos_{Xz} \\ L_Y & \cos_{Yx} & \cos_{Yy} & \cos_{Yz} \\ L_Z & \cos_{Zx} & \cos_{Zy} & \cos_{Zz} \end{bmatrix}$$

Equation 3.15

For transformation of a coordinate vector given in the local coordinate system to the global coordinate system the following matrix multiplication was used;

$$\begin{bmatrix} 1 \\ P_X \\ P_Y \\ P_Z \end{bmatrix} = \begin{bmatrix} 1 & 0 & 0 & 0 \\ L_X & \cos_{XX} & \cos_{XY} & \cos_{XZ} \\ L_Y & \cos_{YX} & \cos_{YY} & \cos_{YZ} \\ L_Z & \cos_{ZX} & \cos_{ZY} & \cos_{ZZ} \end{bmatrix} \cdot \begin{bmatrix} 1 \\ P_x \\ P_y \\ P_z \end{bmatrix}$$

Equation 3.16

or

$$[P_G] = \begin{bmatrix} 1 & \vdots & 0 & 0 & 0 \\ \dots & \dots & \dots & \dots & \dots \\ [L] & \vdots & & [R] & \end{bmatrix} \cdot [P_L] = [T][P_L]$$

Equation 3.17

where  $[P_G]$  is the global coordinate vector,  $[L]$  is the local to global translation vector,  $[R]$  is the local to global rotation matrix and  $[P_L]$  is the local coordinate vector. The inverse of the transformation matrix is not orthogonal therefore its inverse which gives the position of the global frame with regard to the local is;

$$[T]^{-1} = \begin{bmatrix} 1 & \vdots & 0 & 0 & 0 \\ \dots & \dots & \dots & \dots & \dots \\ -[R]^T[L] & \vdots & & [R]^T & \end{bmatrix}$$

Equation 3.18

The transformation matrix was used to transform joint centre positions and sensor displacements between local segment and global coordinate systems.

### 3.1.11. Inverse Dynamics Calculations

Inverse dynamics was used to derive net joint force and net joint moments of force from the combination of measured kinematics, segment inertial parameters and measured external forces. Calculations began at the most proximal or terminal segment, i.e. the hands and the feet. At the feet the external forces were measured using the force plates. It was assumed that no external forces acted on the club. The net joint reaction forces and moments acting at the more distal end of a segment were equal in magnitude and opposite in sign to those acting on the proximal end of the adjacent segment according to Newton's third law. Calculations proceeded proximally up the kinetic chain. Calculations from each end of the chain met at the L5/S1 or lower trunk joint.

Standard biomechanics approaches were used to perform inverse dynamics calculations (Robertson et al., 2004). The example calculates joint kinetics at the ankle and is adapted from the example provided by Robertson et al. (2004).

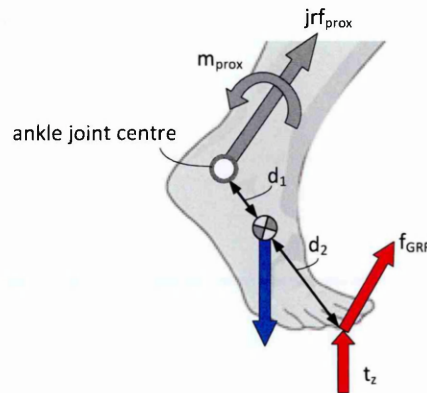


Figure 14 Free body diagram of the foot showing the force and moments acting at the centre of mass

In order to calculate kinetics of the foot segment, all the necessary parameters were first transformed into the foot local coordinate system from the global coordinate system. Firstly, the translational dynamics were calculated;

$$\overrightarrow{jrf_{ankle\_x}} = m\ddot{x}_{CM} - m\vec{g}_x - \vec{f}_{GRF\_x}$$

Equation 3.19

$$\overrightarrow{jrf_{ankle\_y}} = m\ddot{y}_{CM} - m\vec{g}_y - \vec{f}_{GRF\_y}$$

Equation 3.20

$$\overrightarrow{jrf_{ankle\_z}} = m\ddot{z}_{CM} - m\vec{g}_z - \vec{f}_{GRF\_z}$$

Equation 3.21

Where  $\overrightarrow{jrf_{ankle\_x}}$ ,  $\overrightarrow{jrf_{ankle\_y}}$ ,  $\overrightarrow{jrf_{ankle\_z}}$  are the components of the ankle joint reaction force;  $g$  is the acceleration resulting from gravity;  $m$  is the segment mass;  $\ddot{x}_{CM}$ ,  $\ddot{y}_{CM}$ ,  $\ddot{z}_{CM}$  are the segment centre of mass linear acceleration components;  $\vec{f}_{GRF\_x}$ ,  $\vec{f}_{GRF\_y}$ ,  $\vec{f}_{GRF\_z}$  are the orthogonal components of the GRF; and  $m\vec{g}_x$ ,  $m\vec{g}_y$ ,  $m\vec{g}_z$  are the components of the weight of the segment in the LCS.

For rotational dynamics, taking moments about the segment centre of mass, the joint moment at the ankle  $j\vec{m}_{ankle}$  in three dimensions is;

$$jm_{ankle\_X} = I_{XX}\alpha_X + (I_{ZZ} - I_{YY})\omega_{ZZ}\omega_{YY} - m_{GRF\_X} - m_{JRF\_X} - t_x$$

Equation 3.22

$$jm_{ankle\_Y} = I_{YY}\alpha_Y + (I_{XX} - I_{ZZ})\omega_{XX}\omega_{ZZ} - m_{GRF\_Y} - m_{JRF\_Y} - t_y$$

Equation 3.23

$$jm_{ankle\_Z} = I_{ZZ}\alpha_Z + (I_{YY} - I_{XX})\omega_{YY}\omega_{XX} - m_{GRF\_Z} - m_{JRF\_Z} - t_z$$

Equation 3.24

where  $I_{XX}$ ,  $I_{YY}$ ,  $I_{ZZ}$  are components of moment of inertia vector;  $\alpha_X$ ,  $\alpha_Y$ ,  $\alpha_Z$  represent the components of the segment angular acceleration;  $\omega_{XX}$ ,  $\omega_{YY}$ ,  $\omega_{ZZ}$  represent the components of angular velocity;  $t_x$ ,  $t_y$ ,  $t_z$  are the ground reaction torques;  $m_{GRF\_X}$ ,  $m_{GRF\_Y}$ ,  $m_{GRF\_Z}$  are the components of the moment resulting from the GRF and  $m_{JRF\_X}$ ,  $m_{JRF\_Y}$ ,  $m_{JRF\_Z}$  are the components of the moment resulting from the joint reaction force;

$$\vec{m}_{JRF} = \vec{d}_1 \times j\vec{r}f_{ankle}$$

Equation 3.25

where  $\vec{d}_1$  is the vector of the  $xyz$  distance between the centre of mass and the proximal joint centre and  $j\vec{r}f_{ankle}$  is the vector of the  $xyz$  components of the proximal joint reaction force.

$$\vec{m}_{GRF} = \vec{d}_2 \times \vec{f}_{GRF}$$

Equation 3.26

where  $\vec{d}_2$  is the vector of the  $xyz$  distance between the centre of mass and the centre of pressure.

Using Newtons 3<sup>rd</sup> law the moments and forces calculated for the segment were reversed in sign and assumed to act on the distal end of the adjacent segment. All force and moment calculations were conducted in the local coordinate system of the segment so were transformed into the global and then into the local coordinate system of the adjacent segment before the next set of calculations could proceed;

$$[J\vec{M}_{Ankle}] = [T_{local2global}][j\vec{m}_{Ankle}]$$

Equation 3.27

$$[j\vec{m}_{distl\_shank}] = [T_{global2local}][J\vec{M}_{Ankle}]$$

Equation 3.28

For the shank, all the necessary parameters including the ankle joint reaction forces and moments from the foot segment calculations were transformed into the local coordinate system of the shank (figure 15). The same process was necessary for the thigh, hip and so on. The equations for the shank and thigh were analogous to the foot segment with the exception that the *GRF* components were replaced by the components of the distal joint reaction force;

$$j\vec{r}f_{prox} = m\vec{a}_{CM} - m\vec{g} - j\vec{r}f_{distal}$$

Equation 3.29

$$j\vec{m}_{prox} = I\alpha - (\vec{d}_1 \times \vec{f}_{jrf_{prox}}) - (\vec{d}_2 \times \vec{f}_{jrf_{dist}}) - j\vec{m}_{distal}$$

Equation 3.30

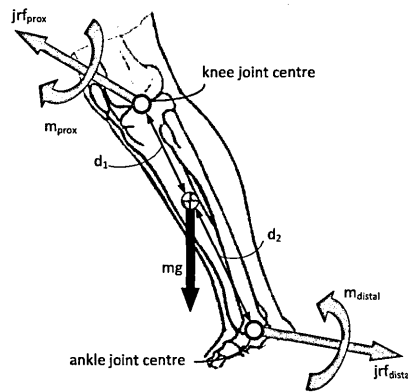


Figure 15 Free body diagram of the shank

### 3.1.12. Special cases

#### 3.1.12.1. The Pelvis

At the pelvis, two *JRF* and *JM* act on the right and left hip joints as shown in the free body diagram below (figure 16). As such, both sets of *JRF* and *JM* are integrated into the translational and rotational dynamics equations.

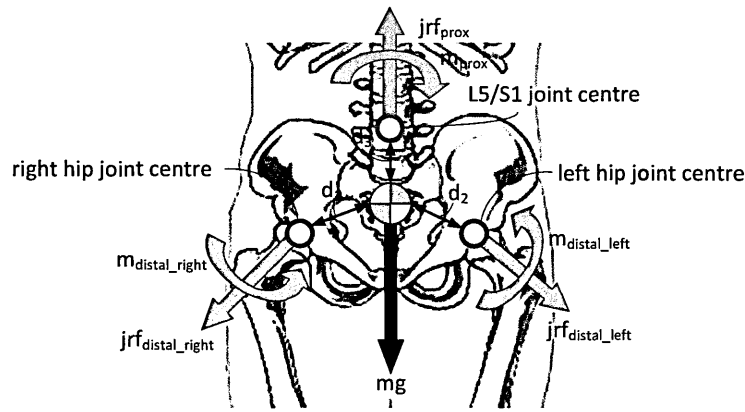


Figure 16 Pelvis free body diagram of joint moment and joint reaction force calculations

### 3.1.12.2. The Club

The hands were assumed to grip the club 12cm from the top of the grip. It was assumed that no external forces or moments acted at the end of the club head (figure 17). Therefore the equations were;

$$\overrightarrow{jrf}_{hand_x} = m\ddot{x}_{CM} - m\vec{g}_x$$

Equation 3.31

$$\overrightarrow{jrf}_{hand_y} = m\ddot{y}_{CM} - m\vec{g}_y$$

Equation 3.32

$$\overrightarrow{jrf}_{hand_z} = m\ddot{z}_{CM} - m\vec{g}_z$$

Equation 3.33

$$m_{hand_x} = I_{XX}\alpha_x + (I_{ZZ} - I_{YY})\omega_{ZZ}\omega_{YY}$$

Equation 3.34

$$m_{hand_y} = I_{YY}\alpha_y + (I_{XX} - I_{ZZ})\omega_{XX}\omega_{ZZ}$$

Equation 3.35

$$m_{hand_z} = I_{ZZ}\alpha_z + (I_{YY} - I_{XX})\omega_{YY}\omega_{XX}$$

Equation 3.36

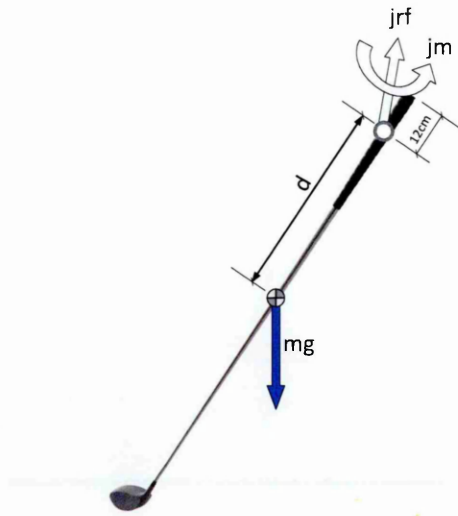


Figure 17 Free body diagram of the club segment. No external forces or moments were assumed to act on the club segment, where  $d$  = distance from the centre of mass to the hand grip,  $m$  = club mass,  $g$  = acceleration due to gravity,  $jrf$  = joint reaction force,  $jm$  = joint moment

### 3.1.13. Model indeterminacy

The closed loop formed by the arms and club resulted in an indeterminate system and so an assumption had to be made as to the distribution of the forces and moments between the two arms. It was assumed that the distal joint reaction force and distal joint moments were distributed equally between the two arms. This was the same approach adopted by Nesbit et al. (2007).

### 3.1.14. Calculation sequence

Inverse dynamics calculations began at opposite ends of the linked segment model; at the left and right feet and at the hands (figure 18). Calculations beginning at the feet were used to estimate joint moments at the ankles, knees, hips, proximal pelvis and proximal mid trunk joint, i.e. T8/T9 joint. Joint moment estimates for the hands, wrists, elbows, shoulders, and upper trunk were a result of calculations beginning at the club end of the kinematic chain.

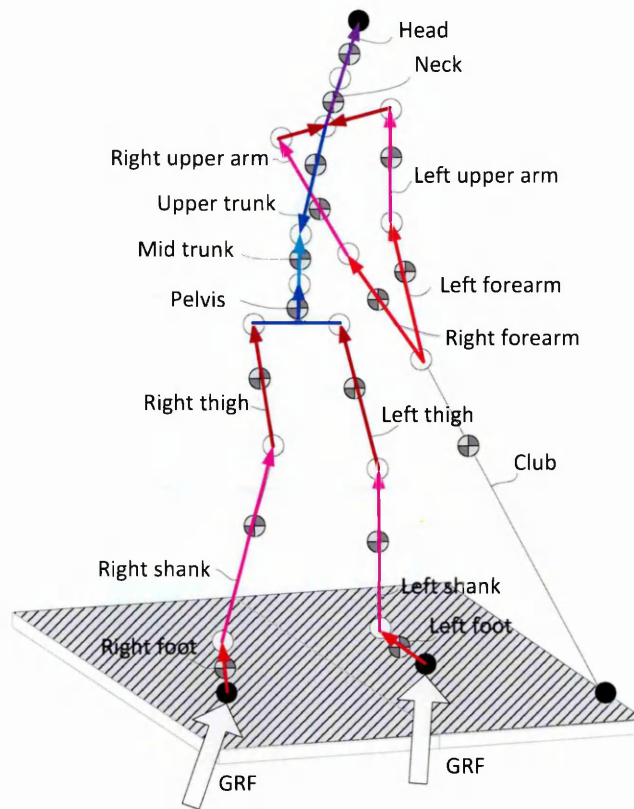


Figure 18 Golphysics linked segment model calculation sequence indicated by arrows. Two recursive strategies were used beginning at the feet and the hands and meeting at the T8/T9 intervertebral joint.

### 3.2. Sample

8 male category 1 golfers as indicated by the CONGU Unified Handicapping System divisions were recruited for the study (mean age  $30 \pm 14$ , height  $182.9 \pm 6.4$ m, weight  $86.2 \pm 18.1$ kg). Participants were therefore of handicap 5 or less with 5 of the sample classed as professional golfers (table 4). All participants were right handed. The sample size and number of trials were determined from the availability of suitable participants, and the practical time allowance for data processing and analysis. All participants were free from injury which may have affected performance at the time of data collection. Written informed consent was obtained from all participants and the ethics committee of Sheffield Hallam University granted approval for the study (see APPENDIX L: Golf Swing Data Collection - Participant Information Sheet, APPENDIX M: Golf Swing Data Collection - Ethics Form and APPENDIX N: Golf Swing Data Collection - Risk Assessment Form).

Table 4 Participant details

Participant #	Age	Height (cm)	Weight (kg)	Official handicap
1	19	190.3	71.4	Pro
2	38	184.8	95.3	T Pro
3	18	186.3	84.7	(+) 3
4	22	176.8	68.7	0
5	20	182.8	95.5	0
6	25	186.6	62.4	0
7	61	180.2	110.6	1
8	31	185.9	116.1	4

### 3.3. Filtering

Kinematic data was smoothed using Wavelet De-Noising (WDN). WDN is a time-frequency filtering technique. Time varying filtering techniques have the ability to localise the frequency content of a signal which makes them very useful for applications involving non-stationary kinematic signals, such as those involving impacts, which have a frequency content which varies with time. Whilst digital filtering techniques, such as the Butterworth filter, can isolate the frequency content of a signal, they cannot distinguish when these components occurred in time. Sharp, high frequency transient components like those caused by impacts are often over-smoothed (Knudson and Bahamonde, 2001; Nunome et al., 2006). WDN techniques process the signal at various scales and resolutions, decomposing it into high frequency, low resolution details and low frequency, high resolution approximations. Decomposition is achieved by dilation and translation of a basic mother wavelet and noise is removed via thresholding of the coefficients. WDN has been applied to biomedical signals (Singh and Tiwari, 2006), artificial biomechanical signals (Ismail and Asfour, 1999; Wachowiak et al., 2000) and more recently, to badminton racket kinematics (Domone et al., 2012).

The raw displacement data were padded to a dyadic length using reflection which also helped to reduce endpoint problems (Smith, 1989). The mother wavelet was selected by calculating the cross correlation coefficient of the signal with 17 different mother wavelets; this process was repeated for each signal to be filtered. Hard thresholding was used as it was better able to maintain the amplitude of spikes in the data than soft thresholding (Buckheit and Donoho, 1995). Translation invariant de-noising (Coifman and Donoho, 1995) was employed to reduce 'pseudo-Gibbs' artefacts which have been shown to be problematic (Giakas et al., 2000; Wachowiak et al., 2000). A semi-

automatic thresholding technique was implemented similar to methods used by Wachowiak et al. (2000). The threshold ( $\lambda$ ) was set to a multiple ( $\alpha$ ) of the standard deviation ( $\sigma$ ) of the wavelet coefficients at each decomposition level  $i$  ( $\lambda = \alpha_i \sigma_i$ ).

The application of a smoothing routine to each component of a unit quaternions  $q_N$  directly does not maintain unity due to the non-linearity of the unit quaternion space (Hsieh et al., 1998). In order to maintain unity, quaternions were first differentiated into angular velocities using equation 3.14 (pg. 62). Wavelet denoising was then applied to each dimension of the angular velocity. It was found that double differentiation of smoothed linear displacements resulted in 'pseudo-Gibbs' artefacts in some cases and therefore double differentiation after smoothing was avoided. As such, for linear and angular accelerations, WDN was applied to the noisy velocity signals and then differentiated (figure 19).

Following empirical experimentation thresholds were determined as follows; for angular velocity,  $\alpha_1 = 6.0$ ,  $\alpha_2 = 3.5$ ,  $\alpha_3 = 3.0$ ,  $\alpha_4 = 1.0$ , coefficients in the remaining levels were not thresholded. For angular acceleration thresholds were increased to,  $\alpha_1 = 15.0$ ,  $\alpha_2 = 10.0$ ,  $\alpha_3 = 4.0$ ,  $\alpha_4 = 1.0$ ; this was analogous to lowering the cut off frequency for higher order derivatives (Giakas and Baltzopoulos, 1997). For linear acceleration thresholds were increased to,  $\alpha_1 = 20.0$ ,  $\alpha_2 = 20.0$ ,  $\alpha_3 = 5.0$ . Velocity and acceleration were calculated from the processed displacement data using the central difference method (section 3.1.9).

To illustrate the effect of WDN, the filtering strategy described above was compared to a conventional second order dual pass Butterworth filter (BWF) with a 12Hz cut-off frequency. The BWF cut-off frequency was determined by residual analysis (Winter, 1990). This method was chosen to represent conventional biomechanical filtering procedures (Kenny et al., 2006). Angular acceleration of the club segment in the Y direction for a single exemplar trial is presented in figure 20. From figure 20 it can be seen that WDN preserved the signal features better than BWF which tended to attenuate and widen the higher frequency transients produced by impact ( $t=1.2$  seconds), a finding consistent with other studies (Ismail and Asfour, 1999; Wachowiak et al., 2000).

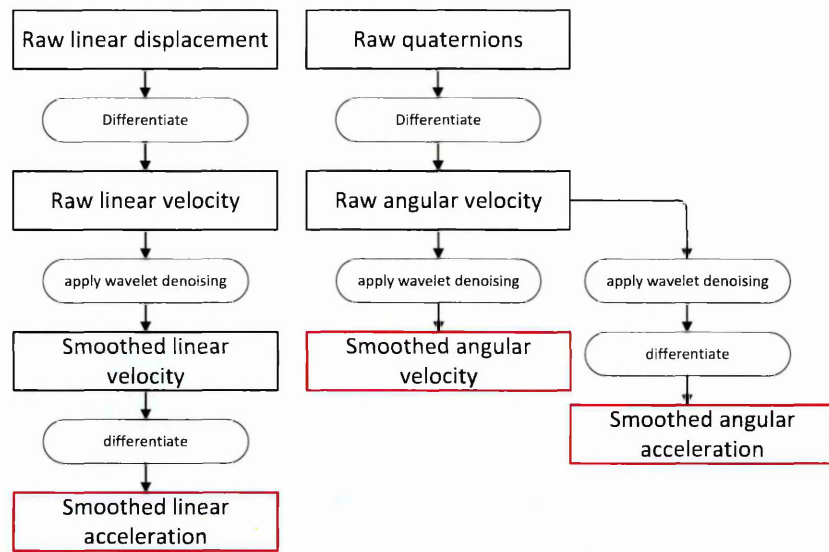


Figure 19 Wavelet de-noising process

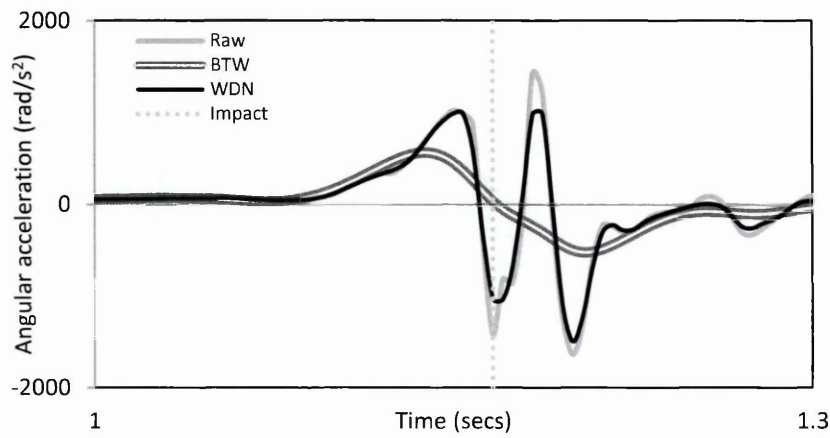


Figure 20 Wavelet De-Noising (WDN) applied to club segment angular acceleration in the Y direction for an exemplar swing trial. WDN is compared to a Butterworth filter (BWF) (cutoff frequency 12Hz) and raw angular acceleration data.

---

## 4. Validation of Inverse Dynamics Solutions

### 4.1. Introduction

The output of inverse dynamics models consists of joint reaction forces and joint moments at inter-segmental joints. Validation of inverse dynamics solutions is difficult due to the absence of a "gold standard" measure for comparison. The over determined nature of inverse dynamics full body models has been exploited for validation purposes. A comparison of joint reaction forces and moments estimated using a 'top down' and 'bottom up' approach at the L5/S1 joint has been used to validate inverse dynamics models applied to lifting (De Looze et al., 1992; Kingma, De Looze, et al., 1996; Kingma, Toussaint, et al., 1996; Plamondon et al., 1996), fast and large trunk movements (Iino and Kojima, 2012), balance recovery (Robert et al., 2007), rowing (Greene et al., 2009), slow speed golf swings (Tsai, 2005) and gait (MacKinnon and Winter, 1993; Riemer et al., 2008). A comparison of joint reaction forces as well as joint moments can reveal which parameters are more likely to be responsible for the error. For example, De Looze et al. (1992) found statistically significant differences between joint moment estimates at the L5/S1 joint during lifting tasks; 4.9 Nm and 22.8 Nm for mean and peak moment differences respectively. However differences for joint force estimates were much smaller (mean 1.47 N). Therefore, the differences in joint moments could be attributed to errors in moment arm lengths, segment moments of inertia and angular acceleration since these did not affect joint reaction force calculations (De Looze et al., 1992).

A comparison of the measured and the predicted ground reaction force (GRF) has been described as a more 'rigorous' test of validity since these are two completely independent measures of the same force (De Looze et al., 1992). The net GRF is calculated as the summed product of every segment's mass and acceleration, minus the gravity vector. The net GRF is then compared to the GRF measured by the force plates by summing the GRFs for both feet. A limitation of this method is that results will not be affected by errors in segment moment arm length, angular velocity, and segment moments of inertia since these are not included in the calculation of force (De Looze et al., 1992). Furthermore, the prediction of GRF uses all body segments in the kinematic chain, as such, the reported residual may be maximised due to the accumulation of error as calculations proceed distally. This method of validation has

been applied to standing broad jumps (Pezzack and Norman, 1981), rapid knee bends (Pezzack and Norman, 1981), planar lifting tasks (De Looze et al., 1992; Freivalds et al., 1984; Kingma, Toussaint, et al., 1996), and asymmetric lifting tasks (Kingma, De Looze, et al., 1996; Kromodihardjo and Mital, 1986). For asymmetric lifting tasks, mean force differences were statistically insignificant and ranged between 0.5-5.1 N (Kingma, De Looze, et al., 1996). Peak force differences were statistically significant for horizontal components, ranging between 15.2-28.0 N. Results of this type of analysis have been shown to be highly influenced by task type; for sagittal plane lifting tasks, the overall performance of a geometric and a proportional model applied to the same data set was compared (De Looze et al., 1992). Results showed systematic errors in the proportional model for back lifting tasks, however, for leg lifting tasks, systematic errors were reported for the geometric model.

Studies utilising these methods of validation have mainly been concerned with slow simple movements such as lifting (De Looze et al., 1992; Kingma, De Looze, et al., 1996; Kingma, Toussaint, et al., 1996; Plamondon et al., 1996). A more recent study compared joint moments at the L5/S1 joint for validation of inverse dynamics applied to fast and large trunk movements (Iino and Kojima, 2012). It was reported that the same level of validity was achieved as for previous lifting studies; mean RMS errors for moments at the L5/S1 joint were less than 10 Nm for all components (Iino and Kojima, 2012). However, movements were constrained to the spine and were artificial in nature. Tsai (2005) investigated the validity of inverse dynamics derived joint moments at the L5/S1 joint during a slow speed golf swing. Mean RMS joint moment differences were 11.1 Nm, 13.2 Nm and 9.5 Nm for lateral bending, flexion-extension and axial rotation respectively. Whilst this is one of the few studies that considered a more complex movement, it is important to note that this validation was performed on "slow speed" swings only. It was stated that during testing, the optical motion measurement system used was not fast enough (120Hz) to track the markers on the wrists, hands, and club during the downswing with a normal swing speed. Previous studies have indicated that greater movement speeds increase the susceptibility of inverse dynamics solutions to error (Larvière and Gagnon, 1998; Pearsall and Costigan, 1999; Plamondon et al., 1996). For example, during asymmetric lifting, the maximum joint moment difference at the L5/S1 joint was increased by 11 Nm, 11 Nm and 8 Nm

for sagittal, longitudinal and transverse components respectively for normal compared to fast lifting speeds (Plamondon et al., 1996).

The aim of this study was to apply previously used methods of validation to an inverse dynamics model of the golf swing. This was achieved using three methods; 1) a comparison of the measured and predicted ground reaction forces at the feet, 2) a comparison of the top down and bottom up calculated joint reaction forces at the T8/T9 joint and 3) a comparison of the top down and bottom up calculated joint moments at the T8/T9 joint. To examine the effect of speed increase, the swing was split into two phases for the analysis; the backswing and the downswing. During the downswing, segments move through the same range of motion as during the backswing in approximately one third of the time (Novosel and Garrity, 2004); the ratio of the backswing time ( $T_b$ ) to downswing time ( $T_d$ ) in this study was  $T_b/T_d \approx 3.5$ .

## 4.2.Method

Data collection methods have been outlined previously in chapter 3 (pg.44). The sample used as outlined in previous sections (3.2) were eight male category one golfers as indicated by the CONGU Unified Handicapping System divisions (mean age  $30 \pm 14$  years, height  $182.9 \pm 6.4$ m, weight  $86.2 \pm 18.1$ kg). Three representative driver swings from each participant were used. All participants provided written informed consent and were free from injury which may have affected performance at the time of data collection. Ethical approval was obtained from the research ethics committee of the Faculty of Health and Wellbeing at Sheffield Hallam University (see appendix L-N for participant information sheet and ethics forms).

### 4.2.1. Data Analysis

The three components of joint moments and joint reaction forces at the T8/T9 joint were compared for the top down and bottom up inverse dynamics models. Joint moments from the top down and bottom up models at the T8/T9 joint acting on the mid trunk segment were compared. Joint reaction forces are presented in the local coordinate system of the mid trunk segment which was defined such that the x, y and z axes were predominantly anterior-posterior, vertical and medial-lateral respectively. Joint moments were defined such that rotations about the x, y and z axes were predominantly lateral-bending, axial rotation and flexion-extension respectively. For

ground reaction force comparison, the measured ground reaction forces were summed for the two force plates. The predicted ground reaction force was calculated by summing the joint reaction forces at the proximal end of the feet. Comparisons between measured and predicted ground reaction forces were made for the force components in all three dimensions in the global coordinate system. Swing data was cropped to begin at take away and end three frames before impact. This was necessary in order to eliminate impact artifacts from the double differentiated acceleration data. It was hypothesised that differences between forces and moments at the T8/T9 joint during the downswing would be greater than during the backswing. To test this hypothesis the backswing and downswing were analysed separately so that comparisons between them could be made. For details on how the backswing and downswing were defined see section 3.1.4.3 (pg. 49).

The mean and peak moments at the T8/T9 joint were calculated for the top down and bottom up models for all time series. Subsequently the mean and standard deviation across all participants and trials was calculated. A paired sample *t*-test was performed to test for systematic differences between the means using top down and bottom up models as repeated measures. RMS error of difference between time series of the joint moments at the T8/T9 joint were calculated for all trials. Pearson's correlation coefficients were also computed for all trials. This tested for the strength of the linear relationship between joint moment time series. The same statistical analysis was used for the three components of top down and bottom up joint reaction forces at the T8/T9 joint and the measured and predicted ground reaction forces. IBM SPSS Statistics (Version 21) was used for all analyses. See APPENDIX O: Table of Assumptions (pg. 59) for a summary of the assumptions made by the test statistics used.

## 4.3.Results

### 4.3.1. Measured compared to predicted GRF

At takeaway the vertical ground reaction forces were close to body weight and horizontal components were approximately zero as the player was stationary (figure 21). For the backswing, the differences between the mean and peak estimated and measured ground reaction forces were statistically significant for the anterior-posterior ( $t(23) = 13.4, p = 0.00, t(23) = -10.4, p = 0.00$ ) and medial-lateral components

( $t(23) = 4.7$ ,  $p = 0.00$ ,  $t(23) = -5.8$ ,  $p = 0.00$ ). Figure 21 represents a typical example of the time series of the measured and estimated ground reaction forces. During the downswing, mean and peak ground reaction forces were higher than during the backswing. The difference between mean predicted and measured GRF was significant for the medial lateral direction ( $t(23) = -6.1$ ,  $p = 0.00$ ) (table 5). Peak force differences during the downswing were statistically significant for all components with the highest difference of 331.3 N in the medial-lateral direction ( $t(23) = -12.3$ ,  $p = 0.00$ ). This difference was equivalent to 66.7% of the peak predicted force. Peak forces were predicted to be over 300 N higher than measured for the horizontal components of force (table 6).

Coefficients of correlation between the measured and estimated ground reaction forces were highest during the backswing for all components in comparison to the downswing (table 7). During the backswing, the anterior-posterior component of force had the lowest coefficients of correlation (median  $r = 0.74$ ) and largest range 0.17-0.89. For the downswing, correlation coefficients were only marginally lower for the vertical components of force than during the backswing. For the horizontal components of force correlation coefficients were reduced and of similar magnitude (median  $r = 0.60$  and  $r = 0.64$  for the anterior-posterior and medial-lateral components respectively). RMS differences were highest for the horizontal components in agreement with correlation coefficient results.

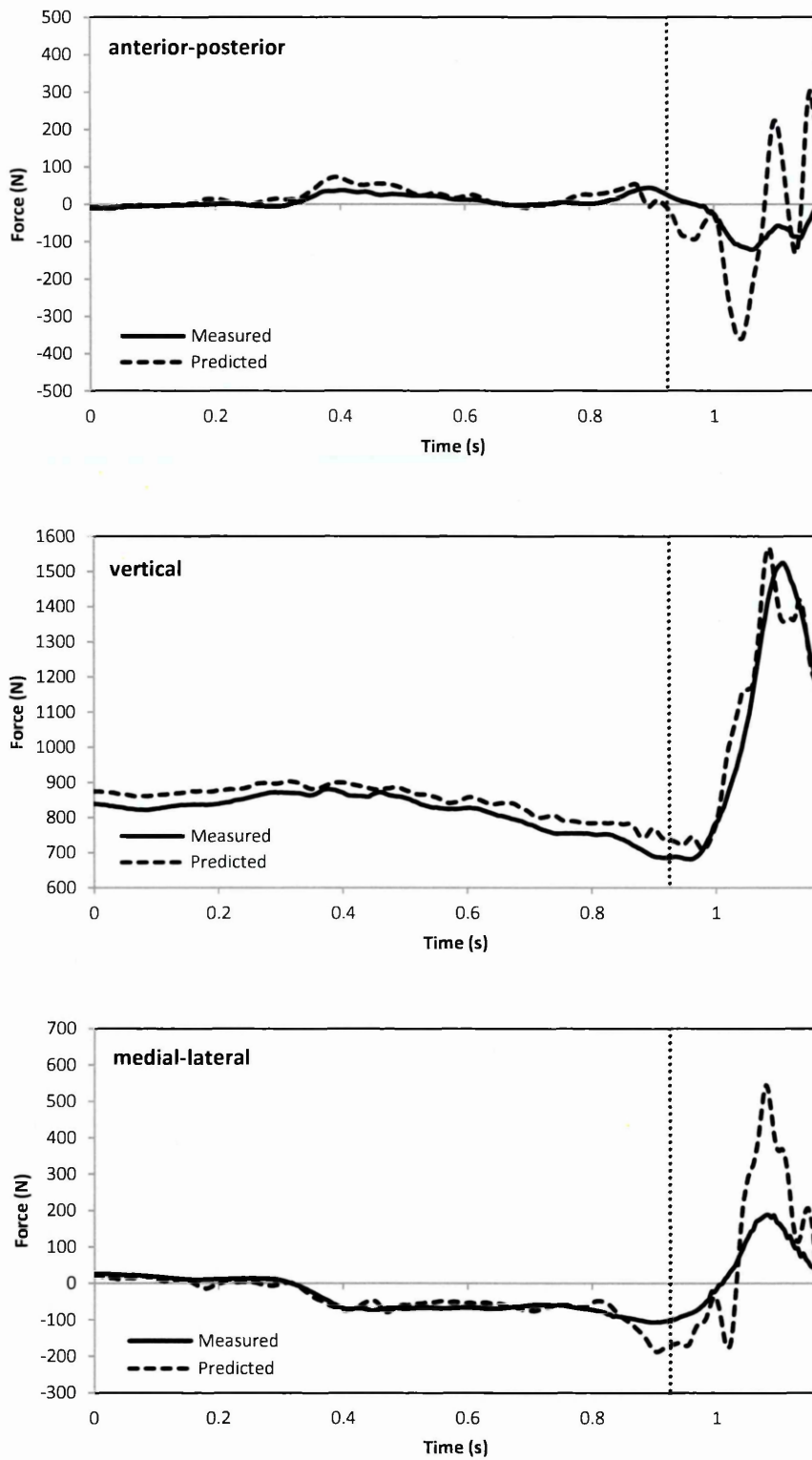


Figure 21 A representative example of the time series of the measured (solid line) and predicted (---) ground reaction force comparisons. Swing begins at take-away and ends 3 frames before impact. The vertical dotted line indicates top of backswing.

**Table 5 Mean measured and predicted GRF and the difference between measured and predicted GRF averaged across all participants and trials.**

	Mean force (N)							
	Measured	(SD)	Predicted	(SD)	Mean error	(SD)	t(23)	p
<b>Backswing</b>								
anterior-posterior	2.4	5.67	10.6	6.15	-8.2	2.36	13.4	0.000*
vertical	893.4	169.53	891.0	163.79	2.4	39.20	0.2	0.816
medial-lateral	-46.5	17.39	-49.6	17.09	3.1	2.56	4.7	0.000*
<b>Downswing</b>								
anterior-posterior	-12.7	19.47	-13.1	22.25	0.4	12.89	-0.1	0.902
vertical	1035.4	182.08	1022.4	146.49	13.0	59.71	0.8	0.412
medial-lateral	-12.8	46.72	14.7	58.45	-27.5	17.43	-6.1	0.000*

Significant differences between measured and predicted GRF components are indicated by an asterisk ( $\alpha=0.05$ ).

**Table 6 Peak measured and predicted GRF and the difference between measured and predicted GRF averaged across all participants and trials.**

	Absolute peak force (N)							
	Measured	(SD)	Predicted	(SD)	Mean error	(SD)	t(23)	p
<b>Backswing</b>								
anterior-posterior	31.5	12.49	69.1	24.54	-37.5	14.00	-10.4	0.000*
vertical	948.8	172.06	958.5	185.10	-9.7	40.06	-0.9	0.365
medial-lateral	159.0	43.26	204.5	25.45	-45.4	30.52	-5.8	0.000*
<b>Downswing</b>								
anterior-posterior	125.3	33.50	439.2	147.38	-314.0	144.52	-8.4	0.000*
vertical	1409.4	206.00	1525.6	170.36	-116.2	116.67	-3.9	0.002*
medial-lateral	165.2	41.14	496.5	119.83	-331.3	104.01	-12.3	0.000*

Significant differences between measured and predicted GRF components are indicated by an asterisk ( $\alpha=0.05$ ).

**Table 7 RMS differences and Pearson correlation coefficients between measured and predicted GRF**

	Coefficient of correlation		RMS difference (N)			
	Median	Range	Median	Range		
<b>Backswing</b>						
anterior-posterior	0.74	0.17	0.89	15.3	10.8	27.4
vertical	1.00	0.97	1.00	37.3	20.1	53.8
medial-lateral	0.92	0.90	0.99	19.2	12.6	37.8
<b>Downswing</b>						
anterior-posterior	0.60	0.15	0.87	134.4	116.6	151.7
vertical	0.97	0.91	0.99	115.8	81.1	179.4
medial-lateral	0.64	0.30	0.95	139.8	127.1	196.6

#### 4.3.2. Top down vs. bottom up calculated joint reaction forces and moments at the T8/T9 joint

Figure 22 and figure 23 present a typical example of the predicted joint reaction forces and moments at the T8/T9 joint respectively (for the same participant and trial as in figure 21). All joint forces and moments are presented in the local coordinate system of the mid trunk segment. The example shows a close agreement between the bottom-up and top-down calculated joint reaction forces for the medial-lateral and anterior-posterior components of force during the backswing. Similarly there was a close agreement between the bottom-up and top-down calculated moments for the lateral bending and axial rotation moments during the backswing. For the vertical force component there was a systematic offset between the top-down and bottom-up calculated joint reaction forces during the backswing (figure 22). Vertical forces had a mean difference of 0.1 N and an absolute peak difference of -14.5 N; this was the lowest of the three force components. The highest peak force difference was -20.4 N for the medial-lateral direction. For the downswing, differences were increased; medial-lateral forces had the highest mean difference of 77 N and the anterior-posterior direction had the highest peak difference of 197 N.

There were significant differences between the top down/bottom up mean joint moments for lateral bending and flexion extension components during the backswing (table 8). This indicated systematic differences in the prediction of joint moments between the top down and bottom up models. For the downswing, differences in the mean joint moments were increased and significant for all components. Absolute peak differences were highest and close to significant for lateral bending during the backswing (table 9). During the downswing, peak differences were again increased and highest for flexion extension moments. Significant differences were reported for lateral bending and flexion extension components. As shown in figure 23, the top down model consistently estimated flexion-extension joint moments at the T8/T9 to be higher than predicted by the bottom up model. This produced an offset in joint moment time series most evident during the backswing. For all components of joint reaction forces and moments, median coefficients of correlation were smaller for the downswing than the backswing (table 10). RMS differences were higher during the downswing than the backswing for all components of JRF and joint moments. Lateral bending moments had the greatest RMS differences during the downswing.

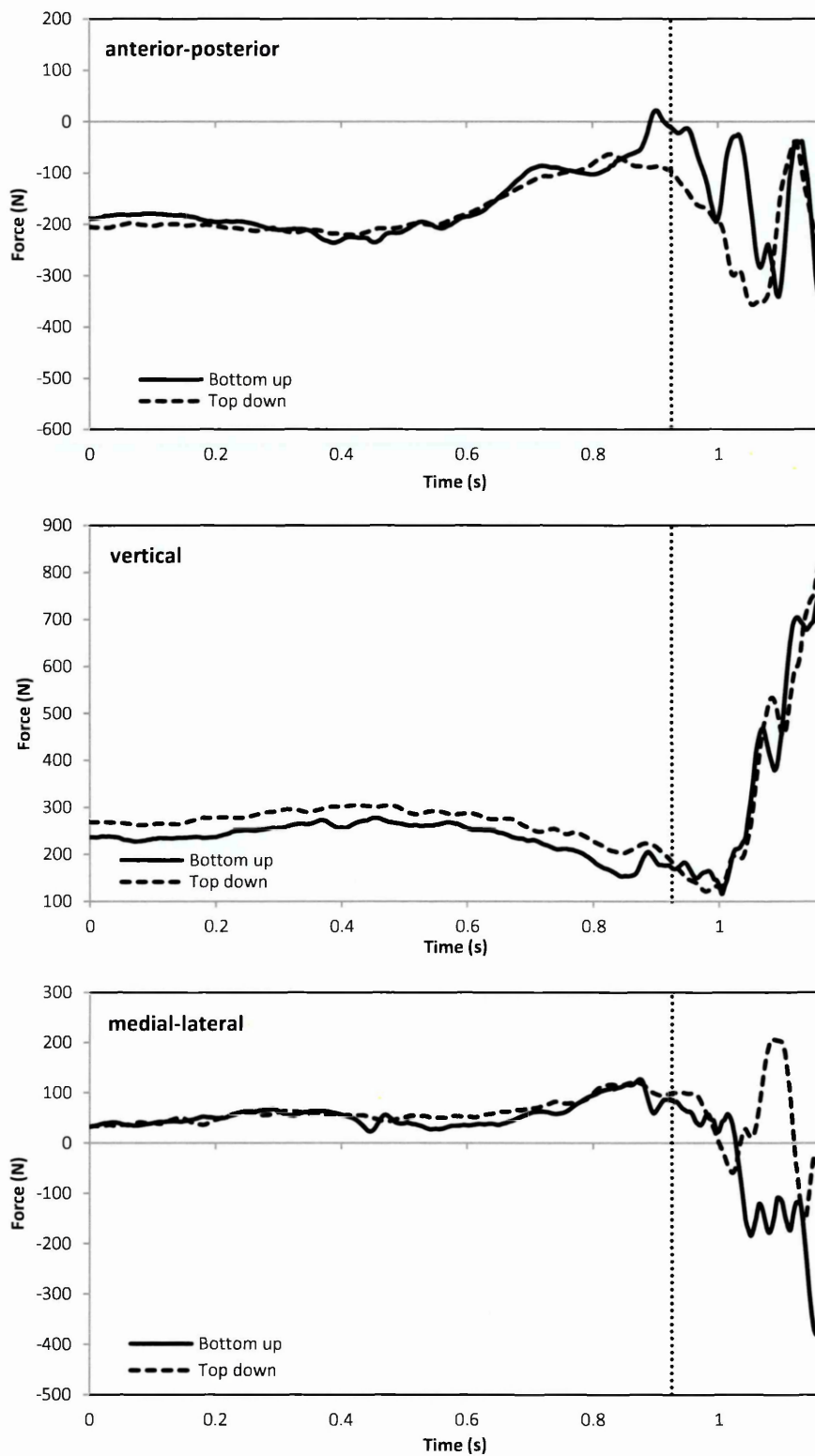


Figure 22 A typical example of the time series of the top down (---) and bottom up (solid line) joint reaction force comparisons at the T8/T9 joint. Swing begins at take-away and ends 3 frames before impact. The vertical dotted line indicates top of backswing.

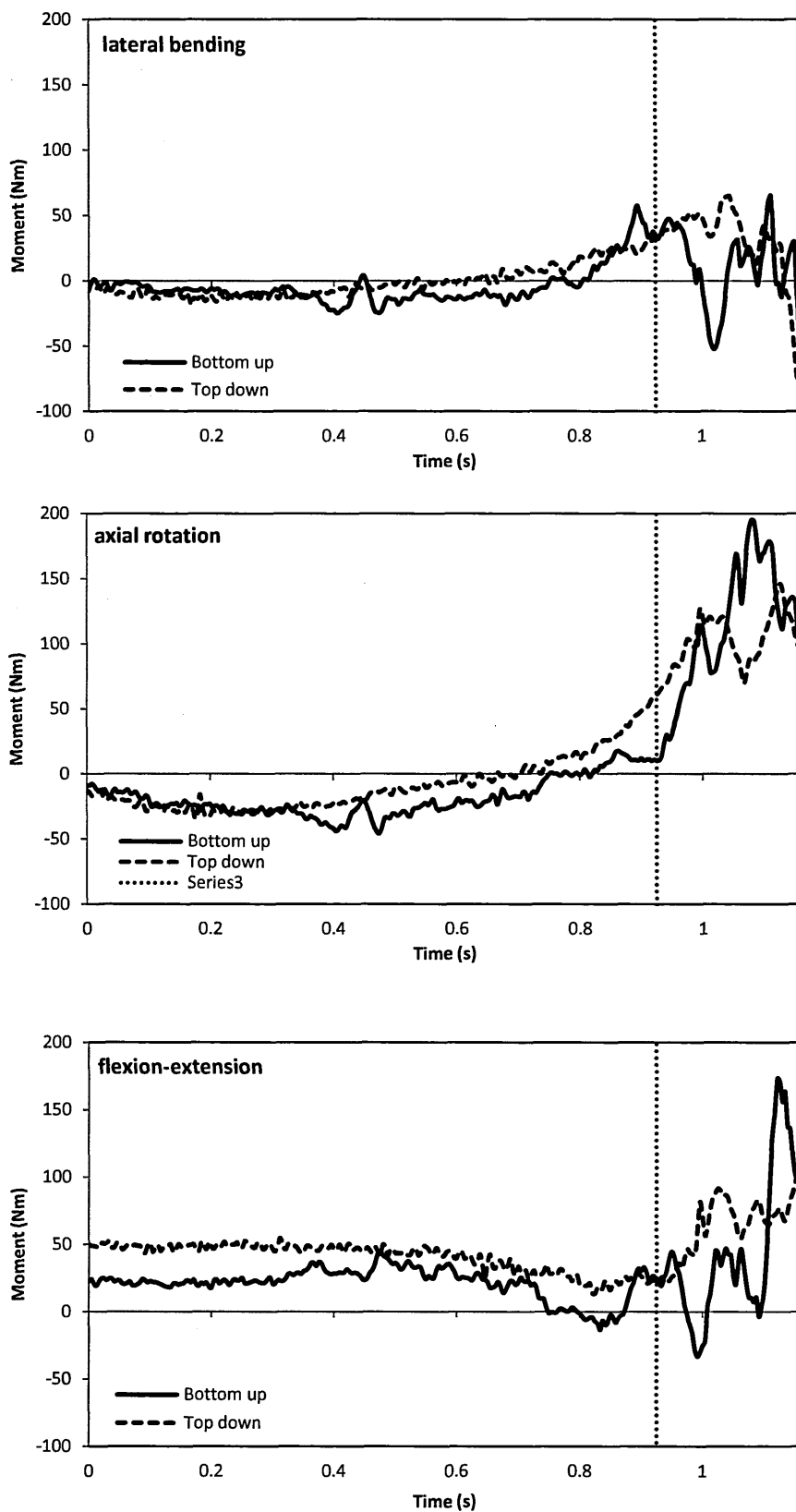


Figure 23 A typical example of the time series of the top down (---) and bottom up (solid line) joint moment comparisons at the T8/T9. Swing begins at take-away and ends 3 frames before impact. The vertical dotted line indicates top of backswing.

**Table 8 Mean joint reaction forces and moments for the top down and bottom up models and the difference between top down and bottom up models averaged across all participants and trials.**

	Mean joint reaction forces (N) and moments (Nm)							
	Top down	(SD)	Bottom up	(SD)	Mean difference	(SD)	t(23)	p
<b>Backswing</b>								
<i>Forces (N)</i>								
anterior-posterior	-104.8	46.03	-113.8	42.10	9.0	13.24	-2.6	0.020*
vertical	314.3	58.65	314.3	59.45	0.1	35.47	0.0	0.995
medial-lateral	76.3	25.95	79.9	23.78	-3.6	8.87	1.6	0.139
<i>Moments (Nm)</i>								
lateral bending	2.0	4.56	-13.7	6.87	15.7	6.15	-9.9	0.000*
axial rotation	-7.9	2.32	-8.9	5.81	1.0	5.45	-0.7	0.490
flexion-extension	38.8	7.23	22.7	10.12	16.1	10.60	-5.9	0.000*
<b>Downswing</b>								
<i>Forces (N)</i>								
anterior-posterior	-91.3	60.41	-99.5	84.52	8.3	49.50	-0.6	0.529
vertical	369.6	75.90	388.5	83.83	-18.9	59.07	1.2	0.236
medial-lateral	36.8	47.97	-40.2	49.95	77.0	25.29	-11.8	0.000*
<i>Moments (Nm)</i>								
lateral bending	51.3	15.57	20.7	10.58	30.6	11.62	-10.2	0.000*
axial rotation	67.1	19.85	72.9	19.91	-5.8	9.50	2.4	0.033*
flexion-extension	41.6	11.83	25.3	13.26	16.3	9.87	-6.4	0.000*

Significant differences between top down and bottom up calculated moments and forces are indicated by an asterisk ( $\alpha=0.05$ ).

**Table 9 Absolute peak joint reaction forces and moments for the top down and bottom up models and the difference between top down and bottom up models averaged across all participants and trials.**

	Absolute peak joint reaction forces (N) and moments (Nm)							
	Top down	(SD)	Bottom up	(SD)	Mean difference	(SD)	t(23)	p
<b>Backswing</b>								
<i>Forces (N)</i>								
anterior-posterior	161.3	54.52	177.7	49.02	-16.4	23.92	-2.7	0.019*
vertical	367.5	79.74	382	81.34	-14.5	53.65	-1.0	0.313
medial-lateral	119.0	35.95	139.4	38.12	-20.4	25.79	-3.1	0.008*
<i>Moments (Nm)</i>								
lateral bending	28.6	6.74	36.5	12.16	-7.8	14.26	-2.1	0.051
axial rotation	48.1	12.61	43.1	16.74	5.0	11.61	1.7	0.116
flexion-extension	54.2	10.56	46.7	12.35	7.5	17.13	1.7	0.111
<b>Downswing</b>								
<i>Forces (N)</i>								
anterior-posterior	263.4	114.58	421.8	197.20	-158.5	139.37	-4.4	0.001*
vertical	765.3	182.81	755.8	120.07	9.4	162.55	0.2	0.825
medial-lateral	333.8	71.00	352.1	125.22	-18.4	170.77	-0.4	0.683
<i>Moments (Nm)</i>								
lateral bending	100.5	12.23	120.1	31.03	-19.6	31.58	-2.4	0.031*
axial rotation	118.9	26.58	138.7	41.91	-19.8	38.84	-2.0	0.068
flexion-extension	99.6	30.46	147.4	31.37	-47.8	43.33	-4.3	0.001*

Significant differences between top down and bottom up calculated moments and forces are indicated by an asterisk ( $\alpha=0.05$ ).

Table 10 RMS differences and Pearson correlation coefficients between top down and bottom up joint reaction forces and joint moments at the T8/T9 joint. RMS differences are in Newtons and newton metres for forces and moments respectively.

	Coefficients of correlation			RMS difference		
	Median	Range		Median	Range	
<b>Backswing</b>						
<i>Forces</i>						
anterior-posterior	0.96	0.77	0.99	24.7	14.4	57.7
vertical	0.99	0.69	1.00	41.9	16.8	78.3
medial-lateral	0.84	0.32	0.94	17.6	12.7	48.7
<i>Moments</i>						
lateral bending	0.46	0.04	0.72	18.6	10.9	24.4
axial rotation	0.92	0.80	0.98	8.2	5.3	16.8
flexion-extension	0.69	0.49	0.81	19.2	8.7	37.8
<b>Downswing</b>						
<i>Forces</i>						
anterior-posterior	0.36	0.03	0.81	132.1	106.9	206.9
vertical	0.88	0.52	0.98	106.5	51.0	303.9
medial-lateral	0.38	0.18	0.76	146.3	123.2	236.7
<i>Moments</i>						
lateral bending	0.29	0.05	0.72	49.5	26.1	75.0
axial rotation	0.60	0.06	0.81	32.6	15.2	46.0
flexion-extension	0.47	0.02	0.70	44.4	32.0	60.1

#### 4.4. Discussion

A three dimensional full body linked segment model was constructed. The validity of the model was tested by comparing top down and bottom up joint reaction forces (JRF) and joint moments (JM) at the T8/T9 joint estimated during the golf swing. In addition, the predicted ground reaction forces (GRF) using a top down approach were compared to measured ground reaction forces. For this analysis, the swing was split into two phases; the backswing and the downswing in order to investigate how the validity of inverse dynamics solutions was affected by an increase in segment acceleration.

In general, mean and peak differences between GRF, JRF and JM were greatest during the downswing. Similarly, coefficients of correlation were lowest and RMS differences were greatest during the downswing for all components exemplified by an increase in RMS differences of 119.1 N, 78.5 N and 120.6 N for the anterior-posterior, vertical and medial-lateral ground reaction force components respectively (table 7). Joint moment RMS differences were increased during the downswing by 30.9 Nm, 24.4 Nm and 25.2 Nm for lateral bending, axial rotation and flexion-extension respectively (table 10).

Also, joint reaction force RMS differences were increased by as much as 128.7 N during the downswing. The increase in error may have been related to the increase in acceleration of the body segments during the downswing. Table 11 is a comparison of

absolute peak segment angular acceleration between the backswing and the downswing averaged across all participants and trials. As shown, angular acceleration of every segment was higher during the downswing compared to the backswing. Peak angular acceleration differences were greatest for the upper body segments exemplified by increases of  $647 \text{ rad/s}^2$  and  $466 \text{ rad/s}^2$  for the club and forearm in the y direction. Previous studies have shown that for lifting tasks, an increase in lifting speed led to an increase in the mean and RMS difference in top down and bottom up calculated joint moments at the L5/S1 joint (Kingma, De Looze, et al., 1996; Larvière and Gagnon, 1998; Plamondon et al., 1996). This increase in error has been attributed to a poor estimation of segment acceleration owing to deformation of the segments and marker displacement relative to the underlying bone (Iino and Kojima, 2012). Previous studies have indicated that the disparity in force and moment differences between speed conditions was particularly evident when the movement was changing direction (Iino and Kojima, 2012; Larvière and Gagnon, 1998). From figure 23 it can be seen that the magnitude of the joint reaction forces in the anterior-posterior and medial lateral directions during some parts of the downswing were decreasing for the top down model, whilst at the same time, were increasing for the bottom up model. This was also the case for all components of joint moments. In some instances, this even led to a positive force or moment for the bottom up model at the same time as a negative moment for the top down model. This was an indication that, for open chain movements, through periods of high acceleration, inverse dynamics solutions can be subject to errors which have the capacity to significantly affect the interpretation of resultant joint moments depending on which model is used.

Table 11 Absolute peak segment angular acceleration differences in the global coordinate system during the backswing and downswing. Peak angular accelerations were averaged across all swings and participants.

	Absolute peak angular acceleration ( $\text{rad/s}^2$ )								
	Backswing			Downswing			Difference		
	X	Y	Z	X	Y	Z	X	Y	Z
<b>Top down segments</b>									
Club	85	77	63	515	724	385	430	647	323
Right forearm	84	69	62	736	535	558	652	466	496
Upper trunk	38	46	20	120	104	90	82	58	70
<b>Bottom up segments</b>									
Pelvis	26	47	18	106	91	60	80	44	42
Right thigh	29	38	27	141	232	138	112	193	111
Right shank	21	36	28	52	89	64	31	53	37

Differences in the measured and predicted vertical ground reaction forces during the slower parts of the swing, i.e. at takeaway, reflected the whole body mass modelling errors. For example, the geometric model for the participant shown in figure 21 overestimated whole body mass by 2.7 kg ( $\approx 27$  N), and the vertical ground reaction force difference at take-away was approximately 35N. The geometric model predicted whole body mass with a mean error of 1.1 kg (1.4%) for the 8 participants and the largest difference was 4.8 kg (5.0%). Mean and peak vertical force differences during the backswing were under 10 N and not significant. This was similar to lifting studies which reported peak differences of 5.5 N in the vertical direction (Kingma, De Looze, et al., 1996). This was especially encouraging as Kingma et al. (1996) adjusted individual segment densities in order to compensate for whole body mass modelling error. This mass modelling error was also apparent in the joint reaction force differences; from figure 22 it can be seen that there is a clear vertical force offset during the backswing. At take-away the vertical force at the T8/T9 joint from the top down model was approximately 32 N higher than the bottom up model. This difference was therefore approximately equal to the whole body mass modelling error.

A comparison of joint moments from the top down and bottom up models at the T8/T9 joint provided additional information with regard to validation; errors in the estimation of joint rotation centres, segment's centres of mass, segmental moments of inertia as well as error in the point of application of the ground reaction force yield residual moments without generating residual force (De Looze et al., 1992; Kingma, De Looze, et al., 1996). There was a noticeable offset between flexion-extension moments during the backswing for top down and bottom up models which was present in all swings (figure 23). Whilst this validation method was unable to determine which model was the most accurate, other studies have suggested the bottom up model provided the best estimate of joint moments (De Looze et al., 1992; Kingma, De Looze, et al., 1996; Larvière and Gagnon, 1998). The basis of this argument is that the trunk which in these studies was included in the top down model is the most difficult to model due to 1) difficulties in obtaining a reliable estimate of trunk COM due to breathing causing volumetric changes and the varied density of the trunk tissues, 2) the trunk being the least rigid body segment so that there are large movements of the centre of mass within the trunk when the participant bends forward, 3) the trunk having the largest mass and as such errors in the centre of mass can have

a strong influence on lateral bending and flexion-extension moments (Kingma, De Looze, et al., 1996). For this study the trunk was split between the two models; the top down model included the upper trunk and the bottom up model included the mid trunk segment. Therefore, errors in modelling the trunk were distributed more evenly between the top down and bottom up models than previous studies. A source of error unique to the bottom up model was the measurement of the ground reaction force. In particular, errors may have been introduced in the calculation of the point of application of the ground reaction force; this would affect moments not forces and therefore explains the absence of a similar offset in the force comparisons. Errors in the point of application of the ground reaction force may have been due to 1) errors in the force plate measurements, 2) errors in the alignment of the Polhemus coordinate system with the force plate coordinate system, 3) errors in the alignment of the metal distortion correction function (see mapping, section 5.4.2) and the Polhemus coordinate system.

Previous studies concerned with the validation of inverse dynamics solutions have investigated lifting tasks (De Looze et al., 1992; Kingma, De Looze, et al., 1996; Larvière and Gagnon, 1998; Plamondon et al., 1996), balance recovery (Robert et al., 2007), trunk movements (Iino and Kojima, 2012) and the golf swing at slow speed (Tsai, 2005). For two dimensional symmetric lifting, Kingma et al. (1996) found peak GRF differences were significant for horizontal components exemplified by differences of 28.0 N and 20.4 N for the anterior-posterior and medial-lateral components respectively. For the golf swing, peak GRF differences were higher. However, during the backswing the difference followed the same pattern as lifting with significant differences for horizontal forces of 37.5 N and 45.4 N for posterior-anterior and lateral bending components respectively. During the downswing, peak GRF differences were significantly different for all components with the model overestimating the ground reaction force magnitude in all directions. Horizontal peak GRF differences reached 331 N (table 6). This high horizontal GRF difference for the golf swing could be due to the highly asymmetric nature of the movement in comparison to lifting movements, the higher acceleration of the segments and the increased complexity of the movement.

Iino and Kojima (2012) investigated the validity of inverse dynamics solutions for fast and large rotational movements of the trunk. Peak joint moments of 156 Nm and 188 Nm were of similar magnitudes to the downswing for lateral bending and flexion-extension respectively (120 Nm and 147 Nm respectively, table 9). However, for axial rotation, peak moments were 38 Nm and therefore most similar to moments generated during the backswing. It was reported that the same level of validity could be achieved for fast and large trunk movements as lifting tasks with mean RMS errors less than 10 Nm for all tasks and components (Iino and Kojima, 2012). For the downswing median RMS differences reached 49.5 Nm (table 10). This difference in results may have been due to the nature of the trunk rotations; movements were performed in isolation of each other and concentrated on rotation of the pelvis and upper trunk segments only. Therefore, although the speed was high, the complexity of the movement was limited and other segments such as the arms and legs would have had less influence on the estimated moments at the L5/S1 joint. Tsai (2005) investigated the validity of inverse dynamics derived joint moments at the L5/S1 joint during a slow speed golf swing. Mean RMS joint moment differences were lower than reported here; 11.1 Nm, 13.2 Nm and 9.5 Nm for lateral bending, flexion-extension and axial rotation respectively. However, it is important to note that this validation was performed on "slow speed" swings. Although no information on trunk rotation speed was provided, the 'slow speed' movements were likely to be controlled and not entirely representative of real golf swings. Hence, errors from soft tissue motion caused by wobbling mass which increase with acceleration (Denoth et al., 1985) were likely to have had a smaller effect on the results.

A limitation of these methods of validation was that nothing could be learnt about the individual sources of error or how they contribute to the total residual error.

Furthermore, these methods were unable to provide information about the error at different joints and how this error propagates through the kinematic chain. Top down/bottom up comparisons by their nature do not account for two sources of error; the orientation of the anatomical coordinate system and the joint centre location of the joint where the two models meet (Kingma, De Looze, et al., 1996), in this case the mid trunk segment.

Other methods of validation that have been used by previous studies include a comparison between the measured anterior-posterior position of the centre of mass and the predicted COM. This equality can only be evaluated during static tasks and was therefore not applicable to this study. A comparison of predicted and known loads at the hands has been used for validation of a lifting task (De Looze et al., 1992). For lifting, determination of the loads at the hands was relatively simple and could be calculated analytically. For the golf swing, measurement of the forces acting on the hands is a complex task; an instrumented club with strain gauges in the grip has been used in the past (Koike et al., 2006) however this is a technically difficult solution to implement. Furthermore, the accuracy with which forces at the hands could be measured is likely to be less than the accuracy with which ground reaction forces can be measured. Therefore a comparison of the predicted and measured GRF was the preferred method of validation.

#### **4.5. Conclusion**

Differences in ground reaction forces, joint reaction forces and joint moments at the T8/T9 joint were higher for the downswing than the backswing. This increase in modelling error may have been due to the increase in acceleration of the body segments during the downswing which was greatest for the upper body segments. The high acceleration, complex nature of the golf swing resulted in a reduced validity compared to previous studies concerned with lifting, fast trunk rotations and slow speed golf swings. A comparison of joint forces and moments at the T8/T9 joint from a top down and bottom up model did not account for error in the orientation of the anatomical coordinate system and the joint centre location of the mid trunk joint where the two models meet since they are included in both analyses. A comparison of the measured and predicted GRF is advantageous as it compares two completely independent measures. However, this method of validation will not be affected by errors in moment arms or segment moments of inertia. Furthermore, since all body segments are included in the prediction of the GRF the reported residual may be maximised due to the accumulation of error as calculations proceed down the kinematic chain.

In the absence of a 'gold standard' measurement, these validation methods provide a useful way to compare the validity of inverse dynamics solutions. However, each has

its own limitations and only limited information can be extracted from such analyses. Therefore, to fully explore the effect of errors in input variables on joint forces and moments derived using inverse dynamics analysis, knowledge of the uncertainty in inverse dynamics solutions is required.

## 5. Quantification of Inaccuracy Magnitudes

### 5.1. Identification of inaccuracies

The aim of this section is to identify the inaccuracies in input parameters that will be used in the uncertainty analysis of inverse dynamics solutions. It is important that all input parameters and sources of error be considered in order that the analysis explores the uncertainty as a totality and results are realistic. The sources of error that can be quantified through experiments will be identified whilst those that cannot will be subject to an in depth literature review from which inaccuracy bounds will be extracted. In this thesis the terms error, inaccuracy and uncertainty are defined as in Reimer et al. (2008); *error* refers to the difference between the true value and a calculated or measured value; *inaccuracy* is defined as the range of error associated with an input variable to an inverse dynamics model or calculation and *uncertainty* is the magnitude of the maximum possible error in inverse dynamics analysis.

The following equations were used to calculate three dimensional segment net joint reaction forces (*JRF*) and net joint moments (*JM*) (Robertson et al., 2004);

$$\overline{JRF}_{prox} = m\vec{a}_{CM} - m\vec{g} - \overline{JRF}_{dist}$$

Equation 5.1

Where  $\overline{JRF}_{prox}$  is the vector describing the proximal joint reaction force,  $m$  is the segment mass,  $\vec{a}_{CM}$  is the linear acceleration vector of the centre of mass,  $m\vec{g}$  is the gravity force vector and  $\overline{JRF}_{dist}$  is the distal force vector,

$$\overline{JM}_{prox,x} = I_{XX}\alpha_x + (I_{ZZ} - I_{YY})\omega_{ZZ}\omega_{YY} - (d_{1x} \times JRF_{prox,x}) - (d_{2x} \times JRF_{dist,x}) - \overline{JM}_{dist,x}$$

Equation 5.2

$$\overline{JM}_{prox,y} = I_{YY}\alpha_y + (I_{XX} - I_{ZZ})\omega_{XX}\omega_{ZZ} - (d_{1y} \times JRF_{prox,y}) - (d_{2y} \times JRF_{dist,y}) - \overline{JM}_{dist,y}$$

Equation 5.3

$$\overline{JM}_{prox,z} = I_{ZZ}\alpha_z + (I_{YY} - I_{XX})\omega_{YY}\omega_{XX} - (d_{1z} \times JRF_{prox,z}) - (d_{2z} \times JRF_{dist,z}) - \overline{JM}_{dist,z}$$

Equation 5.4

Where  $\overline{JM}_{prox}$  is the vector describing the proximal joint moment,  $I$  is the moment of inertia matrix,  $\alpha$  is the angular acceleration matrix,  $\vec{d}_1$  is the vector of the  $xyz$  distance between the COM and the proximal joint centre and  $\vec{d}_2$  is the vector of the  $xyz$

distance between the COM and the distal joint centre and  $\overline{JM}_{dist}$  is the distal joint moment vector.

These equations assume that the local coordinate system is aligned with the principle axis of the segment. Given the equations above, net joint moments are a function of segment principle moments of inertia  $I_{XX}, I_{YY}, I_{ZZ}$ , segment angular acceleration  $\alpha$ , segment angular velocity  $\omega$ , ground reaction forces  $GRF$  (for the ankle joints), distal and proximal moment arms  $\vec{d}_1, \vec{d}_2$  respectively, and the proximal and distal joint reaction force  $\overline{JRF}_{prox}, \overline{JRF}_{dist}$  respectively;

$$JRF = f(m, \vec{d}_{CM}, \overline{JRF}_{dist})$$

Equation 5.5

$$JM = f(I, \alpha, \omega, JRF, GRF, \vec{d}_1, \vec{d}_2, \overline{JRF}_{prox}, \overline{JRF}_{dist})$$

Equation 5.6

Figure 24 & figure 25 show the parameters used to calculate net joint reaction forces and net joint moments using inverse dynamics and the steps used to derive them. The inaccuracy of the parameters highlighted in pink will be quantified in the subsequent sections of this chapter.

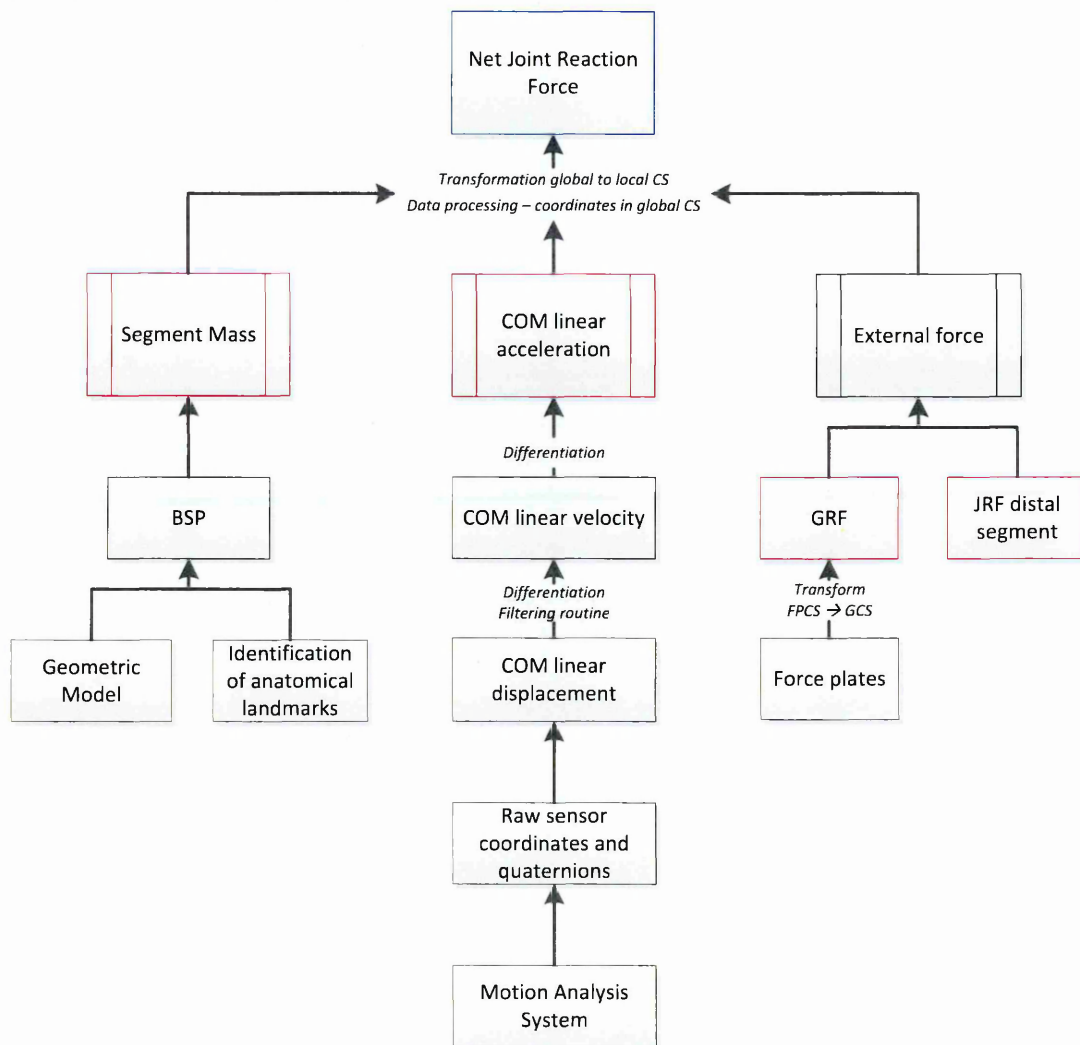


Figure 24 Flow chart of parameters used in the computation of the proximal net joint reaction force using inverse dynamics. BSP = body segment parameters; COM = centre of mass; GRF = ground reaction forces; JRF = joint reaction force; FPCS = force plate coordinate system; LCS = local coordinate system; GCS = global coordinate system. Pink boxes indicate input parameters which were included in the uncertainty analysis.



### 5.1.1. Sources of Inaccuracy

Table 12 shows the sources of inaccuracy that will be quantified experimentally and those which will be extracted from the literature. The majority of inaccuracy parameters will be determined experimentally and will therefore be specific to the data collection methods used in this thesis. It was not possible to quantify soft tissue artefact and joint centre location error using experiments due to ethical, time and cost constraints. An in-depth literature review will be used to inform the quantification of these inaccuracies. Refer to APPENDIX O: Table of Assumptions, pg. 59, for a summary of the assumptions made during the quantification of inaccuracy parameters.

Table 12 Methods of error quantification for input parameters

Parameter	Sub parameter	Inaccuracy quantification method	
		Experimental	Literature Review
Segment mass	-	✓	
COM linear acceleration	sensor linear displacement	✓	
External force	force plate measurements	✓	
Segment moment of inertia	-	✓	
COM angular acceleration	sensor angular position	✓	
COM angular velocity	sensor angular position	✓	
Moment arm length	COP	✓	
	Segment COM	✓	
	joint centre location		✓
Moment arm length	STA		✓
COM linear acceleration	STA		✓
COM angular acceleration	STA		✓
COM angular velocity	STA		✓

COM = centre of mass; COP = centre of pressure; STA = soft tissue artefact

## 5.2. Body Segment Parameter Inaccuracy

### 5.2.1. Introduction

Body segment inertial parameters (BSP) are required for the kinetic analysis of human motion (Durkin and Dowling, 2006). Individual specific BSP can be estimated using geometric models. Geometric models generally make two primary assumptions; the shape of the segment can be accurately modelled using a series of symmetric geometric shapes and the density of a segment is uniform throughout (Wicke and Dumas, 2010). One of the simplest methods that have been used to quantify the accuracy of geometric models is a comparison between the measured total body mass and the total mass predicted by summing all segments of the geometric model. Jensen (1978) used a photogrammetric method to generate a model consisting of a series of

stacked elliptical discs, two centimetres wide. An average error of estimated whole body mass of less than 2% was reported (Jensen, 1978). Hatze (1980) developed a more complex 17 segment model using 242 anthropometric measurements and a non-uniform density function; the average whole body mass error of the model was less than 3% with a maximum error of 5%. Yeadon (1990) developed a geometric model consisting of 40 geometric solids specified by 95 anthropometric measurements. 'Stadium' solids were used to represent the trunk segments which were reported to provide a more accurate approximation of the trunk cross-section than ellipsoids (Yeadon, 1990). The associated whole body mass estimation error of 2.3% was comparable to more complex models. In all three of these studies a maximum of just 4 participants were used for validation. Whilst Yeadon (1990) and Hatze (1980) used a mix of males and females, they were all of similar age and described as 'athletic'. Jensen (1978) selected a more diverse sample of participants who were representative of three different body types however only 3 participants were used in total and they were all boys of similar age. Therefore, the accuracy of the models reported may differ when applied to larger, more diverse samples. Assessments of accuracy using total body mass comparisons do not provide any information on the ability of these models to estimate individual segment mass. Furthermore, this method does not provide any measure of the accuracy with which segment centre of mass or moments of inertia can be estimated.

Dual X-Ray Absorptiometry (DXA) is used to measure bone density and body composition and has been accepted as a standard against which geometric models can be compared for accuracy (Durkin and Dowling, 2003; Wicke and Dumas, 2010; Wicke et al., 2009). Wicke et al. (2009) measured the accuracy of trunk inertia estimates from 5 geometric models using 25 females and 25 males of college age. DXA had the ability to accurately measure the volume and density of the whole body and comparisons of segment mass, centre of mass and moments of inertia were possible. Results showed that individual segment mass errors were higher than predicted using whole body mass comparisons (Wicke et al., 2009). This increase in error may have also been due in part to a larger and more diverse sample which included both males and females. These studies were limited to assessing the accuracy of the moment of inertia about anteroposterior axis due to the attenuation elements of the DEXA scan

being in the frontal plane. Durkin and Dowling (2006) performed a similar comparison of the lower leg BSP estimates. The geometric model proposed by Hanavan (1964) was compared to a newly developed elliptical solid model. A large and diverse sample of 40 participants was divided into four categories according to age and sex. Results showed that accuracy of BSP estimates was dependant on the age and gender of the group (Durkin and Dowling, 2006). However such technologies are expensive and can be inaccessible. It has been shown that inertia estimates are most sensitive to the volume function with density having only a small secondary influence (Ackland et al., 1988; Wicke and Dumas, 2010).

The aim of this study was to determine the accuracy with which a geometric model was capable of estimating the geometry of human body segments and subsequently, by assuming uniform density, estimate BSP. Participants were recruited based on body type so that the sample was representative of the participants used for golf swing data collection. The results were used to define segment specific inaccuracy bounds for mass, centre of mass location and principle moments of inertia.

### 5.2.2. Methods

#### *Participants*

Participants were three healthy males ( $21.0 \pm 2.0$  years;  $103.1 \pm 30.3$  kg;  $188.4 \pm 4.3$  cm) with different body morphologies classified using Heath & Carter's (1967) method as a balanced ectomorph (BE), a balanced mesomorph (BM) and a mesomorph-endomorph (ME) (table 13). Ethics approval was granted by the faculty of Health and Wellbeing at Sheffield Hallam University (see appendix H, I and J for participant information sheet and ethics forms).

**Table 13 Somatotype classification of the three participants using the Heath Carter method (1967)**

	Balanced Ectomorph	Mesomorph Endomorph	Balanced Mesomorph
Age (year)	19	21	23
Height (cm)	187.8	193.0	184.4
Mass (kg)	79.9	137.3	92.0
Somatotype	2 - 3 - 4	6 - 8 - 0.5	3 - 8 - 1.5
Sum 7 (mm)	58.6	152.0	72.5
% Body Fat	11.3	22.8	13.6

### *Geometric Model*

The Golphysics geometric model used in this study was described previously (section 3.1.5, pg. 50). For this study the head, feet and hand segments were excluded from the analysis. During scanning, the participant was required to hold stands either side of them to minimise movement. Therefore, complete scans of the hands could not be obtained. Similarly, the feet were in contact with the floor so could not be scanned. Although scans of the head and neck were attempted, they were un-usable due to too much participant movement.

### *Data Collection*

To assess participant somatotype, bone widths, depths and skin fold measurements were taken using a tape measure and body callipers as required. Height and weight were also measured. The volumes of the torso, dominant leg and arm were measured using a Model Maker D100 non-contact laser scanner (Metris, Leuven, Belgium).

To minimise body movement during scanning, participants gripped two tripods placed either side of them. The tripods were adjusted to a suitable height for each participant. Participants wore thin, elasticated body suits to eliminate interference caused by body hair during the scan (figure 26). The locations of 67 anatomical landmarks were identified with retro-reflective markers (10mm) stuck to the body suits. These were visible on the scans during data processing.



Figure 26 The three participants marked up in preparation for the laser scan, left to right: mesomorph-endomorph, balanced mesomorph, balanced ectomorph

### Data Analysis

After data cleaning and surface reconstruction, segmentation of the scanned data was performed with reference to the anatomical landmarks identified with retro-reflective markers. Three markers were required to create segmentation planes; medial, lateral and posterior markers were placed at each segmentation plane. The scanned segments were imported into Pro-Engineer (Parametric Technology Co., Waltham, MA, USA) and BSP were calculated using the software assuming a uniform segment density (table 1, pg. 54). These values were used as the criterion value against which all other data was compared. Each segment's local coordinate system was defined such that the  $x$ ,  $y$  and  $z$  axes were along the antero-posterior (ap), longitudinal (long) and medio-lateral (ml) planes respectively. Measurements of the width and depth at each segmentation plane were taken directly from the scanned segments using the Pro-Engineer software. The width was defined as the distance between the lateral and medial markers and depth was the distance between the anterior and posterior markers. Segment length was the distance from the centre of the distal segmentation plane to the centre of the proximal plane. This data was then used to build the stadiums and elliptical solids representing each body segment according to Yeadon (1990). Formula for calculation of mass, centre of mass and principle moments of inertia of stadium solids and elliptical solids are presented in the appendix (APPENDIX A: Body segment parameters equations, pg. 1).

### 5.2.3. Results

Table 14 Error in segment mass estimates for the three participants

Segment	Mean mass(kg)±SD		Error (kg)			Mean Error (kg)±SD	Mean % error±SD		
			ME	BM	BE				
Forearm	1.83	±0.56	0.11	0.06	0.10	0.09	±0.02	5.02	±1.68
Upper Arm	3.20	±1.07	0.44	0.49	0.70	0.54	±0.14	18.79	±9.27
Shank	5.27	±1.69	0.63	0.40	0.07	0.37	±0.28	6.54	±4.20
Thigh	15.50	±4.54	-2.16	-0.78	0.60	-0.78	±1.38	-3.45	±8.21
Pelvis	11.49	±2.95	0.52	0.57	-0.25	0.28	±0.46	2.48	±4.38
Mid trunk	17.18	±3.66	1.43	0.98	2.01	1.47	±0.52	8.90	±4.21
Upper trunk	15.12	±6.19	-0.44	-0.16	-0.17	-0.25	±0.16	-1.61	±0.36

Mean and SD error are compared to laser scan. A negative value indicates the model underestimated the mass of the segment. ME = mesomorph-endomorph; BM = balanced-mesomorph; BE = balanced-ectomorph.

Table 15 Error in longitudinal centre of mass (COM) estimates for the three participants

Segment	Mean COM location (cm) $\pm$ SD		Error (cm)			Mean Error (cm) $\pm$ SD	Mean % error $\pm$ SD		
			ME	BM	BE				
Forearm	11.22	$\pm$ 0.47	-0.15	-0.25	0.74	0.11	$\pm$ 0.55	1.01	$\pm$ 4.90
Upper Arm	10.82	$\pm$ 1.05	0.09	0.25	-0.46	-0.04	$\pm$ 0.37	-0.17	$\pm$ 3.35
Shank	26.48	$\pm$ 1.80	-0.36	-0.11	0.28	-0.07	$\pm$ 0.32	-0.21	$\pm$ 1.19
Thigh	27.36	$\pm$ 1.76	-0.03	-1.11	-0.44	-0.53	$\pm$ 0.55	-1.89	$\pm$ 1.87
Pelvis	6.75	$\pm$ 0.29	-0.01	0.02	-0.05	-0.01	$\pm$ 0.04	-0.16	$\pm$ 0.52
Mid trunk	12.36	$\pm$ 1.70	0.13	0.51	0.95	0.53	$\pm$ 0.41	4.06	$\pm$ 2.73
Upper trunk	8.29	$\pm$ 1.40	-0.05	-0.28	-0.16	-0.16	$\pm$ 0.11	-2.12	$\pm$ 1.58

Mean and SD error are compared to laser scan. A negative value indicates the model underestimated the mass of the segment. ME = mesomorph-endomorph; BM = balanced-mesomorph; BE = balanced-ectomorph.

Table 16 Error in antero-posterior centre of mass (COM) estimates for the three participants

Segment	Mean COM location (cm) $\pm$ SD		Error (cm)			Mean Error (cm) $\pm$ SD	
			ME	BM	BE		
Forearm	-0.12	$\pm$ 0.49	-0.42	0.24	0.54	0.12	$\pm$ 0.49
Upper Arm	0.03	$\pm$ 0.41	0.21	-0.51	0.21	-0.03	$\pm$ 0.41
Shank	-1.16	$\pm$ 0.17	1.04	1.09	1.36	1.16	$\pm$ 0.17
Thigh	1.58	$\pm$ 0.64	-1.49	-0.99	-2.26	-1.58	$\pm$ 0.64
Pelvis	0.38	$\pm$ 0.48	-0.85	-0.40	0.10	-0.38	$\pm$ 0.48
Mid trunk	0.72	$\pm$ 0.69	-0.08	-0.63	-1.45	-0.72	$\pm$ 0.69
Upper trunk	-0.05	$\pm$ 0.22	0.08	-0.18	0.25	0.05	$\pm$ 0.22

Mean and SD error are compared to laser scan. A negative value indicates the model underestimated the mass of the segment. ME = mesomorph-endomorph; BM = balanced-mesomorph; BE = balanced-ectomorph.

Table 17 Error in medio-lateral centre of mass (COM) estimates for the three participants

Segment	Mean COM location (cm) $\pm$ SD		Error (cm)			Mean Error (cm) $\pm$ SD	
			ME	BM	BE		
Forearm	0.24	$\pm$ 0.11	-0.12	-0.33	-0.26	-0.24	$\pm$ 0.11
Upper Arm	-0.62	$\pm$ 0.35	0.68	0.94	0.25	0.62	$\pm$ 0.35
Shank	1.09	$\pm$ 0.17	-0.94	-1.28	-1.04	-1.09	$\pm$ 0.17
Thigh	-0.37	$\pm$ 0.63	0.88	0.57	-0.33	0.37	$\pm$ 0.63
Pelvis	0.40	$\pm$ 0.60	-0.95	0.25	-0.48	-0.40	$\pm$ 0.60
Mid trunk	-0.43	$\pm$ 0.27	0.37	0.20	0.73	0.43	$\pm$ 0.27
Upper trunk	0.16	$\pm$ 0.65	-0.24	0.53	-0.76	-0.16	$\pm$ 0.65

Mean and SD error are compared to laser scan. A negative value indicates the model underestimated the mass of the segment. ME = mesomorph-endomorph; BM = balanced-mesomorph; BE = balanced-ectomorph.

Table 18 Error in moment of inertia ( $I_{ap}$ ) estimates about the antero-posterior axis for the three participants

Segment	Mean MOI (kgcm <sup>2</sup> ) $\pm$ SD		Error (kgcm <sup>2</sup> )			Mean Error (kgcm <sup>2</sup> ) $\pm$ SD	Mean % error $\pm$ SD		
			ME	BM	BE				
Forearm	113.2	$\pm$ 48.2	6.8	9.1	5.4	7.1	$\pm$ 1.9	7.0	$\pm$ 3.3
Upper Arm	264.6	$\pm$ 96.1	-1.2	-7.1	34.1	8.6	$\pm$ 29.2	4.0	$\pm$ 10.4
Shank	833.1	$\pm$ 360.9	230.3	114.9	58.1	134.4	$\pm$ 40.2	15.5	$\pm$ 5.8
Thigh	3048.3	$\pm$ 1222.5	-516.4	-144.5	76.7	-194.7	$\pm$ 156.4	-4.2	$\pm$ 8.2
Pelvis	804.2	$\pm$ 430.2	86.1	83.1	-35.6	44.5	$\pm$ 69.4	5.9	$\pm$ 11.2
Mid trunk	1804.1	$\pm$ 501.0	247.9	253.9	167.1	222.9	$\pm$ 48.5	12.8	$\pm$ 4.1
Upper trunk	1164.5	$\pm$ 811.9	-11.9	65.2	15.2	22.8	$\pm$ 39.1	3.4	$\pm$ 4.4

Mean and SD error are compared to laser scan. A negative value indicates the model underestimated the mass of the segment. ME = mesomorph-endomorph; BM = balanced-mesomorph; BE = balanced-ectomorph.

Table 19 Error in moment of inertia ( $I_{long}$ ) estimates about the longitudinal axis for the three participants

Segment	Mean MOI (kgcm <sup>2</sup> ) $\pm$ SD		Error (kgcm <sup>2</sup> )			Mean Error (kgcm <sup>2</sup> ) $\pm$ SD	Mean % error $\pm$ SD		
			ME	BM	BE				
Forearm	20.3	$\pm$ 11.8	1.8	0.3	1.5	1.2	$\pm$ 0.8	6.6	$\pm$ 5.3
Upper Arm	60.1	$\pm$ 39.8	20.0	5.1	-1.3	7.9	$\pm$ 10.9	8.9	$\pm$ 11.8
Shank	107.8	$\pm$ 64.9	14.3	8.3	-1.3	7.1	$\pm$ 7.9	5.6	$\pm$ 6.9
Thigh	959.1	$\pm$ 499.6	-316.2	-137.3	20.6	-144.3	$\pm$ 168.5	-11.0	$\pm$ 13.2
Pelvis	1208.9	$\pm$ 498.3	92.1	28.2	-19.7	33.5	$\pm$ 56.1	2.2	$\pm$ 3.7
Mid trunk	2288.4	$\pm$ 697.6	295.1	186.7	-195.5	95.4	$\pm$ 257.7	3.5	$\pm$ 11.4
Upper trunk	2349.9	$\pm$ 1500.8	-290.5	-172.9	-105.9	-189.8	$\pm$ 93.5	-8.5	$\pm$ 1.4

Mean and SD error are compared to laser scan. A negative value indicates the model underestimated the mass of the segment. ME = mesomorph-endomorph; BM = balanced-mesomorph; BE = balanced-ectomorph.

Table 20 Error in moment of inertia ( $I_{mi}$ ) estimates about the medio-lateral axis for the three participants

Segment	Mean MOI ( $\text{kgcm}^2$ ) $\pm$ SD	Error ( $\text{kgcm}^2$ )			Mean Error ( $\text{kgcm}^2$ ) $\pm$ SD	Mean % error $\pm$ SD	
		ME	BM	BE			
Forearm	110.1 $\pm$ 47.2	8.7	11.4	4.8	8.3 $\pm$ 3.3	8.3	$\pm$ 4.7
Upper Arm	254.1 $\pm$ 91.9	6.6	0.3	30.5	12.4 $\pm$ 15.9	5.5	$\pm$ 7.9
Shank	825.4 $\pm$ 361.4	237.1	112.4	57.2	135.6 $\pm$ 92.2	15.7	$\pm$ 5.9
Thigh	2848.6 $\pm$ 1099.8	-510.0	-125.2	81.1	-184.7 $\pm$ 300.0	-4.2	$\pm$ 8.9
Pelvis	1642.0 $\pm$ 842.4	86.1	83.1	-35.6	44.5 $\pm$ 69.4	2.7	$\pm$ 5.3
Mid trunk	2377.8 $\pm$ 1237.5	247.9	253.9	167.1	160.7 $\pm$ 90.5	7.5	$\pm$ 4.6
Upper trunk	2752.5 $\pm$ 1738.7	-11.9	65.2	15.2	22.8 $\pm$ 39.1	1.3	$\pm$ 1.7

Mean and SD error are compared to laser scan. A negative value indicates the model underestimated the mass of the segment. ME = mesomorph-endomorph; BM = balanced-mesomorph; BE = balanced-ectomorph.

### Segment Mass

Segment mass was estimated with a mean error of 5.2% (table 14). The highest percentage errors were for the upper arm and mid trunk with errors of 18.8% and 8.9% respectively. The mass of the upper trunk was consistently underestimated for all three participants and the mass of the thigh and pelvis was both under- and over-estimated.

### Segment COM

Mean COM error was 0.19, 0.23 and 0.07 cm along the longitudinal (table 15), antero-posterior (table 16) and medio-lateral (table 17) axes respectively. Errors in centre of mass location ranged from 0.01 – 1.58 cm. Centre of mass location was the most accurately estimated parameter exemplified by errors of less than 2.2% for the shank, thigh, pelvis, upper arm, forearm and upper trunk for longitudinal centre of mass location.

### Segment MOI

Mean MOI error was 6.3% for the antero-posterior axis (table 18), 1.04% for the longitudinal axis (table 19) and 5.2% in for the medio-lateral axis (table 20). MOI about the medio-lateral and anteroposterior axes for the limb segments tended to be less accurately estimated than trunk segments. In particular the shank segment produced the highest errors of 15.5% and 15.7% for MOI about the anteroposterior and medio-lateral axes respectively. For longitudinal MOI the thigh, upper arm and upper trunk produced high errors of -11.0%, 8.9% and -8.5% respectively. For medio-lateral and antero-posterior moments of inertia, the shank was the least accurately estimated segment with errors of 15.5% and 15.7% respectively.

#### 5.2.4. Discussion

The aim of this study was to quantify the error involved in the estimation of BSP using a geometric model similar that developed by Yeadon (1990). Error in mass, centre of

mass and moments of inertia estimations for individual segments was quantified which was an advancement over previous studies which had considered only whole body mass errors (Hatze, 1980; Jensen, 1978; Yeadon, 1990). It should be noted however that the methods used in this study were not able to consider BSP error caused by the uniform density assumption which would affect whole body mass comparisons. Overall the findings were similar to previous studies which used DXA scanning for gold standard comparisons (Durkin and Dowling, 2003; Wicke and Dumas, 2010; Wicke et al., 2009). Past studies have reported average whole body mass errors of 2, 3 and 2.3% for geometric models developed by Jensen (1978), Hatze (1980) and Yeadon (1990) respectively. Consideration of individual segment errors resulted in a mean segment mass error of 5.2%. For the upper arm the mean error was 18.79% which was considerably larger than had been previously reported for whole body mass comparisons (Hatze, 1980; Jensen, 1978; Yeadon, 1990).

The mass of the upper arm and mid trunk segments were the least accurately estimated with errors of 18.8% (0.54 kg) and 8.9% (1.5 kg) respectively. Figure 27 shows a scanned upper arm segment overlaid with an elliptical solid used to model its shape. The orientation of the segmentation plane at the shoulder and the eccentric shape particularly at the proximal end made this segment difficult to model with a symmetrical elliptical solid. Similarly, the shape eccentricity at the top of the thigh (figure 28) resulted in the mass being both over and underestimated for the three participants with different morphologies. Of the trunk segments, the mid trunk mass was the least accurately estimated. The mid trunk was the only trunk segment to be modelled using a single stadium solid. The accuracy of trunk segment inertial parameter estimates has been suggested to be highly dependent on the number of shapes used to model it (Erdmann, 1997). It is possible that the volume of the mid trunk and therefore the mass could be better approximated with the use of more than one stadium solid. However this would increase the number of anatomical landmarks to be digitised and therefore calibration time which may not be desirable. The upper trunk mass was consistently underestimated for all participants; this highlighted the difficulty in capturing the contours of the upper chest even though 3 stadium solids were used to model it. The forearm mass was estimated with good accuracy exemplified by a mean error of 0.09 kg (5.02%). Figure 28 shows the shape of the forearm was approximated by two stacked elliptical solids well. There was no clear

relationship between segment mass and the error magnitude. Observation of the images (figure 27 & figure 28) suggests error was more a result of the eccentricity of the shape of the segment which did not necessarily relate to volume or mass of the segment.

The geometric model assumed the centre of mass was located along the longitudinal axis of each segment so that the geometric shapes were symmetric about the longitudinal axis. Mean COM error was 0.02, 0.2 and 0.07 cm in the longitudinal, antero-posterior and medio-lateral axes respectively. For the longitudinal COM this was equivalent to a 0.07% error making the COM the most accurately estimated parameter. Moment of inertia was estimated with the least accuracy supporting the findings of Wicke et al. (2009). To calculate the MOI, the mass and moment arm length (i.e. the distance from the proximal end to the COM) are used, therefore any error in these parameters will contribute to the error in moments of inertia. In addition, the squaring of the moment arm means this error will contribute to a greater extent (two times the amount) than mass error due to propagation of error (Taylor, 1997).

The majority of upper trunk moments of inertia were underestimated. This was most likely due to the cavities created using stadium solids to represent the shape; this finding was also reported for ellipses (Wicke et al., 2009). Trunk MOI estimates were less accurate for the medio-lateral axis than the antero-posterior axis. This was due to the transverse cross sectional areas of the trunk not being symmetrical especially about the medio-lateral axis (Wicke and Dumas, 2010). Previous studies have reported this to be particularly predominant in areas such as the lumbar region for obese people or the chest area of a muscular man (Wicke and Dumas, 2010).

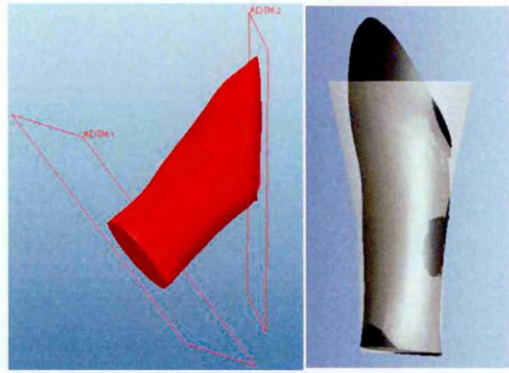


Figure 27 Upper arm segment (ME); segmentation planes of the upper arm defined by anatomical landmarks; Right: scanned upper arm in dark grey with transparent elliptical solid overlaid aligned at the origin along the longitudinal axis.

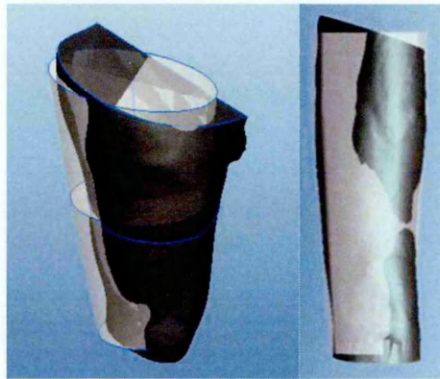


Figure 28 Left: Thigh (ME), solid thigh scanned segment and transparent stacked elliptical solids aligned at origin along the longitudinal axis. Right: Forearm (ME), solid forearm scanned segment and transparent stacked elliptical solids aligned at the origin along the longitudinal axis.

In this study the laser scans used for 'gold standard' comparisons were limited to volume measurements and did not include measurements of segment density. This meant error in BSP as a result of the uniform density assumption was not considered and this may change the reported error. However, it has been shown that BSP estimates are most sensitive to the volume function with density having only a small secondary influence (Ackland et al., 1988; Wicke and Dumas, 2010). Furthermore, the scanning technique used was advantageous over previously used DEXA scanning techniques which were limited to assessing the accuracy of the moment of inertia about one plane (Durkin and Dowling, 2006).

Accuracy of BSP estimates has been shown to be dependent on the age, body type and gender (Durkin and Dowling, 2003; Wicke et al., 2009). It was therefore important that participants were chosen which represented the diversity expected during golf swing data collection trials. For this reason the sample consisted of three body types; participants were classified as mesomorph-endomorph, balanced-mesomorph and a

balanced-ectomorph. The sample covered the extremes of the body types likely to be included in the data collection. Only men were used since no women were to be included in the golf swing trials. Large standard deviations in the results indicated high inconsistencies for all parameters. This was due to the small sample size used due to time constraints in both for testing and data analysis. However it was anticipated that using extreme body types would produce results which reflected the variability expected for a larger sample size. A further limitation was that the analysis did not include the hand, foot, neck or head segments. The participant was required to hold stands either side of them to minimise movement during scanning. This made scanning the hands impossible. Similarly the feet were in contact with the floor so could not be scanned. Scans of the neck and head were attempted but were un-usable since there was too much movement. The segments used were able to provide sufficient information as to the expected overall performance of the geometric model.

#### 5.2.5. Conclusion

This study quantified the error in body segment parameter estimation for the adapted Yeadon geometric model (1990). Three male participants were used which were representative the diversity expected during golf swing data collection trials and three extremes of body type were used. The results were specific to the geometric model used. Errors in segment mass and centre of mass location propagated to moment of inertia error which was the least accurately estimated parameter.

#### *Generation of BSP inaccuracy values*

Three sets of inaccuracy values were formed to reflect the variability in the results (table 21); sets 1, 2 and 3 represented the minimum, mean absolute and maximum error respectively. For COM along the antero-posterior and medio-lateral axes, uncertainties were added to nominal values in units of cm rather than percentages; since the geometric model assumed the COM was along the longitudinal axis resulting in 100% error. For all other parameters uncertainties are percentages of respective nominal values. Since the hand, foot, neck and segments were not included in the study the uncertainty of their BSP parameters are assumed to be the mean uncertainty of all other segments.

Table 21 Three sets of inaccuracies (Set 1: minimum error, set 2: mean error, set 3: maximum error) for body segment parameters including mass, centre of mass and moment of inertia.

Segment	Set 1	Set 2	Set 3
<b>Shank</b>			
Mass (%)	1.70	6.54	9.25
COM ap (cm)	1.04	1.16	1.36
COM long (%)	0.21	0.44	1.28
COM ml (cm)	0.94	1.09	1.28
Iap (%)	8.87	15.50	19.26
Ilong (%)	2.04	5.60	11.13
Iml (%)	8.85	15.70	19.10
<b>Thigh</b>			
Mass (%)	3.45	5.05	10.74
COM ap (cm)	0.99	1.58	2.26
COM long (%)	0.12	1.89	3.84
COM ml (cm)	0.33	0.37	0.88
Iap (%)	4.20	4.23	12.13
Ilong (%)	4.00	13.66	21.08
Iml (%)	4.20	4.32	13.00
<b>Pelvis</b>			
Mass (%)	2.34	2.48	6.23
COM ap (cm)	0.10	0.38	0.85
COM long (%)	0.09	0.16	0.32
COM ml (cm)	0.25	0.40	0.95
Iap (%)	4.22	5.90	9.36
Ilong (%)	1.97	2.20	5.18
Iml (%)	2.70	5.76	16.70
<b>Mid trunk</b>			
Mass (%)	6.26	8.90	13.76
COM ap (cm)	0.08	0.72	1.45
COM long (%)	1.22	4.06	6.65
COM ml (cm)	0.20	0.43	0.73
Iap (%)	3.28	12.80	14.07
Ilong (%)	3.50	8.16	12.89
Iml (%)	7.02	7.50	10.68
<b>Upper trunk</b>			
Mass (%)	1.26	1.61	1.97
COM ap (cm)	0.05	0.08	0.25
COM long (%)	0.53	2.12	3.68
COM ml (cm)	0.16	0.24	0.76
Iap (%)	3.40	6.41	9.15
Ilong (%)	0.57	8.50	12.50
Iml (%)	0.40	1.30	8.10
<b>Upper arm</b>			
Mass (%)	9.98	18.79	28.47
COM ap (cm)	0.03	0.21	0.51
COM long (%)	0.17	0.83	3.88
COM ml (cm)	0.25	0.62	0.94
Iap (%)	0.33	4.00	15.91
Ilong (%)	4.08	8.90	18.94
Iml (%)	0.13	5.50	14.51
<b>Forearm</b>			
Mass (%)	1.01	3.85	6.94
COM ap (cm)	0.12	0.24	0.54
COM long (%)	1.01	1.28	6.64
COM ml (cm)	0.12	0.24	0.33

---

Quantification of Inaccuracy Magnitudes

lap (%)	4.00	4.05	10.61
llong (%)	2.03	6.60	12.35
lml (%)	5.30	8.30	13.73
<b>Mean absolute values</b>			
Mass (%)	3.94	6.52	11.05
COM ap (cm)	0.34	0.62	1.03
COM long (%)	0.48	1.54	3.76
COM ml (cm)	0.32	0.48	0.84
lap (%)	4.04	7.56	12.93
llong (%)	2.60	7.66	13.44
lml (%)	4.09	6.91	13.69

---

---

### 5.3. Force Plate Measurement Inaccuracy

#### 5.3.1. Introduction

In human movement analysis force plates are used to measure ground reaction forces (GRF) and centre of pressure (COP) positions of the feet. Force plates are usually equipped with either strain-gauge transducers or piezoelectric transducers. Errors in force plate measurements manifest themselves in the measured ground reaction forces as well as in the calculation of the centre of pressure (Hsieh et al., 2011). Manufacturer's documentation provides information on the accuracy of force plates however factory specified errors can be altered by various means, such as improper installation, cable malfunction and electrical faults (Chockalingam et al., 2002). Further inaccuracies can be caused by the discrepancy in the alignment of the global coordinate system and plate reference coordinate system (Kim et al., 2007). Most studies which report GRF and COP errors are concerned with application of new *in situ* calibration procedures followed by the application of various correction techniques (Bobbert and Schamhardt, 1990; Collins et al., 2009; Gill and O'Connor, 1997; Goldberg et al., 2009; Hall et al., 1996). *Ad hoc* designed devices that have been used to assess the accuracy of force plate data include instrumented poles (Holden et al., 2003; Lewis et al., 2007), a framework-attached pendulum (Fairburn et al., 2000), a passive moveable plate (Browne and O'Hare, 2000), rectangular steel feet (Middleton et al., 1999), and orthogonal rails and trolleys (Gill and O'Connor, 1997). Most calibration procedures applied static loads or used rigid objects which applied load relatively slowly. This type of loading was often not representative of the load patterns experienced during use (Lewis et al., 2007). Dynamic tests have been recommended for applications which are dependent on a dynamic force profile such as gait or indeed the golf swing (Fairburn et al., 2000). Lewis et al. (2007) used an instrumented pole in combination with a motion analysis system in order to perform *in-situ* calibration checks. The addition of the force transducer provided a full six component load measurement. This was an advance on previous similar studies which, in the absence of a force transducer, could not assess the accuracy of the force magnitude (Holden et al., 2003). Error in force plate measurements has been reported to range from 0.1% to 2.8% (Gill and O'Connor, 1997) of the force magnitude and from 0.5mm (Hsieh et al., 2011) to 8.4mm (Lewis et al., 2007) for COP position along a single axis. The variation in force plate measurement error reported in the literature may be due to the

magnitude of loads applied which ranged from 50-1600N, the type of loading, the force plate model and the *in-situ* conditions. It has also been shown that the position of load application effected the results; COP and GRF errors generally increased with distance from the centre of the force plate (Chockalingam et al., 2002; Hsieh et al., 2011; Middleton et al., 1999). Therefore, experiments attempting to fully characterise the accuracy of force plates should include measurement positions that cover the whole area of the platform.

The aim of this study was to quantify errors in force plate measurements. Errors in force and centre of pressure measurements for two force plates (KISTLER type 9128C, Kistler Instrumente AG, Winterthur, Switzerland) were experimentally quantified *in situ*. An instrumented pole was used to manually apply dynamic forces which were able to provide an independent measure of force for comparison to force plate measurements. Force was applied to 77 different known locations to characterise error over the entire surface of each force plate.

### 5.3.2. Method

#### *Data collection*

Tests were performed with two force plates (KISTLER type 9128C, Kistler Instrumente AG, Winterthur, Switzerland), installed in the laboratory floor according to the manufacturer's specifications. The plates were connected to electronic amplifier units (KISTLER type 5233A, Kistler Instrumente AG, Winterthur, Switzerland) and the 8 output signals from each unit were sampled at 600 Hz.

#### Measurement of static vertical force error

For quantification of vertical force error, static weights of  $\approx 10\text{kg}$  increments from  $\approx 10\text{-}50\text{kg}$  were placed on the centre of each the plate and the force output was recorded directly using Bioware software (Kistler Instrumente AG, Winterthur, Switzerland). The static weights were measured on weighing scales ( $\pm 0.01\text{g}$ ) and compared to force plate output. For further information see APPENDIX C: Force plate and force transducer calibration, pg. 7.

#### Measurement of dynamic vertical and shear force error

For application of point loads an instrumented pole was used (figure 30). The instrumented pole allowed for measurement of both magnitude and direction of

forces applied to the force plate. The design of the pole insured only axial loads were applied; the top end of the pole was a pointed tip that fitted into the handle so that no torque could be applied, therefore loading was along the long axis of the pole only. The other end was a pointed tip which could be accurately placed at the desired location. The pole was fitted with nine retro-reflective markers (figure 1). The pole's orientation was determined from the tracked optical marker positions using a 12 camera motion analysis system (Motion Analysis Corporation, Santa Rosa, CA, USA) operating at 200Hz. During a static trial, markers were placed on the 'TIP' and 'TOP' of the pole in order to define a direction vector along the centre of the pole's axis (figure 29). During dynamic trials, the TIP and TOP markers were removed and the remaining seven tracked markers were used to recreate the virtual position of the TIP and TOP markers using Visual3D (C-Motion, Inc., Rockville, MD, USA). Though this only required the coordinates of three or more non-collinear points, seven markers were used to increase the accuracy of the estimation of the position of these virtual points (Challis, 1995).

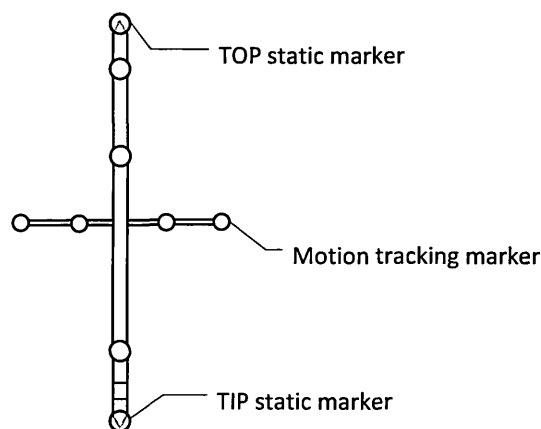


Figure 29 Instrumented pole showing static trial set up with 'TIP' and 'TOP' markers shown. These were removed during dynamic trials.

The axial pole force was measured by a transducer (type STA-1-100, LCM Systems, Newport, UK) located near the tip of the pole. The transducer had an accuracy of  $<\pm 0.03\%$  of rated load (100 kg). Calibration of the transducer was achieved as follows; the transducer was dynamically loaded for 5 seconds in the centre of the force plate. The pole was held upright so that applied loads were vertical. The load ranged from 0-430N which was the upper limit of the transducer. Vertical force data from the force plate measured directly through BioWare software was compared to output from transducer. This process was repeated three times in the centre of each plate. Lines

of best fit were fitted to plots of transducer output against reference vertical force in order to extract conversion equations. Vertical force output from the force plate was calibrated using the results from the static vertical force tests with known weights described above. For further information see APPENDIX C: Force plate and force transducer calibration, pg. 7.

The amplified output of the transducer was sampled through the A/D channels of the motion analysis system allowing synchronous data collection. A rectangular grid placed on the force plate surface had lines with spacings of 50 mm (11 lines parallel to the x axis and 7 lines parallel to the y axis). Measurements were made at each of the 77 grid intersections (figure 30). At each grid intersection, the pole was dynamically loaded for 5 seconds by the experimenter. The pole was moved through a range of angles to generate shear forces ( $\approx \pm 50^\circ$  from the vertical).

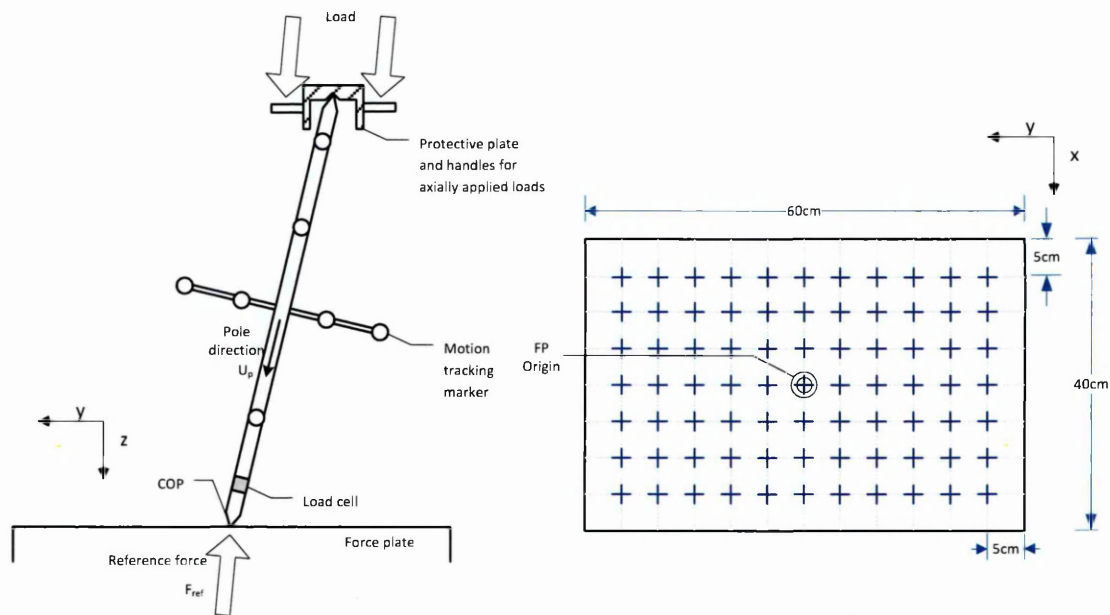


Figure 30 Experimental apparatus used for quantification of force plate measurement error. (Left) Instrumented pole used for application and dynamic point loads with marker set during measurement trials. (Right) A grid was laid on plate surface to apply forces at known positions. The crosses represent each of the 77 measurement locations which were spaced 5cm apart.

### Data Analysis

For dynamic trials, force output from the force plates were compared to the reference transducer forces. The resultant force  $F_{ref}$  measured by the transducer was decomposed into its three mutually perpendicular components  $F_x, F_y, F_z$ . The locations of the virtual TIP and TOP markers along the vertical axis of the pole were

recreated using the remaining seven markers in Visual 3D (C-Motion, Rockville, MD). For conversion to the force plate coordinate system three markers placed at known locations on the force plate were used to create a local coordinate system during a static trial. Transformation matrices were created to transform tracked coordinates of the TIP and TOP markers to local coordinate system and then force plate coordinate system. The length of the pole  $l$  was defined as shown in equation 5.7;

$$l = \sqrt{(TIP_x - TOP_x)^2 + (TIP_y - TOP_y)^2 + (TIP_z - TOP_z)^2}$$

Equation 5.7

The following relationships were used to determine the individual force components  $F_x, F_y, F_z$ ;

$$\cos\theta_x = \frac{TIP_x - TOP_x}{l}$$

Equation 5.8

$$\cos\theta_y = \frac{TIP_y - TOP_y}{l}$$

Equation 5.9

$$\cos\theta_z = \frac{TIP_z - TOP_z}{l}$$

Equation 5.10

$$F_x = F\cos\theta_x$$

Equation 5.11

$$F_y = F\cos\theta_y$$

Equation 5.12

$$F_z = F\cos\theta_z$$

Equation 5.13

where subscripts  $x, y$  and  $z$  refer to the coordinates in the force plate coordinate system;  $\theta_{x,y,z}$  is the angle of the pole in the force plate coordinate system along the  $x, y$  and  $z$  axis respectively. Reference COP measurements in the  $x$  and  $y$  directions were taken from the grid placed on top of the plates. The grid was computer generated and aligned with all four sides of each plate. The sixteen channel force plate

output was converted to force and COP using calculations in appendix (APPENDIX B: Force platform calculations).

### 5.3.3. Results

For static vertical loading experiments, the maximal difference between the measured vertical force  $F_z$  and actual  $F_z$  was 1% (table 22). This was within accuracy specifications given by the manufacturer. For dynamic point loading experiments the accuracy of the force plate was decreased; at the centre of the plate the mean absolute error in  $F_z$  was 3.1% (2.1 N) of the mean force. The maximum  $F_z$  error increased to 11.8% of the actual  $F_z$  when the plate was loaded away from the centre. Mean shear force error was 27.5% (2.3 N) and 94.1% (2.5 N) for  $F_x$  and  $F_y$  respectively. During dynamic loading trials forces in the  $x$ ,  $y$  and  $z$  directions reached 200, 100, and 400 N respectively.

Table 22 Mean absolute errors for force and centre of pressure measurements

	Mean	±SD	Max	Min
<b>Static loads</b>				
$F_z$ (N)	0.90	±0.58	2.20	0.045
$F_z$ (%)	0.36	±0.26	1.00	0.045
<b>Dynamic loads</b>				
$F_x$ (N)	2.3	±1.5	8.5	0.5
$F_x$ (%)	27.5	±38.6	408.5	3.9
$F_y$ (N)	2.5	±1.8	9.1	0.4
$F_y$ (%)	94.1	±169.2	1527.9	5.5
$F_z$ (N)	4.9	±2.2	10.9	1.7
$F_z$ (%)	3.7	±2.1	11.8	1.2
COP $_x$ (cm)	0.55	±0.37	1.27	0.02
COP $_y$ (cm)	0.79	±0.54	1.98	0.07

Errors for COP $_x$  ranged from 0.002 – 1.27 cm and for COP $_y$  ranged from 0.007 to 1.98 cm (table 22 & table 23). Figure 31 shows vectors of mean COP errors at each of the grid positions. The vector pattern is symmetrical about the centre of the plate. Vectors appear to be attracted to the closest transducer outlined in black.

**Table 23** Mean COP absolute error for both plates showing distance away from plate centre, all measurements are in cm

Point of application y axis	Point of application x axis							
	±0cm		±5cm		±10cm		±15cm	
	COPx	COPy	COPx	COPy	COPx	COPy	COPx	COPy
±0cm	0.09	0.18	0.43	0.73	0.12	0.10	0.84	0.14
±5cm	0.20	0.30	0.40	0.73	0.07	0.45	0.80	0.44
±10cm	0.19	0.63	0.62	0.95	0.24	0.93	0.80	1.07
±15cm	0.10	0.53	0.86	1.06	0.81	1.71	0.87	1.81
±20cm	0.27	0.31	0.94	0.51	1.10	0.25	1.03	0.95
±25cm	0.23	1.09	0.47	1.23	0.68	1.58	0.99	1.37

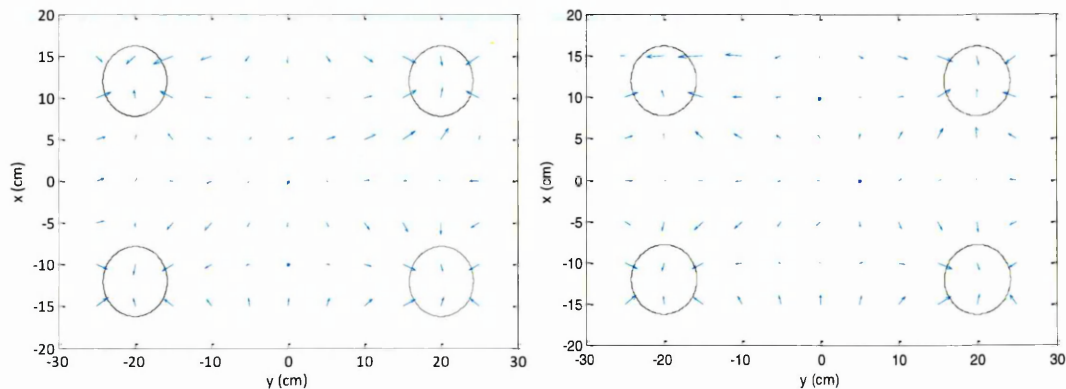


**Figure 31** Vectors of mean centre of pressure errors (blue arrows) for each grid position on each force plate showing position of transducers in platforms outlines in black

#### 5.3.4. Discussion

Vertical force measurement using static weights was shown to be highly accurate with a mean error of 0.36% for forces ranging between  $\approx 96$ -476 N. For dynamic point load tests, in the centre of the plate, this error was increased to 3.7% for forces of similar magnitudes (10 - 400 N). This was consistent with previous studies which reported that the accuracy of force plates for single point loads was less than for a load distributed over a greater area (Bobbert and Schamhardt, 1990; Middleton et al., 1999; Schmiedmayer and Kastner, 2000). In most biomechanics applications, including golf, forces are applied over a finite area in the form of a distribution of pressure and shear force (Schmiedmayer and Kastner, 2000). Previous studies have indicated that the magnitude of the error is dependent on the load distribution; the error in COP for a point load has been shown to be higher than a load distributed load across the sole of the foot during the stance phase of gait (Schmiedmayer and Kastner, 2000). Bobbert and Schamhardt (1990) suggested this was because point application of force would result in greater bending on the plate than a distributed force and therefore increased

force plate deformation. Therefore, inaccuracies quantified in this study are likely to be representative of the upper bound inaccuracies expected during the golf swing.

The load application technique used in this study insured shear forces were generated in order that the accuracy of shear forces as well as vertical forces could be assessed. The relative error of shear force in the x and y directions were substantially larger than vertical force error. This may in part have been due to the low shear forces generating during testing;  $F_x$  and  $F_y$  had ranges of  $\approx \pm 200$  N and  $\pm 100$  N respectively whilst  $F_z$  had a range of 10-400 N. These increased errors may have been partially caused by a reduced signal to noise ratio for smaller forces (Chockalingam et al., 2002). Additionally, shear force reference measurement required sensor tracking to measure pole orientation and the instrumented pole to measure reference forces. Both systems were carefully calibrated although each would have included some measurement error.

The accuracy of centre of pressure deteriorated towards the edges of the force plate, a finding consistent with other studies (Bobbert and Schamhardt, 1990; Middleton et al., 1999). Furthermore, errors seemed to be symmetrical about the centre of the plate and 'attracted' to the transducer closest to the point of force application, a finding consistent with Bobbert and Schamhardt (1990). In general, mean COP errors in the x direction were smaller than the y direction however this was not always the case for each individual measurement. Previous studies reported accuracy in the x direction twice that of the accuracy in the y direction (Bobbert and Schamhardt, 1990; Gill and O'Connor, 1997; Middleton et al., 1999). This difference between studies may have been due to the dissimilarities in loading conditions; previous studies used static vertical loading so shear force was minimised and did not contribute to COP error to the same extent as in this study. Individual force component error has been ascribed to the non-linearity of a transducer's response to the applied load, cross talk, different offset voltages of individual transducers and electronic noise (Browne and O'Hare, 2000; Schmiedmayer and Kastner, 1999). However, since a non-uniform response was observed, particularly for COP error, this is an indication that, in addition to the possible causes of errors listed, there was deformation of the top plate (Browne and O'Hare, 2000; Schmiedmayer and Kastner, 1999). This bending possibly introduced systematic errors which were dependent on point of force application (Cappello et al.,

2011) as shown by the greatest non linearity near the edges of the plate (Cedraro et al., 2009; Chockalingam et al., 2002). Centre of pressure error may have been higher in this study than others due to the relatively small vertical force magnitude; Chockalingam et al. (2002) found that a minimum vertical force of 113 N was required for COP prediction within 0.3 cm.

### 5.3.5. Conclusion

The accuracy with which force plates can measure forces and centre of pressure for a single point load were determined in this study. Previous studies have suggested that the expected accuracy during the golf swing where pressure is distributed over a larger area, i.e. the sole of the foot, would be greater than indicated in this experiment (Bobbert and Schamhardt, 1990; Middleton et al., 1999; Schmiedmayer and Kastner, 2000). In addition, maximum force magnitudes produced in this experiment were lower than maximum forces expected during the golf swing which may also have produced accuracy than would be expected (Chockalingam et al., 2002). Errors quantified were therefore representative of the higher range of errors expected during the golf swing. Maximum errors may be most similar to the error expected during the follow through on the back foot when most of the weight would be on the front foot. Three sets of inaccuracies representing the minimum (set 1), mean (set 2) and maximum (set 3) errors for force and centre of pressure are shown in table 24. Inaccuracies were based on dynamic loading as this experimental condition better replicated dynamic loading of the feet during the golf swing.

Table 24 Inaccuracy sets for force and centre of pressure measurements

	Set 1	Set 2	Set 3
<b>Dynamic loading</b>			
Fx (N)	0.5	2.3	8.5
Fy (N)	0.4	2.5	9.1
Fz (N)	1.7	4.9	10.9
COPx (cm)	0.02	0.55	1.27
COPy(cm)	0.07	0.79	1.98

## 5.4. Kinematic Measurement Inaccuracy

### 5.4.1. Introduction

In biomechanics, electromagnetic tracking systems are used to measure the motion of the body. They allow for a full three dimensional analysis of motion with 6 degrees of

freedom. Systems such as the Polhemus Liberty system (Polhemus Inc., Colchester, VT, USA) can use up to 16 sensors with a sampling rate of up to 240 Hz suitable for capturing high velocity motion such as the golf swing. Polhemus is an electromagnetic tracking system consisting of a magnetic field transmitter and receiver (sensor) couple. The position and orientation of each sensor is determined through a comparison of the strength of received signal to the strength of the emitted pulse. Unlike stereo photogrammetric systems, tracked data from electromagnetic systems benefit from requiring little or no post processing and they do not suffer from marker occlusion during movement trials. However, such electromagnetic motion analysis systems are subject to inaccuracies in sensor measurements due to noise. For example, for the Polhemus Liberty system, the manufacturer states that within a 90 cm source to sensor collection range the static accuracy of the system running at 240 Hz is 0.76 mm RMS for the  $x$ ,  $y$  and  $z$  positions and  $0.15^\circ$  RMS for orientation (Polhemus Inc., Colchester, VT, USA). Richards et al. (1999) found that the accuracy of an electromagnetic system was linearly dependant on the sensor's distance from the transmitter, even inside the manufacturers recommended volume. Furthermore, electromagnetic systems can be affected by distortions caused by metal or conductive material near the sensors or transmitter (Bull et al., 1998; Jaberzadeh et al., 2005; Milne et al., 1996; Ng et al., 2009). Calibration or 'mapping' techniques can be used to account for static errors. Calibration techniques compensate for distortion error through experimentally established differences between the true sensor positions and that reported by the tracking system. Mapping techniques assume that transmitter's position and surrounding metal does not move (Kindratenko, 2000).

The aim of this study was to assess the accuracy of the Polhemus Liberty system (Polhemus Inc., Colchester, VT, USA) for the quantification of kinematic measurement noise. To achieve this, the variance of sensor position and orientation was quantified (Challis and Kerwin, 1996). The effect of metal distortion from the force plates that sit within the test volume was also investigated. In the second part of this study, a map was applied to correct for distortions in sensor measurements caused by the metal force plates which were situated within the test volume. The effect of mapping on the measurement noise was quantified.

### 5.4.2. Methods

#### Data collection

The experimental set up was identical to that used for golf swing data collection (figure 32) and the test volume had dimensions of 100 x 250 x 200 cm in the  $x$ ,  $y$  and  $z$  directions respectively (figure 35). The electromagnetic system used was the Polhemus Liberty system (Polhemus Inc., Colchester, VT, USA). The transmitter or source box was securely positioned on a plastic stand that remained in a fixed position throughout testing. Within the test volume two force plates (KISTLER type 9128C) were embedded into the floor (figure 32 and figure 35). Each force plate had dimensions of 40 x 60 cm and was situated approximately 40 cm from the emitter in the  $x$  direction and -80 cm in the  $y$  direction.

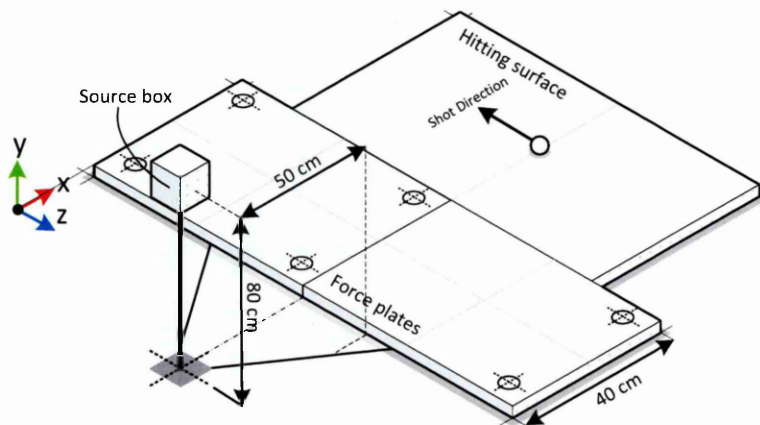


Figure 32 Lab set-up showing position of transmitter (source box) in relation to force plates.

Noise magnitude was assessed by mounting two sensors to a rigid bracket and measuring the variance in their relative positions and orientations at a number of locations within the test volume. Two Polhemus Liberty sensors (Polhemus Inc., Colchester, VT, USA) were securely fixed to a plastic bracket approximately 49.5 cm apart (figure 33).

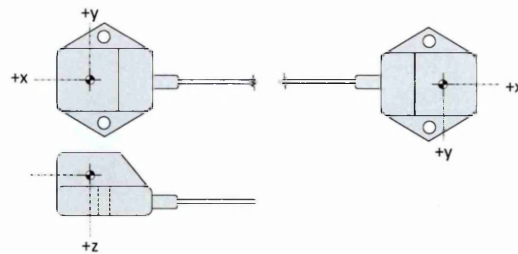


Figure 33 Polhemus sensors. Positions of the electrical centre and local coordinate system of sensors are shown.

A custom made plastic tube apparatus had slots at three predefined heights (65 cm, 145 cm and 225 cm) which the bracket holding the sensors could sit in (figure 34). Static measurements were made with the bracket held parallel to the  $z$  and  $y$  axes in turn. Dynamic measurements were made by manually spinning the bracket through  $360^\circ$  in the vertical plane at a slow velocity ( $\approx 1.26$  rad/s). A second bracket was used for measurements parallel to the  $x$  axis and horizontal spinning trials ( $\approx 1.26$  rad/s). Sensors were secured 49.5 cm apart. This bracket could slot over the top of the tube apparatus and could be secured at each of the three heights using a dowel. This allowed for static measurements along the  $x$ ,  $y$  and  $z$  axes and dynamic measurements about the horizontal and vertical planes for three heights of 65 cm, 145 cm and 225 cm. The tube apparatus was moved through a grid of 16 positions within the test volume (figure 35). All trials were collected at 240 Hz for 5 seconds.

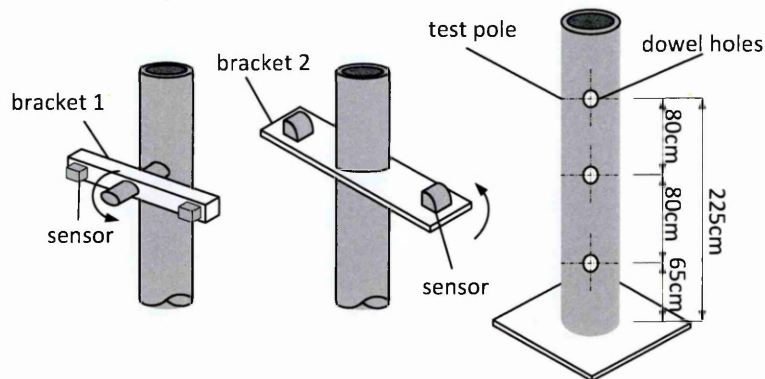


Figure 34 Test pole and brackets upon which sensors were mounted during testing.

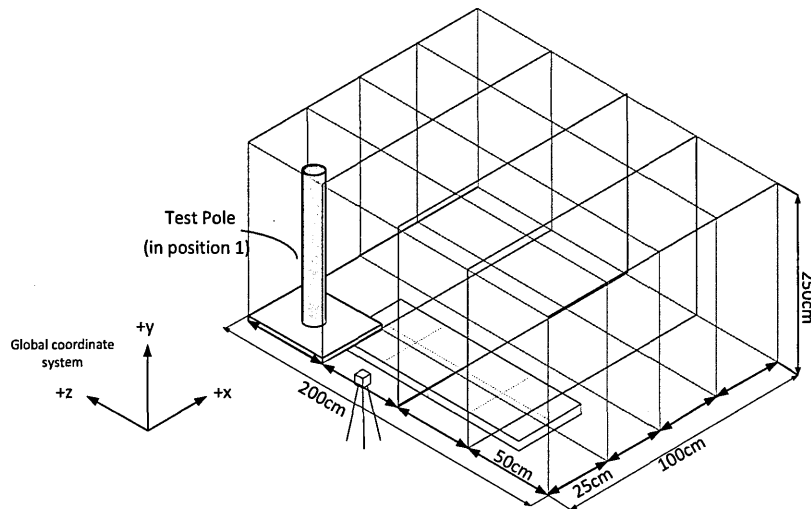


Figure 35 Grid positions for testing. The test pole is shown in the first grid position, there were sixteen grid positions in total which covered a test volume which had dimensions of 100x250x200cm along the x, y and z directions respectively.

### *Mapping*

In second part of the data collection, the effect of mapping on the position and orientation variance was investigated. For further details of the mapping process used by Golphysics see section 3.1.3.2 (pg. 46). To test the effects of mapping the rigid bracket with two sensors fixed to it was used. The bracket was held over the force plates and moved around the test volume above the force plates in a random pattern for 20 seconds. Measurements made outside the map i.e. less than 40 cm from the force plate's surface were removed before data processing. This process was repeated three times. Variance of the relative position and orientation of the sensors was calculated for each trial for comparisons to unmapped data.

### *Data Analysis*

To analyse the random noise in sensor position and orientation the variance of the relative distance and orientation of the two sensors was calculated. This was analogous to the methods used by Challis and Kerwin (1996) to analyse the random noise in kinematic measurements introduced by the digitisation process which quantified the variance in the estimation of the centre of mass and joint orientation angles. Variance ( $var(x)$ ) was defined as follows;

$$var(x) = \frac{1}{N-1} \sum_{i=1}^N (x_i - \mu)^2$$

Equation 5.14

Where  $N$  was the sample size,  $x_i$  the  $i$ th observation, and  $\mu$  the sample mean. At each measurement position data was collected for 5 seconds at 240 Hz and the variance in the relative position and orientation of the two sensors was calculated. Relative measures of position and orientation of the two sensors were used so that dynamic trials could be analysed in the same way as static trials.

### Distance

The resultant Euclidean distance  $D_{RES}$  between the electrical centres of the sensors  $s_1$  and  $s_2$  was calculated as follows;

$$D_{RES} = \sqrt{(s_{1x} - s_{2x})^2 + (s_{1y} - s_{2y})^2 + (s_{1z} - s_{2z})^2}$$

Equation 5.15

where subscripts  $x$   $y$  and  $z$  refer to the global coordinates along the  $x$   $y$  and  $z$  axes respectively.

### Orientation

Unit quaternions were used to represent sensor orientation. For further details on quaternions see section 3.3 (pg. 70). For each frame, quaternions were used to form rotation matrices  $R_G$  for each sensor using standard methods described previously (Equation 3.1, pg. 49). Using the rotation matrices for sensors 1 and 2 in the global coordinate system,  $[R_{G1}]$  and  $[R_{G2}]$ , the matrix of relative positions  $[R_{12}]$  was defined according to Zatsiorsky (1998) as;

$$[R_{12}] = [R_{G1}]^{-1}[R_{G2}]$$

Equation 5.16

From Zatsiorsky (1998), the rotation matrix of Euler angles could be expressed as elements of the 3 x 3 rotation matrix  $[R] = [R_Z][R_{y'}][R_{x''}]$  where  $[R_Z][R_{y'}][R_{x''}]$  are the matrices of sequential rotations for a  $Zy'x''$  rotation sequence;

$$R_{12} = \begin{bmatrix} \cos 11 & \cos 12 & \cos 13 \\ \cos 21 & \cos 22 & \cos 23 \\ \cos 31 & \cos 32 & \cos 33 \end{bmatrix}$$

$$= \begin{bmatrix} \cos \alpha \cos \beta & \cos \alpha \sin \beta \sin \gamma - \sin \alpha \cos \gamma & \cos \alpha \sin \beta \cos \gamma + \sin \alpha \sin \gamma \\ \sin \alpha \cos \beta & \sin \alpha \sin \beta \sin \gamma + \cos \alpha \cos \gamma & \sin \alpha \sin \beta \cos \gamma - \cos \alpha \sin \gamma \\ -\sin \beta & \cos \beta \sin \gamma & \cos \beta \cos \gamma \end{bmatrix}$$

Equation 5.17

Elements in the combined matrix represented direction cosines between axes of the two reference frames, expressed as a function of Euler angles. Euler angles for the  $Zy'x''$  sequence were therefore obtained from the rotation matrix  $[R_{12}]$  as follows;

$$A(Z) = \tan^{-1} \left( \frac{\cos 21}{\cos 11} \right) = \alpha_i$$

Equation 5.18

$$A(y') = \tan^{-1} \left( -\frac{\cos 31}{\sqrt{\cos_{11}^2 + \cos_{11}^2}} \right) = \beta_i$$

Equation 5.19

$$A(x'') = \tan^{-1} \left( -\frac{\cos 31}{\sqrt{\cos_{11}^2 + \cos_{11}^2}} \right) = \gamma_i$$

Equation 5.20

The mean variances of the Euler angles  $var(\alpha)$ ,  $var(\beta)$ ,  $var(\gamma)$  were calculated for each measurement position for both static and dynamic trials.

### 5.4.3. Results

#### *Static trials (unmapped)*

For two sensors separated by a distance of  $\approx 49.5$  cm the mean variance in relative distance during static trials was  $0.03 \text{ cm}^2$  (table 25). The mean variance in the relative orientation of the sensors was  $0.01^{\circ 2}$  (table 25). For displacement and orientation the maximum variance was  $1.45 \text{ cm}^2$  and  $0.45^{\circ 2}$  respectively, which was a large increase from mean values. It is believed that the spread of both the distance and orientation variance was affected by the metal in the force plates. This had the effect of increasing the variance for measurements near to force plates.

Table 25 Variance associated with the measurement of distance and orientation between two sensors for the Polhemus Liberty system

	Variance		
	Mean	Minimum	Maximum
<b>Distance(cm<sup>2</sup>)</b>			
Static	0.026	0.00001	1.451
Dynamic	0.397	0.00052	3.193
<b>Orientation (deg<sup>2</sup>)</b>			
Static	0.010	0.0001	0.445
Dynamic	0.368	0.0007	3.439

### Dynamic trials (Unmapped)

Dynamic trials produced higher mean and maximum variances than static trials for both displacement and orientation. The mean variance was  $0.40 \text{ cm}^2$  and  $0.37^\circ^2$  for displacement and orientation respectively (table 25). Figure 36 shows a histogram of the magnitude of the variance of the distance between the two sensors. The plot aggregates all of the dynamic measurements. Figure 36 also shows a histogram of the magnitude of the variance in relative sensor orientation. Like static trials it is thought that the spread of variance was affected by the metal in the force plates for the measurements made closest to the plates.

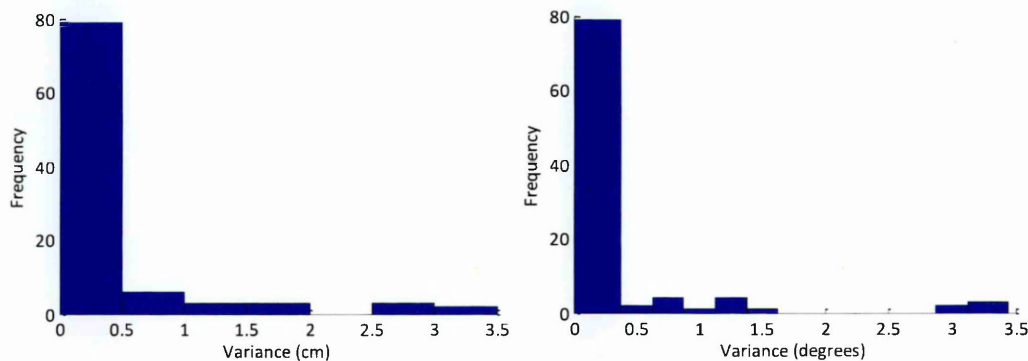


Figure 36 Histograms of variance for dynamic trials associated with the measurement of relative distance (left) and orientation (right) of two sensors for the Polhemus Liberty system

### Effect of force plates

At the lowest measurement height (65 cm), with sensors closest to the force plates, measurement variance was significantly increased for both static (table 26) and dynamic trials (table 27). During these trials the sensors were as low as 40 cm from the force plates. With the exclusion of the lowest set of trials the maximum variance was reduced from  $1.45 \text{ cm}^2$  to  $0.54 \text{ cm}^2$  for displacement and from  $0.45^\circ^2$  to  $0.12^\circ^2$  for orientation for static trials. Similarly, for dynamic trials maximum variance was reduced from 3.19 cm and  $3.44^\circ$  to 1.62 cm and  $1.58^\circ$  for displacement and orientation

respectively. Figure 37 and figure 38 show histograms of the variance of distance and orientation respectively for each of the three measurement heights. For heights of 145 cm and 225 cm the range of variance was substantially reduced for both distance and orientation.

**Table 26** Variance associated with the measurement of distance and orientation between sensors for the Polhemus Liberty system in relation to vertical distance from the force plates for static trials

Vertical distance from force plates (cm)	Variance in displacement (cm <sup>2</sup> )			Variance in orientation (deg <sup>2</sup> )		
	Mean	Min	Max	Mean	Min	Max
65	0.03648	0.00001	1.45061	0.0146	0.0001	0.4454
145	0.02623	0.00001	0.53848	0.0037	0.0001	0.1196
225	0.01626	0.00064	0.40004	0.0124	0.0026	0.0892

**Table 27** Variance associated with the measurement of distance and orientation between sensors for the Polhemus Liberty system in relation to vertical distance from the force plates for dynamic trials

Vertical distance from force plates (cm)	Variance in displacement (cm <sup>2</sup> )			Variance in orientation (deg <sup>2</sup> )		
	Mean	Min	Max	Mean	Min	Max
65	0.7902	0.0034	3.1925	0.814	0.021	3.439
145	0.0303	0.0005	0.1143	0.068	0.001	0.635
225	0.3707	0.0152	1.6209	0.222	0.006	1.576

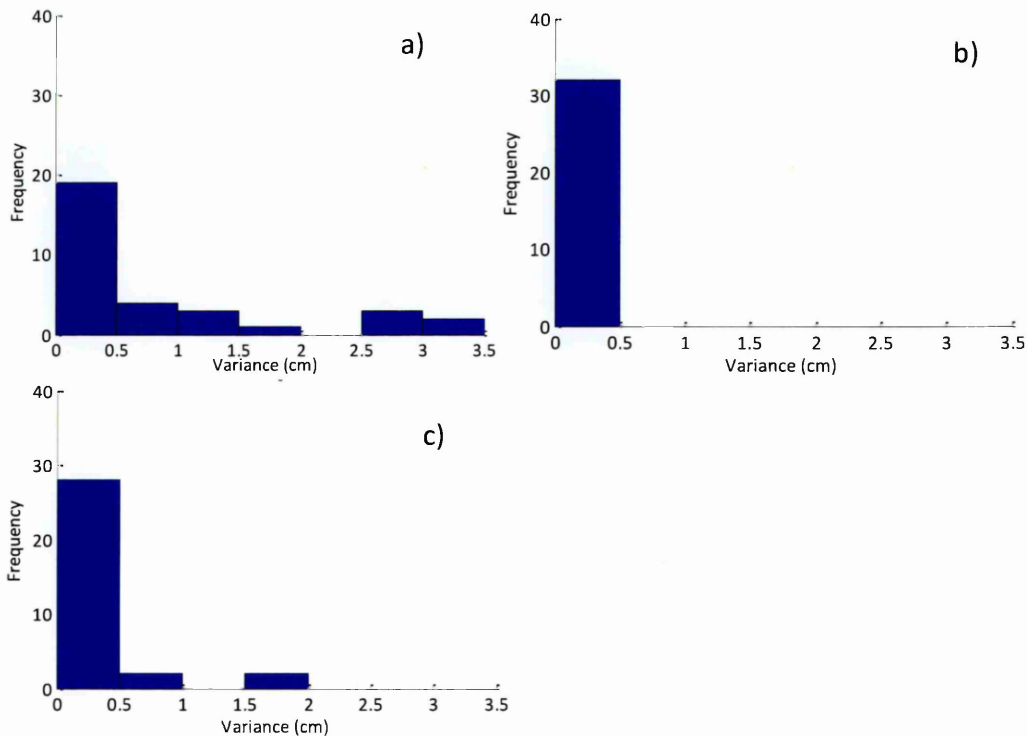


Figure 37 Histogram of variance associated with the measurement of distance between sensors for a) 65cm b) 145cm c) 225cm above the force plates for dynamic trials

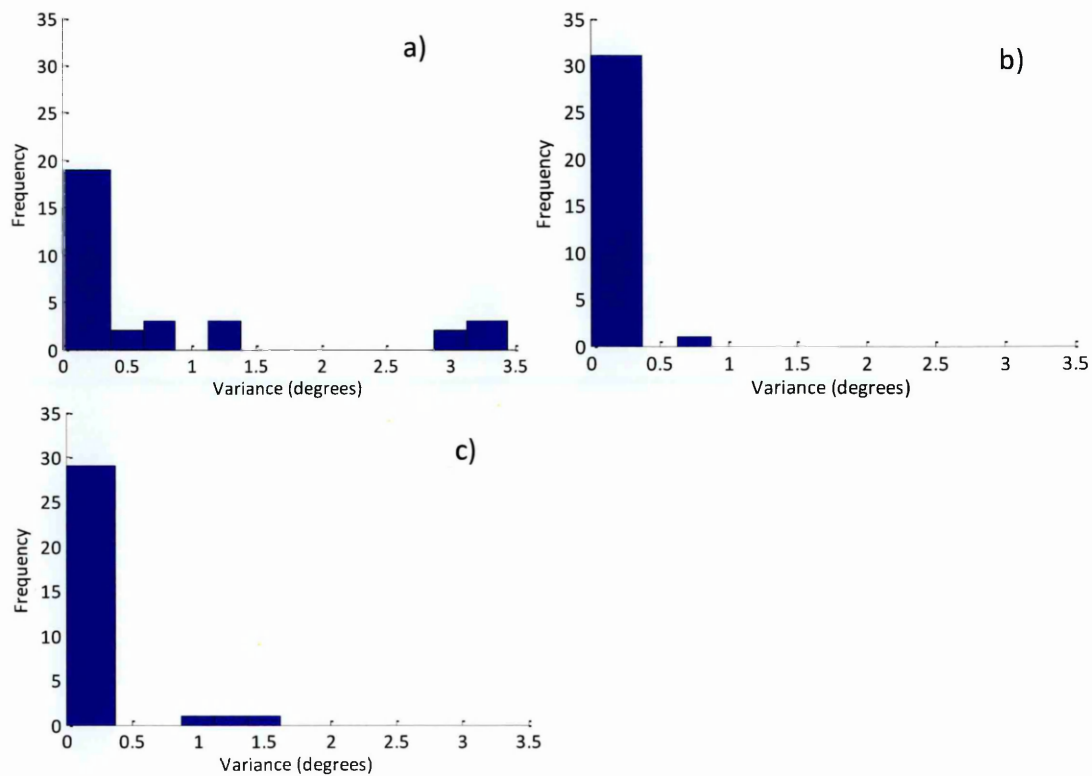


Figure 38 Histogram of variance associated with the measurement of orientation between sensors for a) 65 cm b) 145 cm c) 225 cm above the force plates for dynamic trials

### *Distance from source box*

Figure 39 and figure 40 show the variance plotted against the resultant distance between the sensors and the transmitter for displacement and orientation respectively. Distance was measured as resultant distance from the source box electrical centre to the centre of the bracket upon which the sensors were fixed. These plots exclude the lowest measurements which were affected by distortion from the metal in the force plates; this distortion made the relationship between sensor variance and distance from the transmitter less clear. Some scatter was present which could have been caused by distortions in the magnetic field. Excluding these outliers, there appeared to be a general trend in the data that suggested an increase in transmitter to sensor distance also increased the measurement variance. This relationship was evident for both static and dynamic trials.

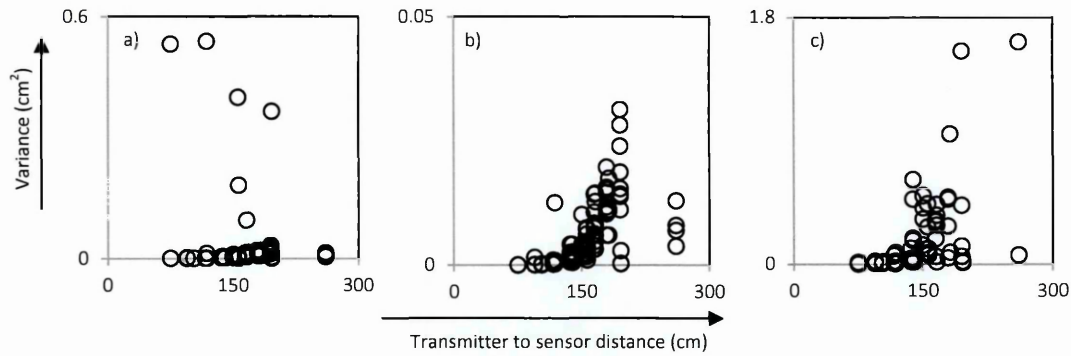


Figure 39 Variance in distance between the two sensors as a function of distance from the transmitter for (a,b) static and (c) dynamic trials. Plot (b) for static trials is a zoomed in version of plot (a); exclusion of outliers highlighted the trend that variance increased with distance from the transmitter.

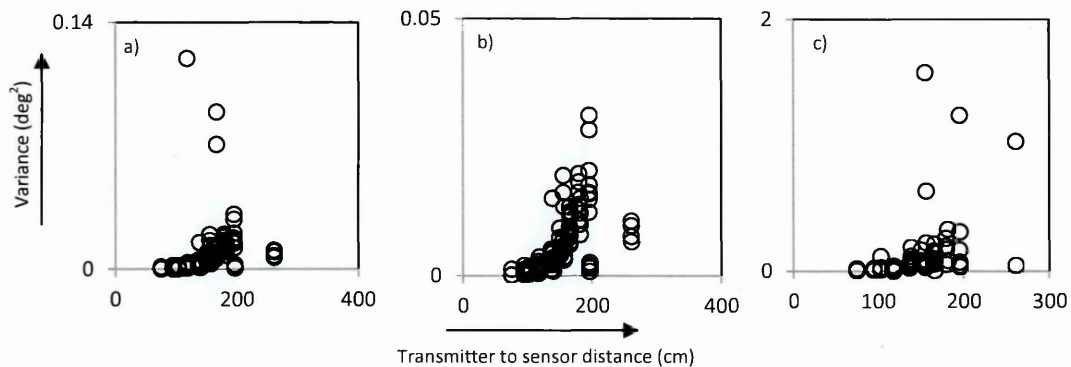


Figure 40 Variance in relative orientation of the two sensors as a function of distance from the transmitter for static (a, b) and dynamic (c) trials. Plot (b) for static trials is a zoomed in version of plot (a); exclusion of outliers highlighted the trend that variance increased with distance from the transmitter.

### Effect of mapping

Mapping was able to reduce the variance of both the relative position and orientation of two sensors within the test volume (table 28). The range of variance in sensor position was reduced from 0.203-0.300  $\text{cm}^2$  to 0.014-0.038  $\text{cm}^2$  using mapping. For orientation, unmapped variance ranged between 0.192-1.579  $\text{deg}^2$ . This range was reduced to 0.044 - 0.461  $\text{deg}^2$  using the map.

The variance of the unmapped trials in table 28 was similar in magnitude to the variance of the dynamic trials in table 25. For example, the mean position variance for dynamic trials was 0.307  $\text{cm}^2$  (table 25). This was comparable to the mean variance of 0.272  $\text{cm}^2$  for unmapped trials in table 18. This was an indication that although the methods used to collect the data were different they produced equivalent results.

Table 28 Variance in the relative position of two sensors for<sup>6</sup> dynamic trials with and without mapping.

	Variance		
	Test 1	Test 2	Test 3
<b>Distance(cm<sup>2</sup>)</b>			
Unmapped	0.203	0.399	0.214
Mapped	0.014	0.014	0.038
<b>Orientation(deg<sup>2</sup>)</b>			
Unmapped			
x	1.208	1.408	0.518
y	0.489	1.320	0.193
z	0.192	1.579	0.991
Mapped			
x	0.333	0.070	0.096
y	0.461	0.044	0.103
z	0.098	0.073	0.074

#### 5.4.4. Discussion

In this study the noise variance of the Polhemus Liberty electromagnetic system was evaluated. The variance of the relative positions and orientations of two sensors fixed to a rigid bracket was calculated at various positions within the test volume. The system was found to have a mean position and orientation variance of 0.03 cm<sup>2</sup> and 0.01°<sup>2</sup> for static trials within a sensor to emitter range of 45 – 200 cm. This was within useful operational ranges but out of the optimal operational range (<90 cm) as specified by the manufacture. Comparisons to other studies was difficult since results were specific to the experimental set up which included metallic force plates. The mean standard deviation ( $\sqrt{var}$ ) for static trials of 0.17 cm and 0.1° was higher than that reported by Richards (1999) who reported a RMS error of 0.01 cm and 0.06° for relative sensor distance and orientation measurements respectively. The differences in results could be attributed to the different systems used and the different measurement ranges; Richards (1999) used Skill Technologies Phoenix system and measurements were made at 45 cm from the transmitter, which was the minimum sensor to transmitter distance used in this study. Additionally, Richards (1999) did not include any metal in close proximity to the sensors. Other similar studies have reported orientation errors of 1.4±0.8° (Ng et al., 2009) and -1.65±0.60° (Pearcy and Hindle, 1989) using the Polhemus 3 Space Fastrack. In this study, removing the apparent distortion caused by the metal in the force plates reduced the mean static variance to 0.02 cm<sup>2</sup> and 0.008°<sup>2</sup> (i.e. standard deviations of 0.15 cm and 0.09°). Dynamic trials had a greater variance than static trials for both position and orientation. This was in agreement with the increased error for dynamic trials

---

reported by Richards (1999) who observed an increase of 0.29cm and 2.05° in positional and orientation error respectively.

The metal in the force plates was shown to increase the measurement variance for both static and dynamic trials and for both displacement and orientation. Bull et al. (1998) investigated the effect of metal on the accuracy of the Flock of Birds electromagnetic system. Mild steel cylinders placed within 150mm of the transmitter or receiver had a significant detrimental effect on the accuracy, with a maximum translational error of  $\approx 3.4$ cm. Ng et al. (2009) used the 3-Space Fastrack<sup>TM</sup> system (Polhemus Navigation Science Division, Colchester, VT, USA) to determine the effects of ferrous metal in rowing ergometers on tracking accuracy. There was an increased error of 4° in measurement angle. The magnitude of the distortion was dependent on both the type of metal and the size of the metal source (Nixon et al., 1998) and will differ between systems which use different excitation frequencies (Kindratenko and Bennett, 2000). Mapping was able to reduce the variance in position and orientation. Mean variance in position was reduced from 0.27 to 0.02 cm<sup>2</sup> and the mean variance in orientation was reduced from 0.88 to 0.15 deg<sup>2</sup> for dynamic trials.

For the majority of measurements, the variance in both position and orientation was shown to increase with distance from the transmitter (figure 39 and figure 40). Dynamic measurements at the greatest height (225 cm) and therefore furthest from the emitter showed more variance when compared to the middle level which was at the same height as the transmitter (145 cm) for both position and orientation: exemplified by an increase in mean variance of from 0.03cm and 0.068° to 0.37cm and 0.22° (table 27). Richards (1999) reported that the accuracy of the system was linearly dependant on the sensor's distance from the emitter, even inside the optimal range specified by the manufacturer. Similarly, Bull et al. (1998) found positional error to increase proportionally with the measured distance from the emitter within the optimal operational zone. Bull et al. (1998) performed measurements in 25 mm steps over a range of 150-900 m and as such these finer measurements would have provided a much more detailed assessment of distance effects than this experiment. Since the objective of this study was to quantify the accuracy over the entire test volume, finer detailed analysis of distance effects were not required, however results indicate the same general trends.

The results presented are only applicable to particular test set up and system and will vary for other applications. The quantification of noise in kinematic measurements made the assumption that errors were random in nature and the effects of systematic errors were not considered though they may have affected the results. Further work could include a test set up whereby the positions of sensors are accurately known so that a 'gold standard' measurement could be used for comparison. It would also be interesting to know how the rate of acceleration of sensors affects the noise; results suggest an increase in noise for moving sensors however the relationship between sensor acceleration rates and noise was not investigated.

#### 5.4.5. Conclusion

The presence of metal force plates in the test volume caused large amount of distortion in the lower third of the test volume nearest the plates. The application of mapping was able to reduce the effect of distortion on sensor position and orientation variance. Variance in both position and orientation tended to increase with distance from the emitter however the relationship wasn't as strong as had been reported previously (Bull et al., 1998; Richards, 1999). Mean variance for static trials away from the force plates was  $0.02 \text{ cm}^2$  and  $0.008^{\circ 2}$  within a transmitter to sensor range of 45 – 200 cm. For dynamic trials the variance increased to a mean of  $0.2 \text{ cm}^2$  and  $0.15^{\circ 2}$  for displacement and orientation respectively. Inaccuracy sets for the uncertainty analysis will be based on mapped dynamic trials as this condition was most representative of the expected variance during the golf swing. Three sets of inaccuracies were extracted from the results to represent noise variance in kinematic measurements; sets 1, 2, 3 reflected the minimum, mean and maximum amount of variance measured for mapped dynamic trials (table 29).

Table 29 Three sets of inaccuracies (Set 1: minimum, Set 2: mean, Set3: maximum) of position and orientation variance for the Polhemus Liberty system based on mapped dynamic measurements

Set	Displacement variance ( $\text{cm}^2$ )	Orientation variance ( $\text{deg}^2$ )
1	0.01	0.01
2	0.15	0.08
3	0.46	0.23

---

## 5.5. Soft Tissue Artefact and Joint Centre Location Inaccuracy: A literature review

### 5.5.1. Introduction

Soft tissue artefact can be defined as the relative displacement between the skin markers or sensors and the underlying bone. STA is due to movement of the soft tissue, stretching of the skin and stimulation of muscles, which is not accounted for when reconstructing skeletal movement (Andersen et al., 2012). The quantification of this error usually requires invasive techniques which are beyond the scope of this thesis due to ethical constraints. However, a large body of work exists around the quantification of STA and so error magnitudes will be sourced from the literature. STA will not only affect measured kinematics but also the estimated joint centre locations since they are saved in the sensor coordinate system during calibration. Therefore STA will also introduce error in the distal and proximal moment arm lengths.

Linked segment models assume a geometric centre for each joint. Errors in locating joint centres can arise from a number of sources such as anthropometric measurements, marker location and regression uncertainty (Schwartz and Rozumalski, 2005). Methods to determine joint centre location error require measurement of the true joint centre location which can be difficult. Cadaveric specimens have been used for direct measurement of joint centres (Isman and Inman, 1969; Seidel et al., 1995). Alternative methods use imaging techniques such as radiography (Bell et al., 1989) or MRI scans (Campbell et al., 2009). Such techniques are beyond the scope of this thesis due to ethical, cost and resource constraints. Therefore, error in joint centre location will be determined from a review of the literature.

A review of the literature relating the quantification of Soft Tissue Artefact (STA) during motion analysis measurement and errors in locating joint centres was carried out. These are both sources of error which will affect the uncertainty in net joint reaction forces and net joint moments derived through inverse dynamics. This section aims to 1) quantify the expected error in kinematic measurements caused by the relative motion between the sensors and the underlying bone known as STA and 2) quantify the expected error in the location of joint centres.

This literature review was used to identify, appraise and summarise research evidence related to the research aims above. An approach based on a similar review of STA affecting the lower limbs during human movement was used (Peters et al., 2010). The process for each began with a search of the literature for relevant papers defined by the search criteria. The search strategies including the databases and journals searched are listed. The titles and abstracts found were checked against the criteria for eligibility and relevance. The review aimed to provide an objective appraisal of evidence using a transparent and repeatable methodology. Conclusions were used to support decision making with regard to inaccuracy bounds used in the uncertainty analysis.

### 5.5.2. Soft Tissue Artefact

For the quantification of STA, inclusion criteria reflected the experimental set up; Polhemus sensors (figure 41) were strapped to body segments using elastic straps secured with Velcro (figure 2, pg. 48).

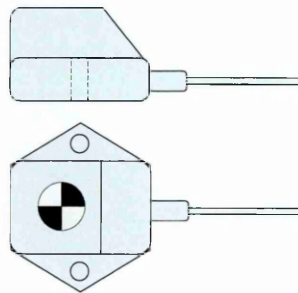


Figure 41 Schematic diagram of a Polhemus sensor

### 5.5.3. Methods

#### *Search Strategy*

An electronic search of the following international databases related to the subject areas of biomechanics or health for published reports was performed in June 2012; Science Direct, PubMed, Scopus and Google Scholar. The search was limited to literature reporting studies involving human subjects with abstracts written in English and full papers that were available online. The search terms included the following key terms: 'skin movement', 'soft tissue displacement', 'artefact', 'motion analysis' and 'error'. A manual search of the reference lists of relevant studies also identified articles for the review.

---

***Inclusion Exclusion Criteria***

The titles and abstracts of articles identified by the search strategy were assessed; articles were included when they fulfilled the following criteria: (1) functional tasks were investigated, (2) there was an implied or documented objective to quantify STA, (4) 2D or 3D motion analysis techniques were used, (5) the full scientific paper and abstract were available online, (6) markers or sensors were placed at mid segment locations. Excluded from the study were articles using simulated or artificial error. Since sensors are placed at mid segment locations (figure 2, pg. 48) articles purely concerned with skin markers placed in the local vicinity of joint centres were also excluded.

***Data Extraction***

A customised data extraction form based on previous reviews of similar subject areas (Peters et al., 2010; Piriya-prasarth and Morris, 2007) was used (table 30). The data extraction table required the following information; number of participants, age, BMI, motion analysis technique, gold standard measure, limitations and conclusions. A complimentary form was used to summarise the functional task characteristics of each study, the themes were; segment, activity, speed and range of movement (table 33).

***Similarity Assessment***

A similarity assessment form was designed to objectively rate the likeness of each study's conditions to the conditions used for golf swing analysis with the Polhemus system (table 35). A scored checklist (table 34) was used to assess each article against 4 questions relating to the similarity of the functional task, speed of movement, marker attachment method and marker location. Each question was given a rating out of 3.

**5.5.4. Results*****Search Yield***

The initial electronic search of the selected databases yielded 456 published articles. Hand searching of article reference lists identified an additional 4 scientific articles. Following the application of inclusion and exclusion criteria, 31 articles were selected for review. Results tables Table 31 & Table 32 present the reported STA from the studies reviewed. Direct measures (table 31) relate to the actual movement of the

markers with respect to the underlying bone and indirect measures (table 32) report the effect of STA on joint angles and segment translations.

Table 30 Data extraction table from reviewed articles which quantified STA

Ref	No. Partici pants	Age (mean $\pm$ SD)	BMI	Task	Motion Analysis	Gold Standard	Limitations	Conclusions
Akbarshahi et al., 2010.	4	30 $\pm$ 3	22.4	knee flexion, hip rotation, treadmill walking and step up	3D	X-ray	Small sample size, static images between movements.	STA for the thigh larger than the shank. STA was subject, task and location dependent.
Alexander et al., 2001	1	46	27.5	step up	3D	External fixation device	Small sample, limited range of movement, external fixation device may alter normal motion	Accounting for changing shape of the limb segment can lead to as substantial improvement in estimates of skeletal kinematics.
Amis et al., 2008	20	-	-	pivot shift test - knee flexion/extension	3D (electromagnet ic)	Intra-cortical pins	Minimal movement, slow velocity, no details on subjects provided.	Electromagnetic tracking system could be used to assess knee laxity with acceptable accuracy.
Andersen et al., 2010	6	26 $\pm$ 4.7	24.5	gait	3D	Intra-cortical pins	Small sample size, invasive, limited to one joint.	Optimised idealised joint constraints for the knee produced no overall improvement in the validity of skin marker derived kinematics.
Benoit et al., 2006	8	26	24.6	walking and lateral cutting	3D	Intra-cortical pins	Small sample, invasive, STA may have been reduced by sterile bandages around pins, pins may have affected motion	3D kinematics significantly affected by STA using skin markers, standard error of measurement can improve errors.
Cappozzo et al., 1996	7	23	23.6	walking and cycling, knee flexion and hip rotation	3D	External fixation device	Small sample size, external fixator may effect normal movement, fracture may alter results.	Markers located above anatomical landmarks near joints experience the largest STA (0-40mm).
Cereatti et al., 2009	4 (cadavers)	-	-	hip rotations	3D	Intra-cortical pins	Small sample, cadavers, no assessment of pelvic STA influence on HIC determination.	Hip joint centre errors caused by STA were variable among subjects, methods and skin marker cluster configurations (1.4-38.5mm).
Chen et al., 2011	20	26 $\pm$ 3	24.6	jaw opening and closing	3D	Trans-oral frame	Trans-oral device may interfere with natural chewing movement, device may move relative to underlying bone.	Middle and side face markers had large displacements compared to nose bridge markers.
Cook et al., 2002	1	48	25.5	humeral rotation and adduction/abduction	3D (electromagnet ic)	Intra-cortical pins	Small sample, slow velocity, limited range of movement	Dynamic measurement of slow velocity humeral motion can be achieved with RMSE's less than 8° with a surface humeral cuff.
Cutti et al., 2005	6	31 $\pm$ 6	23.9	humeral internal/external rotation	3D	Analytical	Small sample size, small range of movement, no gold standard.	Strong influence of STA over the estimation of upper-arm kinematics was shown. Subject specific compensation techniques recommended.
Cutti et al., 2006	6	35 $\pm$ 6	24	5 arm movement tasks	3D	Analytical	No gold standard, small sample.	Compensation technique reduced RMS due to STA from 9° to 3° for the upper arm
Garling et al., 2007	10	67	30	step up task	Fluoroscopy	Fluoroscopy	Small sample, alignment of epicondylar axis between subjects may cause large variability in results	Large STA found during stair task, kinematics presented with error bounds recommended.
Hamming et al., 2012	19	35	26.3	raising arm and rotation	3D (electromagnet ic)	Intra-cortical pins	Slow velocity movements, pins may affect normal motion.	Thermoplastic humeral cuff was accurate except when measuring axial rotations of the arm. Error increased for subject with BMI greater than 25.
Heneghan et al., 2010	30	24 $\pm$ 3.1	21.1 $\pm$ 3.4	thoracic axial rotation and single arm elevation.	Digital callipers	Ultrasound	Only static measurements at max rotation, callipers may have underestimated STA	Large variability of STA within the thoracic region; most occurring in the mid thoracic region.
Holden et al., 1997	3	33	17.5	walking	3D	Percutaneous skeletal tracker	Small sample size, no evaluation of movement around the lateral ankle	Greatest errors were along and around the longitudinal axis of the shank. Errors in knee joint net forces and moments were greatest during the stance phase of gait.
Houck et al., 2004	2	37	25.8	gait	3D	Intra-cortical pins	Small sample, invasive, possible effects of anaesthetic on movement.	Femoral tracking device useful in recording tibio-femoral angles and displacement for the first 85% of stance phase during gait.

Karduna et al., 2001	9	33	<36	humeral rotations	3D (electromagnetic)	Intra-cortical pins	Small sample, skin tension may have bent pins, restricted movement, slow velocity	Methods produced "reasonably" accurate representations of scapular motion.
Kuo et al., 2011	10	78±6.5	25.9	sit to stand	3D	Fluoroscopy	Small sample, knee joint centre definition accuracy may have affected results.	STA led to significant underestimation of flexion and internal rotation angles of the knee.
Lucchetti et al., 1998	3	34	22.6	walking	3D	Analytical	Small sample, no gold standard, cumbersome procedure.	Compensation method allows accurate measurement of joint movements that undergo even minimal variations that would otherwise be hidden by error.
Manal et al., 2000	7	25.6±1.9	1 overweight, 6 average	walking	3D	Percutaneous skeletal tracker	Small sample, limited range of movement, external fixation device may alter normal motion	Tibial rotation was best estimated using four markers attached to a rigid shell positioned over the lateral shank.
Manal et al., 2003	7	-	24.6	walking	3D	Percutaneous skeletal tracker	Small sample, skeletal trackers could alter normal performance.	Tibial translation estimates have a minimum error of 3mm using standard motion capture methods and moulded shell targets strapped to shank.
Reinschmidt et al., 1997	5	28.6±4.3	24.3	walking	3D	Intra-cortical pins	Small sample, invasive, some markers moved outside small capture volume during collection	Knee rotations are affected by substantial errors using external skin marker.
Reinschmidt et al., 1997	3	25.7±2.1	24.5	running	3D	Intra-cortical pins	Small sample, invasive	High STA larger than shank STA. Flexion/extension were the only knee rotations that were accurately estimated using skin markers during running.
Ryu et al., 2009	1	42	21.1	Knee motion	3D	External fixation device	Small sample, invasive, fixation device may have altered normal movement	Effective STA compensation was achieved through AL displacement modelling.
Sangeux et al., 2006	11	33	-	knee flexion	MRI	MRI	Small capture volume, small sample, no BMI data, limited movement.	Non-invasive method could measure STA with good accuracy and reproducibility.
Schache et al., 2008	20	20.8±4.1	22.2	gait and isolated longitudinal hip rotations	3D	Analytical	No gold standard, sample limited to young, average weight adults, only two motor tasks evaluated.	Non-rigid distal thigh cluster configuration provided the most accurate hip axial rotation profiles.
Shultz et al., 2011	23	-	-	quasi static positions	2D	Fluoroscopy	2D only, BMI not reported, error in digitisation of X-ray images unknown.	Toe off position had the highest STA error for foot bones.
Stagni et al., 2005	2	66	23	stair climbing, step up/down, sit to stand, extension against gravity	3D	Fluoroscopy	Small sample, total knee replacement patients	STA was subject and task specific, proximal thigh largest STA, errors caused by STA can critically affect clinical interpretation of a gait analysis.
Südhoff et al., 2007	18	25	23	knee flexion and gait	X ray	X-ray	Static images between movements, limited number of positions due to ethics, different subjects were used to compare attachment systems.	Of the 3 tested, no method of fixation was able to limit STA in the transverse plane. Epicondyle cuff was the best performance overall.
Tranberg et al., 1998	6	39	-	ankle flexion	2D	2D roentgen photogrammetry	2D, small sample, limited volume, static images.	Largest STA occurred over the most proximal medial malleolus, navicular bone and calcaneus markers.
Tsai et al., 2011	12	22±1.4	25.9	three step stair climbing	3D	Fluoroscopy	Small sample, knee joint centre definition accuracy may have affected results	STA of thigh markers larger than shank, joint centre translations significantly overestimated during stance phase of gait.

Table 31 Direct results obtained from reviewed articles

Segment	Measure of artefact			Activity	Gold Standard	Study	
	AP (mm)	ML (mm)	Long (mm)				
Foot	4.31		0.94	ankle flexion	2D photogrammetry	(Tranberg and Karlsson, 1998)	
Shank	15.8	14.1	16.3	stair climbing	Flouroscopy	(Stagni et al., 2005)	
	9.8	12.6	11.1	Sit to stand	Flouroscopy	(Stagni et al., 2005)	
	6.3	10.3	12.9	step up/down	Flouroscopy	(Stagni et al., 2005)	
	12.5	20.6	13.5	knee extension	Flouroscopy	(Stagni et al., 2005)	
	6	10	2	stair climbing	Flouroscopy	(Tsai et al., 2011)	
	30	2	10	sit to stand	Flouroscopy	(Kuo et al., 2011)	
	4.0-18.3 (range, all directions)			knee flexion	External fixator	(Ryu et al., 2009)	
	5.5	2.5	8.6	knee flexion,	X-ray flouroscopy	(Akbarshahi et al., 2010)	
	3.4	1.3	4.3	hip rotation	X-ray flouroscopy	(Akbarshahi et al., 2010)	
	6	3.3	8.4	gait (treadmill)	X-ray flouroscopy	(Akbarshahi et al., 2010)	
	4.3	2.7	6.9	step up	X-ray flouroscopy	(Akbarshahi et al., 2010)	
	14.1	11.8	8.3	gait	Percutaneous skeletal tracker	(Manal et al., 2003) <sup>n</sup>	
	Thigh	30	28	20	stair climbing	Flouroscopy	(Tsai et al., 2011)
		5	5	30	sit to stand	Flouroscopy	(Kuo et al., 2011)
17.4		31.1	14.7	stair climbing	Flouroscopy	(Stagni et al., 2005)	
28.5		28.4	17.5	Sit to stand	Flouroscopy	(Stagni et al., 2005)	
14.5		16.1	14.9	step up/down	Flouroscopy	(Stagni et al., 2005)	
11.1		13.7	12.8	knee extension	Flouroscopy	(Stagni et al., 2005)	
6.8		9.6	8.6	knee flexion,	X-ray flouroscopy	(Akbarshahi et al., 2010)	
8.1		2.4	10.4	hip rotation	X-ray flouroscopy	(Akbarshahi et al., 2010)	
6.2		7.6	9.7	gait (treadmill)	X-ray flouroscopy	(Akbarshahi et al., 2010)	
5.9		12.6	10.7	step up	X-ray flouroscopy	(Akbarshahi et al., 2010)	
5.47		4.68	5.35	gait	none	(Schache et al., 2008)	

<sup>n</sup> moulded shell, Velcro strap; <sup>o</sup> rigid wand cluster

Table 32 Indirect results obtained from reviewed articles. STA artefact was quantified as either the effect of STA on joint angles and segment translations or the relative motion between the bone embedded coordinate system and the marker defined coordinate system.

Segment	Measurement of artefact		Activity	Gold standard	Ref
	Translation (mm)	Rotation (°)			
Foot	16.4	0.7	gait	2D Flouroscopy	(Shultz et al., 2011)
	4.31	2.3	ankle flexion	2D roentgen photogrammetry	(Tranberg and Karlsson, 1998)
Shank	6.8	3.6	gait	intra-cortical bone pins	(Benoit et al., 2006)
	8	6.3	cutting	intra-cortical bone pins	(Benoit et al., 2006)
	10.9	9.6	step up	Flouroscopy	(Garling et al., 2007) <sup>a</sup>
	8.3	3.6	step up	Flouroscopy	(Garling et al., 2007) <sup>b</sup>
	10.5	8	gait	Percutaneous skeletal tracker	(Holden et al., 1997) <sup>c</sup>
		7.9	running	intracortical pins	(Reinschmidt, Bogert, Nigg, et al., 1997)
	9.00	15	knee flexion	MRI	(Sangeux et al., 2006) <sup>d</sup>
	2.4	1.9	knee flexion/extension	bone pins	(Amis et al., 2008) <sup>e</sup>
	3.9	4.2	gait	intracortical pins	(Houck et al., 2004) <sup>f</sup>
		9.8	gait	intracortical pins	(Andersen et al., 2010)
	0.25	0.37	step up	external fixation device	(Alexander and Andriacchi, 2001)
		4	gait	percutaneous skeletal tracker	(Manal et al., 2000) <sup>g</sup>
		8.1	gait	intracortical bone pins	(Reinschmidt, Bogert, Nigg, et al., 1997)
		6.4	4.5	knee flexion	X ray
	2.8	2.4	knee flexion	X ray	(Südhoff et al., 2007) <sup>i</sup>
	8.8	8.8	knee flexion	X ray	(Südhoff et al., 2007) <sup>j</sup>
Thigh	16.6	5.2	step up	Flouroscopy	(Garling et al., 2007) <sup>a</sup>
	7.5	7.7	step up	Flouroscopy	(Garling et al., 2007) <sup>b</sup>
	14.5	3	hip external	external fixators	(Cappozzo et al., 1996)

	22	11	rotation		
	±3.6	±5.6	knee flexion	MRI	(Sangeux et al., 2006) <sup>d</sup>
			knee flexion/extension	bone pins	(Amis et al., 2008) <sup>e</sup>
		10.3	gait	intracortical bone pins	(Reinschmidt, Bogert, Lundberg, et al., 1997)
	19.6	8.1	gait	none	(Lucchetti et al., 1998)
	8.2		hip rotation	intracortical pins	(Cereatti et al., 2009)
	7.9	2.4	knee flexion	X ray	(Südhoff et al., 2007) <sup>h</sup>
	6	3.2	knee flexion	X ray	(Südhoff et al., 2007) <sup>i</sup>
	7.1	5.1	knee flexion	X ray	(Südhoff et al., 2007) <sup>j</sup>
Thorax T12	5.11		axial rotation/ arm elevation	ultrasound imaging	(Heneghan and Balanos, 2010)
Thorax T6	16.57		axial rotation/ arm elevation	ultrasound imaging	(Heneghan and Balanos, 2010)
Thorax T1	7.93		axial rotation/ arm elevation	ultrasound imaging	(Heneghan and Balanos, 2010)
Scapular	-	11.4	humeral rotations	bone pins	(Karduna et al., 2001) <sup>k</sup>
	-	10	humeral rotations	bone pins	(Karduna et al., 2001) <sup>l</sup>
Upper Arm	-	9	5 arm movement tasks	artefact free embedded frame	(Cutti et al., 2006)
	-	3	humeral internal/external rotation	none	(Cutti et al., 2003) <sup>n</sup>
	-	4.8	scapular plane abduction	transcortical pins	(Hamming et al., 2012) <sup>m</sup>
	-	5.5	forward flexion	transcortical pins	(Hamming et al., 2012) <sup>m</sup>
	-	14.3	axial rotations	transcortical pins	(Hamming et al., 2012) <sup>m</sup>
	1.3	3.8	flexion	humeral fixator - bone pins	(Cook and Paula, 2002)
	2.1	3.5	scapular plane abduction	humeral fixator - bone pins	(Cook and Paula, 2002)
	0.5	7.5	internal/external rotation	humeral fixator - bone pins	(Cook and Paula, 2002)
Face	12.83	12.6	jaw opening and closing	transoral rigid frame	(Chen et al., 2007)

<sup>a</sup>Plate mounted markers; <sup>b</sup>Strap mounted markers; <sup>c</sup>Shell mounted markers; <sup>d</sup>Plastic plates; <sup>e</sup>Splint mounted electromagnetic sensors; <sup>f</sup>femoral tracking device - clamped onto condyles and skin markers; <sup>g</sup>rigid shell with under-wrap; <sup>h</sup>wand and strapped shells; <sup>i</sup>epicondyle cuffs; <sup>j</sup>flat plastic blocks with straps; <sup>k</sup>double sided tape; <sup>l</sup>base, adjustable arm and footpad; <sup>m</sup>thermoplastic cuff; <sup>n</sup>elastic cuff.

Table 33 Movement speed and range of movement reported for reviewed articles

Segment	Activity	Speed (m/s)	ROM			Ref	
			Ext/Flex	Ab/Ad	Ext/Int		
Foot	ankle flexion	static	50	-	-	Tranberg et al., 1998	
Shank	gait	'self-paced'	41	-	-	Manal et al., 2003	
		'self-paced'	30	3	9	Benoit et al., 2006	
		1.1-1.3	-	-	-	Holden et al., 1997	
		1.56 - 1.79	-	-	10	Houck et al., 2004	
		-	36.6	8	10	Andersen et al., 2010	
		1.11-1.36	-	-	8	Manal et al., 2000	
	Thigh	treadmill walking	1.6±0.2	55	10	10	Reinschmidt et al., 1997a
			0.78	55	6	12	Akbarshahi et al., 2010
		running	2.9±0.2	40	18	20	Reinschmidt et al., 1997b
		sit to stand	-	80	30	10	Stagni et al., 2005
			-	55	3	8	Kuo et al., 2011
		knee flexion	-	90	13	10	Akbarshahi et al., 2010
			static	90	-	-	Sangeux et al., 2006
		Thigh	step up	static	70	-	-
-				50	9	7	Akbarshahi et al., 2010
hip rotation			-	6	5	4	Akbarshahi et al., 2010
cut	-		45	5	15	Benoit et al., 2006	
gait	1.20-1.12		-	-	-	Lucchetti et al., 1998	
	1.25±0.14		-	-	-	Schache et al., 2008	
treadmill walking	0.78		55	6	12	Akbarshahi et al., 2010	
sit to stand	-		80	30	10	Stagni et al., 2005	
	'self-paced'	65	2	7	Kuo et al., 2011		
knee flexion	-	25	-	-	Südhoff et al., 2007		
	-	90	13	10	Akbarshahi et al., 2010		
step up	-	50	9	7	Akbarshahi et al., 2010		
hip rotation	-	6	5	4	Akbarshahi et al., 2010		

Quantification of Inaccuracy Magnitudes

		-	60	40	30	Cereatti et al., 2009
	pivot shift test	-	50	-	-	Amis et al., 2008
Thorax	thoracic axial rotation	static	-	-	38	Heneghan et al., 2010
	humeral rotation	-	-	150	-	Karduna et al., 2001
Upper Arm	humeral rotation	'slow'	135	-	-	Cutti et al., 2005
		-	-	-	7	Hamming et al., 2012
	humeral forward flexion	-	-	-	120	Hamming et al., 2012
	scapular plane abduction	-	-	-	120	Hamming et al., 2012
		10 °/s	-	70	30	Cook et al., 2002
	internal/external rotation	20 °/s	111	10	60	Cook et al., 2002

Table 34 Similarity form used in literature review, questions were scored out of 3

#	Question
1	How similar was the activity?
2	Were segmental velocities of a similar magnitude?
3	Were the markers or sensors placed at mid segment locations?
4	How similar was the markers fixation method?

Table 35 Similarity analysis results from reviewed articles

Ref	Question Number				Total (/12)
	1	2	3	4	
Schache et al., 2008.	2	2	3	2	9
Holden et al., 1997	1	2	3	3	9
Manal et al., 2000.	1	2	3	3	9
Manal et al., 2003	1	2	3	3	9
Cutti et al., 2005.	2	1	3	3	9
Hamming et al., 2012.	2	1	3	2	8
Südhoff et al., 2007.	2	0	3	3	8
Benoit et al., 2006	2	2	3	1	8
Reinschmidt, 1997.	2	3	2	1	8
Garling et al., 2007.	1	1	2	3	7
Cutti et al., 2006.	2	1	3	1	7
Karduna et al., 2001.	2	1	1	3	7
Lucchetti et al., 1998.	1	2	3	1	7
Cook et al., 2002	2	1	2	2	7
Sangeux et al., 2006.	1	0	3	2	6
Tsai et al., 2011	1	2	2	1	6
Kuo et al., 2011.	1	1	3	1	6
Akbarshahi et al., 2010.	2	1	2	1	6
Andersen et al., 2012.	1	2	2	1	6
Andersen et al., 2010	1	2	2	1	6
Houck et al., 2004.	1	2	1	2	6
Reinschmidt et al., 1997.	1	2	2	1	6
Stagni et al., 2005.	2	1	2	1	6
Alexander et al., 2001.	1	1	3	1	6
Cereatti et al., 2009	2	1	2	1	6
Heneghan et al., 2010.	2	0	2	1	5
Cappozzo et al., 1996	2	1	1	1	5
Tranberg et al., 1998	1	0	3	1	5
Amis et al., 2008.	1	1	1	2	5
Ryu et al., 2009.	1	1	2	1	5
Chen et al., 2011	1	1	1	1	4
Shultz et al., 2011	1	0	1	1	3

*Similarity of reviewed articles*

The similarity of functional tasks to the golf swing received either a 1 or 2 out of 3 since most studies were concerned with clinical applications and therefore isolated joint movements such as knee flexion/extension (Akbarshahi et al., 2010; Amis et al., 2008; Ryu et al., 2009; Sangeux et al., 2006; Stagni et al., 2005; Südhoff et al., 2007), hip rotation (Cappozzo et al., 1996), arm elevation/rotation (Cook and Paula, 2002; Cutti et al., 2003; Hamming et al., 2012; Heneghan and Balanos, 2010; Karduna et al., 2001), and ankle flexion (Tranberg and Karlsson, 1998). The abundance of such studies was an indication that the invasive nature and resources required to quantify STA were more justifiable within a clinical context. The impairment of movement due to bone pins (Holden et al., 1997) may have also been a factor that limited the type of movement that was investigated. Studies looking at more dynamic tasks such as gait (Akbarshahi et al., 2010; Andersen et al., 2010; Benoit et al., 2006; Holden et al., 1997; Houck et al., 2004; Lucchetti et al., 1998; Manal et al., 2003, 2000; Reinschmidt, Bogert, Nigg, et al., 1997; Schache et al., 2008; Shultz et al., 2011), stair climbing (Stagni et al., 2005; Tsai et al., 2011) or running (Reinschmidt, Bogert, Nigg, et al., 1997) involved more than one joint and movement in multiple planes simultaneously; these more complex movements were most similar to the golf swing.

The velocity of movements were only reported in 11 out of the 31 studies reviewed (table 33) with 4 studies quantifying STA using static imaging techniques (Heneghan and Balanos, 2010; Sangeux et al., 2006; Südhoff et al., 2007; Tranberg and Karlsson, 1998). The speed at which participants walked or ran was given for 9 studies however no information on the linear or rotational velocity of individual segments was given. One study was found which reported rotational velocities of up to 20°/s for upper arm rotation (Cook and Paula, 2002). For the golf swing angular velocities of up to 426°/s, 549°/s, 762°/s and 2144°/s for the pelvis, upper trunk, lead arm and club respectively have been measured (Yontz, 2010). No study reported segmental velocities approaching those experienced by the upper body during the golf swing.

The location of markers in relation to joint centres was used as exclusion criteria since it had been reported that markers placed at joint centres would move more relative to bone than mid segment markers (Cappozzo et al., 1996). Moulded shells or thermoplastic cuffs upon which markers were placed were secured near to the middle

of the segment using straps (Amis et al., 2008; Garling et al., 2007; Hamming et al., 2012; Holden et al., 1997; Manal et al., 2003, 2000; Sangeux et al., 2006; Südhoff et al., 2007); this type of marker attachment method was most similar to the method used in this thesis.

Of the studies reviewed, 15 different marker attachment methods were used, with 4 studies comparing STA using different marker attachment methods (Cereatti et al., 2009; Manal et al., 2000; Schache et al., 2008; Südhoff et al., 2007). Marker attachment methods varied with respect to the location on a segment, the physical characteristics of the marker set and method used to attach the marker array to the segment. The majority of studies used unconstrained markers attached directly to the skin using double sided tape; this is the least similar marker attachment method to the Polhemus system. Other methods mounted markers to moulded plates or cuffs thereby constraining inter marker distances. Electromagnetic systems used sensors to track the motion of the segment making the thermoplastic shells most similar to the Polhemus sensors. Sensors are generally larger and heavier than skin markers. Methods used to attach sensors included double sided tape, plastic splints and mounts secured with elasticated straps.

### *Participants*

Sample sizes ranged from 1-30, with 23 articles which used 10 participants or less (table 30). The majority of studies recruited people of similar age and body type; only one study deliberately selected a range of body types in order to assess the effects of BMI on STA (Hamming et al., 2012). Some articles provided insufficient information on the physical characteristics of participants by not reporting BMI or age statistics (Amis et al., 2008; Cereatti et al., 2009; Shultz et al., 2011).

### *Movement Analysis Techniques*

Optical systems were used in 15 studies for movement analysis with Schultz et al. (2011) the only study to use 2D video motion analysis rather than 3D. 4 studies used electromagnetic tracking systems (table 30). The remainder of studies used either fluoroscopy, X-ray, MRI or ultrasound imaging for both the principal measurement of kinematics and gold standard comparisons. Physically invasive gold standard techniques used were intracortical bone pins, percutaneous trackers and external fixation devices. 4 studies did not have a 'gold standard' as such and used analytical

methods (Cutti et al., 2006, 2003; Lucchetti et al., 1998; Schache et al., 2008).

Limitations of invasive techniques include the possibility of pin bending (Benoit et al., 2006; Karduna et al., 2001), incisions which may affect the way the skin would naturally stretch and move (Akbarshahi et al., 2010) and natural body movement impingement due to pain (Holden et al., 1997). Non-invasive techniques used in some of the more recent studies avoided various limitations of invasive methods however X-ray and MRI were only able to capture still or quasi-static images (Sangeux et al., 2006; Südhoff et al., 2007) and radiation limited the number of images that could be taken (Amis et al., 2008). Fluoroscopy allowed for free movement whilst simultaneously capturing motion of both the skin markers and the underlying bone, however capture volume was limited so the type of task that could be examined was restricted (Stagni et al., 2005).

#### *Quantification of STA*

Both direct and indirect measurements of STA were reported; direct measurements refer to the translation of markers relative to the underlying bone (table 31) whereas indirect measurements reported the effect of STA on joint angles and segment translations (table 32). In order to report STA, studies used a various combinations of statistical measures such as the mean, RMSE, standard deviation, maximum and range. Some studies used clusters of skin markers to determine an average STA measure whereas others reported STA with relation to just one marker creating additional inconsistencies in the way in which STA was quantified. The lack of similarity of statistical measures made it difficult to analyse results and to make comparisons between studies.

#### **5.5.5. Discussion**

STA was quantified through different methods, for different segments, for different tasks and using different marker attachment techniques. There was a lack of homogeneity of data and this was confirmed by disparity of results and the inconsistencies of conclusions between studies.

The lower extremities have been the subject of most research in this area. Only 2 studies reported STA for the foot (Shultz et al., 2011; Tranberg and Karlsson, 1998). Maximum reported values were 4.31 mm and 16.4 mm for Tranberg et al. (1998) and Schultz et al. (2011) respectively. The large difference between STA magnitudes was

thought to be due to the marker type (Shultz et al., 2011). Marker triads were more susceptible to movement relative to the skin due to larger inertia and greater distance between COM from marker attachment site than an individual spherical marker (Shultz et al., 2011). Studies found were in agreement that thigh STA was larger than shank STA (Akbarshahi et al., 2010; Andersen et al., 2012; Cappozzo et al., 1996; Garling et al., 2007; Kuo et al., 2011; Reinschmidt, Bogert, Lundberg, et al., 1997; Reinschmidt, Bogert, Nigg, et al., 1997; Stagni et al., 2005; Tsai et al., 2011). For the shank the maximum reported STA was 30mm during sit to stand tasks (Kuo et al., 2011). This was for a single skin marker placed on the femoral epicondyle. Markers placed further away from the knee joint centre at the tibial tuberosity and head of the fibula were subject to STA of up to 10 mm (Kuo et al., 2011). The highest reported STA for the thigh was 31.1 mm during stair climbing (Stagni et al., 2005) for a single skin marker. Reinschmidt et al. (1997) stated that the STA of the shank could be neglected in comparison to thigh STA during gait; the effect of STA on knee flexion/extension was  $<1.8^\circ$  for the shank compared to  $>6^\circ$  for the thigh. These findings were attributed to the inertia caused by a greater amount of soft tissue in the thigh than the shank (Reinschmidt, Bogert, Lundberg, et al., 1997). However, for running, Reinschmidt et al. (1997) reported an additional cause. Video analysis showed that skin markers placed on the top of large muscles such as the quadriceps were subject to STA caused by muscle activity to greater extent than inertial effects (Reinschmidt, Bogert, Nigg, et al., 1997).

Only one study was found which quantified STA of the trunk; Heneghan et al. (2010) reported thorax STA to range between 5.1 - 16.6 mm with the largest effects around the mid thoracic region. This study reported the maximum displacement of skin markers from a neutral position to full spinal rotation. STA may have been higher than would be expected than using straps and sensors as it has been reported that unconstrained skin markers were among the worst fixation method for STA error during gait (Manal et al., 2000).

Upper arm STA was reported for indirect measurements with a maximal rotational artefact of  $14.3^\circ$  using a thermoplastic cuff during axial rotations (Hamming et al., 2012) and maximal translations of 2.1 mm during scapular plane abductions (Cook and Paula, 2002). A wide range of movements for upper arm STA was investigated however all

---

movements were carried out at a slow velocity. No study was found that quantified STA for the forearm, pelvis or lumbar segments.

10 studies were found which compared STA during different functional tasks. For the thigh and shank 3 studies reported STA of skin markers to be task specific (Akbarshahi et al., 2010; Benoit et al., 2006; Schache et al., 2008). Benoit et al. (2006) reported STA during lateral cutting was greater than during gait. The relationship between skin and pin derived kinematic profiles was also found to differ considerably between participants (Benoit et al., 2006). Schache et al. (2008) investigated the effect of four different thigh cluster marker configurations on STA during gait and hip longitudinal rotation. All four cluster marker sets consistently underestimated hip axial rotation during longitudinal rotation whilst all cluster configurations overestimated the amplitude of hip axial rotation during gait. In conflict with these findings, Cappozzo et al. (1996) found lower extremity STA to be a factor of joint angle irrespective of motor task when comparing gait, cycling, knee flexion and hip external rotation tasks. For the upper arm all three studies found reported task dependant STA (Cook and Paula, 2002; Cutti et al., 2003; Hamming et al., 2012).

A relationship between STA magnitude and range of motion for the knee (Manal et al., 2003), hip (Cappozzo et al., 1996), upper arm (Hamming et al., 2012) and thorax (Heneghan and Balanos, 2010) was observed for simple movements. Cappozzo et al. (1996) found the magnitude of STA of a marker located on the greater trochanter to vary linearly with respect to hip joint flexion angle during a hip external rotation task. Hamming et al. (2012) found STA error increased with upper arm flexion angle. Heneghan et al. (2010) reported that STA of the thorax and range of arm motion demonstrated a moderately strong association. Manal et al. (2003) stated that the magnitude of STA followed the knee flexion profile. On the other hand Sangeaux et al. (2006) found rotation parameters for the thigh and shank did not express a trend during knee flexion. In the same study where a relationship between the STA of a skin marker on the greater trochanter and hip joint angle was reported, no relationship between STA magnitude and ankle joint angle for the malleolus marker was found (Cappozzo et al., 1996). Other studies have reported no relationship between STA magnitude and segment motion during more complex tasks like gait with STA varying randomly (Benoit et al., 2006; Holden et al., 1997; Manal et al., 2000).

The Body Mass Index (BMI) of the participant has been shown to affect STA; Cutti et al. (2003) found participants with less muscle mass had lower STA in the upper arm during shoulder rotation and arm abduction tasks than participants with the highest BMI. Cereatti et al. (2009) found participants with larger thigh circumferences had more STA during gait trials. Similarly Hamming et al. (2012) commented that during investigations of axial rotations of the upper arm, the exclusion of participants with a BMI greater than 25 (overweight) would significantly reduce error. These findings indicate that STA is larger in places where soft tissue thickness is greater (Gao and Zheng, 2008). Even studies which have used relatively homogenous samples have reported participant specific STA (Akbarshahi et al., 2010; Andersen et al., 2010; Garling et al., 2007; Reinschmidt, Bogert, Lundberg, et al., 1997; Stagni et al., 2005; Tsai et al., 2011). One of the smallest samples used by Akbarshahi et al. (2010) consisted of 4 male participants with a mean age of  $30\pm 3$  and mass of  $71\pm 7$  kg. Knee flexion extension STA was larger for participants 2 and 3 whereas knee abduction/adduction was larger for participants 3 and 4 during gait.

Six studies investigated the effects of fixation method used to attach markers or sensors to body segments on STA (Garling et al., 2007; Holden et al., 1997; Karduna et al., 2001; Manal et al., 2000; Schache et al., 2008; Südhoff et al., 2007). The primary source of STA error irrespective of attachment method is the relative movement between markers and underlying bone (Manal et al., 2000). A second source of error was identified as the deformation of the marker configuration which causes inter marker distances to change; this is the case when multiple skin markers are used to determine the movement of a segment (Manal et al., 2000). It was shown that during gait, unconstrained skin markers at the proximal end of the shank were among the worst for STA error in comparison to a rigid shell which was under-wrapped (Manal et al., 2000). Südhoff et al. (2007) compared 5 different fixation devices and found that that a distal clamp reduced STA compared to an elastic strap on the thigh and shank however no system could limit STA in the transverse plane during gait. The discrepancy in STA between methods may have been inflated in this study since different participants were used to compare fixation devices.

Another factor that has been considered is the location of marker attachment on a segment. Cappozzo et al. (1996) and Tranberg et al. (1998) found that the more

proximal areas of the thigh and foot were subject to larger movement than the distal areas. This was consistent with findings reported by Akbarshahi et al. (2010) where STA for the shank and thigh in the vicinity of joint centres was larger than mid-segment regions for 4 different functional tasks. This study also found that the most accurate skin-marker cluster was different for each task and each plane of motion. Kuo et al. (2011) and Tsai et al. (2011) reported different patterns and magnitudes of STA for markers placed on different regions of the thigh during sit to stand and stair ascent tasks respectively.

Studies characterising the nature of STA have produced contradictory results with some studies reporting that STA introduces systematic errors and other studies concluding STA to be random in nature (Peters et al., 2010). Studies have reported consistent patterns of STA between participants (Akbarshahi et al., 2010; Benoit et al., 2006; Garling et al., 2007; Shultz et al., 2011), only within participants (Andersen et al., 2010; Manal et al., 2003) or no consistent pattern whatsoever (Kuo et al., 2011). A major area of research is in the development of correction techniques or kinematic models to reduce the effects of STA in motion analysis (Alexander and Andriacchi, 2001; Andersen et al., 2012, 2010; Cutti et al., 2006; Lucchetti et al., 1998; Ryu et al., 2009). Models have been based on the assumption that STA is not random or sinusoidal in nature but systematic (Andersen et al., 2010; Ryu et al., 2009) and as such task and participant specific correction algorithms have been developed.

STA has been shown to be a major source of error in human movement analysis, the magnitude of which can obscure the movement itself; Reinschmidt et al. (1997a) found that during gait and running tasks the effect of STA on knee rotation was in some cases as high as the measured motion. Stagni et al. (2005) reported similar findings for stair climbing, step ups and sit to stand tasks. Schache et al. (2008) recommended caution when using hip rotational estimates for research or clinical applications. However, Amis et al. (2008) reported that even in the presence of STA, results were clinically useful in determining knee laxity. It is important to note that this study used specially developed splints and mounts to attach electromagnetic sensors to the femoral epicondyles and movement ranges were limited and controlled.

### 5.5.6. Conclusion

The objective of this literature review was to gain as much information as possible in order to inform selection of STA inaccuracy bounds. Studies considered in the search were limited to English papers which had abstracts available electronically so some papers could have been overlooked. Since only one reviewer performed the data extraction and similarity assessment process the subjective nature of the task was increased compared with larger scale systematic reviews, however all attempts were made to remain as objective as possible; this was achieved by following strict protocols in the reviewing process.

The literature falls short of providing STA measures for complex, high acceleration motions like the golf swing. Unsurprisingly no study was found which attached Polhemus sensors to body segments in exactly the same way as shown in figure 2 (pg. 48) however studies using plates or thermoplastic cuffs secured with elastic strapping were thought to be most similar. There exists a great deal of controversy over the characteristics of STA with conclusions from many studies contradicting each other. The disparity in reported STA magnitudes makes selecting inaccuracy bounds difficult. The participant, task, segment and marker attachment method specific nature of STA adds to the problem. In addition, since it has been shown that STA magnitude is not constant throughout a specific task or movement, applying a constant error bound to the kinematic data will not be exact in any case.

#### *Selection of inaccuracy bounds*

STA contributes to error in the measured kinematics and the distal and proximal moment arm lengths. Table 36 shows the inaccuracy sets used to represent STA during the uncertainty analysis. Moment arm inaccuracies were based on direct measurements (table 31) and represent the minimum, mean and maximum STA reported. For kinematic measurements, inaccuracies were based on the minimum, mean and maximum artefact magnitudes for indirect measurements (table 32) since a rotation and a translation is required. Mean inaccuracies,  $\bar{x}$ , were based on weighted averages of the reported STA magnitudes. Weights were given based on similarity scores (table 35) as follows;

$$\bar{x} = \frac{\sum_{i=1}^n w_i x_i}{\sum_{i=1}^n w_i}$$

Equation 5.21

where  $w_i$  was the similarity score for study  $i$  and  $x_i$  was the reported STA error.

Table 36 Inaccuracy sets for proximal and distal moment arms and kinematics caused by STA

Parameter	Set 1(min)	Set 2 (mean, $\bar{x}$ )	Set 3(max)
<b>Moment arm</b>			
ap (mm)	3.4	9.1	28.4
ml (mm)	1.3	9.2	31.1
long (mm)	0.94	7.8	30
<b>Kinematic data</b>			
translation (mm)	0.25	9.7	19.6
rotation (°)	0.7	7.4	15

Set 1 represented the minimum reported STA from all reviewed studies; Set 2 represented the weighted average of STA with the most similar studies given the highest weighting; Set 3 represented the maximum reported STA from all reviewed studies.

### 5.5.7. Joint Centre Location

For each joint of the geometric model a geometric centre is assumed. During calibration the location of the proximal joint centre for a particular segment is saved in the segment's sensor coordinate system. Therefore, during inverse dynamics calculations, in segment local coordinate system, the relative distance of the joint centre to the COM remains fixed whilst the position of application of the distal JRF can change. The aim of this literature review is to quantify the expected inaccuracy in the location of joint centres. As such, only studies which have considered the joint centre definitions used by the geometric model developed for this study will be included (table 37).

Table 37 Joint centre definitions used by geometric model to define each joint centre

Joint	Joint centre definition
Ankle	midpoint of the lateral and medial malleoli
Knee	midpoint of the lateral and medial epicondyle
Hip	Method of Bell et al. (1989) - predictive approach*
Lower trunk	midpoint of the iliac crests
Mid trunk	midpoint of the right and left ribs at the height of the xiphoid process
Upper trunk	midpoint of the right and left acromion process
Shoulder	Method of Schmidt et al. (1999) - offset approach**
Elbow	midpoint of medial and lateral epicondyles
Wrist	midpoint of the radial and ulnar styloids
Neck	midpoint of sternal notch and T2

\*Bell et al. (1989) defined the hip joint centre ( $HJC$ ) as a function of pelvis width ( $PW$ ) as follows;  
 $HJC_x = -0.19PW$   $HJC_y = -0.30PW$   $HJC_z = 0.36PW$

where subscripts x, y, and z are the coordinates of the right hip joint centre in the pelvis anatomical coordinate system and  $PW$  is the distance between the right and left anterior superior iliac spines.

\*\*Schmidt et al. (1999) defined the shoulder joint centre at a position 7 cm vertically below the acromion process.

---

### 5.5.8. Methods

#### *Search Strategy*

An electronic search of the following international databases related to the subject areas of biomechanics or health for published reports was performed in July 2012; Science Direct, PubMed, Scopus and Google Scholar. The search was limited to literature reporting studies of human subjects with abstracts written in English. The search terms were customised to each database and included the following key terms: 'joint centre location', 'accuracy', 'kinematics', 'joint kinematics', 'validation', 'rotation centre' and 'error'. In addition separate searches were conducted for each joint; ankle, knee, hip, mid trunk, upper trunk, shoulder, elbow, neck and wrist. A manual search of the reference lists of relevant studies also identified articles for the review.

#### *Inclusion Criteria*

The titles and abstracts of articles retrieved from the search strategy were assessed; articles were included when they satisfied the following criteria: (1) accuracy of joint centre definition quantified, (2) joint centre definition matched that used by the geometric model as shown in table 37, (4) formal scientific papers and abstracts.

#### *Data Extraction*

A customised data extraction form (table 38) was developed based on previous systematic reviews of similar subject areas (Peters et al., 2010; Piriyaarasarth and Morris, 2007). The major data extraction themes were; participants, age, BMI, joint, gold standard, limitations, conclusions.

Table 38 Data extraction table from reviewed articles which quantified joint centre location error

Ref	Participants	Mean Age±SD	Mean weight/ height	Joint	Gold Standard	Limitations	Conclusions
Bell et al., 1989	7	46.6	78kg/ 1.7m	hip	Radiographs	small number of participants, all male	Hip joint centre predicted with best accuracy using a combination of two newly developed regression model outperformed other established methods but results were sample specific
Campbell et al., 2009	10	24±2	76kg/1.8m	shoulder	MRI	Small sample, all male, palpation reliability may have contributed to error	Transepicondylar axis closely approximates the optimal knee flexion axis
Churchill et al., 1998	15	cadavers	-	knee	Radiographs	measurement reliability	Joint centre locations were provided with reasonable accuracy, more sophisticated models should be used when higher accuracy is required
De Leva et al., 1996	6	cadavers	-	hip, shoulder, knee, ankle, wrist	Radiographs	selective sub-set of data from previous study, 2D	The use of skeletal landmarks to determine the axis of the ankle joint was feasible
Isman and Inman, 1969	46	cadavers	-	ankle	Axis locating device	Cadavers, relies on measurement reliability and simulated movement	Functional methods performed significantly better than predictive methods for locating hip joint centre
Leardini et al., 1999	11	29±5.8	76kg/ 1.8m	hip	Roentgen stereo photogrammetric analysis	small sample size, all male, palpation error	Orientation and location of elbow joint axis was determined relative to marker based coordinates
MacWilliams et al., 2010	25	-	-	elbow	Functional method	skin motion artefact, no true measure of joint centre	Proposed new method for determine lower extremity joint axes was a precise and practical alternative to the standard clinical approach.
Schwartz and Rozumalski, 2005	1	-	-	knee and hip	Functional method	no accuracy measurement only accuracy indicators, small sample, no true measure of joint centre	HJC cannot be accurately located as a function of pelvic width alone, but requires estimation as a function of pelvic height and depth as well.
Seidel et al., 1995	65	cadavers	-	hip	Direct measurements in-vitro	Used cadavers, relied on measurement reliability in vitro	A suitable approximation of the position and orientation of the mean optimal flexion axis was acquired in vivo
Stokdijk et al., 1998	10	30.8±9.8	-	elbow	Mean Optimal Instantaneous Helical Axes	skin movement error, uncontrollable pro-supination, variability in movement, no true axis of rotation established	
Veeger et al., 1996	5	cadavers	80kg/1.8m	elbow	Optimal Mean Instantaneous Helical Axes	small sample, cadavers, no true measure of joint centre	Forearm movements could be modelled with a two DOF model
Veeger et al., 1997	5	cadavers	-	elbow	Optimal Mean Instantaneous Helical Axes	Small sample, cadavers, no true joint centre location established	Shoulder joint can be modelled as ball and socket joint with 3 DOF and elbow a double hinge joint with 2 DOF

## 5.5.9. Results

*Search Yield*

The initial search yielded 211 published articles. Following application of inclusion and exclusion criteria, 11 articles were found for review. There was a lack of papers reporting the accuracy of the specific methods of defining joint centres (table 37) particularly for the shoulder, wrist and trunk joints.

Table 39 Reported joint centre error for studies identified in the literature review

Joint	Method	Direction	Error (Mean±SD)	Participants	Ref
Ankle	Mid malleoli (most prominent)	AP	11±4mm	46	(Isman and Inman, 1969)
		Long	12±4mm		
	% distance from LM	Long	3.2±0.8%	6	(de Leva, 1996)
Knee	Transepicondylar axis	AP	7.4mm	1	(Schwartz and Rozumalski, 2005)
		ML	-6.5mm		
		Long	-1.0mm		
	Distance from medial epicondyle point	AP	0.2±2.4mm	15	(Churchill et al., 1998)
		Long	0.14±2.7mm		
	Distance from lateral epicondyle point	AP	0.2±2.7mm	15	(Churchill et al., 1998)
Long		0.6±2.9mm			
	% distance from TIB	Long	3.2±0.8%	6	(de Leva, 1996)
Hip	Bell et al. (1989)	3D	10.7mm	7	(Bell et al., 1989)
	Bell et al. (1989)	AP	5.8±4.4mm	65	(Seidel et al., 1995)
		ML	5.8±4.2mm		
	Bell et al. (1989)	Long	7.5±5.6mm	11	(Leardini et al., 1999)
		AP	-7.2±5.5mm		
		Long	-18.7±10.3mm		
	ML	5.3±9.7mm			
	RMS	23.3±10.3mm			
	% distance from GT	Long	0.7±1.6%	6	(de Leva, 1996)
Shoulder	Schmidt et al. (1999)	3D	50±3.2mm	10	(Campbell et al., 2009)
	% distance from ACR	Long	10.4±1.5%	6	(de Leva, 1996)
Elbow	Lateral Epicondyle	AP	18.6±7.2mm	10	(Stokdijk et al.,

		Long	8.1±6.6mm		1999)
Lateral Epicondyle		AP	4.4mm	5	(Veeger et al., 1996)
		Long	6mm		
Lateral epicondyle		AP	8.3mm	5	(Veeger et al., 1997)
		Long	1.9mm		
Midpoint of humeral epicondyles		AP	12.3±4.7mm	25	(MacWilliams et al., 2010)
		Long	12.3±6mm		
Wrist	% distance from STYL	Long	0.6±1.5%	6	(de Leva, 1996)

LM: Most lateral point on the Lateral Malleolus, ACR: Acromion, most lateral point on the lateral margin of the acromial process of the scapula, TIB: Tibiale, most proximal point on the medial margin of the head of the tibia, GT: Greater Trochanter, STYL: stylium, distal tip of the styloid process of the radius

### Participants

Five out of eleven studies determined joint centre locations of cadavers (table 38).

These samples consisted mainly of older people and were therefore not representative of the general population (Isman and Inman, 1969). Of these studies, the largest sample size was 65 (Seidel et al., 1995). The remaining six studies were performed *in vivo*. On the whole sample sizes were small and relatively homogenous. Schwartz and Rozumalski (2005) used only a single participant in order to validate a new method for defining knee joint centre location and gave no details on participant characteristics. The largest sample size of living participants was used by MacWilliams et al. (2010) who recruited 25 participants consisting of 11 females and 14 males although no further information on participant characteristics was given.

### Techniques

Six studies used *in vitro* methods to quantify joint centre location and axes of rotation (Churchill et al., 1998; de Leva, 1996; Isman and Inman, 1969; Seidel et al., 1995; Veeger et al., 1996, 1997). Dissected specimens were manually manipulated to simulate movement in order that kinematic methods could be used to determine rotation axes. For example, Isman and Inman (1969) used cadaver leg specimens to determine the ankle joint centre; the tibia was securely clamped whilst the adjoining talus segment was rotated. The point of least motion indicated the position of the optimal axis of rotation. The position of this axis in relation to anatomic landmarks was also measured. Veeger et al. (1996) calculated the Optimal Mean Helical Axes of

the glenohumeral centre of rotation, elbow flexion extension axis and forearm pronation-supination axis. The scapula was fixed to a measuring table and the arm was free to move. Electromagnetic sensors were attached directly to bones to track arm movement therefore excluding any skin motion artefacts. A similar study by Churchill et al. (1998) used electromagnetic tracking of cadaveric leg specimens to calculate optimal knee axes using a compound hinge algorithm (Churchill et al., 1998). Cadaveric legs were attached to a loading jig which could simulate load bearing squatting activity. Rotations which did not occur about the flexion and longitudinal rotation axes and any translations were residuals. Flexion and longitudinal rotation axes were optimised by adjusting their positions until residuals were minimised. These were compared to the transepicondylar axis constructed by passing a line through the digitized positions of the medial and lateral epicondyle points. Cadaveric studies require the removal of all constraining tissues around the joint to facilitate the observation of joint motion (Isman and Inman, 1969). Therefore, the results of such studies will only reflect the effects of the shape of articular surfaces and negate the effects of constraints due to ligaments, capsules and tendons (Isman and Inman, 1969). Other studies made direct measurements on cadaveric specimens (de Leva, 1996; Seidel et al., 1995). Seidel et al. (1995) measured the hip joint centre, defined as the centre of the acetabular rim, of 65 de-fleshed pelvises using a ruler. De Leva (1996) determined the longitudinal distance from bony landmarks to the joint centres from a subset of data from Chandler et al. (1975) based on six cadavers. Joint centres were identified using methods defined by Clauser et al. (1969) based on cine-radiology on living participants.

Three of the studies found used imaging techniques to directly measure the position of joint centres in vivo (Bell et al., 1989; Leardini et al., 1999; Ng et al., 2009). Bell et al. (1989) found the three dimensional location of the hip joint centre using radiographs of participants' pelvises. However, no information on the accuracy of this 'gold standard' method was reported. Leardini et al. (1999) assessed the accuracy of hip joint centre location prediction methods using roentgen stereo photogrammetric analysis. Hip joint centre was defined as the centre of the femoral head which could be located with an accuracy of <3.5mm. Campbell et al. (2009) used MRI imaging to determine the true position of the glenohumeral joint centre (GHJC); defined as the centre of the humeral head. The accuracy of MRI relied upon the digitisation of

images. The reliability with which the GHJC could be determined was  $1.0\pm 0.2\text{mm}$  and  $0.7\pm 0.4\text{mm}$  for intra- and inter-tester assessment respectively.

The remaining studies used formal mathematical techniques to determine joint centres and reported the location with respect to anatomical landmarks. Stokdijk et al. (1999) used an electromagnetic tracking system to measure the relative motion of the forearm and upper arm during flexion extension of the elbow. The mean helical axis was then determined and the average position of the flexion-extension axis with respect to the lateral epicondyle was reported. Schwartz and Rozumlski (2005) based estimations of knee joint centre on the kinematic constraint that adjacent body segments share a single common point. True joint parameters were not measured so validation was achieved through various indirect indicators such as comparison to existing literature. MacWilliams et al. (2010) used functional methods to determine the joint centre locations of the glenohumeral joint and the elbow joint. In these studies, joint centres and axes were determined relative to skin markers and therefore relied on accurate marker placement (MacWilliams et al., 2010). Skin motion artefact may have also effected results (MacWilliams et al., 2010). These studies provided no gold standard measure of the true joint centre location (Stokdijk et al., 1999).

### *Quantification*

Many of the methods used produced information on the position of axis of rotation with respect to anatomical landmarks (Churchill et al., 1998; Isman and Inman, 1969; MacWilliams et al., 2010; Stokdijk et al., 1999; Veeger et al., 1996, 1997). This limited error quantification to translations along the antero-posterior and longitudinal axes of the segment only. Studies reporting the hip and shoulder joint centres were able to locate the true joint centre locations in three dimensions from radiograph images (Bell et al., 1989; Leardini et al., 1999; Seidel et al., 1995). Therefore, these studies were able to report three dimensional hip and shoulder joint centre errors using regression and offset methods respectively. Campbell et al. (2009) chose to present shoulder joint centre estimation error in terms of the Euclidean distance and provided no information on individual axes error. The study by De Leva et al. (1996) was the only study found which reported distance between longitudinal joint centre location and anatomical landmarks as a percentage. This relative error would be useful for comparisons between other similar studies which may have used different populations.

#### 5.5.10. Discussion

For the Golphysics linked segment model, the joint centre is an idealised point that is assumed to lie on the longitudinal axis of a segment. The proximal joint centre is assumed to maintain a fixed position relative to the segment centre of mass in the local coordinate system. Errors in locating joint centres arise from error in anthropometric measurements, marker miss-location and regression uncertainty (Schwartz and Rozumalski, 2005). This review was concerned with studies which quantified the accuracy of joint centre definitions used in the geometric model (table 37). The number of relevant studies was diminished considerably in this respect. A total of 11 studies were found which provided error estimations for six joints. No studies were found which quantified error in the neck joint centre or any of the trunk joints. The lack of studies reporting error in trunk joint centre definitions indicated the difficulty in quantifying this error. Spinal motion occurs at the intervertebral joints between adjacent vertebrae and is summation of the intervertebral motion occurring at all mobile spine joints (Wua et al., 2002). Linked segment models split the trunk into segments and assume regional motion in this section of the spine. For example, mid trunk spinal motion is the motion that occurs between the pelvis and the upper trunk joint centres. The rotational centre of such motion is extremely difficult to locate and as such so is quantifying the error in this measurement.

Studies which used radiographs or direct measurement of cadaveric specimens as a 'gold standard' provided the best estimate of joint centre accuracy (Bell et al., 1989; Campbell et al., 2009; Churchill et al., 1998; Isman and Inman, 1969; Leardini et al., 1999; Seidel et al., 1995) as a measure of the true joint centre was provided. Other types of study used functional methods to estimate joint centre locations and related these to location of anatomical landmarks (MacWilliams et al., 2010; Schwartz and Rozumalski, 2005; Stokdijk et al., 1999; Veeger et al., 1996, 1997). The accuracy of functional trials in determining joint centre location is affected by three things; soft tissue artefact of markers on the skin during the functional task, movement of the predicted joint centre during the task, and the actual error in the functional method for predicting joint centre location (MacWilliams et al., 2010). Since no true measurement of joint centre location was attempted in these studies, results were considered to be a less accurate representation of the error.

From table 39 it can be seen that the highest errors in joint centre location estimates were reported for the predictive methods of the shoulder and the hip (Campbell et al., 2009; Leardini et al., 1999). Campbell et al. (2009) reported a resultant shoulder joint centre error of  $50 \pm 3.2$  mm using the method proposed by Schmidt et al. (1999) for a sample of 20 males of similar body type and age. The method used to determine shoulder joint centre was a generic 7cm vertical offset from the acromion process. In the derivation of this offset method Schmidt et al. (1999) describe the 7cm as an average location determined visually using a ruler, though it is not clear whether this was based on one participant or the 10 participants used in the proceeding sections of the paper. In any case this was a small sample. Individual variations are not taken into account and accuracy is reliant on the tester's ability to accurately locate the position of the acromion process. The intra- and inter-tester reliability with which the acromion process could be located was  $3 \pm 4$  mm and  $5 \pm 3$  mm respectively (Campbell et al., 2009). This indicated that the error reported was primarily a factor of the generic and arbitrary nature of the method. Leardini et al. (1999) reported hip joint centre error using predictive equations of Bell et al. (1989). The regression equation is based on the inter ASIS distance. RMS errors of  $23.3 \pm 10.3$  mm were reported with errors consistently largest in the longitudinal direction for all 11 participants. These results were higher than errors reported by Bell et al. (1989) which could have been due to the differences in sample sizes or the analysis techniques (Leardini et al., 1999).

The smallest errors reported were for the knee joint (Churchill et al., 1998). 15 cadavers were used and optimal flexion and longitudinal rotational axes were determined using kinematic methods. It was found that the knee had two primary axes of rotation and that the flexion axis was closely approximated by the transepicondylar axis.

#### 5.5.11. Conclusion

There was a lack of studies reporting error in joint centre locations. Of the 10 joints used in the geometric model, errors in estimating the location of just 6 were quantified in the literature. No quantification of joint centre error was found for the trunk or neck joints. Comparisons between studies were difficult due to the variety of methods used and small sample sizes. Studies which used 'gold standard' imaging techniques such as MRI provided more valid results than others which used functional methods

such as the Optimal Mean Helical Axis. It is for this reason that inaccuracy bounds were based on studies which used imaging techniques where possible.

### *Selection of inaccuracy bounds*

Error in joint centre location will affect the proximal and distal moment arm distance. Moment arms will be perturbed along each axis. For inaccuracy bounds, studies which used a 'gold standard' comparison were preferred and so where possible inaccuracies were based purely on these studies. For the elbow joint, error values were based on functional joint centre comparison studies since no 'gold standard' studies were found. Inaccuracy values of joints for which no studies were found were based on the overall mean values of all other joints. Table 40 shows the three sets of inaccuracy values used in the uncertainty analysis. Set 1 was representative of the smallest mean error reported. If only one study was available this was equal to the mean minus one standard deviation. Set 2 was based on the mean error of all studies for that joint. Set 3 was the highest error value reported; if only one study was available this was equal to the mean error plus one standard deviation. For the shoulder, the error in the Euclidean distance reported by Campbell et al. (2009) was split into its components along the  $x$ ,  $y$  and  $z$  axes ( $e_{ml}$ ,  $e_{ap}$ ,  $e_{long}$ ) assuming the same error along each;

$$e_{ml} = e_{ap} = e_{long} = \sqrt{\frac{\text{Euclidean distance error}^2}{3}}$$

Equation 5.22

Table 40 Inaccuracy sets (mm) for proximal and distal moment arms caused by error in joint centre location

Segment	Set 1			Set 2			Set 3		
	AP	ML	Long	AP	ML	Long	AP	ML	Long
Ankle	7.0	8.0	8.0	11.0	-	12.0	15.0	-	16.0
Knee	0.2	-	0.1	2.9	-	0.37	5.6	-	0.6
Hip	5.8	5.3	7.5	6.5	5.6	13.1	7.2	5.8	18.7
Shoulder	27.0	27.0	27.0	28.9	28.9	28.9	30.7	30.7	30.7
Elbow	4.4	-	1.9	10.9	-	7.1	18.6	-	12.3
Mean (all other joints)	4.4	6.7	4.5	7.2	5.6	8.1	10.9	9.1	11.6

### **5.6.Noise in derivatives obtained from kinematic measurement data**

Lanshammar (1980) developed a formula which estimated the amount of noise expected to remain in a signal after differentiation and filtering. This was the maximal precision (or minimal variance) with which derivatives could be obtained from

measurement data. This method of estimating inaccuracies in kinematic derivatives has been used previously for sensitivity analysis of joint moments during three dimensional lifting and elbow flexion (Challis and Kerwin, 1996; Larivière and Gagnon, 1999a). Measurement data were assumed to be signals with added white noise (equation 5.23);

$$f(t) = s(t) + e(t)$$

Equation 5.23

Where  $s(t)$  is the  $k$ th order derivative estimated from the measurement data and  $e(t)$  was white noise i.e. not correlated between samples with a mean values of zero (Challis and Kerwin, 1996). The variance of the estimated  $k$ th order derivative  $\sigma_k^2$  was defined as;

$$\sigma_k^2 \geq \sigma_{k,min}^2 = \frac{\sigma_f^2 T \omega_b^{2k+1}}{\pi(2k+1)}$$

Equation 5.24

Where  $\sigma_{k,min}^2$  = the minimal variance;  $\sigma_f$  = the standard deviation of the measurement noise;  $T$  = the sampling interval;  $\omega_b$  = the bandwidth of the signal in radians ( $\omega_b = 2\pi f_b$ ); where  $f_b$  is the sample bandwidth of the signal. This formula makes a series of assumptions; the signal is bandlimited, the noise contaminating the signal is white and the frequency response of the differentiator is ideal. These assumptions mean that the formulae gives minimum estimates of variance (Challis and Kerwin, 1996). Lanshammar's equation was used to estimate the minimal variance with which angular velocity, angular acceleration and linear acceleration could be measured given the errors caused by sensor measurement noise and soft tissue artefact quantified in previous sections (5.4 & 5.5).

### 5.6.1. Sensor measurement noise

The variance in the displacement measurements using the Polhemus system was quantified previously (section 5.4). Systematic errors caused by metal distortion were reduced using mapping techniques. It was assumed that the variance calculated during the experiment was representative of the random noise present throughout swing trials. Lanshammar's equation (1982) assumed that variables were normally distributed. Tests for normality were conducted using SPSS software (IBM SPSS

Statistics 19.0, SPSS Inc., Chicago, IL). Normality tests were performed on the dynamic measurements for both the resultant distance and relative orientations of two sensors fixed to a rigid bracket. Results showed that static and dynamic measurements for both orientation and position had a normal distribution.

The measured variance quantified in section 5.4 was representative of the variance of two sensors since relative position and orientations were used. This was necessary to allow for variance in dynamic trials to be calculated. From statistics theory (Weisstein, 2013), the distribution of the sum of two independent normally distributed variables  $X$  and  $Y$  with means and variances  $\mu_X, \sigma_X^2$  and  $\mu_Y, \sigma_Y^2$  is another normal distribution with variance;

$$\sigma_{X+Y}^2 = \sigma_X^2 + \sigma_Y^2$$

Equation 5.25

Assuming the two sensors have equal variance in their measurements the variance of a single sensor was estimated as;

$$\sigma_{sensor}^2 = \frac{\sigma_{X+Y}^2}{2}$$

Equation 5.26

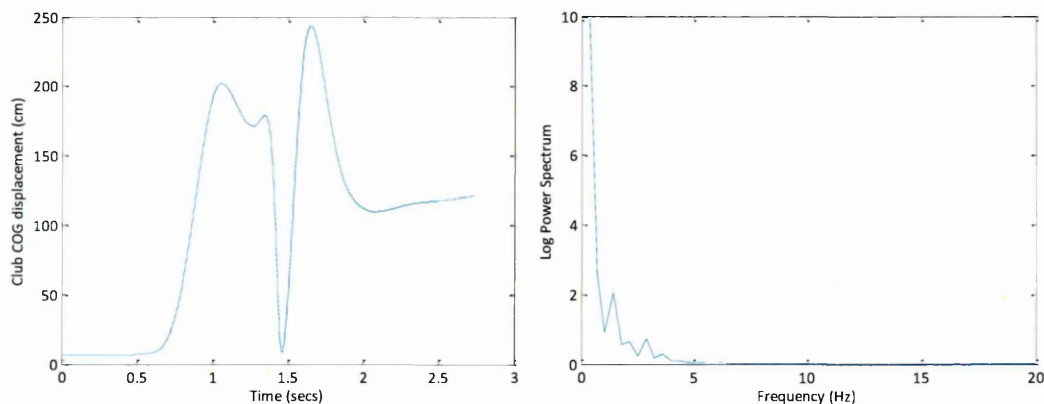
Given equation 5.26 the inaccuracy sets quantified previously (section 5.4) were adjusted as shown in table 41.

Table 41 Three sets of inaccuracies (Set 1: minimum, Set 2: mean, Set3: maximum) of position and orientation variance for the Polhemus Liberty system based on mapped dynamic measurements

Set	Displacement variance (cm <sup>2</sup> )		Orientation variance (° <sup>2</sup> )	
	2 sensors	1 sensor	2 sensors	1 sensor
1	0.01	0.01	0.04	0.02
2	0.15	0.08	0.15	0.08
3	0.46	0.23	0.46	0.23

For application of the formula, the bandwidth of the signals was required. The bandwidth is defined as the difference in the upper and lower frequencies contained within a signal (Giakas, 2004). The frequency components of the signal describing the movement and orientation of the centre of mass of body segments during the golf swing were determined and the bandwidth was computed using standard frequency

analysis techniques (Giakas, 2004) as follows; a Fourier transform of the signal was obtained using MATLAB (MATLAB Release 2010b, The MathWorks, Inc., Natick, Massachusetts, United States). The power spectrum was used to determine the amplitudes of each frequency; this was calculated as the sum of the squares of the real and imaginary parts for each frequency component obtained from the Fourier transform. The power of each frequency component was expressed as a percentage of the overall all power. By progressively adding the power the cumulative power spectrum was calculated. The bandwidth of the signal was taken as the frequency at which 99% of the signal was accounted for using a cumulative spectral analysis (figure 42). This process was repeated for a sample of swing trials. The sample consisted of unfiltered signals from the driver trials of 8 participants. All segments were considered and a total of 15 displacement and 15 orientation signals were used. Mean signal bandwidths were 6Hz and 5Hz for displacement and orientation respectively. The standard deviations of noise for derivatives were calculated as shown in table 42.



**Figure 42** Representative example of method used to calculate signal bandwidth. (Left) Club COM displacement in the y direction. (Right) Cumulative power spectrum of COM displacement of club, 99% of the signal is contained within 6.2 Hz.

Table 42 Minimal noise variance in COG linear and angular velocity and acceleration calculated from the equations of Lanshammar (1980)

	Standard deviation of noise	Signal bandwidth	Standard deviation of noise for derivatives	
			1	2
<b>Position</b>	<i>cm</i>	<i>Hz</i>	<i>ms<sup>-1</sup></i>	<i>ms<sup>-2</sup></i>
Set 1	0.08	6	0.00	0.12
Set 2	0.27	6	0.01	0.39
Set 3	0.48	6	0.02	0.68
<b>Orientation</b>	<i>rad</i>		<i>rads<sup>-1</sup></i>	<i>rads<sup>-2</sup></i>
Set 1	0.15	5	0.07	1.77
Set 2	0.27	5	0.13	3.26
Set 3	0.48	5	0.23	5.71

### 5.6.2. Soft Tissue Artefact

There exists a controversy over the characteristics of STA and many studies have produced contradictory conclusions. STA has been shown to introduce systematic as well as random errors (Peters et al., 2010). Some studies have used the apparent systematic nature of STA to develop task and participant specific correction algorithms (Andersen et al., 2010; Ryu et al., 2009). This approach requires collection of data for a specific motor task and/or participant. No such data exists for the golf swing at present. Even for relatively well studied motor tasks, compensation techniques based on the characterisation of STA have not been able to provide satisfactory estimates of skeletal motion in in vivo experiments (Leardini et al., 2005). Other compensation techniques have treated STA as random or arbitrary noise (Alexander and Andriacchi, 2001; Andriacchi et al., 1998; Cheze et al., 1995; Lu and O'Connor, 1999; Söderkvist and Wedin, 1993; Spoor and Veldpaus, 1980). For example Dumas et al.(2009) simulated STA by adding sinusoidal zero-mean random noise to marker trajectories. Oberhofer et al.(2009) investigated the error propagation from STA to muscle tendon lengths predicted by a musculo-skeletal model during gait. STA was modelled as a normally distributed isotropic error function around the reference skin marker trajectories. Standard deviations of the error function were used to account for STA. This method of describing STA was based on the original findings of Woltring et al. (1985). Modelling STA as random noise does not allow for the observed relationship between STA magnitude and range of motion which has been reported for the knee (Manal et al., 2003), hip (Cappozzo et al., 1996), upper arm (Hamming et al., 2012) and thorax (Heneghan and Balanos, 2010). The participant specific nature of STA is also

difficult to model using a random function (Akbarshahi et al., 2010; Andersen et al., 2010; Cereatti et al., 2009; Cutti et al., 2003; Gao and Zheng, 2008; Garling et al., 2007; Reinschmidt, Bogert, Lundberg, et al., 1997; Stagni et al., 2005; Tsai et al., 2011).

For input into the uncertainty analysis, STA were assumed to be normally distributed around the segment centre of gravity positions as previously proposed to analytically estimate errors in joint kinematics (Oberhofer et al., 2009; Woltring, 1994; Woltring et al., 1985). Whilst there are limitations to this approach discussed above, it is a widely used method of modelling STA and will provide a measure of the upper bound effect of STA on the uncertainty of joint moment estimates. The STA errors synthesised from the literature (section 5.5) were input into the equations of Lanshammar (1980) in order to estimate the effect of STA on the calculation of derivatives (table 43). The bandwidths of the signals were estimated as described previously (section 5.6.1).

Table 43 Minimal noise variance in linear and angular velocity and acceleration due to STA calculated from the equations of Lanshammar (1980)

	Standard deviation of STA noise	Signal bandwidth	Standard deviation of noise for derivatives	
			1	2
<b>Position</b>	<i>(m)</i>	<i>Hz</i>	<i>ms<sup>-1</sup></i>	<i>ms<sup>-2</sup></i>
Set 1	0.00025	6	0.001	0.036
Set 2	0.0097	6	0.047	1.379
Set 3	0.0196	6	0.095	2.786
<b>Orientation</b>	<i>(rad)</i>		<i>rads<sup>-1</sup></i>	<i>rads<sup>-2</sup></i>
Set 1	0.012	5	0.05	1.10
Set 2	0.129	5	0.48	11.64
Set 3	0.262	5	0.97	23.59

---

## 6. Taylor Series Uncertainty Analysis

### 6.1. Introduction

An appreciation of how inaccuracies in input parameters contribute to uncertainties in inverse dynamics solutions is important for the interpretation of joint moments (Challis and Kerwin, 1996; Riemer et al., 2008). Knowledge of this uncertainty dictates the confidence that can be placed in the results and any conclusions that may be drawn from them (Challis, 2008). The Guide to the Expression of Uncertainty in Measurement (GUM), jointly developed by various international metrological and standards bodies, defines uncertainty as a "parameter, associated with the result of a measurement, that characterizes the dispersion of the values that could reasonably be attributed to the measurand" (ISO, 1995). The uncertainty describes the range of values within which the solution could lie and is a quantitative indication of the quality of the result (White and Farrance, 2004). As well as being recognised as an integral part of the validation process for any model approximating a living system (Henninger et al., 2010; Roache, 1998), uncertainty analyses are particularly important for inverse dynamics solutions which are difficult to validate since comparison to a 'gold standard' measurement is often not possible (Anderson et al., 2007).

Uncertainty in inverse dynamics solutions can originate from a variety of approximations and assumptions made during the modelling process. Inverse dynamics analysis seeks to apply the principles of mechanics to living tissue and as such there will be insufficiencies in the formulation of the model describing the physics of the real world (Henninger et al., 2010). For example, body segments are assumed to be rigid, with fixed inertial parameters. Furthermore, it is assumed that the shape of the body can be represented by a series of symmetrical geometric shapes (Yeadon, 1990). The non-invasive measurement of skeletal kinematics is subject to errors from soft tissue artefact (STA) (Leardini et al., 2005) and will be affected by the precision limits of the motion measurement system (Lanshammar, 1980). The measurement of external forces can contain error in both the force magnitude and centre of pressure location (Lewis et al., 2007). Moment arms are subject to inaccuracies caused by error in the estimation of joint centre locations, segment centre of mass and soft tissue artefact (STA). Furthermore, inverse dynamics is particularly susceptible to uncertainties due to the nature of the calculation procedure; using the Newton Euler

---

method, the net joint reaction force and moment acting on the distal end of one segment are assumed equal in magnitude and opposite in sign to those acting on the proximal end of the adjacent segment. It is this iterative nature of inverse dynamics that further compound the propagation of error as calculations proceed up the kinematic chain (Riemer et al., 2008).

Much of the previous literature concerned with error propagation in inverse dynamics solutions has utilised sensitivity analyses. A sensitivity analysis can be used to determine the influence of input parameter inaccuracy on the model output, scaling the relative importance of the inputs (Henninger et al., 2010; Roache, 1998). A single model input is perturbed by an order of magnitude whilst the others are held constant. Sensitivity analyses applied to inverse dynamics analysis have been carried out for gait (Challis, 1996; Holden and Stanhope, 1998; McCaw and DeVita, 1995; Pearsall and Costigan, 1999; Ren et al., 2008; Silva and Ambrosio, 2004; Stagni et al., 2000), lifting (Gagnon and Gagnon, 1992; Kingma, De Looze, et al., 1996; Kingma, Toussaint, et al., 1996; Larivière and Gagnon, 1999b; Plamondon et al., 1996), overarm throwing (Challis, 1996) and elbow flexion (Challis and Kerwin, 1996). Despite previous research theorizing that the effects of input parameter error would be most apparent during open chain, high acceleration activities (Challis and Kerwin, 1996; Pearsall and Costigan, 1999), the types of tasks which have been investigated are generally slow and simple. The main limitation of sensitivity analyses is that it is extremely arduous and time consuming to account for all possible combinations of errors, particularly for models which have a large number of input variables (Challis, 2007).

Unlike sensitivity studies which focus on one or two sources of error, uncertainty analyses are able to consider the inaccuracies in all input parameters and how they contribute to the total uncertainty in the solution (Riemer et al., 2008). They are also characterised by a greater focus on the quantification of inaccuracies in input parameters. Despite the evident importance of this type of analysis, knowledge of the uncertainty in inverse dynamics derived joint moments is limited. The Taylor Series Method (TSM) for error propagation has been used to estimate how inaccuracies in input parameters contribute to the total uncertainty in joint moment estimates for sagittal plane gait (Riemer et al., 2008), a single segment in fixed axis rotation (Andrews and Mish, 1996) and symmetrical lifting (Desjardins et al., 1998). Most

previous work utilising TSM has focused on only two or three input parameters and the effects of these inaccuracies in isolation of each other (Andrews and Mish, 1996; Desjardins et al., 1998). Riemer et al. (2008) presented a more rigorous uncertainty analysis of inverse dynamics solutions looking at the effects of 21 input parameter inaccuracies on joint moment estimates during sagittal plane gait. Inaccuracies were quantified for BSPs, joint centre location, force plate measurements, kinematic measurements, motion capture system measurements and segment angle error. Segment angle and BSP were identified as the parameters which made the greatest contribution to the joint moment uncertainty. Results were concerning with uncertainty magnitudes reaching 236% of peak joint moments. The Monte Carlo (MC) method is an alternative uncertainty propagation analysis method that has been applied to inverse dynamics solutions during gait (Langenderfer et al., 2008; Nguyen et al., 2007; Reinbolt et al., 2007). Error values are randomly generated for each input parameter based on its estimated probability distribution. The Monte Carlo method has been described as the 'gold standard' of probabilistic methods (Laz and Browne, 2010). However, this method is computationally expensive since many thousands of trials must be performed for convergence to the correct solution. Like TSM, studies which have used Monte Carlo simulations have assumed parameter independence and uniform error distributions since there was no prior knowledge of the correlation between input parameters, therefore, output distributions were possibly overestimated (Reinbolt et al., 2007). Reinbolt et al. (2007) reported that inaccuracies in axis position and orientation of body segments had the greatest effect on joint moment uncertainties. Studies utilising the MC method have tended to consider a smaller number of input parameters than TSM studies. For example, Nguyen et al. (2007) considered only BSP inaccuracies, Langenderfer et al. (2008) considered BSP and anatomical landmark identification inaccuracies and Reinbolt et al. (2007) considered inaccuracies in joint parameters, BSP and kinematic noise. Furthermore, Reinbolt et al. (2007) presented results for the left leg only. The small number of parameters considered in these studies may be due to the large amount of processing time required to perform such analyses, a major limitation of this method.

The aim of this study was to estimate the uncertainty in joint moments derived using inverse dynamics for the golf swing. The golf swing was used as a motion representative of a complex, high acceleration, open chain movement involving the

whole body. The Taylor Series Method for error propagation was used to estimate the upper bound uncertainty based on three sets of inaccuracy estimates for input parameters defined previously (chapter 5). It was expected that uncertainty in joint moments for the golf swing would be higher than the uncertainty reported by previous literature for slower tasks such as gait.

## 6.2. Methods

The procedures outlined in chapter 3 provide information on the experimental set up, data collection protocols (section 3.1, pg. 44) and sample used for this study (section 3.2, pg. 69).

### 6.2.1. Taylor Series Method for Propagation of Uncertainty

To calculate the effects of input parameter inaccuracies on the uncertainties in joint moments the combined standard uncertainty was determined using methods recommended by The Guide to the Expression of Uncertainty in Measurement (GUM) (ISO, 1995).

In general, a measurand  $Y$  is not measured directly, but is determined from  $N$  other quantities or input parameters  $X_1, X_2, \dots, X_N$  through the functional relationship  $f$ :

$$Y = f(X_1, X_2, \dots, X_N)$$

Equation 6.1

The general formula for propagation of uncertainty using a first order Taylor Series approximation is (Taylor, 1997);

$$u_c(y) = \sqrt{\sum_{i=1}^N \left(\frac{\partial f}{\partial x_i}\right)^2 u^2(x_i)}$$

Equation 6.2

where  $f$  is the function given in equation 6.1 and each  $u(x_i)$  is the inaccuracy in each input parameter. The combined standard uncertainty,  $u_c(y)$ , is an estimated standard deviation that characterises the dispersion of values that could reasonably be attributed to the measurand  $Y$  (ISO, 1995).

Equation 6.2 assumes that inaccuracies in input parameters are independent and random. As the relationship between parameters is not known, equation 6.2 can be re-written as;

$$u_c(y) \leq \sqrt{\sum_{i=1}^N \left(\frac{\partial f}{\partial x_i}\right)^2 u^2(x_i)}$$

Equation 6.3

Whether or not the inaccuracies are independent and random, equation 6.3 always gives an upper bound on  $u_c(y)$  (Taylor, 1997). This is often an overstatement of the uncertainty  $u_c(y)$  because there may be partial cancellation of the error in the input parameters  $x_1, \dots, x_n$  (Taylor, 1997).

In equation 6.3 the derivatives are estimated by developing a partial differential equation of the prediction variable with respect to the input parameter. In some cases the development of the resulting differential equations can be problematic; for three dimensional inverse dynamics the derivation of the partial differential equations is complex and lengthy. The solution can be approximated using numerical methods (Coleman and Steele, 2009). To accomplish the linearization numerically the procedure recommended by GUM (1995) was used;

Equation 6.2 can be written as;

$$u_c(y) = \sqrt{\sum_{i=1}^N [c_i u(x_i)]^2}$$

Equation 6.4

where

$$c_i \equiv \frac{\partial f}{\partial x_i}$$

Equation 6.5

The combined standard uncertainty  $u_c(y)$  may be calculated numerically by replacing  $c_i u(x_i)$  in equation 6.4 with

$$Z_i = \frac{1}{2} \{f[x_1, \dots, x_i + u(x_i), \dots, x_N] - f[x_1, \dots, x_i - u(x_i), \dots, x_N]\}$$

Equation 6.6

This was the approach used in this study. Proof of the numerical method for approximation of the Taylor Series expansion is presented in the appendix (APPENDIX D: Calculation of the combined standard uncertainty). For a summary of the assumptions made when using the Taylor Series method see APPENDIX O: Table of Assumptions (pg.59).

A custom application was written to allow alterations to be made individually to each of the input parameters of the joint moment equations. The application had the capacity to alter each input parameter by absolute amounts or percentages as required. Input files were created in excel; for each run of the inverse dynamics model, a segment, parameter and perturbation amount was specified. For every swing, and each of the 17 segments, each input parameter was perturbed according to the inaccuracy magnitudes defined previously (chapter 5) so that a total of 640 excel files were produced for each swing. Each file contained the three dimensional perturbed joint moment time series for each joint of the linked segment model. Each of these output files was processed in MATLAB (MATLAB 8.2, The MathWorks Inc., Natick, MA, 2013) whereby the inaccuracy values were combined as shown in equation 6.4.

### 6.2.2. Quantification of inaccuracies in input parameters

The quantification of inaccuracies in input parameters are described in detail elsewhere for inaccuracies in; 1) GRF (table 24, pg. 116), 2) linear acceleration, 3) angular acceleration, 4) angular velocity, 5) BSP (table 21, pg. 106), 6) centre of pressure (table 24, pg. 116), and 7) moment arm lengths. Note that inaccuracies due to STA and joint centre location contributed to inaccuracy in moment arm lengths and kinematics. Similarly, inaccuracies due to STA and motion marker noise contributed to inaccuracies in kinematics (table 44). Three sets of inaccuracy parameters were synthesised for each input variable to reflect the range of values reported in chapter 5 (for a complete list of the inaccuracy sets for each parameter and segment see - APPENDIX E: Complete list of inaccuracy values for sets 1, 2 and 3).

Table 44 Inaccuracy sets for kinematic measurements. These were the sum of errors quantified for motion marker noise and STA.

Parameter	Cause of inaccuracy		Total inaccuracy
	Noise	STA	
<b>Angular Velocity (rads<sup>-1</sup>)</b>			
Set 1	0.07	0.05	0.12
Set 2	0.13	0.48	0.61
Set 3	0.23	0.97	1.20
<b>Angular Acceleration (rads<sup>-2</sup>)</b>			
Set 1	1.77	1.10	2.87
Set 2	3.26	11.64	14.90
Set 3	5.71	23.59	29.30
<b>Linear acceleration (ms<sup>-2</sup>)</b>			
Set 1	0.12	0.04	0.16
Set 2	0.39	1.38	1.77
Set 3	0.68	2.79	3.47

### 6.2.3. Data Analysis

All joint moments and uncertainty values obtained using the three sets of inaccuracies were normalised in time as a percentage of the swing cycle which began at takeaway and ended three frames before impact using spline interpolation (MATLAB 8.2, The MathWorks Inc., Natick, MA, 2013). The mean and standard deviation of joint moments and uncertainties were calculated for each 1% of the swing. Absolute peak joint moments were calculated for the baseline moments ( $JM_0$ ) as well as for the moments with added uncertainty ( $JM_0 + u_c(JM)$ ). To quantify the effect of uncertainty the percentage of uncertainty relative to peak moments was calculated by dividing the maximum estimated uncertainty by the absolute peak moment. Temporal characteristics were also investigated by reporting the change in timing of peak joint moments due to uncertainty. Joint moments were normalised with respect to the weight and height of the participant to allow for comparisons between participants. Sensitivity coefficients were used to calculate the relative contribution of each parameter to the total uncertainty, calculated as follows;

$$S_i = Z_i/u(x_i)$$

Equation 6.7

where  $S_i$  is the sensitivity coefficient for parameter  $i$ ,  $Z_i$  is evaluated numerically by calculating the change in  $y$  due to a change in  $x_i$  of  $+u(x_i)$  and of  $-u(x_i)$  as in equation 6.6 and  $u(x_i)$  is the inaccuracy associated with parameter  $x_i$ . Sensitivity coefficients were averaged over the swing cycle to provide a ranking of each input parameter's contribution to the uncertainty (Laz and Browne, 2010).

## 6.3.Results

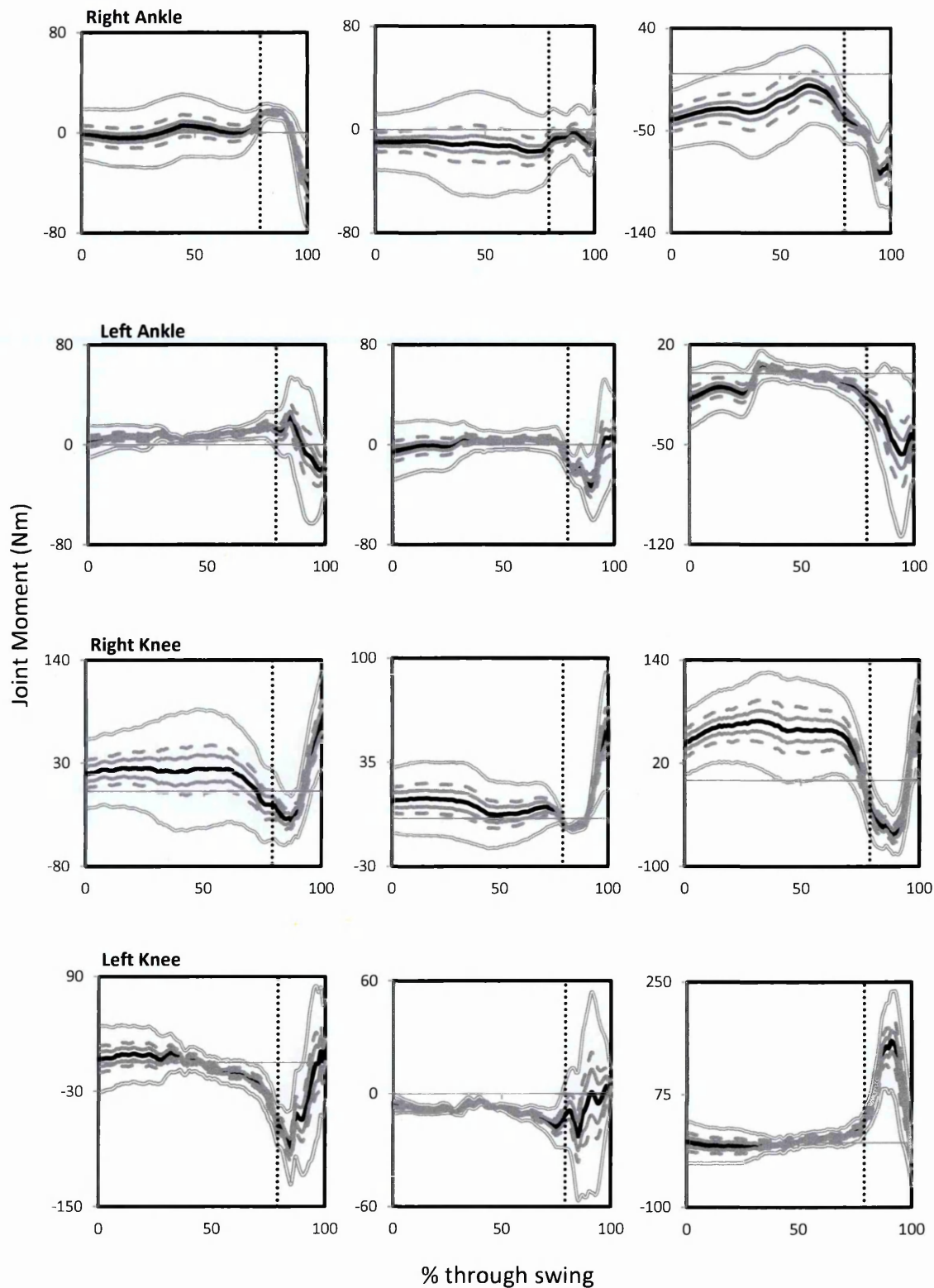


Figure 43 Time varying joint moment estimates (thick black line) and  $\pm U_1$ ,  $\pm U_2$ ,  $\pm U_3$  confidence limits (thin grey, dotted grey and double grey lines respectively) derived using set 1, 2 and 3 inaccuracy values respectively. Joint moments are presented in the local coordinate system of the distal segment. Vertical dotted line indicates top of backswing event. Joints are ordered distal to proximal. From left to right plots represent lateral-bending, axial rotation and flexion-extension moments respectively. Swing begins at takeaway and ends three frames before impact.

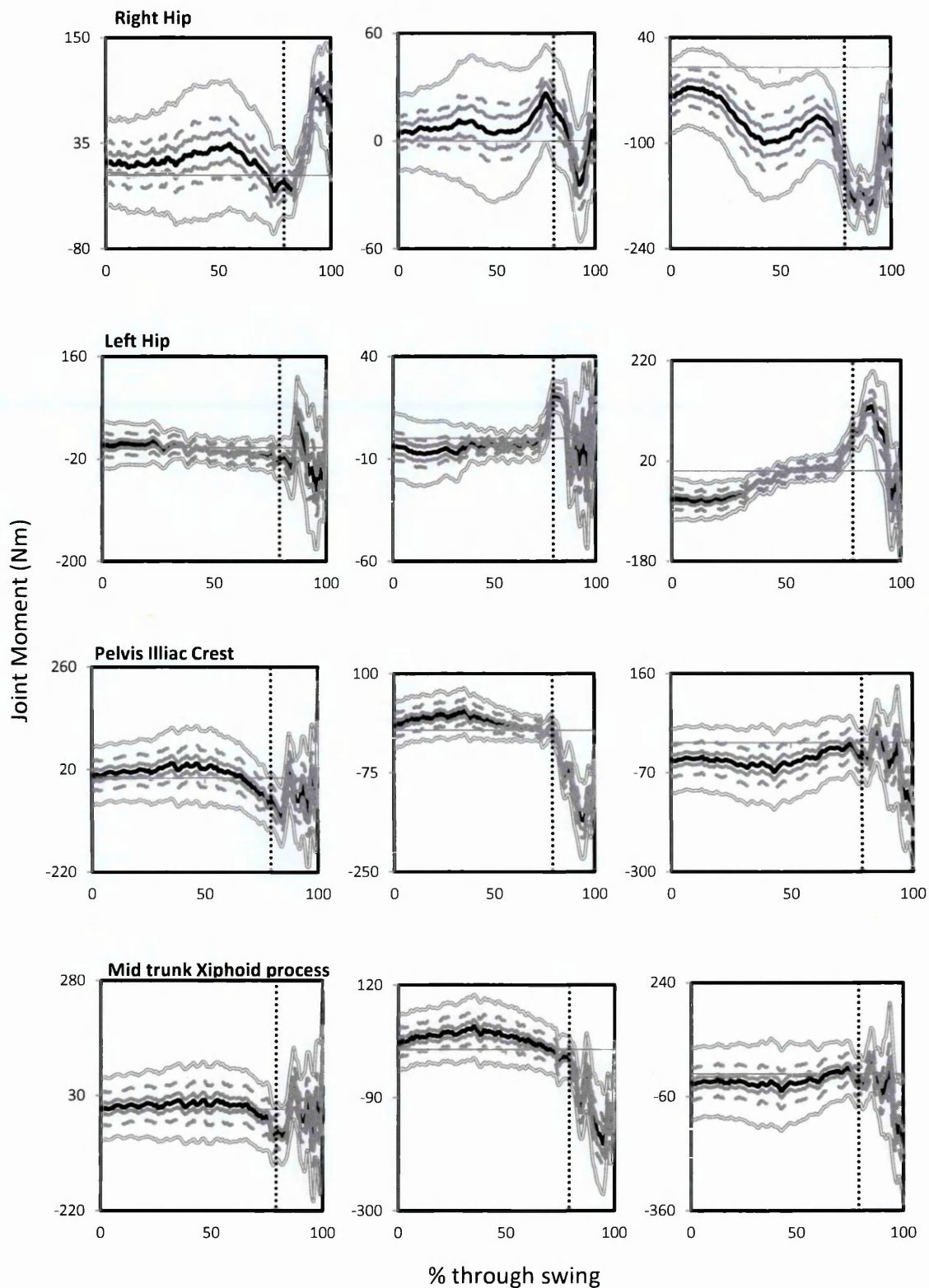


Figure 44 Time varying joint moment estimates (thick black line) and  $\pm U_1$ ,  $\pm U_2$ ,  $\pm U_3$  confidence limits (thin grey, dotted grey and double grey lines respectively) derived using set 1, 2 and 3 inaccuracy values respectively. Joint moments are presented in the local coordinate system of the distal segment. Vertical dotted line indicates top of backswing event. Joints are ordered distal to proximal. From left to right plots represent lateral-bending, axial rotation and flexion-extension moments respectively. Swing begins at takeaway and ends three frames before impact.

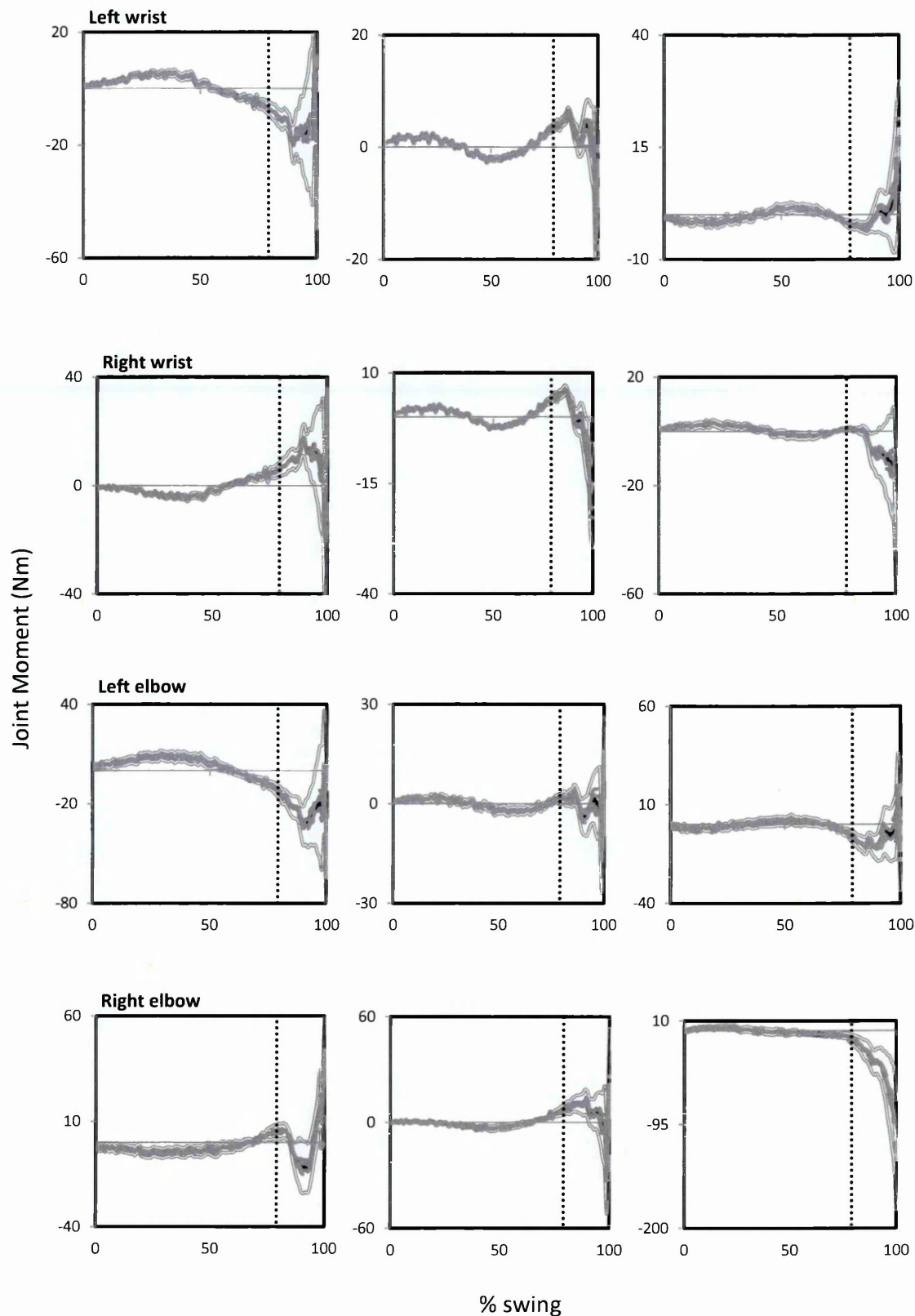


Figure 45 Time varying joint moment estimates (thick black line) and  $\pm U_1$ ,  $\pm U_2$ ,  $\pm U_3$  confidence limits (thin grey, dotted grey and double grey lines respectively) derived using set 1, 2 and 3 inaccuracy values respectively. Joint moments are presented in the local coordinate system of the distal segment. Vertical dotted line indicates top of backswing event. Joints are ordered distal to proximal. From left to right plots represent lateral-bending, axial rotation and flexion-extension moments respectively. Swing begins at takeaway and ends three frames before impact.

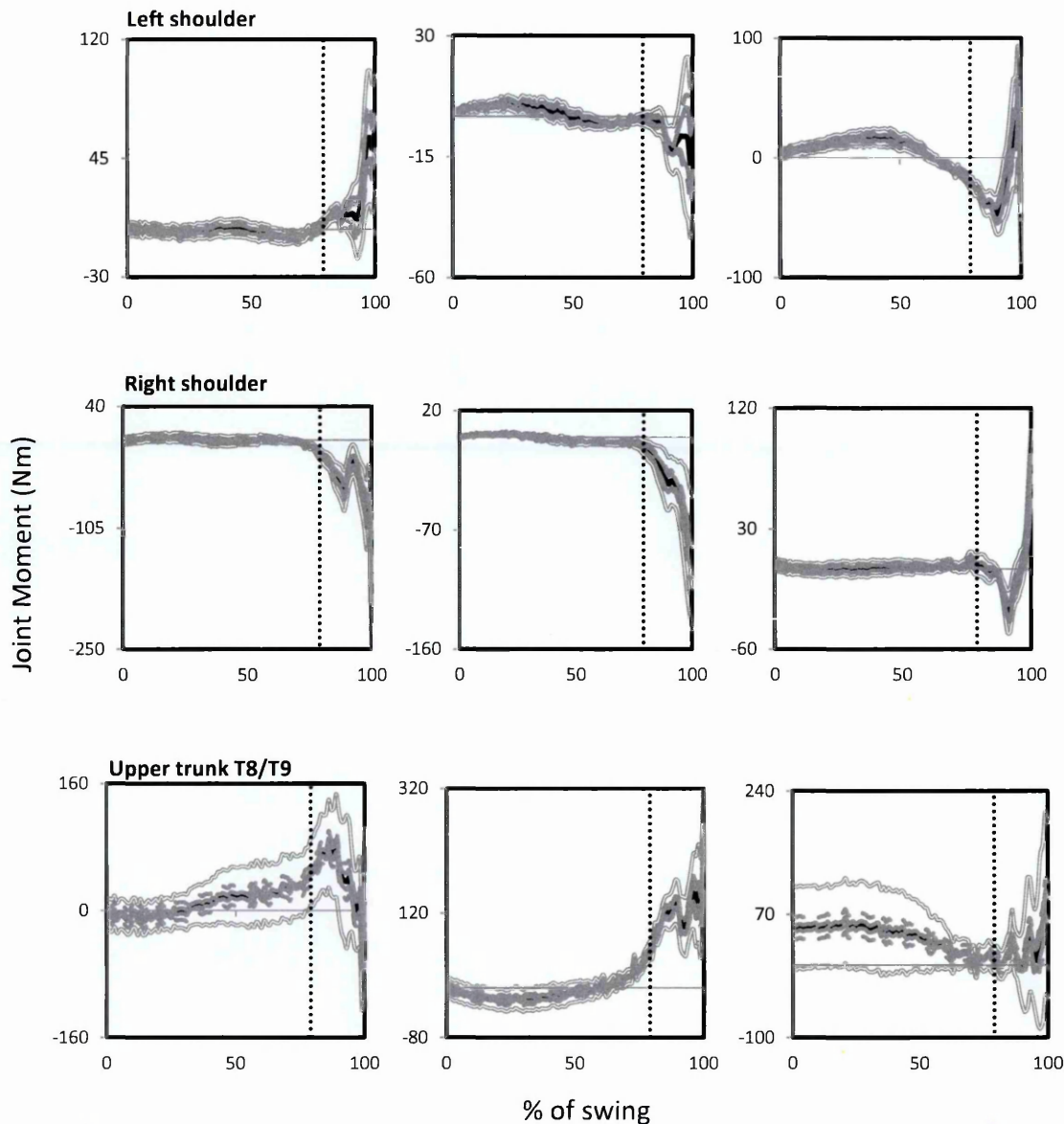


Figure 46 Time varying joint moment estimates (thick black line) and  $\pm U_1$ ,  $\pm U_2$ ,  $\pm U_3$  confidence limits (thin grey, dotted grey and double grey lines respectively) derived using set 1, 2 and 3 inaccuracy values respectively. Joint moments are presented in the local coordinate system of the distal segment. Vertical dotted line indicates top of backswing event. Joints are ordered distal to proximal. From left to right plots represent lateral-bending, axial rotation and flexion-extension moments respectively. Swing begins at takeaway and ends three frames before impact.

The magnitude of the uncertainties in the estimated joint moments varied over time (figure 47 and figure 48) however they did not resemble the moment profiles (figure 43, figure 44, figure 45 and figure 46). For the ankle, knee and hip joints of the right and left legs the uncertainty resembled the ground reaction force profiles (figure 49). Similar trends were observed for all sets of inaccuracies (APPENDIX G: Uncertainty figures for inaccuracy sets 2 and 3). The joint moment uncertainties were smaller for the more distal joints and larger for the more proximal joints for the both the top down and bottom up models (figure 47 & figure 48). This demonstrated the

---

accumulation of error inverse dynamics solutions as calculations proceeded up the kinematic chain. Uncertainties peaked just before impact for top down and bottom up models (figure 47 & figure 48).

For the top down model, mean and maximum uncertainties were similar for joints of the left and right arms particularly for the backswing (table 45 & table 47). Mean and maximum uncertainties during the downswing were higher than during the backswing for all segments. This reflected the increase in mean joint moments during the downswing which was apparent for all segments with the exception of left hand axial rotation moments. During the backswing, the mean and maximum uncertainty was lowest for axial rotation for all segments despite this not always being the smallest mean joint moment component. The upper trunk had the largest mean uncertainty during both the backswing and the downswing for the top down model.

For the bottom up model, the mean and maximum uncertainties differed between the joints of the left and right legs (table 46 & table 48). The mean and maximum uncertainties of the right ankle, knee and hip were greater than the left during the backswing. During the downswing, the reverse was true with uncertainties of the left ankle, knee and hip joints greater than those for the right side joints. This reflected the joint moment pattern during the swing; during the backswing when most of the player's weight was over the back foot, joint moments were higher for the right leg joints than the left. During the downswing, weight was transferred to front foot and joint moments were higher for the left leg joints.

For the top down model, the maximum estimated uncertainties relative to peak joint moments was highest for the lateral bending components of the left shoulder during the backswing, exemplified by values of 32.2%, 57.7% and 95.3% for sets 1, 2 and 3 respectively (table 45 & table 47). The relative uncertainties did not always increase as calculations proceeded proximally up the kinematic chain; for set 1 inaccuracies the upper trunk joint had a small relative uncertainty of 13.3% for lateral bending and the more distal shoulder joints had the largest overall relative uncertainty (32.2% and 26.8% for lateral bending of the left and right shoulder respectively). For set 3 inaccuracies, the left and right wrists had the highest relative uncertainty of up to 200.4% in the flexion-extension direction. For the bottom up model, the relative uncertainty was highest for the lateral bending component of the mid trunk joint during the backswing

---

exemplified by values of 62.8% 155.8% and 319% for sets 1, 2 and 3 respectively (table 46 & table 48). For the downswing the highest estimated uncertainty relative to peak joint moment was for axial rotation of the knee (50.8%, 88.0% and 219% for sets 1, 2 and 3 respectively).

The parameters that had the most influence on joint moment uncertainty at the mid trunk joint (the most proximal joint of the bottom up model) were moment arm lengths of the right side limbs during the backswing (figure 51). For lateral bending and axial rotation components, moment arm uncertainty in the z direction was most influential. For flexion-extension moments moment arms were most influential in the x direction. For the downswing moment arms of the left side limbs were most influential. As inaccuracies were increased from set 1 to set 2, centre of mass accelerations had more of an influence for lateral bending and axial rotation in the z direction and in the x direction for flexion-extension (table 61, pg. 30). Moment arms of the knee were also among the top five most influential parameters. For set 3, results were similar to set 1 inaccuracies with moment arms having the greatest influence on the uncertainty at the mid trunk joint. For the top down model, the upper trunk proximal moment arm had the largest influence for all components of moment arms and sets of inaccuracies (figure 51 and table 62). The proximal moment arm of the shoulders was the second most influential parameter. For set 2, upper trunk COM acceleration and angular acceleration were the most influential parameters. Set 3 inaccuracies were dominated by upper trunk moment arm uncertainties and also COM acceleration uncertainties. For top down uncertainties there was no difference in directions about which moments arms were most influential between the backswing and downswing as there was for the bottom up model.

Uncertainties affected the timings of peak joint moments (table 49). For the top down model the right shoulder axial rotation peak joint moment was changed by 174.0 ms, 283.3 ms and 560.8 ms for sets 1, 2 and 3 respectively. For the bottom up model the difference in timing of peak joint moments ranged from 9.0-521.9 ms and 0-97.4 ms for the backswing and the downswing respectively.

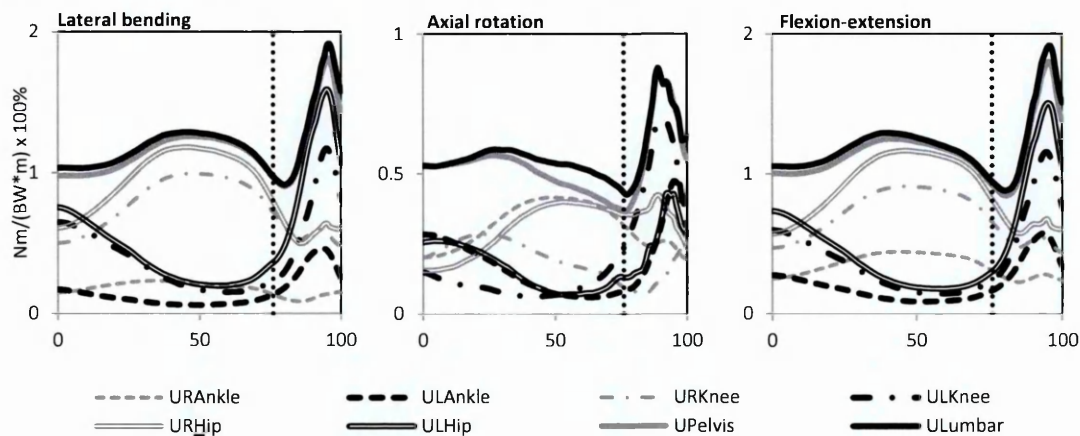


Figure 47 Bottom up joint moment uncertainties based on set 1 inaccuracy values, moments are presented in the local coordinate system of the distal segment. Moments were normalised with respect to the body weight and height of each participant before being averaged across all trials and participants for each 1% of the swing duration. Vertical dotted line indicates top of backswing event, swing begins at takeaway and ends three frames before impact.

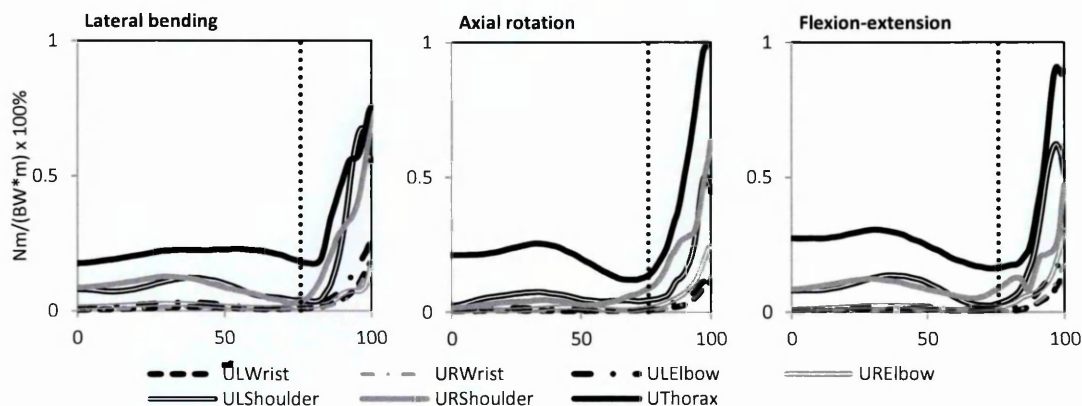


Figure 48 Top down joint moment uncertainties based on set 1 inaccuracy values. Moments are presented in the local coordinate system of the distal segment. Moments were normalised with respect to the body weight and height of each participant before being averaged across all trials and participants for each 1% of the swing duration. Vertical dotted line indicates top of backswing event, swing begins at takeaway and ends three frames before impact.

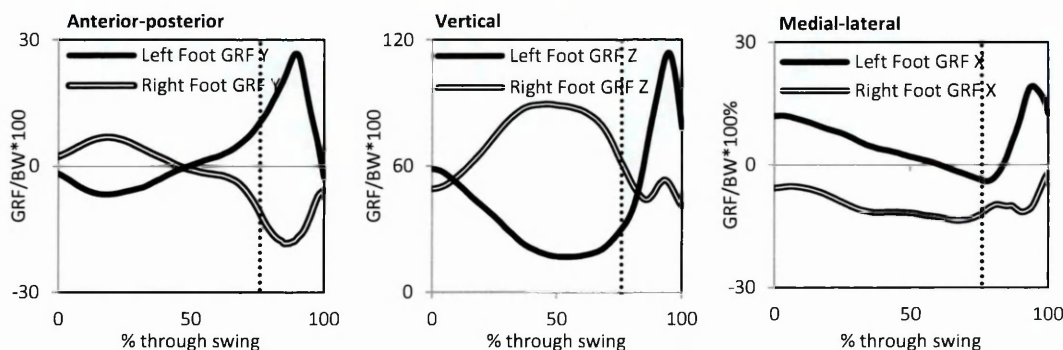


Figure 49 Ground reaction force profiles in global coordinate system normalised by body weight for comparison to uncertainty profiles. Mean GRFs of all participants are presented. Vertical dotted line indicates top of backswing event, swing begins at takeaway and ends three frames before impact.

Table 45 Uncertainty analysis results for set 1 inaccuracy values for the upper body joints

Joint	Backswinging			Downswinging			Max U	% contribution	% contribution
	Mean JM	Mean U	Max JM	Mean JM	Mean U	Max JM			
<b>Left wrist</b>									
lateral bending	0.06	0.01	0.57	0.02	0.02	0.02	0.18	16.6	2.7
axial rotation	0.07	0.01	0.27	0.01	0.01	0.01	0.11	22.0	3.8
flexion extension	-0.07	0.01	0.25	0.01	0.01	0.01	0.14	33.8	5.8
<b>Right wrist</b>									
lateral bending	-0.04	0.01	0.45	0.02	0.02	0.02	0.17	20.3	3.6
axial rotation	0.06	0.01	0.28	0.01	0.01	0.01	0.13	14.8	3.8
flexion extension	0.06	0.01	0.31	0.01	0.01	0.01	0.17	15.2	4.8
<b>Left elbow</b>									
lateral bending	0.18	0.02	0.79	0.03	0.03	0.03	0.25	13.4	4.1
axial rotation	0.02	0.01	0.18	0.02	0.02	0.02	0.12	19.0	10.7
flexion extension	-0.08	0.02	0.45	0.03	0.03	0.03	0.24	23.7	5.9
<b>Right elbow</b>									
lateral bending	-0.12	0.02	0.36	0.03	0.03	0.03	0.16	13.9	7.6
axial rotation	0.01	0.01	0.4	0.02	0.02	0.02	0.25	27.4	5.3
flexion extension	-0.02	0.02	0.57	0.03	0.03	0.03	0.29	5.7	5.4
<b>Left shoulder</b>									
lateral bending	-0.05	0.08	0.42	0.13	0.13	0.13	0.73	20.9	32.2
axial rotation	0.08	0.05	0.43	0.08	0.08	0.08	0.54	54.7	21.2
flexion extension	0.37	0.09	1.15	0.14	0.14	0.14	0.66	21.3	12.5
<b>Right shoulder</b>									
lateral bending	0.04	0.09	0.56	0.13	0.13	0.13	0.69	14.3	26.8
axial rotation	-0.05	0.04	0.55	0.09	0.09	0.09	0.60	12.7	19.1
flexion extension	0.02	0.09	0.48	0.13	0.13	0.13	0.45	17.0	27.7
<b>Upper trunk</b>									
lateral bending	0.72	0.21	1.95	0.25	0.25	0.25	0.77	16.2	13.3
axial rotation	-0.38	0.20	3.01	0.26	0.26	0.26	1.04	11.7	8.8
flexion extension	2.45	0.25	3.7	0.31	0.31	0.31	0.97	21.2	8.5

JM: Joint moment normalised by body weight and height (Nm/(BW\*m)\*100%); U = uncertainty (Nm/(BW\*m)\*100%)

Table 46 Uncertainty analysis results for set 1 inaccuracy values for the lower body joints

Joint	Backswinging			Downswinging			Max U	Max JM	Mean U	% contribution	Max U	% contribution
	Mean JM	Mean U	Max U	Mean JM	Mean U	Max U						
<b>Right ankle</b>												
lateral bending	0.96	0.20	1.81	0.24	0.18	1.02	0.24	1.81	0.12	15.6	0.20	9.8
axial rotation	-0.22	0.34	1.17	0.43	0.29	1.04	0.43	1.17	0.26	48.5	0.35	25.5
flexion extension	-2.04	0.38	3.06	0.45	0.28	4.05	0.45	3.06	0.26	15.7	0.39	7.0
<b>Left ankle</b>												
lateral bending	0.07	0.10	1.1	0.18	0.18	2.3	0.18	1.1	0.32	21.7	0.49	21.1
axial rotation	-0.30	0.14	1.27	0.29	0.29	1.04	0.29	1.27	0.26	28.0	0.49	15.5
flexion extension	-0.63	0.15	1.51	0.28	0.28	4.05	0.28	1.51	0.39	21.5	0.60	15.3
<b>Right knee</b>												
lateral bending	0.93	0.81	2.3	1.02	1.02	3.65	1.02	2.3	0.58	48.5	0.83	21.1
axial rotation	-0.31	0.21	1.04	0.30	0.30	1.04	0.30	1.04	0.13	31.6	0.27	17.5
flexion extension	1.33	0.75	4.05	0.94	0.94	3.45	0.94	4.05	0.53	26.3	0.77	14.9
<b>Left knee</b>												
lateral bending	-0.52	0.33	3.65	0.66	0.66	1.22	0.66	3.65	0.69	21.2	1.21	20.0
axial rotation	-0.19	0.10	0.94	0.25	0.25	0.94	0.25	0.94	0.49	33.2	0.76	50.8
flexion extension	0.75	0.30	3.45	0.61	0.61	3.45	0.61	3.45	0.71	24.5	1.19	11.1
<b>Right hip</b>												
lateral bending	0.33	0.98	3.33	1.22	1.22	3.33	1.22	3.33	0.61	42.0	0.99	15.0
axial rotation	-0.14	0.30	1.38	0.43	0.43	1.38	0.43	1.38	0.36	31.9	0.48	27.7
flexion extension	-3.83	0.96	8.03	1.21	1.21	8.03	1.21	8.03	0.65	16.7	0.98	7.7
<b>Left hip</b>												
lateral bending	0.13	0.38	2.57	0.77	0.77	2.57	0.77	2.57	1.01	33.7	1.66	32.3
axial rotation	0.09	0.15	1.23	0.28	0.28	1.23	0.28	1.23	0.26	25.6	0.53	27.1
flexion extension	-1.14	0.37	5.57	0.75	0.75	5.57	0.75	5.57	0.93	14.4	1.57	15.6
<b>Pelvis</b>												
lateral bending	0.76	1.12	2.41	1.29	1.29	2.41	1.29	2.41	1.30	60.4	1.85	25.9
axial rotation	0.82	0.50	2.89	0.59	0.59	2.89	0.59	2.89	0.64	21.2	1.00	12.3
flexion extension	-2.45	1.12	3.99	1.28	1.28	3.99	1.28	3.99	1.25	33.8	1.86	19.9
<b>Mid trunk</b>												
lateral bending	1.00	1.16	2.43	1.32	1.32	2.43	1.32	2.43	1.35	62.8	1.97	27.1
axial rotation	0.66	0.54	2.79	0.63	0.63	2.79	0.63	2.79	0.66	24.0	1.04	12.3
flexion extension	-1.35	1.16	2.94	1.33	1.33	2.94	1.33	2.94	1.32	49.7	1.99	20.9

JM: Joint moment normalised by body weight and height (Nm/(BW\*m)\*100%); U = uncertainty (Nm/(BW\*m)\*100%)

Table 47 Uncertainty analysis results for set 2 and 3 inaccuracy values for the upper body joints

Joint	Backswinging						Downswinging					
	Set 2			Set 3			Set 2			Set 3		
	Mean U	Max U	%	Mean U	Max U	%	Mean U	Max U	%	Mean U	Max U	%
<b>Left wrist</b>												
lateral bending	0.02	0.03	5.1	0.07	0.15	27.2	0.11	0.37	33.5	0.62	1.93	174.4
axial rotation	0.01	0.02	7.6	0.02	0.04	16.7	0.07	0.22	44.1	0.17	0.51	103.0
flexion extension	0.02	0.03	12.1	0.06	0.10	40.5	0.08	0.29	69.6	0.22	0.80	200.4
<b>Right wrist</b>												
lateral bending	0.02	0.03	6.7	0.06	0.16	37.1	0.09	0.32	37.7	0.46	1.39	156.4
axial rotation	0.01	0.02	7.3	0.02	0.05	16.7	0.07	0.23	26.3	0.17	0.55	63.4
flexion extension	0.02	0.03	10.0	0.07	0.12	40.9	0.10	0.39	34.2	0.49	1.73	154.7
<b>Left elbow</b>												
lateral bending	0.06	0.08	9.7	0.17	0.24	30.6	0.19	0.50	26.2	0.78	2.01	104.2
axial rotation	0.03	0.04	24.7	0.07	0.10	60.8	0.11	0.24	39.2	0.30	0.79	119.9
flexion extension	0.06	0.07	16.9	0.12	0.17	39.0	0.18	0.52	53.0	0.52	1.54	157.7
<b>Right elbow</b>												
lateral bending	0.05	0.07	18.6	0.13	0.19	54.4	0.11	0.32	26.8	0.43	1.18	95.9
axial rotation	0.02	0.04	10.8	0.06	0.13	31.7	0.16	0.47	52.1	0.47	1.57	181.2
flexion extension	0.06	0.08	14.7	0.15	0.24	46.5	0.21	0.65	12.7	0.98	3.00	58.7
<b>Left shoulder</b>												
lateral bending	0.18	0.23	57.7	0.28	0.38	95.3	0.46	1.13	32.3	0.87	2.28	66.0
axial rotation	0.08	0.13	31.5	0.15	0.23	55.9	0.28	0.78	80.1	0.59	1.50	152.8
flexion extension	0.18	0.24	20.9	0.32	0.44	39.0	0.44	0.98	31.7	1.06	2.54	82.3
<b>Right shoulder</b>												
lateral bending	0.17	0.23	46.2	0.29	0.38	78.5	0.43	1.12	23.2	0.99	3.04	62.0
axial rotation	0.07	0.14	29.1	0.14	0.28	57.5	0.40	0.95	20.0	1.11	2.86	60.4
flexion extension	0.17	0.22	46.7	0.29	0.41	89.1	0.27	0.68	25.7	0.62	1.63	62.1
<b>Upper trunk</b>												
lateral bending	0.78	0.85	46.2	1.91	2.66	145.5	1.05	1.61	33.8	3.23	6.00	125.0
axial rotation	0.46	0.53	18.1	1.02	1.21	41.4	0.86	1.70	19.2	2.14	4.73	53.5
flexion extension	0.90	1.03	28.1	2.96	3.93	106.9	1.12	2.02	44.7	3.73	8.17	181.6

U = uncertainty (Nm/(BW\*m)\*100%)

Table 48 Uncertainty analysis results for set 2 and 3 inaccuracy values for the lower body joints

Joint	Backswing						Downswing					
	Set 2			Set 3			Set 2			Set 3		
	Mean U	Max U	%	Mean U	Max U	%	Mean U	Max U	%	Mean U	Max U	%
<b>Right ankle</b>												
lateral bending	0.48	0.58	37.3	1.34	1.64	106.4	0.28	0.49	23.7	0.77	1.38	67.2
axial rotation	0.80	1.02	116.1	2.28	2.90	329.4	0.62	0.83	61.0	1.75	2.35	172.7
flexion extension	0.88	1.06	36.8	2.22	2.70	93.4	0.61	0.91	16.4	1.57	2.29	41.5
<b>Left ankle</b>												
lateral bending	0.23	0.44	52.2	0.64	1.21	144.5	0.76	1.16	50.5	2.14	3.24	141.8
axial rotation	0.35	0.69	66.6	0.97	1.91	189.1	0.61	1.16	36.5	1.68	3.14	99.5
flexion extension	0.36	0.66	50.5	0.91	1.67	128.6	0.90	1.37	35.2	2.22	3.38	86.5
<b>Right knee</b>												
lateral bending	1.43	1.78	84.5	3.57	4.44	212.0	1.05	1.46	37.1	2.60	3.65	91.9
axial rotation	0.38	0.53	55.7	0.93	1.30	137.6	0.24	0.50	33.1	0.57	1.22	78.9
flexion extension	1.49	1.84	51.5	3.35	4.13	116.3	1.06	1.52	29.4	2.39	3.43	66.3
<b>Left knee</b>												
lateral bending	0.65	1.18	37.6	1.55	2.90	93.0	1.24	2.10	34.7	3.06	5.18	85.6
axial rotation	0.19	0.45	60.0	0.46	1.11	147.7	0.86	1.31	88.0	2.14	3.24	219.2
flexion extension	0.65	1.21	48.8	1.46	2.72	109.8	1.48	2.38	22.3	3.41	5.45	50.9
<b>Right hip</b>												
lateral bending	1.93	2.33	42.0	4.32	5.30	182.3	1.38	1.94	29.5	2.92	4.38	66.8
axial rotation	0.55	0.78	31.9	1.30	1.84	136.9	0.65	0.86	49.9	1.51	1.94	112.9
flexion extension	1.99	2.40	16.7	4.17	5.09	71.4	1.50	2.03	15.9	3.06	4.28	33.6
<b>Left hip</b>												
lateral bending	1.10	1.61	71.3	2.10	3.49	154.4	2.03	3.08	60.1	4.51	7.05	136.7
axial rotation	0.32	0.52	47.8	0.70	1.19	109.1	0.52	0.96	48.8	1.14	2.08	106.1
flexion extension	1.09	1.62	31.3	2.05	3.36	64.8	2.00	3.06	30.2	4.27	6.63	65.3
<b>Pelvis</b>												
lateral bending	2.56	2.81	130.8	5.40	6.03	281.9	2.89	3.76	52.8	6.31	8.75	121.3
axial rotation	1.31	1.48	52.9	2.47	2.83	102.0	1.53	2.37	30.3	2.96	4.35	53.5
flexion extension	2.90	3.20	85.1	5.42	6.00	158.3	3.21	4.64	47.4	5.98	8.62	92.7
<b>Mid trunk</b>												
lateral bending	3.02	3.26	155.8	6.03	6.65	319.1	3.39	4.42	61.3	7.21	10.92	150.1
axial rotation	1.38	1.59	61.0	2.68	3.05	116.9	1.61	2.32	28.0	3.15	4.63	55.1
flexion extension	3.30	3.61	137.9	6.29	7.02	261.2	3.70	5.24	53.1	6.99	11.35	120.2

U = uncertainty (Nm/(BW\*m)\*100%)

Table 49 Effect of uncertainty on the timing of absolute peak joint moments

Joint	Difference in timing of peak joint moments due to uncertainty (ms)					
	Backswing			Downswing		
	Set 1	Set 2	Set 3	Set 1	Set 2	Set 3
<b>Left wrist</b>						
lateral bending	35.4	56.8	254.0	0.9	0.5	-70.3
axial rotation	-3.8	-6.8	-6.8	-7.6	-5.7	-3.1
flexion extension	0.0	6.3	-58.3	0.5	1.7	-5.4
<b>Right wrist</b>						
lateral bending	-17.5	-17.5	-51.0	4.7	1.4	-29.2
axial rotation	0.0	0.0	-53.0	-0.3	0.3	50.2
flexion extension	0.0	39.4	70.5	5.7	10.9	-6.8
<b>Left elbow</b>						
lateral bending	50.2	198.6	298.1	4.2	5.4	-83.5
axial rotation	47.4	57.5	103.6	-1.4	-3.0	-4.9
flexion extension	-0.2	14.2	105.6	-6.4	-16.5	-59.0
<b>Right elbow</b>						
lateral bending	-76.6	-232.8	-400.0	-8.0	-8.3	-12.7
axial rotation	-0.9	-5.0	-9.4	12.2	40.5	13.7
flexion extension	25.3	117.7	315.3	0.0	0.0	0.5
<b>Left shoulder</b>						
lateral bending	51.0	92.4	34.2	0.2	0.2	-0.5
axial rotation	120.5	143.2	150.5	7.5	-5.6	-47.2
flexion extension	83.5	106.1	156.1	-18.4	-28.0	-81.3
<b>Right shoulder</b>						
lateral bending	60.2	214.9	258.0	0.9	1.4	8.7
axial rotation	174.0	283.3	560.8	0.0	0.0	-0.3
flexion extension	-109.0	-138.5	-146.0	0.0	0.0	0.2
<b>Upper trunk</b>						
lateral bending	-5.2	-6.6	-33.7	32.3	32.5	38.4
axial rotation	-59.9	-59.9	-59.9	-10.6	-10.6	-15.8
flexion extension	-12.2	-12.2	-24.3	-7.8	-7.3	-8.0
<b>Right ankle</b>						
lateral bending	17.2	19.3	81.9	6.9	6.9	36.6
axial rotation	94.6	98.6	213.5	-24.0	-24.0	-75.9
flexion extension	-26.0	-31.4	-40.5	2.6	2.6	-9.9
<b>Left ankle</b>						
lateral bending	-39.1	-128.8	-109.5	11.8	23.3	59.5
axial rotation	16.8	42.7	285.6	1.4	-1.0	-9.7
flexion extension	-41.5	-99.7	-162.0	-1.9	9.7	-10.2
<b>Right knee</b>						
lateral bending	169.4	139.6	65.6	-22.2	-28.0	-22.9
axial rotation	19.3	63.9	230.2	-13.2	-16.7	-32.8
flexion extension	80.6	63.2	125.9	-5.7	-10.4	-30.2
<b>Left knee</b>						
lateral bending	91.3	91.3	521.9	8.9	-12.0	-97.4
axial rotation	127.8	127.8	289.2	-26.2	-58.9	-39.4
flexion extension	46.4	46.4	142.5	-1.0	-3.1	-9.5
<b>Right hip</b>						
lateral bending	176.6	245.8	258.9	2.4	3.3	-15.1
axial rotation	-57.8	-80.2	-86.8	68.6	71.0	87.7
flexion extension	-17.4	9.0	295.1	1.2	1.2	3.6
<b>Left hip</b>						
lateral bending	64.8	234.2	284.4	-17.5	-32.3	-31.1
axial rotation	90.6	210.6	240.3	-8.9	-48.3	-71.4
flexion extension	-116.7	-195.8	-197.2	-1.6	-1.9	-18.2
<b>Pelvis</b>						
lateral bending	182.1	172.9	150.9	-10.6	-35.8	-24.5
axial rotation	114.4	139.1	131.3	-0.5	-1.9	-18.1
flexion extension	-95.1	-296.9	-337.2	3.6	32.8	71.0
<b>Mid trunk</b>						
lateral bending	10.9	61.1	30.4	-19.1	-32.6	-32.5
axial rotation	158.7	229.5	204.2	0.0	-0.2	-2.1
flexion extension	-184.5	-241.1	-93.6	25.9	47.2	47.4

## 6.4. Discussion

Following a comprehensive analysis of inaccuracies in joint moment input parameters the Taylor series method (Taylor, 1997) for error propagation was used to estimate the uncertainty in joint moments calculated using inverse dynamics analysis. This approach was applied to three dimensional joint moments during the golf swing. Three sets of inaccuracy estimates for input parameters of inverse dynamics calculations were determined from a set of experimental data, complimented where necessary by data from the literature (chapter 5). The results provided an important insight into uncertainty in joint moments for high acceleration, complex motions which has yet to be established in the literature.

Joint moment uncertainty showed similar trends between inaccuracy sets, however the magnitude of the uncertainty for sets 1, 2 and 3 were not always in proportion to each other. This was due to the way in which the parameter inaccuracy sets were defined; sets 1, 2 and 3 were representative of the minimum, mean and maximum inaccuracies quantified in chapter 5. These inaccuracy sets did not necessarily increase in proportion to each other. Figure 50 shows the inaccuracy magnitudes of sets 1 and 2 as a percentage of the inaccuracy magnitudes for set 3. It can be seen that, for COM acceleration for example, the inaccuracy magnitude for set 1 was very small (1%) in comparison to set 2 (79%).

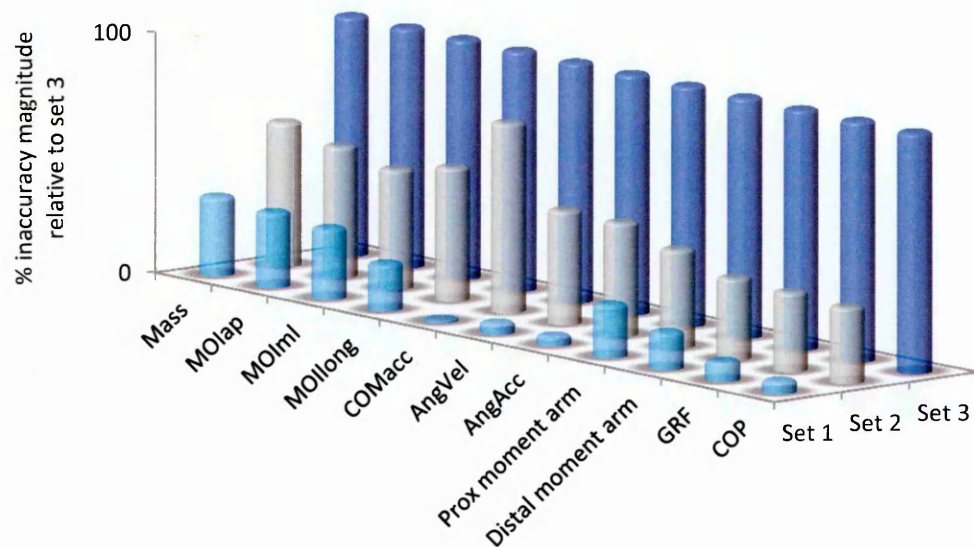


Figure 50 The relative magnitude of inaccuracy sets 1, 2 and 3. The magnitude of inaccuracies for sets 1 and 2 are presented as percentages of set 3. For parameters with direction or segment specific inaccuracies, mean inaccuracy values are presented.

Uncertainties did not follow joint moment profiles. For the lower body joints, uncertainties were similar in shape to the ground reaction force profiles for either foot (figure 49, pg. 175). This was consistent with the findings of Riemer et al. (2008) who reported similar shape of uncertainties to ground reaction forces for lower body joint moments during the single support phase of sagittal plane gait. The characteristics of the uncertainty for the lower body joints changed as the swing progressed from the backswing to the downswing. During the backswing, uncertainties of the right ankle, knee and hip joints were greatest. During the downswing, the uncertainties of the left ankle, knee and hip were greatest. These uncertainties reflected the joint moment pattern as weight was transferred from the back to front foot. For the top down model, there was not such a clear difference in uncertainty between left and right arm joints. This may have been a result of the assumptions made during the modelling process; to solve the indeterminacy caused by the club and arms forming a closed loop the forces were distributed equally between the right and left arms (section 3.1.13). Different partitioning strategies may affect the relative magnitude of the uncertainty between the left and right wrist, elbow and shoulder joints.

Analysis of the peak uncertainties relative to peak joint moments provided further insight into the effect that uncertainty could have on the interpretation of joint moments. The uncertainty relative to the peak joint moment can be substantial and ranged from 3% - 329% of the absolute peak moment; therefore, in some cases the relative uncertainty was higher than the joint moment itself. The magnitude of peak uncertainty relative to the peak joint moment did not always increase as calculations proceeded proximally; joints with the highest relative uncertainty were the shoulders and the upper trunk for the top down model and the right ankle and mid trunk joints for the bottom up model. The large magnitude of the relative uncertainty should be considered for studies concerned with joint moments; in biomechanics research, joint moments have been used to assess the effects of interventions on performance and compare skill levels and techniques to determine key performance indicators (Bahamonde and Knudson, 2003; Elliott et al., 2003; Gatt et al., 1998; Iino and Kojima, 2011). This is often achieved through a comparison of between group differences relative to within group differences using an  $F$  or  $t$ -test. Uncertainty in the joint moment estimates may lead to a smaller  $t$ -statistic which may no longer be significant

therefore altering the conclusions about the effectiveness of the intervention or importance of a performance indicator.

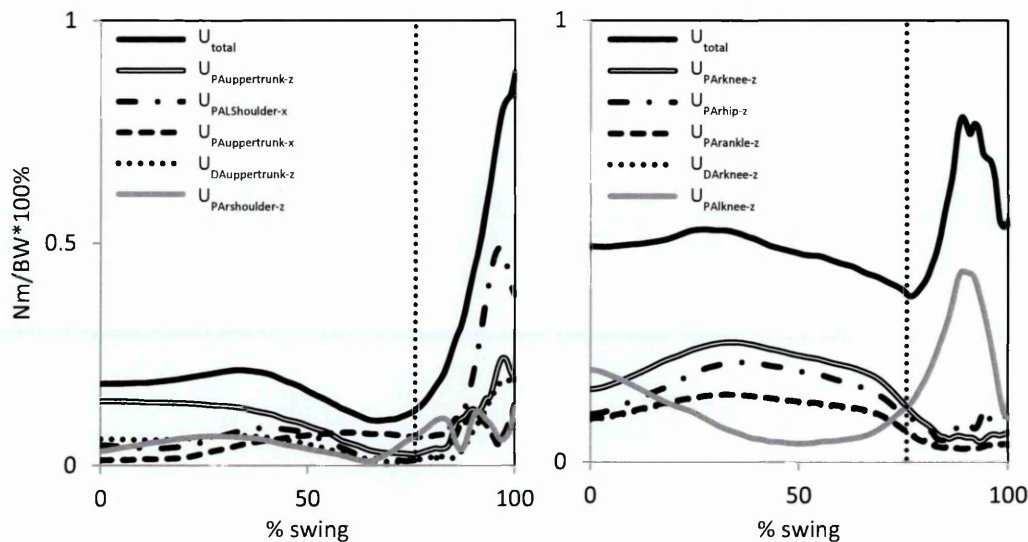


Figure 51 Example of main contributors to uncertainty in joint moments (normalised by height and weight) using set 1 inaccuracy values. (Left) at the upper trunk joint using the top down model and (right) at the lower trunk joint using the bottom up model. U: uncertainty; PA: proximal moment arm; DA: distal moment arm.

Examination of the parameters which had the most influence on joint moment uncertainty revealed the most dominant error sources (figure 51). The 5 most influential parameters accounted for an average of 30% of the total uncertainty at the most proximal joints of the top down and bottom up models. For both the top down and bottom up models these were the proximal moment arms and centre of mass accelerations. For the lower body model, uncertainties were influenced by the weight distribution patterns; during the backswing when most of the weight was over the back foot, proximal moment arms of the right side limbs were most influential in the  $z$  direction. For the downswing when the body weight was transferred forward over the front foot, proximal moment arms of the left side limbs were most influential in the  $x$  direction. For the upper body model, the proximal moment arm of the upper trunk in all three dimensions had the largest influence on joint moment uncertainty. The proximal moment arm of the shoulder was second most influential parameter. For the top down model there was no difference in directions about which moment arm lengths were most influential between the backswing and downswing as there was for the bottom up model. This may have been influenced by the assumption of an equal force distribution between the arms and may not be the case with different partitioning strategies. Uncertainty in moment arm lengths can be attributed to

inaccuracies caused by soft tissue artefact, joint centre location error and centre of mass error. Kinematic error can be attributed to soft tissue artefact and noise in the motion analysis measurement system. This finding was consistent with other studies which have reported that STA was among the largest source of error in joint moment estimations (Cappozzo et al., 1996; Leardini et al., 2005; Riemer et al., 2008).

The substantial uncertainties which could affect joint moment estimations reported in this study highlight the importance of reducing or correcting for the inaccuracies involved in inverse dynamics solutions. Results can be used to inform the best method of improving the model and data collection methods. This study has shown that moment arm inaccuracies had the most influence on the uncertainty and therefore, an important area in future research design is reducing STA and inaccuracies in joint centre location and segment centre of mass locations.

Optimisation methods offer an alternative way of improving the accuracy of inverse dynamics solutions. They have been used to reduce uncertainty effects by creating cost functions based on minimising the force and moment residuals at the feet. Riemer et al. (2008) reported that uncertainties in joint moments were mainly influenced by errors in segment angles mostly associated with soft tissue artefacts. Based on these findings a method was designed to increase accuracy through optimisation of angular position data used to describe segment motion (Riemer and Hsiao-Wecksler, 2008). Angular data was computed using a constrained non-linear optimisation algorithm with a cost function that minimised the difference between the measured and predicted GRF. Other studies have used similar methods to optimise BSP estimates (Vaughan et al., 1982b), GRF and segment motion measurements (Kuo, 1998) and segment acceleration (Cahouet et al., 2002). The results of this study dictate that optimisation of the moment arm lengths and centre of mass accelerations would result in the greatest improvement in accuracy of inverse dynamics solutions for the golf swing.

The temporal characteristics of the joint moment profiles were affected by uncertainties. Uncertainties had the capacity to change the timing of peak joint moments by as much as 560ms for the right shoulder joint. Timings were most affected during the backswing. Segmental sequencing analysis has been applied to kinematics in order to establish optimal motion patterns during the golf swing

(Anderson et al., 2006; Kenny et al., 2008). Such studies have tested for statistically significant differences in both the timing and the magnitude of peak kinetic energy between segments. There is considerable scope for establishing these patterns for joint moments in golf. If these patterns are to be established, studies must take into consideration the effect of uncertainty on the timings and magnitudes of peak joint moments. Table 49 (pg. 180) shows that, due to uncertainty, the timing of the peak moment for the pelvis could be delayed by 71ms, whilst the timing of the upper trunk peak joint moment could be 8.0ms earlier than predicted. This would result in a smaller time difference between peak moments for these two segments. A statistically significant difference seen in the results could in fact not be significant once uncertainty is taken into account.

There was a lack of studies available for comparison to the results of this study. Andrews and Mish (1996) found uncertainties reached 12% of baseline joint moments for a single segment in fixed axis rotation. Only BSP errors of  $\pm 5\%$  were considered. Desjardins et al. (1998) reported that external force uncertainty had the greatest effect on the L5/S1 moment output for lower body joints during a lifting task. Segment mass had the greatest effect on the upper body joints. Input parameters were perturbed by  $\pm 5\%$  and these were perturbed in isolation of each other. The Monte Carlo Method is an alternative uncertainty propagation analysis method which has been applied to inverse dynamics solutions during gait (Langenderfer et al., 2008; Nguyen et al., 2007; Reinbolt et al., 2007). Reinbolt et al. (2007) found axis position and orientation of body segments had the largest effect on joint moments (Reinbolt et al., 2007). STA was shown not to have a significant effect on the uncertainties; however this was modelled as a continuous noise function with amplitudes of 0.25-1 cm which was considerably smaller than the STA magnitude used in this study. The range of STA used by Reinbolt et al. (2007) was not large enough to represent the expected STA experienced by some segments during the golf swing. Langenderfer et al. (2008) reported 56-156% variability in joint moments and joint reaction forces from nominal base values for BSP and anatomical landmark identification errors during the stance phase of gait. These studies which have investigated uncertainty using Monte Carlo simulations have been concerned with gait analysis and therefore comparisons to golf swing joint moment uncertainty characteristics are difficult. These Monte Carlo studies have focussed on inaccuracies in only a limited number of parameters. This is

---

most likely due to the increased processing time required to run Monte Carlo simulations.

From previous literature the most comprehensive study of a similar nature involved the estimation of uncertainties in joint moment estimates during sagittal plane gait (Rierner et al., 2008). Peak uncertainty relative to peak joint moments was reported to range between 6% - 236% (Rierner et al., 2008). Maximum relative uncertainties were therefore higher for the golf swing. Differences in the results may be due to dissimilarity in the movements analysed and the way in which the inaccuracies were defined. For this study, the quantification of inaccuracies in input parameters were specific to the experimental set up; inaccuracies in all but two input parameters were quantified using experiments with the same equipment used for data collection. Reimer et al. (2008) relied mainly on data from previous studies to extract inaccuracy sets. In addition, Rierner et al. (2008) used only two sets of inaccuracies, whereas it was thought more appropriate to use three in order to better characterise the range of inaccuracies which could affect joint moment estimations during a high acceleration golf swing.

The Taylor Series Method for propagation of error provided an upper bound of joint moment uncertainties (Taylor, 1997). The limitations of the Taylor series method (TSM) for quantification of error propagation are fully acknowledged in this thesis. TSM is only approximate for non-linear models and does not provide a complete description of the estimated uncertainty (Hills and Trucano, 1999). Perturbations are assumed to occur simultaneously in the worst possible combinations and based on this assumption the extreme condition or upper bound of uncertainty is output. Monte Carlo (MC) simulations have been described as the 'gold standard' of probabilistic techniques (Laz and Browne, 2010). The MC method is able to fully characterise the range of possible outcomes and their likelihood. However, the MC method is computationally expensive and would require a large amount of processing time if all sources of inaccuracy considered in this study were to be included (Laz and Browne, 2010). The use of TSM provided a more efficient method to quantify uncertainty bounds for a large number of input parameters. Furthermore, without knowledge of the correlation between input parameters, MC simulations, like TSM, assume parameter independence and uniform error distributions, therefore, output distributions will possibly be

---

overestimated (Reinbolt et al., 2007). The TSM uncertainty analysis provided knowledge of the most influential parameters affecting joint moment uncertainty. This information could be used to prioritise the parameters to include in subsequent Monte Carlo simulations thereby making implementation more manageable.

### **6.5.Conclusion**

The uncertainty of joint moment estimates during the golf swing was substantial and ranged from 3% - 329% of the peak joint moment. This was higher than previously reported for sagittal plane gait (Riemer et al., 2008) indicating that for high acceleration, open chain movements, uncertainty in inverse dynamics derived joint moments is increased. The uncertainty analysis was able to identify the input parameters which made the greatest contribution to joint moment uncertainty. These were the proximal moment arms and the centre of mass accelerations. Uncertainty also affected the timing of peak joint moments which could affect the interpretation of joint moments. The quantification of joint moment uncertainties provides important information relating to the interpretation of joint moments; without knowledge of the uncertainties useful conclusions cannot be drawn.

## 7. Summary, conclusion and future research

It is the purpose of this chapter to summarise the results presented in the previous chapters relating to validation and uncertainty in joint moments calculated using inverse dynamics analysis. Validation and knowledge of the uncertainty in solutions is of critical importance in interpretation of results from any biomechanical computational model. Previous research has suggested that the iterative nature of inverse dynamics calculations and the large potential for propagation of error as calculations proceed up the kinematic chain made inverse dynamics solutions particularly susceptible to error. The primary motivation for this thesis was the lack of knowledge of the uncertainty in the estimation of joint moments derived through inverse dynamics analysis for open chain, high acceleration movements. The golf swing was used to provide a mechanical basis for this analysis. It was representative of a highly complex skill involving the coordination of many body segments moving at high accelerations in multiple planes. The task of validating the output of inverse dynamics analysis is not trivial since there is usually no 'gold standard' measure for comparison. Therefore, this was achieved using a two tier approach which included the use so called "validation" techniques and an uncertainty analysis. The validation analysis was expected to provide some insight into the accuracy of inverse dynamics solutions, however there were major limitations associated with these methods. Uncertainty analyses have been recognised as an integral part of the validation process, particularly for models which are difficult to validate or cannot be validated (Anderson et al., 2007).

The validity of the model was tested by comparing top down and bottom up joint reaction forces (JRF) and joint moments (JM) at the T8/T9 joint estimated during the golf swing. In addition, the predicted ground reaction forces (GRF) using a top down approach were compared to measured ground reaction forces. For this analysis, the swing was split into two phases; the backswing and the downswing. In general, mean and peak differences between GRF, JRF and JM were greatest during the downswing. The apparent increase in modelling error may have been related to the increase in acceleration of the body segments during the downswing. It had been reported previously that for lifting tasks, an increase in lifting speed led to an increase in the residuals between the top down and bottom up calculated joint moments at the L5/S1

---

joint (Kingma, De Looze, et al., 1996; Larvière and Gagnon, 1998; Plamondon et al., 1996). Results indicated that, for open chain movements, through periods of high acceleration, inverse dynamics solutions can be subject to errors which have the capacity to significantly affect the interpretation of joint moments depending on which model is used. A limitation of these methods of validation is that nothing can be learnt about the individual sources of error or how they contribute to the total residual error. Furthermore, these methods were unable to provide information about the error at different joints and how this error propagates through the kinematic chain.

Uncertainty was quantified using the Taylor Series Method for propagation of error (Taylor, 1997). The first challenge in implementing this method was quantifying the inaccuracy magnitudes for each input parameter. The inaccuracies in body segment parameters, ground reaction force, centre of pressure location and kinematics were determined experimentally. Inaccuracies caused by Soft Tissue Artefact (STA) and error in joint centre locations were extracted from the literature due to ethical constraints associated with measurement of these errors. Three sets of inaccuracies were used to account for the range of inaccuracies produced from experimentation and reported in the literature. The results of the Taylor Series analysis provided an estimate of the upper bound uncertainty as it was assumed that input parameters were random and uncorrelated. A common approach was taken when defining the three inaccuracy sets for each input parameter; set 1 was representative of the minimum inaccuracy, set 2 the mean and set 3 the maximum inaccuracy. This approach was standardised for all input parameters. The relative magnitude of the inaccuracies between sets was not always proportional and this reflected the way in which they were selected. Re-running the uncertainty analysis three times with a minimum, mean and maximum set of inaccuracies provided a range of results to better characterise the uncertainty.

Accurately estimating the magnitude of inaccuracies in input parameters was essential for realistic results as it directly effects the predicted uncertainty bounds (Laz and Browne, 2010). Difficulties in obtaining realistic inaccuracy values were compounded by the assumption implicit to the Taylor Series Method that error in input parameters were random in nature and that the magnitude of the error was constant throughout the motion. This simplification was more appropriate for some parameters than

others. For example inaccuracies in the estimation of segment mass were unlikely to change significantly during the golf swing motion. However, the error in the estimation of the centre of mass positions and moments of inertia of the less rigid segments such as those in the trunk were likely to change considerably during the golf swing as segments moved through a large range of motion at high speed. For Soft Tissue Artefact (STA), a fixed magnitude of random error does not allow for the observed relationship between STA magnitude and range of motion which has been reported for the knee (Manal et al., 2003), hip (Cappozzo et al., 1996), upper arm (Hamming et al., 2012) and upper trunk (Heneghan and Balanos, 2010). Other studies have used the apparent systematic nature of STA to develop task and participant specific correction algorithms (Andersen et al., 2010; Ryu et al., 2009) and this may have been a more appropriate method of modelling STA. This approach would require collection of data for a specific motor task and no such data exists for the golf swing at present.

The quantification of BSP inaccuracy was specific to the geometric model used. This was an improvement on other studies which based their inaccuracy values on a combination of inaccuracy values reported in the literature for a range of BSP estimates using both geometric and proportional models (Riemer et al., 2008). A range of body types were used to account for the possible range of body types used in the main data collection. This was important as accuracy of BSP estimates has been shown to be dependent on the age, body type and gender (Durkin and Dowling, 2006; Wicke et al., 2009). The method used was able to provide segment specific inaccuracy values for most body segments. Body segments excluded from the analysis were the hands, feet, and head and neck segments. Inaccuracy values for these segments were based on mean values of all other segments. Though this was not ideal, it was thought that this was a reasonable estimate of inaccuracy since the same techniques were used to model these segments as the others. The use of a laser scanner provided volumetric measurements of each segment which were used for 'gold standard' comparisons. The laser scanner did not have the ability to measure segment density. This meant error in BSP as a result of the uniform density assumption was not considered and this may have increased the reported error. However, it has been shown that BSP estimates are most sensitive to the volume function with density having only a small secondary influence (Ackland et al., 1988; Wicke and Dumas, 2010).

The accuracy with which force plates were able to measure both forces and centre of pressure location for a single point load were determined. Both static and dynamic tests were used however inaccuracies were based on dynamic loading as this experimental condition better replicated dynamic loading of the feet during the golf swing. Previous studies suggested that the expected accuracy of the force plates during the golf swing, where pressure is distributed over a larger area, i.e. the sole of the foot, would be greater than indicated in this experiment (Bobbert and Schamhardt, 1990; Middleton et al., 1999; Schmiedmayer and Kastner, 2000). In addition, maximum force magnitudes achieved in this experiment were lower than the maximum forces expected during the golf swing. This may have also resulted in lower accuracy than would be expected during the golf swing (Chockalingam et al., 2002). Inaccuracies quantified may be most similar to the error expected during the follow through on the back foot when most of the weight is over the front foot. Therefore, inaccuracies were representative of the upper bound and the influence of inaccuracy in ground reaction forces and centre of pressure position on the uncertainty in joint moments was possibly overestimated.

The noise variance of the Polhemus Liberty electromagnetic system was evaluated; the variance of the relative positions and orientations of two sensors fixed to a rigid bracket was calculated at various positions within the test volume. The effect of mapping techniques to correct for distortions caused by metal in the force plates was also investigated. Dynamic trials had a greater variance than static trials for both position and orientation. The metal in the force plates was shown to increase the measurement variance for both static and dynamic trials. For the majority of measurements, the variance in both position and orientation was shown to increase with distance from the transmitter. Quantification of the variance in sensor position and orientation did not consider the effects of systematic errors although they may have affected the results. Further work should include a test set up whereby the positions of the sensors are accurately known therefore providing a true 'gold standard' measurement for comparison. The presence of metal force plates in the test volume caused a large amount of distortion in the lower third of the test volume nearest the plates. Mapping was able to reduce the variance of both position and orientation near the force plates and inaccuracy values were based on the mapped data for dynamic measurements.

Soft tissue artefact (STA) is the relative displacement between the skin markers or sensors and the underlying bone. STA contributed to the inaccuracy in the measured kinematics and the distal and proximal moment arm lengths. Methods to quantify STA were beyond the scope of this thesis due to ethical constraints therefore STA magnitudes were sourced from the literature. The literature was not able to provide STA measures for complex, high acceleration motions like the golf swing. There exists a great deal of controversy over the characteristics of STA with conclusions from many studies contradicting each other. The disparity in reported STA magnitudes made the selection of inaccuracy bounds difficult. This disparity was due to the participant, task, segment and marker attachment method specific nature of STA. In addition, since some studies have shown the magnitude of STA to vary throughout a specific task or movement, applying a constant error bound to the kinematic data was not ideal. In order to select the most appropriate inaccuracy magnitudes, each study reviewed which had quantified STA was given a similarity score which rated the similarity of the activity, movement velocity and marker attachment method to the golf swing data collection methods used in this thesis. Mean inaccuracy values (set 2) were based on the weighted averages of each study.

Error in joint centre location contributed to the inaccuracy in the proximal and distal moment arm distance. Methods to quantify inaccuracies in joint centre location estimates were beyond the scope of this thesis so these were synthesised from the literature. A total of 11 studies were found which provided error estimations for six joints. Inaccuracies in joint centre location estimates were joint specific for the ankle, knee, hip, shoulder and elbow. No studies were found which quantified error in the neck joint centre or any of the trunk joints. The lack of studies reporting error in trunk joint centre definitions indicated the difficulty in quantifying this error experimentally. Error values of joints for which no studies were found were based on the overall mean values of all other joints. Studies which used 'gold standard' imaging techniques such as MRI provided more relevant results than others which used functional methods such as the Optimal Mean Helical Axis. It is for this reason that inaccuracy bounds were based on studies which used imaging techniques where they were available.

Lanshammar's prediction equation (1980) was used to estimate the minimal variance with which angular velocity, angular acceleration and linear acceleration could be

measured given the errors caused by sensor measurement noise and soft tissue artefact. It was assumed that the variance in sensor position and orientation calculated during experiments was representative of the random noise present throughout swing trials. Similarly, STA was assumed to be normally distributed around the segment centre of gravity positions as previously proposed to analytically estimate errors in joint kinematics (Oberhofer et al., 2009; Woltring, 1994; Woltring et al., 1985). For application of Lanshammar's equation, variables were assumed to be normally distributed and band limited. The band limit of the signals was estimated using standard frequency analysis techniques. For a signal to be band limited it must be suitably amplified up to the cut-off frequency up to which no signal is allowed to pass (Challis and Kerwin, 1996). No filter is ideal and therefore no signal is perfectly band-limited.

The input parameters around which the uncertainty analysis was based were selected from the components of the joint reaction force and joint moment calculations. This provided a clear basis from which to examine the sources of inaccuracy which contributed to the uncertainty in inverse dynamics solutions. However, not all possible sources of inaccuracy were included in this study. The rigid body assumption implicit to inverse dynamics calculations was not considered directly; segment lengths may vary significantly over time (Zhang et al., 2004) and the assumption of rigid segments has been shown to be particularly unsuited to high impact movements (Gruber et al., 1998). The effect of filtering on kinematic noise was not considered. It was expected that noise in the measured kinematics would have been reduced once filtering had been applied so that the resulting inaccuracy would have been lower than quantified in section 5.6. The inclusion of some error sources would have required the components of the inverse dynamics calculations to be broken down in to their fundamental parts; for example, error in anatomical landmark locations and anatomical coordinate system orientation. These sources of error were instead included in the uncertainty analysis as contributing to the quantified inaccuracy in estimating other parameters. For example, error in the anatomical landmark locations contributed to the inaccuracy in BSP estimates.

The uncertainty in joint moment estimates during the golf swing was quantified using the Taylor Series Method for propagation of error. Results were representative of the

upper bound uncertainty since parameters were considered uncorrelated and random (Taylor, 1997). Uncertainties were found to increase as calculations proceeded proximally with the mid trunk and the upper trunk joints experiencing the highest uncertainty. The uncertainty profiles for the lower body joints followed the ground reaction force profiles for either foot and not the joint moment profiles. During the backswing, uncertainty was greatest for the back leg joints when most of the weight was over the back foot. As weight was transferred to the front foot during the downswing, the uncertainty of the front leg joints were highest. For the upper body joints, which were not influenced by GRF, there was no clear difference between the uncertainty magnitudes of the left and right arms. The assumption that loads were equally distributed between the arms - required to solve the indeterminacy problem - may have affected the uncertainty patterns between the arms. Uncertainties reached 339% of the peak joint moment magnitude. This was higher than previously reported for sagittal plane gait (Riemer et al., 2008). The joints with the highest uncertainty relative to peak joint moment were the shoulders and the upper trunk for the top down model and the right ankle and mid trunk for the bottom up model. In general, relative uncertainties were highest for the lower body joints.

The magnitude of the uncertainty relative to the peak joint moment was highest during the downswing. This agreed with the results of the validation study which indicated that during the downswing, when segments were moving at the maximum acceleration, joint moment estimations were the most susceptible to error. The increase in acceleration of the segments also changed which joints had the highest uncertainties; for the backswing, relative uncertainty was highest for the left shoulder and mid trunk joints whereas for the downswing, uncertainties were highest for the knee and the wrist joints.

The parameters which had the most influence on joint moment uncertainty were the moment arms and the centre of mass acceleration. Uncertainty in moment arm lengths was attributed to STA, joint centre location error and centre of mass error. Kinematic error was attributed to STA and motion marker noise. Uncertainties affected the temporal characteristics of the joint moment profiles. For, example, the timing of peak joint moments of the right shoulder joint was altered by 560ms when

uncertainties were considered. This could have a significant effect on sequencing patterns used to analyse joint moments during the golf swing.

The research findings of this thesis provide an important insight into the magnitude of uncertainty in inverse dynamics solutions that should be expected for other high acceleration movements. It is acknowledged that the uncertainty reported may change for movements other than the golf swing however, results are generalizable to other high acceleration, open chain activities providing they are interpreted in the context of the movement analysed and the data collection methods used.

### **7.1.Future research**

This thesis has quantified the upper bound uncertainty in joint moments estimated for the golf swing which was representative of a high acceleration, open chain movement. The uncertainty bounds characterise the range of values within which the joint moments could lie and quantitatively indicate the quality of the joint moment estimations. In addition, this analysis has provided information on the most influential parameters affecting the performance of inverse dynamics analysis and to what extent.

The results of this uncertainty analysis are important to any research utilising joint moment estimates both for the golf swing and other high acceleration, open chain activities. Only with knowledge of the uncertainty involved in the estimation of joint moments can future research provide meaningful conclusions. The amount of uncertainty acceptable can be determined by considering the use that will be made of the result (Coleman and Steele, 2009). In the context of sports biomechanics, joint moments are commonly used to compare skill level, movement speed, or movement technique in order to establish key performance indicators (Greene et al., 2009; Iino and Kojima, 2011; Nunome et al., 2002) and assess the risk of injury due to joint loading (Bahamonde and Knudson, 2003; Elliott et al., 2003; Ferdinands et al., 2009; Fleisig et al., 1995; Kawasaki et al., 2005; Sabick, 2004). In golf, joint moments have been used to determine the influence of shoe type and skill level on knee loading patterns for rehabilitation suitability (Gatt et al., 1998), to examine the correlation between hip moments and club head velocity as a performance indicator (Stewart and Haigh, n.d.) and to describe swing mechanics (Nesbit and Serrano, 2005; Nesbit, 2005). These studies typically look for relationships between joint moment magnitudes and skill level (Bahamonde and Knudson, 2003; Gatt et al., 1998; Iino and Kojima, 2011) or

other performance indicators such as club head velocity (Stewart and Haigh, n.d.). In comparing skill level, statistically significant differences in the peak joint moments between two groups representing skilled and less-skilled players highlight crucial performance differences which could be used to improve performance. With knowledge of the uncertainty provided by this study, it can be determined whether or not these differences are real or most likely due to measurement error; if uncertainty bounds are smaller than the difference between two group means this will provide confidence that this was a real effect.

Future work can also utilise the results of this uncertainty analysis to direct improvements to data collection methods and modelling techniques in the most efficient and cost-effective way. Moment arm inaccuracy was found to have a primary influence on uncertainty in joint moment estimates and this was attributed to STA, centre of mass location inaccuracy and joint centre location inaccuracy. Reducing these inaccuracies will have the greatest effect on decreasing the overall uncertainty in joint moment estimates and therefore an important area in future research design is the minimisation of these errors. To reduce the effect of STA, sensor attachment methods should be carefully considered; studies have shown the location of sensor attachment as well as the method used to attach the sensor affected the magnitude of STA (Manal et al., 2000). There are a number of different methods that can be used to define joint centres; these include regression equations (Bell et al., 1989), 2D and 3D offsets (Anglin and Wyss, 2000; Schmidt et al., 1999) and functional methods (Churchill et al., 1998; Leardini et al., 1999). The accuracy of functional joint centre methods have been shown to be more accurate than regression methods (Campbell et al., 2009; Leardini et al., 1999) so these may be worth including for future research.

In conclusion, the results of this uncertainty analysis are important to any future research utilising joint moment estimates both for the golf swing and other high acceleration, open chain activities. There is significant scope for establishing key performance indicators of a successful swing using joint moments as at present research of this type has received little attention. Only with knowledge of the uncertainty involved in the estimation of joint moments can future research provide meaningful conclusions. Ultimately, this research provides the first step in uncovering

the potential for joint moment analysis applied to high acceleration, open chain movements in the future.

## **7.2.Conclusion**

The purpose of this thesis was to investigate the validity and uncertainty of inverse dynamics solutions applied to high acceleration movements. The golf swing was used to provide a mechanical basis for this analysis; it was representative of a highly complex skill involving the coordination of many body segments moving at high accelerations in multiple planes. The high acceleration, complex nature of the golf swing resulted in a reduced validity compared to previous studies concerned with lifting, fast trunk rotations and slow speed golf swings. The residuals between the measured and predicted GRF were greatest during the downswing. Similarly, the residuals between the joint reaction forces and moments at the upper trunk joint measured using a top down and bottom up mechanical analysis were greatest during the downswing. It was shown that for open chain movements, through periods of high acceleration, inverse dynamics solutions can be subject to errors which have the capacity to significantly affect the interpretation of resultant joint moments depending on whether a top down or bottom up mechanical analysis is used.

Uncertainty in joint moment estimations was greatest for downswing where segments were moving with the greatest acceleration. The magnitude of the uncertainty was substantial and ranged from 6-339% of the peak joint moment magnitude.

Inaccuracies in proximal moment arms and centre of mass accelerations had the most influence on the joint moment uncertainty and this uncertainty had the capability to alter the timing of peak joint moments by as much as 560ms. For the backswing, the peak uncertainty relative to the peak joint moment was highest for the left shoulder and mid trunk joints. For the downswing the peak uncertainty relative to the peak joint moment was highest for the knee and the wrist joints. The magnitude of the uncertainty quantified in this study provides clear evidence that uncertainty must be taken into account when interpreting joint moments estimated using inverse dynamics as it has the capacity to considerably affect the conclusions of such studies.

**Word count 64,086**

---

## Bibliography

- Ackland, D.C., Lin, Y.-C., Pandy, M.G., 2012. Sensitivity of model predictions of muscle function to changes in moment arms and muscle-tendon properties: a Monte-Carlo analysis. *J. Biomech.* 45, 1463–71.
- Ackland, T., Henson, P., Bailey, D., 1988. The uniform density assumption: Its effect upon the estimation of body segment inertial parameters. *Int. J. Sport Biomech.* 4, 146–155.
- Akbarshahi, M., Schache, A.G., Fernandez, J.W., Baker, R., Banks, S., Pandy, M.G., 2010. Non-invasive assessment of soft-tissue artifact and its effect on knee joint kinematics during functional activity. *J. Biomech.* 43, 1292–301.
- Akutagawa, S., Kojima, T., 2005. Trunk rotation torques through the hip joints during the one- and two-handed backhand tennis strokes. *J. Sports Sci.* 23, 781–93.
- Alexander, E.J., Andriacchi, T.P., 2001. Correcting for deformation in skin-based marker systems. *J. Biomech.* 34, 355–61.
- Alkjaer, T., Simonsen, E.B., Dyhre-Poulsen, P., 2001. Comparison of inverse dynamics calculated by two- and three-dimensional models during walking. *Gait Posture* 13, 73–7.
- Alonso, F.J., Castillo, J.D., Pintado, P., 2005. Application of singular spectrum analysis to the smoothing of raw kinematic signals. *J. Biomech.* 38, 1085–1092.
- Amis, A. a., Cuomo, P., Rama, R.B.S., Giron, F., Bull, A.M.J., Thomas, R., Aglietti, P., 2008. Measurement of Knee Laxity and Pivot-Shift Kinematics With Magnetic Sensors. *Oper. Tech. Orthop.* 18, 196–203.
- Andersen, M.S., Benoit, D.L., Damsgaard, M., Ramsey, D.K., Rasmussen, J., 2010. Do kinematic models reduce the effects of soft tissue artefacts in skin marker-based motion analysis? An in vivo study of knee kinematics. *J. Biomech.* 43, 268–73.
- Andersen, M.S., Damsgaard, M., Rasmussen, J., Ramsey, D.K., Benoit, D.L., 2012. A linear soft tissue artefact model for human movement analysis: Proof of concept using in vivo data. *Gait Posture* 35, 606–11.
- Anderson, A.E., Ellis, B.J., Weiss, J.A., 2007. Verification, validation and sensitivity studies in computational biomechanics. *Comput. Methods Biomech. Biomed. Engin.* 10, 171–184.
- Anderson, B., Wright, I., Stefanyshyn, D., 2006. Segmental sequencing of kinetic energy in the golf swing. *Eng. Sport* 6.
- Andersson, G.B., Ortengren, R., Schultz, A., 1980. Analysis and measurement of the loads on the lumbar spine during work at a table. *J. Biomech.* 13, 513–520.

- Andrews, J.G., Mish, S.P., 1996. Methods for investigating the sensitivity of joint resultants to body segment parameter variations. *J. Biomech.* 29, 651–654.
- Andriacchi, T.P., Alexander, E.J., Toney, M.K., Dyrby, C., Sum, J., 1998. A point cluster method for in vivo motion analysis: applied to a study of knee kinematics. *J. Biomech. Eng.* 120.
- Andriacchi, T.P., Andersson, G.B., Fermier, R.W., Stern, D., Galante, J.O., 1980. A study of lower-limb mechanics during stair-climbing. *J. Bone Jt. Surg.* 62, 749–457.
- Anglin, C., Wyss, U.P., 2000. Review of arm motion analyses. *Proc. Inst. Mech. Eng. Part H J. Eng. Med.* 214, 541–555.
- Apkarian, J., Naumann, S., Cairns, B., 1989. A Three-Dimensional Kinematic and Dynamic Model of the Lower Limb. *J. Biomech.* 22, 143–155.
- Bahamonde, R.E., Knudson, D., 2003. Kinetics of the upper extremity in the open and square stance tennis forehand. *J. Sci. Med. Sport* 6, 88–101.
- Ball, K., 2006. Weight transfer styles in the golf swing: individual and group analysis.
- Ball, K.A., Best, R.J., 2007. Different centre of pressure patterns within the golf stroke I: Cluster analysis. *J. Sports Sci.* 25, 757–770.
- Bell, L., Pedersen, R., Brand, A., 1989. A comparison of the accuracy of several hip center location prediction methods. *J. Biomech.* 23, 617–621.
- Benoit, D.L., Ramsey, D.K., Lamontagne, M., Xu, L., Wretenberg, P., Renström, P., 2006. Effect of skin movement artifact on knee kinematics during gait and cutting motions measured in vivo. *Gait Posture* 24, 152–64.
- Betzler, N., Monk, S., Wallace, E., Otto, S.R., Shan, G., 2008. From the double pendulum model to full-body simulation: evolution of golf swing modeling. *Sport. Technol.* 1, 175–188.
- Bobbert, M., Schamhardt, H., 1990. Accuracy of determining the point of force application with piezoelectric force plates. *J. Biomech.* 23, 705–710.
- Broker, J.P., Ramey, M.R., 2007. A New Method for Measuring Grip Force and its Distribution During the Golf Swing. *Int. J. Sport. Sci. Coach.* 2, 121–134.
- Brown, S.A., Sepulveda, A.E., 1997. Approximation of System Reliability Using a Shooting Monte Carlo Approach. *AIAA J.* 35, 1064–1071.
- Browne, J., O'Hare, N., 2000. My IOPscience A quality control procedure for force platforms A quality control procedure for force platforms. *Physiol. Meas* 21, 515–524.
- Buckheit, J.B., Donoho, D.L., 1995. Wavelab and Reproducible Research.

- Budney, D.R., Bellow, D.G., 1982. On the swing mechanics of a matched set of golf clubs. *Res. Q. Exerc. Sport* 53, 185–192.
- Bull, A.M.J., Berkshire, F.H., Amis, A.A., 1998. Accuracy of an electromagnetic measurement device and application to the measurement and description of knee joint motion. *Proc. Inst. Mech. Eng. Part H J. Eng. Med.* 212, 347–355.
- Cahouet, V., Luc, M., David, A., 2002. Static optimal estimation of joint accelerations for inverse dynamics problem solution. *J. Biomech.* 35, 1507–1513.
- Caldwell, G.E., Li, L., McCole, S.D., Hagberg, J.M., 1998. Pedal and crank kinetics in uphill cycling. *J. Appl. Biomech.* 14, 245–259.
- Campbell, A.C., Lloyd, D.G., Alderson, J.A., Elliott, B.C., 2009. MRI development and validation of two new predictive methods of glenohumeral joint centre location identification and comparison with established techniques. *J. Biomech.* 42, 1527–1532.
- Campbell, K., Reid, R., 1985. The application of optimal control theory to simplified models of complex human motions: the golf swing. In: Winter, D., Normam, R., Wells, R., Hayes, K., Patla, A. (Eds.), *Biomechanics IX-B. Human Kinetics Baltimore*, pp. 527–538.
- Cappello, A., Bagalà, F., Cedraro, A., Chiari, L., 2011. Non-linear re-calibration of force platforms. *Gait Posture* 33, 724–6.
- Cappozzo, A., Catani, F., Leardini, A., Benedetti, M., Della Croce, U., 1996. Position and orientation in space of bones during movement: experimental artefacts. *Clin. Biomech.* 11, 90–100.
- Cappozzo, A., Leo, T., A, P., 1975. A general computing method for the analysis of human locomotion. *J. Biomech.* 8, 307–320.
- Cedraro, A., Cappello, A., Chiari, L., 2009. A portable system for in-situ re-calibration of force platforms: experimental validation. *Gait Posture* 29, 449–53.
- Cereatti, A., Donati, M., Camomilla, V., Margheritini, F., Cappozzo, A., 2009. Hip joint centre location: an ex vivo study. *J. Biomech.* 42, 818–23.
- Challis, J.H., 1995. A procedure for determining rigid body transformation parameters. *J. Biomech.* 28, 733–737.
- Challis, J.H., 1996. Accuracy of Human Limb Moment of Inertia Estimations and Their Influence on Resultant Joint Moments. *J. Appl. Biomech.* 12, 517–530.
- Challis, J.H., 2007. Data processing and error estimation. In: Payton, C., Bartlett, R. (Eds.), *Biomechanical Evaluation of Movement in Sport and Exercise: The British Association of Sport and Exercise Sciences Guide*. Routledge, pp. 129–152.

- Challis, J.H., 2008. Data processing and error estimation. In: *Biomechanical Evaluation of Movement in Sport*.
- Challis, J.H., Kerwin, D.G., 1996. Quantification of the uncertainties in resultant joint moments computed in a dynamic activity. *J. Sports Sci.* 14, 219–231.
- Chandler, R.F., 1975. *Investigation of Inertial Properties of the Human Body*.
- Chang, Y., Hughes, R.E., Su, F., An, K., 2000. Prediction of muscle force involved in shoulder internal rotation. *J. Shoulder Elb. Surg.* 9, 188–195.
- Chen, C.C., Inoue, Y., Shibara, K., 2007. Numerical study on the wrist action during the golf downswing. *Sport. Eng.* 10, 23–31.
- Cheze, L., Fregly, B.J., Dimnet, J., 1995. A solidification procedure to facilitate kinematic analysis based on video system data. *J. Biomech.* 28, 879–884.
- Chiari, L., Della Croce, U., Leardini, A., Cappozzo, A., 2005. Human movement analysis using stereophotogrammetry. Part 2: instrumental errors. *Gait Posture* 21, 197–211.
- Chirokov, A., 2006. Scattered Data Interpolation and Approximation using Radial Base Functions [WWW Document]. MATLAB Cent. File Exch. URL <http://www.mathworks.co.uk/matlabcentral/fileexchange/10056-scattered-data-interpolation-and-approximation-using-radial-base-functions>
- Chockalingam, N., Giakas, G., Iossifidou, A., 2002. Do strain gauge force platforms need in situ correction? *Gait Posture* 16, 233–7.
- Chow, J., Carlton, L., Lim, Y., Chae, W., Shim, J., Kuenster, A., Kokbun, K., 2003. Comparing the pre- and post-impact ball and racquet kinematics of elite tennis players' first and second serves: a preliminary study. *J. Sports Sci.* 21, 529–537.
- Churchill, D.L., Incavo, S.J., Johnson, C.C., Beynnon, B.D., 1998. The transepicondylar axis approximates the optimal flexion axis of the knee. *Clin. Orthop. Relat. Res.* 111–8.
- Clarke, G.R., 1972. Unequal leg length: An accurate method of detection and some clinical results. *Rheumatology* 11, 385–390.
- Cochran, A.J., Stobbs, J., Britain, G.S. of G., 1968. *The search for the perfect swing: an account of the Golf Society of Great ... Heinemann*.
- Coifman, R.R., Donoho, D.L., 1995. *Translation-Invariant De-Noising*. Springer New York.
- Coleman, H.W., Steele, W.G., 2009. *Experimentation, validation, and uncertainty analysis for engineers*. Wiley.
- Collins, J.J., Whittle, M.W., 1989. Impulsive forces during walking and their clinical implications. *Clin. Biomech.* 4, 179–187.

- Collins, S.H., Adamczyk, P.G., Ferris, D.P., Kuo, A.D., 2009. A simple method for calibrating force plates and force treadmills using an instrumented pole. *Gait Posture* 29, 59–64.
- Consiglieri, L., Pires, E.B., 2009. An analytical model for the ergometer rowing: inverse multibody dynamics analysis. *Comput. Methods Biomech. Biomed. Engin.* 12, 469–79.
- Cook, T.M., Paula, L.M., 2002. Comparison of Surface Sensor and Bone-Fixed Measurement of Humeral Motion. *J. Appl. Biomech.* 18, 163–170.
- Cooper, R.A., Member, S., Boninger, M.L., Vansickle, D.P., Robertson, R.N., Shimada, S.D., 1997. Uncertainty Analysis for Wheelchair Propulsion Dynamics. *IEEE Trans. Rehabil. Eng.* 5, 130–139.
- Crowninshield, R.D., Johnston, R.C., Andrews, J.G., Brand, R.A., 1978. A biomechanical investigation of the human hip. *J. Biomech.* 11, 75–77, 79–85.
- Cunningham, L.S., Kelsey, J.L., 1984. Epidemiology of musculoskeletal impariments and associated disability. *Am. J. Public Health* 74, 574–579.
- Cutti, A.G., Cappello, A., Davalli, A., 2006. In vivo validation of a new technique that compensates for soft tissue artefact in the upper-arm: Preliminary results. *Clin. Biomech.* 21, S13–S19.
- Cutti, A.G., Paolini, G., Troncossi, M., Cappello, A., Davalli, A., 2003. Soft tissue artefact assessment in humeral axial rotation. *Gait Posture* 21, 341–9.
- Davis, L., Clarkson, E., Rolland, J.P., 2006. Predicting accuracy in pose estimation for marker-based tracking. *Second IEEE ACM Int. Symp. Mix. Augment. Reality, 2003. Proceedings.* 28–35.
- De Jalon, J.G., Bayo, E., 2011. *Kinematic and Dynamic Simulation of Multibody Systems–The Real-Time Challenge*, Mechanical. ed. Springer London, Limited.
- De Leva, P., 1996. Joint Center Longitudinal Positions Computed From A Selected Subset of Chandler’s Data. *J. Biomech.* 29, 1231–1233.
- De Looze, M.P., Kingma, I., Bussmann, J.B.J., 1992. Validation of a dynamic linked segment model to calculate joint moments in lifting. *Clin. Biomech.* 161–169.
- Dempster, W.T., 1955. Space requirements of the seated operator. *Wright Patterson Air Force Base WADC-TR-55-159* 55–159.
- Denoth, J., Gruber, K., Ruder, H., Keppler, M., 1985. Forces and torques during sports activities with high accelerations. In: *Biomechanics: Current Interdisciplinary Research*. Springer Netherlands, pp. 663–668.

- Desjardins, P., Plamondon, A., Gagnon, M., 1998. Sensitivity analysis of segment models to estimate the net reaction moments at the L5/S1 joint in lifting. *Med. Eng. Phys.* 20, 153–158.
- Ditlevsen, O., Olesen, R., Mohr, G., 1987. Solution of A Class of Load Combination Problems by Directional Simulation. *Struct. Saf.* 4, 95–109.
- Domholdt, E., 2000. *Physical therapy research: principles and applications*, 2nd ed. Saunders Company, Philadelphia, W.B.
- Domone, S., Wheat, J., Choppin, S., Hamilton, N., Heller, B., 2012. Wavelet based de-noising of non-stationary kinematic signals. In: 30th Annual Conference of Biomechanics in Sports. Melbourne, Australia.
- Donoho, D.L., Johnstone, I.M., 1995. Adapting to unknown smoothness via wavelet shrinkage. *J. Am. Stat. Assoc.* 90, 1200–1224.
- Du, X., Chen, W., 2001. A most probable point-based method for efficient uncertainty analysis. *J. Des. Manuf. Autom.* 4, 47–66.
- Dumas, R., Lafon, Y., Jacquelin, E., Chèze, L., 2009. Soft tissue artefacts: compensation and modelling. *Comput. Methods Biomech. Biomed. Engin.* 12, 103–104.
- Dumas, R., Nicol, E., Chèze, L., 2007. Influence of the 3D inverse dynamic method on the joint forces and moments during gait. *J. Biomech. Eng.* 129, 786–90.
- Durkin, J.L., Dowling, J.J., 2003. Analysis of Body Segment Parameter Differences Between Four Human Populations and the Estimation Errors of Four Popular Mathematical Models. *J. Biomech. Eng.* 125, 515–522.
- Durkin, J.L., Dowling, J.J., 2006. Body segment parameter estimation of the human lower leg using an elliptical model with validation from DEXA. *Ann. Biomed. Eng.* 34, 1483–93.
- Durkin, J.L., Dowling, J.J., Andrews, D.M., 2002. The measurement of body segment inertial parameters using dual energy X-ray absorptiometry. *J. Biomech.* 35, 1575–1580.
- Elliott, B., Fleisig, G., Nicholls, R., Escamilla, R., 2003. Technique effects on upper limb loading in the tennis serve. *J. Sci. Med. Sport* 6, 76–87.
- Elliott, B.C., 2000. Back injuries and the fast bowler in cricket. *J. Sports Sci.* 18, 983–991.
- Eng, J., Pierrynowski, M.R., 1994. The Effect of Soft Foot Orthotics on Three-dimensional Lower-Limb Kinematics During Walking and Running. *J. Am. Phys. Ther. Assoc.* 74, 836–844.
- Erdmann, W.S., 1997. Geometric and inertial data of the trunk in adult males. *J. Biomech.* 30, 679–688.

- 
- Fairburn, P.S., Palmer, R., Whybrow, J., Fielden, S., Jones, S., 2000. A prototype system for testing force platform dynamic performance. *Gait Posture* 12, 25–33.
- Ferdinands, R.E.D., Kersting, U., Marshall, R.N., 2009. Three-dimensional lumbar segment kinetics of fast bowling in cricket. *J. Biomech.* 42, 1616–21.
- Fleisig, G., Andrews, J., Dillman, J., Escamilla, R., 1995. Kinetics of Baseball Pitching with Implications About Injury Mechanisms. *Am. J. Sports Med.* 23, 233–239.
- Fleisig, G.S., Kingsley, D.S., Loftice, J.W., Dinnen, K.P., Ranganathan, R., Dun, S., Escamilla, R.F., Andrews, J.R., 2006. Kinetic comparison among the fastball, curveball, change-up, and slider in collegiate baseball pitchers. *Am. J. Sports Med.* 34, 423–30.
- Fletcher, I.M., Hartwell, M., 2004. Effect of an 8-week combined weights and plyometrics training program on golf drive performance. *J. strength Cond. Res.* 18, 59–62.
- Freivalds, A., Chaffin, D.B., Garg, A., Lee, K.S., 1984. A Dynamic Biomechanical Evaluation of Lifting Maximum Acceptable Loads. *J. Biomech.* 17, 251–262.
- Fritz, J.M., Wainner, R.S., 2001. Examining diagnostic tests: an evidence-based perspective. *Phys. Ther.* 81, 1546–64.
- Fukashiro, S., Paavo, K., Jarvinen, M., Mitsumasa, M., 1995. In vivo achilles tendon loading during jumping in humans. *Eur. J. Appl. Physiol. Occup. Physiol.* 71, 453–458.
- Gagnon, D., Gagnon, M., 1992. The influence of dynamic factors on triaxial net muscular moments at the L5/S1 joint during asymmetrical lifting and lowering. *J. Biomech.* 25, 891–901.
- Gagnon, M., Plamondon, A., Gravel, D., 1993. Pivoting with the load. An alternative for protecting the back in asymmetric lifting. *Spine (Phila. Pa. 1976)*. 18, 1515.
- Ganley, K.J., Powers, C.M., 2004. Determination of lower extremity anthropometric parameters using dual energy X-ray absorptiometry: the influence on net joint moments during gait. *Clin. Biomech.* 19, 50–56.
- Gao, B., Zheng, N.N., 2008. Investigation of soft tissue movement during level walking: translations and rotations of skin markers. *J. Biomech.* 41, 3189–95.
- Garling, E.H., Kaptein, B.L., Mertens, B., Barendregt, W., Veeger, H.E.J., Nelissen, R.G.H.H., Valstar, E.R., 2007. Soft-tissue artefact assessment during step-up using fluoroscopy and skin-mounted markers. *J. Biomech.* 40 Suppl 1, S18–24.
- Gatt, C.J., Pavol, M.J., Parker, R.D., Grabiner, M.D., 1998. Three-dimensional knee joint kinetics during a golf swing. Influences of skill level and footwear. *Am. J. Sports Med.* 26, 285–94.

- Gazzani, F., 1993. Comparative assessment of two algorithms for calibrating stereophotogrammetric systems. *J. Biomech.* 26, 1449–1454.
- Giakas, G., 2004. Power Spectrum Analysis and Filtering. In: Stergiou, N. (Ed.), *Innovative Analyses of Human Movement*. Human Kinetics, Champaign, IL, pp. 223–256.
- Giakas, G., Baltzopoulos, V., 1997. A comparison of automatic filtering techniques applied to biomechanical walking data. *J. Biomech.* 30, 847–850.
- Giakas, G., Stergioulas, L.K., Vourdas, A., 2000. Time-frequency analysis and filtering of kinematic signals with impacts using the Wigner function: accurate estimation of the second derivative. *J. Biomech.* 33, 567–574.
- Giles, L.G.F., Taylor, J.R., 1981. Low-back pain associated with leg length inequality. *Spine (Phila. Pa. 1976)*. 6, 510–521.
- Gill, H.S., O'Connor, J.J., 1997. A new testing rig for force platform calibration and accuracy tests. *Gait Posture* 5, 228–232.
- Goldberg, S.R., Kepple, T.M., Stanhope, S.J., 2009. In situ calibration and motion capture transformation optimization improve instrumented treadmill measurements. *J. Appl. Biomech.* 25, 401–6.
- Greene, A.J., Sinclair, P.J., Dickson, M.H., Colloud, F., Smith, R.M., 2009. Relative shank to thigh length is associated with different mechanisms of power production during elite male ergometer rowing. *Sports Biomech.* 8, 302–17.
- Gruber, K., Ruder, H., Denoth, J., Schneider, K., 1998. A comparative study of impact dynamics: wobbling mass model versus rigid body models. *J. Biomech.* 31, 439–444.
- Hale, S. a, 1990. Analysis of the swing phase dynamics and muscular effort of the above-knee amputee for varying prosthetic shank loads. *Prosthet. Orthot. Int.* 14, 125–35.
- Hall, M.G., Fleming, M.J., Dolan, M.J., Millbank, S.F.D., Paul, J.P., 1996. Static in situ calibration of force plates. *J. Biomech.* 29, 659–665.
- Hamilton, W.R., 1969. *Elements of quaternions*, Vol. I, II. Chelsea Publishing Company.
- Hamming, D., Braman, J.P., Phadke, V., LaPrade, R.F., Ludewig, P.M., 2012. The accuracy of measuring glenohumeral motion with a surface humeral cuff. *J. Biomech.* 45, 1161–8.
- Hanavan, J., 1964. *A Mathematical Model of the Human Body*. No. AFIT-GA-PHYS-64-3. AIR FORCE Aerosp. Med. Res. LAB WRIGHT-PATTERSON AFB OH.
- Hatze, H., 1974. The meaning of the term “biomechanics”. *J. Biomech.* 7, 189–190.

- 
- Hatze, H., 1980. A mathematical model for the computational determination of parameter values of anthropomorphic segments. *J. Biomech.* 13, 833–843.
- Hatze, H., 2002. The fundamental problem of myoskeletal inverse dynamics and its implications. *J. Biomech.* 35, 109–115.
- Heath, B.H., Carter, J.E.L., 1967. A modified somatotype method. *Am. J. Phys. Anthropol.* 27, 57–74.
- Heneghan, N.R., Balanos, G.M., 2010. Soft tissue artefact in the thoracic spine during axial rotation and arm elevation using ultrasound imaging: a descriptive study. *Man. Ther.* 15, 599–602.
- Henninger, H.B., Reese, S.P., Anderson, A.E., Weiss, J.A., 2010. Validation of Computational Models in Biomechanics. *Proc Inst Mech Eng H* 224, 801–812.
- Hills, R., Trucano, T., 1999. Statistical Validation of Engineering and Scientific Models: Background. Sandia Natl. Lab. SAND99-1256 36.
- Hoffman, S.J., 2009. Introduction to kinesiology: studying physical activity. Human Kinetics Publishers, Champaign, IL.
- Holden, J., Stanhope, S., 1998. The effect of variation in knee center location estimates on net knee joint moments. *Gait Posture* 7, 1–6.
- Holden, J.P., Orsini, J. a., Siegel, K.L., Kepple, T.M., Gerber, L.H., Stanhope, S.J., 1997. Surface movement errors in shank kinematics and knee kinetics during gait. *Gait Posture* 5, 217–227.
- Holden, J.P., Selbie, W.S., Stanhope, S.J., 2003. A proposed test to support the clinical movement analysis laboratory accreditation process. *Gait Posture* 17, 205–13.
- Houck, J., Yack, H.J., Cuddeford, T., 2004. Validity and comparisons of tibiofemoral orientations and displacement using a femoral tracking device during early to mid stance of walking. *Gait Posture* 19, 76–84.
- Hsieh, C.C., Fang, Y.C., Wang, M.E., Wang, C.K., Kim, M.J., Shin, S.Y., Woo, T.C., 1998. Noise smoothing for VR equipment in quaternions. *IIE Trans.* 30, 581–587.
- Hsieh, H.-J., Lu, T.-W., Chen, S.-C., Chang, C.-M., Hung, C., 2011. A new device for in situ static and dynamic calibration of force platforms. *Gait Posture* 33, 701–5.
- Hughes, R.E., An, K.N., 1997. Monte Carlo simulation of a planar shoulder model. *Med. Biol. Eng. Comput.* 35, 544–8.
- Hume, P. a, Keogh, J., Reid, D., 2005. The role of biomechanics in maximising distance and accuracy of golf shots. *Sports Med.* 35, 429–49.
- Iino, Y., Kojima, T., 2011. Kinetics of the upper limb during table tennis topspin forehands in advanced and intermediate players. *Sports Biomech.* 10, 361–77.
-

- Iino, Y., Kojima, T., 2012. Validity of the top-down approach of inverse dynamics analysis in fast and large rotational trunk movements. *J. Appl. Biomech.* 28, 420–30.
- Ismail, a R., Asfour, S.S., 1999. Discrete wavelet transform: a tool in smoothing kinematic data. *J. Biomech.* 32, 317–21.
- Isman, R., Inman, V., 1969. Anthropometric studies of the human foot and ankle. *Bull. Prosthet. Res.* 11, 97–108.
- ISO, 1995. Guide to the Expression of Uncertainty in Measurement. International Organization for Standardization (ISO) and the International Committee on Weights and Measures (CIPM), Switzerland.
- Iwatsubo, T., Kawamura, S., Furuichi, K., Yamaguchi, T., 2002. Influence of characteristics of golf club head on release velocity and spin velocity of golf ball after impact. In: Thain, E. (Ed.), *Science and Golf IV*. pp. 410–425.
- Jaberzadeh, S., Scutter, S., Zoghi, M., 2005. Accuracy of an electromagnetic tracking device for measuring hip joint kinematics during gait: effects of metallic total hip replacement prosthesis, source-sensor distance and sensor orientation. *Australas. Phys. Eng. Sci. Med.* 28, 184–9.
- James, C.R., Bates, B.T., Dufek, J.S., 2003. Classification and comparison of biomechanical response strategies for accomodating landing impact. *J. Appl. Biomech.* 19, 106–118.
- Jensen, R.K., 1978. Estimation of the biomechanical properties of three body types using a photogrammetric method. *J. Biomech.* 11, 349–358.
- Jorgensen, T., 1970. On the dynamics of the swing of a golf club. *Am. J. Phys.* 38, 644–651.
- Kahn, H., 1956. Use of Different Monte Carlo Sampling Techniques. In: Meyer, H.A. (Ed.), *Proc. Symp. on Monte Carlo Methods*. John Wiley & Sons, New York, NY, pp. 149–190.
- Kaneko, Y., Sato, F., 2000. The adaptation of golf swing to inertia property of club. In: Haake, S., Subic, A. (Eds.), *The Engineering of Sport*. Blackwell Science: Leeds, pp. 469–476.
- Karduna, A.R., McClure, P.W., Michener, L. a., Sennett, B., 2001. Dynamic Measurements of Three-Dimensional Scapular Kinematics: A Validation Study. *J. Biomech. Eng.* 123, 184–190.
- Kawasaki, S., Imai, S., Inaoka, H., Masuda, T., Ishida, A., Okawa, A., Shinomiya, K., 2005. The lower lumbar spine moment and the axial rotational motion of a body during one-handed and double-handed backhand stroke in tennis. *Int. J. Sports Med.* 26, 617–21.

- Kenny, I.C., McCloy, A.J., Wallace, E.S., Otto, S.R., 2008. Segmental sequencing of kinetic energy in a computer-simulated golf swing. *Sport. Eng.* 11, 37–45.
- Kenny, I.C., Wallace, E.S., Brown, D., Otto, S.R., Kenny, I., Wallace, E., Otto, S., 2006. Validation of a Full-Body Computer Simulation of the Golf Drive for Clubs of Differing Length. *Eng. Sport* 6 11–16.
- Kim, H., Sakurai, S., Ahn, J., 2007. Errors in the Measurement of Center of Pressure (CoP) Computed with Force Plate Affect on 3D Lower Limb Joint Moment During Gait. *Int. J. Sport Heal. Sci.* 5, 71–82.
- Kim, J.H., Abdel-Malek, K., Yang, J., Marler, T., 2006. Prediction and analysis of human motion dynamics performing various tasks. *Int. J. Hum. Factors Model. Simul.* 1, 69–94.
- Kindratenko, V., Bennett, A., 2000. Evaluation of Rotation Correction Techniques for Electromagnetic Position Tracking Systems. In: *Proc. Virtual Environments 2000 Eurographics Workshop.* pp. 13–22.
- Kindratenko, V. V., 2000. A survey of electromagnetic position tracker calibration techniques. *Virtual Real.* 5, 169–182.
- Kingma, I., De Looze, M.P., Toussaint, H.M., Klijnsma, H.G., Bruijnen, T.B.M., 1996. Validation of a full body 3-D dynamic linked segment model. *Hum. Mov. Sci.* 15, 833–860.
- Kingma, I., Toussaint, H.M., De Looze, M.P., Van Dieen, J.H., 1996. Segment inertial parameter evaluation in two anthropometric models by application of a dynamic linked segment model. *J. Biomech.* 29, 693–704.
- Knudson, D., Bahamonde, R., 2001. Effect of endpoint conditions on position and velocity near impact in tennis. *J. Sports Sci.* 19, 839–844.
- Koike, S., Iida, H., Kawamura, T., Fujii, N., Ae, M., 2004. An instrumented bat for simultaneous measurement of forces and moments exerted by the hands during batting. *Eng. Sport.* 5 5, 194–200.
- Koike, S., Iida, H., Shiraki, H., Ae, M., 2006. An Instrumented Grip Handle for Golf Clubs to Measure Forces and Moments Exerted by Each Hand During Swing Motion. *Eng. Sport* 6 6, 137–142.
- Kromodihardjo, S., Mital, A., 1986. Kinetic Analysis of Manual Lifting Activities: Part 1 - Development of a Three-Dimensional Computer Model. *Int. J. Ind. Ergon.* 1, 77–90.
- Kuo, A.D., 1998. A least squares estimation approach to improving the precision of inverse dynamics computations. *J. Biomech. Eng.* 104, 38.
- Kuo, M.-Y., Tsai, T.-Y., Lin, C.-C., Lu, T.-W., Hsu, H.-C., Shen, W.-C., 2011. Influence of soft tissue artifacts on the calculated kinematics and kinetics of total knee replacements during sit-to-stand. *Gait Posture* 33, 379–84.

- Kwon, Y., 1998. BSP Equations [WWW Document]. URL <http://www.kwon3d.com/theory/bspeq/bspeq.html>
- Langenderfer, J.E., Laz, P.J., Petrella, A.J., Rullkoetter, P.J., 2008. An efficient probabilistic methodology for incorporating uncertainty in body segment parameters and anatomical landmarks in joint loadings estimated from inverse dynamics. *J. Biomech. Eng.* 130, 014502.
- Lanshammar, H., 1980. Precision limits on derivatives obtained from measurement data. *Biomech.* VII 586–592.
- Lanshammar, H., 1982. On practical evaluation of differentiation techniques for human gait analysis. *J. Biomech.* 15, 99–105.
- Larivière, C., Gagnon, D., 1999a. The L5 / S1 joint moment sensitivity to measurement errors in dynamic 3D multisegment lifting models. *Hum. Mov. Sci.* 18, 573–587.
- Larivière, C., Gagnon, D., 1999b. The influence of trunk modelling in 3D biomechanical analysis of simple and complex lifting tasks. *Clin. Biomech.* 14, 449–461.
- Larivière, C., Gagnon, D., 1998. Comparison between two dynamic methods to estimate triaxial net reaction moments at the L5/S1 joint during lifting. *Clin. Biomech.* 13, 36–47.
- Lavanon, J., Dapena, J., 1998. Comparison of the kinematics of the full-instep and pass kicks in soccer. *Med. Sci. Sports Exerc.* 30, 917–927.
- Laz, P.J., Browne, M., 2010. A review of probabilistic analysis in orthopaedic biomechanics. *Proc. Inst. Mech. Eng. Part H J. Eng. Med.* 224, 927–943.
- Leardini, A., Cappozzo, A., Catani, F., Toksvig-Larsen, S., Petitto, A., Sforza, V., Cassanelli, G., Giannini, S., 1999. Validation of a functional method for the estimation of hip joint centre location. *J. Biomech.* 32, 99–103.
- Leardini, A., Chiari, L., Della Croce, U., Cappozzo, A., 2005. Human movement analysis using stereophotogrammetry. Part 3. Soft tissue artifact assessment and compensation. *Gait Posture* 21, 212–225.
- Lewis, A., Stewart, C., Postans, N., Trevelyan, J., 2007. Development of an instrumented pole test for use as a gait laboratory quality check. *Gait Posture* 26, 317–22.
- Lu, T.W., O'Connor, J.J., 1999. Bone position estimation from skin marker coordinates using global optimization with joint constraints. *J. Biomech.* 32, 129–134.
- Lucchetti, L., Cappozzo, a, Cappello, a, Della Croce, U., 1998. Skin movement artefact assessment and compensation in the estimation of knee-joint kinematics. *J. Biomech.* 31, 977–84.

- MacKinnon, C.D., Winter, D.A., 1993. Control of whole body balance in the frontal plane during human walking. *J. Biomech.* 26, 633–44.
- MacWilliams, B. a, Sardelli, M.C., Tashjian, R.Z., 2010. A functional axis based upper extremity model and associated calibration procedures. *Gait Posture* 31, 289–91.
- Manal, K., McClay Davis, I., Galinat, B., Stanhope, S., 2003. The accuracy of estimating proximal tibial translation during natural cadence walking: bone vs. skin mounted targets. *Clin. Biomech. (Bristol, Avon)* 18, 126–31.
- Manal, K., McClay, I., Richards, J., Galinat, B., Stanhope, S., 2002. Knee moment profiles during walking: errors due to soft tissue movement of the shank and the influence of the reference coordinate system. *Gait Posture* 15, 10–7.
- Manal, K., McClay, I., Stanhope, S., Richards, J., Galinat, B., 2000. Comparison of surface mounted markers and attachment methods in estimating tibial rotations during walking: an in vivo study. *Gait Posture* 11, 38–45.
- Marras, W.S., Granata, K.P., 1995. A biomechanical assesment and model of axial twisting in the thoraco-lumbar spine. *Spine (Phila. Pa. 1976)*. 20, 1440–1451.
- McCaw, S.T., DeVita, P., 1995. Errors in Alignment of Center of Pressure and Foot Coordinates affect predicted lower extremity torques. *J. Biomech.* 28, 985 –988.
- McGuan, S., 1996. Exploring human adaptation using optimized, dynamic human models. In: 20th Annual Meeting of the American Society of Biomechanics. Atlanta, Georgia, USA, pp. 17–19.
- McLean, S.G., Huang, X., Van Den Bogert, A.J., 2008. Investigating isolated neuromuscular control contributions to non-contact anterior cruciate ligament injury risk via computer cimulation methods. *Clin. Biomech.* 23, 926–937.
- Middleton, J., Sinclair, P., Patton, R., 1999. Accuracy of centre of pressure measurement using a piezoelectric force platform. *Clin. Biomech. (Bristol, Avon)* 14, 357–60.
- Milne, A.D., Chess, D.G., Johnson, J.A., King, G.J.W., 1996. Accuracy of an Electromagnetic Tracking Device: A Study of the Optimal Operating Range and Metal Interference. *J. Biomech.* 29, 791–793.
- Milne, R.D., Davis, J.P., 1992. The role of the shaft in the golf swing. *J. Biomech.* 25, 975–83.
- Miura, K., 2001. Parametric acceleration - the effect of inward pull of the golf club at impact stage. *Sport. Eng.* 4, 75–86.
- Neal, R.J., Wilson, B.D., 1985. 3D kinematics and kinetics of the golf swing. *Int. J. Sport. Biomech.* 1, 221–232.

- Nesbit, S.M., 2005. A Three Dimensional Kinematic and Kinetic Study of the Golf Swing. *J. Sport. Sci. Med.* 4, 499–519.
- Nesbit, S.M., 2007. Development of a full-body biomechanical model of the golf swing. *Int. J. Model. Simul.* 27, 392–404.
- Nesbit, S.M., Serrano, M., 2005. Work and power analysis of the golf swing. *J. Sport. Sci.* an 4, 520–533.
- Ng, L., Burnett, A., Campbell, A., O'Sullivan, P., 2009. Caution: the use of an electromagnetic device to measure trunk kinematics on rowing ergometers. *Sports Biomech.* 8, 255–9.
- Nguyen, T., Baker, R., Pandy, M., 2007. Effect of the variability in segment inertial parametrs on joint moment using monte carlo simulation. *J. Biomech.* 100.
- Nixon, M.A., McCallum, B.C., Fright, W.R., Price, N.B., 1998. The effects of metals and interfering fields on electromagnetic trackers. *Presence Teleoperators Virtual Environ.* 7, 204–218.
- Novosel, J., Garrity, J., 2004. *Tour Tempo*. Doubleday, New York.
- Nunome, H., Asai, T., Ikegami, Y., Sakurai, S., 2002. Three-dimensional kinetic analysis of side-foot and instep soccer kicks. *Med. Sci. Sports Exerc.* 34, 2028–36.
- Nunome, H., Lake, M., Georgakis, A., Stergioulas, L.K., 2006. Impact phase kinematics of instep kicking in soccer. *J. Sports Sci.* 24, 11–22.
- O'Brien, J.F., Bodenheimer, B.E., Brostow, G.J., Hodgins, J.K., 2000. Automatic joint parameter estimation from magnetic motion capture data. In: *Proceedings of the Graphics Interface*. Montreal, Quebec, Canada.
- Oberhofer, K., Mithraratne, K., Stott, N.S., Anderson, I. a, 2009. Error propagation from kinematic data to modeled muscle-tendon lengths during walking. *J. Biomech.* 42, 77–81.
- Pain, M.T.G., Challis, J.H., 2006. The influence of soft tissue movement on ground reaction forces, joint torques and joint reaction forces in drop landings. *J. Biomech.* 39, 119–124.
- Pearcy, M.J., Hindle, R.J., 1989. New method for the non-invasive three-dimensional measurement of human back movement. *Clin. Biomech.* 4, 73–79.
- Pearsall, D.J., Costigan, P.A., 1999. The effect of segment parameter error on gait analysis results. *Gait Posture* 9, 173–183.
- Pearsall, D.J., Reid, J.G., 1994. The study of human body segment parameters in biomechanics. An historical review and current status report. *Sports Med.* 18, 126–40.

- Peters, A., Galna, B., Sangeux, M., Morris, M., Baker, R., 2010. Quantification of soft tissue artifact in lower limb human motion analysis: a systematic review. *Gait Posture* 31, 1–8.
- Pezzack, J.C., Norman, R.W., 1981. A validation of the joint reaction force and resultant moment output of an “n” link plane motion model of the human. *Biomech. VII-A* 260–266.
- Pickering, W., 1998. A computational study of the double pendulum model of the golf swing. In: Haake, S.J. (Ed.), *The Engineering of Sport*. Blackwell Science: London, pp. 353–360.
- Pickering, W.M., Vickers, G.T., 1999. On the double pendulum model of the golf swing. *Sport. Eng. 2*, 161–172.
- Pillet, H., Bonnet, X., Lavaste, F., Skalli, W., 2010. Evaluation of force plate-less estimation of the trajectory of the centre of pressure during gait. Comparison of two anthropometric models. *Gait Posture* 31, 147–52.
- Piriyaprasarth, P., Morris, M.E., 2007. Psychometric properties of measurement tools for quantifying knee joint position and movement: a systematic review. *Knee* 14, 2–8.
- Plagenhoef, S., 1983. Anatomical data for analyzing human motion. *Res. Q. Exerc. Sport* 54, 169–178.
- Plamondon, A., Gagnon, M., Desjardins, P., 1996. Validation of two 3-D segment models to calculate the net reaction forces and moments at the L(5)/S(1) joint in lifting. *Clin. Biomech.* 11, 101–110.
- Portus, M.R., Mason, B.R., Elliott, B.C., Pfitzner, M.C., Done, R.P., 2004. Cricket: Technique factors related to ball release speed and trunk injuries in high performance Cricket fast bowlers. *Sport. Biomech.* 3, 263–284.
- Putnam, C. a, 1993. Sequential motions of body segments in striking and throwing skills: Descriptions and explanations. *J. Biomech.* 26, 125–135.
- Rao, G., Amarantini, D., Berton, E., Favier, D., 2006. Influence of body segments’ parameters estimation models on inverse dynamics solutions during gait. *J. Biomech.* 39, 1531–6.
- Reinbolt, J. a, Haftka, R.T., Chmielewski, T.L., Fregly, B.J., 2007. Are patient-specific joint and inertial parameters necessary for accurate inverse dynamics analyses of gait? *IEEE Trans. Biomed. Eng.* 54, 782–93.
- Reinschmidt, C., Bogert, A.J. Van Den, Lundberg, A., Nigg, B.M., Murphy, N., Alta, T.N.N., 1997. Tibiofemoral and tibioacalcaneal motion during walking : external vs . skeletal markers. *Gait Posture* 6, 98–109.

- Reinschmidt, C., Bogert, A.J. Van Den, Nigg, B.M., Lundberg, A., Murphy, N., 1997. Effect of skin movement on the analysis of skeletal knee joint motion during running. *J. Biomech.* 30, 729–732.
- Ren, L., Jones, R.K., Howard, D., 2008. Whole body inverse dynamics over a complete gait cycle based only on measured kinematics. *J. Biomech.* 41, 2750–9.
- Reyes, M., Mittendorf, A., 1998. A mathematical swing model for a long-driving champion. In: Farrally, M., Cochran, A. (Eds.), *Science and Golf III. Human Kinetics Leeds*, pp. 13–19.
- Richards, J., 1999. The measurement of human motion: A comparison of commercially available systems. *Hum. Mov. Sci.* 18, 589–602.
- Riemer, R., Hsiao-Wecksler, E.T., 2008. Improving joint torque calculations: Optimization-based inverse dynamics to reduce the effect of motion errors. *J. Biomech.* 41, 1503–1509.
- Riemer, R., Hsiao-Wecksler, E.T., Zhang, X., 2008. Uncertainties in inverse dynamics solutions: a comprehensive analysis and an application to gait. *Gait Posture* 27, 578–588.
- Roache, P.J., 1998. *Verification and validation in computational science and engineering*. Hermosa Publishers.
- Robert, T., Chèze, L., Dumas, R., Verriest, J.-P., 2007. Validation of net joint loads calculated by inverse dynamics in case of complex movements: application to balance recovery movements. *J. Biomech.* 40, 2450–6.
- Robertson, D.G., Caldwell, G.E., Hamill, J., Kamen, G., Whittlesey, S.N., 2004. *Research Methods In Biomechanics*. Human Kinetics, Champaign, IL.
- Rubinstein, R.Y., 1981. *Simulation and the Monte Carlo Method*. Wiley, Toronto.
- Ryu, T., Choi, H.S., Chung, M.K., 2009. Soft tissue artifact compensation using displacement dependency between anatomical landmarks and skin markers – a preliminary study. *Int. J. Ind. Ergon.* 39, 152–158.
- Sabick, M.B., 2004. Humeral Torque in Professional Baseball Pitchers. *Am. J. Sports Med.* 32, 892–898.
- Sangeux, M., Marin, F., Charleux, F., Dürselen, L., Ho Ba Tho, M.C., 2006. Quantification of the 3D relative movement of external marker sets vs. bones based on magnetic resonance imaging. *Clin. Biomech.* 21, 984–91.
- Schache, A.G., Baker, R., Lamoreux, L.W., 2008. Influence of thigh cluster configuration on the estimation of hip axial rotation. *Gait Posture* 27, 60–9.
- Schmidt, R., Disselhorst-Klug, C., Silny, J., Rau, G., 1999. A marker-based measurement procedure for unconstrained wrist and elbow motions. *J. Biomech.* 32, 615–21.

- 
- Schmiedmayer, H.B., Kastner, J., 1999. Parameters influencing the accuracy of the point of force application determined with piezoelectric force plates. *J. Biomech.* 32, 1237–42.
- Schmiedmayer, H.B., Kastner, J., 2000. Enhancements in the accuracy of the center of pressure (COP) determined with piezoelectric force plates are dependent on the load distribution. *J. Biomech. Eng.* 122, 523–7.
- Schwartz, M.H., Rozumalski, A., 2005. A new method for estimating joint parameters from motion data. *J. Biomech.* 38, 107–16.
- Schwer, L., 2006. Guide for the verification and validation in computational solid dynamics. *Am. Soc. Mech. Eng. ASME V&V.*
- Seidel, G.K., Marchinda, D.M., Dijkers, M., Soutas-Little, R.W., 1995. Technical Note: Hip Joint Center Location From Palpable Bony Landmarks - A Cadaver Study. *J. Biomech.* 28, 28–31.
- Shultz, R., Kedgley, a E., Jenkyn, T.R., Schultz, R., 2011. Quantifying skin motion artifact error of the hindfoot and forefoot marker clusters with the optical tracking of a multi-segment foot model using single-plane fluoroscopy. *Gait Posture* 34, 44–48.
- Silva, M., Ambrosio, J., 2004. Sensitivity of the results produced by the inverse dynamic analysis of a human stride to perturbed input data. *Gait Posture* 19, 35–49.
- Singh, B.N., Tiwari, A.K., 2006. Optimal selection of wavelet basis function applied to ECG signal denoising. *Digit. Signal Process.* 16, 275–287.
- Smith, G., 1989. Padding point extrapolation techniques for the Butterworth digital filter. *J. Biomech.* 22, 967– 971.
- Söderkvist, I., Wedin, P.Å., 1993. Determining the movements of the skeleton using well-configured markers. *J. Biomech.* 26, 1473–1477.
- Spoor, C.W., Veldpaus, F.E., 1980. Rigid body motion calculated from spatial coordinates of markers. *J. Biomech.* 13, 391–393.
- Springs, E.J., Mackenzie, S.J., 2002. Examining the delayed release in the golf swing using computer simulation. *Sport. Eng.* 5, 23–32.
- Springs, E.J., Neal, R.J., 2001. Shifting a portion of the clubshaft’s mass distally: does it improve performance? *Sport. Eng.* 4, 15–21.
- Stagni, R., Fantozzi, S., Cappello, A., Leardini, A., 2005. Quantification of soft tissue artefact in motion analysis by combining 3D fluoroscopy and stereophotogrammetry: a study on two subjects. *Clin. Biomech.* 20, 320–9.
- Stagni, R., Leardini, A., Cappozzo, A., Benedetti, M.G., Cappello, A., 2000. Effects of hip joint centre mislocation on gait analysis results. *J. Biomech.* 33, 1479–1487.

- Stanic, U., Bajd, T., Valencic, V., Kljajic, M., Acimovic, R., 1977. Standardization of kinematic gait measurements and automatic pathological gait pattern diagnostics. *Scand. J. Rehabil. Med.* 9, 95–105.
- Stewart, S., Haigh, J., n.d. The relationship between hip torque and club head angular velocity in the driver swing of sub 5 handicap golfers 1–10.
- Stokdijk, M., Meskers, C.G., Veeger, H.E., de Boer, Y. a, Rozing, P.M., 1999. Determination of the optimal elbow axis for evaluation of placement of prostheses. *Clin. Biomech.* 14, 177–84.
- Südhoff, I., Van Driessche, S., Laporte, S., de Guise, J. a, Skalli, W., 2007. Comparing three attachment systems used to determine knee kinematics during gait. *Gait Posture* 25, 533–43.
- Suzuki, S., Haake, S.J., Heller, B.W., 2006. Multiple modulation torque planning for a new golf-swing robot with a skilful wrist turn. *Sport. Eng.* 9, 201–208.
- Taylor, J.R., 1997. An introduction to error analysis: the study of uncertainties in physical measurements, Second. ed. University Science Books, Sausalito, CA.
- Tranberg, R., Karlsson, D., 1998. The relative skin movement of the foot: a 2-D roentgen photogrammetry study. *Clin. Biomech.* 13, 71–76.
- Tsai, T.-Y., Lu, T.-W., Kuo, M.-Y., Lin, C.-C., 2011. Effects of soft tissue artifacts on the calculated kinematics and kinetics of the knee during stair-ascent. *J. Biomech.* 44, 1182–8.
- Tsai, Y.-S., 2005. Biomechanical and Physical Characteristics of Trunk and Hip in Golfers with and without Low Back Pain.
- Tsujiuchi, N., Koizumi, T., Tomii, Y., 2002. Analysis of the influence of golf club design on the golf swing. In: Ujihashi, S., Haake, S. (Eds.), *The Engineering of Sport* 4. Blackwell, Oxford, pp. 537–544.
- Tsunoda, M., 2004. Three-deimensional motion analysis and inverse dynamic modelling of the human golf swing. *Eng. Sport.* 5 5, 326–332.
- Valero-Cuevas, F.J., Johanson, M.E., Towles, J.D., 2003. Towards a realistic biomechanical model of the thumb: the choice of kinematic description may be more critical than the solution method or the variability/uncertainty of musculoskeletal parameters. *J. Biomech.* 36, 1019–1030.
- Van Den Bogert, A.J., de Koning, J.J., 1996. On Optimal Filtering for Inverse Dynamics Analysis. In: *Proceedings of the IXth Biennial Conference of the Canadian Society for Biomechanics*. Vancouver, pp. 214–215.
- Vaughan, C.L., 1981. A three-dimensional analysis of the forces and torques applied by a golfer during the downswing. In: Morecki, A., Fidelus, K., Kedzior, K., Witt, A. (Eds.), *Biomechanics VII-B*. University Park Press, Baltimore, MD, pp. 325–331.

- Vaughan, C.L., Hay, J.G., Andrews, J.G., 1982a. Closed loop problems in biomechanics. Part I--a classification system. *J. Biomech.* 15, 197–200.
- Vaughan, C.L., Hay, J.G., Andrews, J.G., 1982b. Closed loop problems in biomechanics. Part II--an optimization approach. *J. Biomech.* 15, 201–10.
- Veeger, D., Yu, B., An, K.N., 1996. Orientation of axes in the elbow and forearm for biomechanical modelling. *Proc. First Conf. ISG* 83–88.
- Veeger, H.E.J., Yu, B., An, K.-N., Rozendal, R.H., 1997. Parameters for modelling the upper extremity. *J. Biomech.* 30, 647–652.
- Versi, E., 1992. “ Gold standard” is an appropriate term. *BMJ Br. Med. J.* 305, 187.
- Viceconti, M., Olsen, S., Nolte, L.P., Burton, K., 2005. Extracting clinically relevant data from finite element simulations. *Clin. Biomech.* 20, 451–454.
- Wachowiak, M.P., Rash, G.S., Quesada, P.M., Desoky, a H., 2000. Wavelet-based noise removal for biomechanical signals: a comparative study. *IEEE Trans. Biomed. Eng.* 47, 360–8.
- Wahrenberg, H., Lindbeck, L., Ekholm, J., 1978. Knee muscular moment, tendon tension force and EMG during a vigorous movement in man. *Scand. J. Rehabil. Med.* 10, 99–106.
- Walker, J.R., 1986. Practical Application Of Variance Reduction Techniques In Probabilistic Assessments. In: *The Second International Conference on Radioactive Waste Management*. Winnipeg, Manito, Canada, pp. 517–521.
- Weisstein, E.W., 2013. Normal sum distribution [WWW Document]. *MathWorld - A Wolfram Web Resour.* URL <http://mathworld.wolfram.com/NormalSumDistribution.html>
- White, G.H., Farrance, I., 2004. Uncertainty of measurement in quantitative medical testing: a laboratory implementation guide. *Clin. Biochem. Rev.* 25, S1.
- White, R., 2006. On the efficiency of the golf swing. *Am. J. Phys.* 74, 1088.
- Wicke, J., Dumas, G.A., 2010. Influence of the volume and density functions with geometric models for estimating trunk inertial parameters. *J. Appl. Biomech.* 26, 26–31.
- Wicke, J., Dumas, G.A., Costigan, P.A., 2009. A comparison between a new model and current models for estimating trunk segment inertial parameters. *J. Biomech.* 42, 55–60.
- Winter, D. a, 1980. Overall principle of lower limb support during stance phase of gait. *J. Biomech.* 13, 923–7.

- Winter, D.A., 1990. Biomechanics and motor control of human movement. Wiley, Toronto.
- Woltring, H.J., 1994. 3-D attitude representation of human joints: a standardization proposal. *J. Biomech.* 27, 1399–1414.
- Woltring, H.J., Huiskes, R., De Lange, A., Veldpaus, F.E., 1985. Finite centroid and helical axis estimation from noisy landmark measurements in the study of human joint kinematics. *J. Biomech.* 18, 379–389.
- Wood, D.E., Donaldson, N., Perkins, T., 1999. Apparatus to measure simultaneously 14 isometric leg joint moments. Part 2: Multi-moment chair system. *Med. Biol. Eng. Comput.* 37, 148–154.
- Wood, G., 1982. Data smoothing and differentiation procedures in biomechanics. *Exerc. Sport Sci. Rev.* 10, 308–362.
- Wua, G., Sieglerb, S., Allardc, P., Kirtleyd, C., Leardini, A., Rosenbaumf, D., Whittleg, M., D'Limah, D.D., Cristofolini, L., Wittej, H., Schmidk, O., Stokes, I., 2002. ISB recommendation on definitions of joint coordinate system of various joints for the reporting of human joint motion—part I: ankle, hip, and spine. *J. Biomech.* 35, 543–548.
- Yeadon, M.R., Morlock, M., 1989. The appropriate use of regression equations for the estimation of segmental inertia parameters. *J. Biomech.* 22, 683–689.
- Yeadon, M.R.R., 1990. The simulation of aerial movement—II. A mathematical inertia model of the human body. *J. Biomech.* 23, 67–74.
- Yontz, N.A., 2010. Determining the correlation between core performance and golf swing kinematics and kinetics.
- Zabala, M.E., Favre, J., Scanlan, S.F., Donahue, J., Andriacchi, T.P., 2012. Three-dimensional knee moments of ACL reconstructed and control subjects during gait, stair ascent, and stair descent. *J. Biomech.* 1–6.
- Zachmann, G., 1997. Distortion correction of magnetic fields for position tracking. *Proc. Comput. Graph. Int.* 213–220.
- Zatsiorsky, V.M., 1998. Kinematics of human motion. Human Kinetics, Champaign, IL.
- Zatsiorsky, V.M., 2002. Kinetics of human motion. Human Kinetics, Champaign, IL.
- Zhang, X., Lee, S.-W., Braido, P., 2004. Towards an integrated high-fidelity linkage representation of the human skeletal system based on surface measurement. *Int J Ind Ergo* 33, 215–227.

## APPENDIX A: Body segment parameters equations

The following equations were used to define the mass ( $m$ ), centre of mass location from the proximal end ( $g_z$ ), and the principle moments of inertia ( $I_{xx}$ ,  $I_{yy}$  and  $I_{zz}$ ) of the geometric solids used to model the body. Calculations assume a uniform density  $\rho$ .

### Semi Ellipsoid

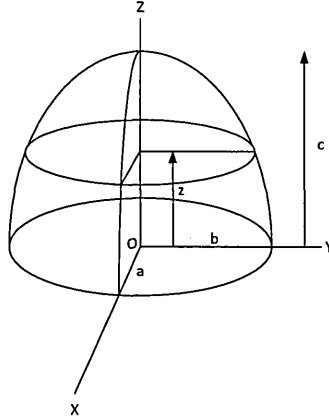


Figure 52 Semi ellipsoid geometric solid

$$m = \frac{2\pi}{3} \rho abc$$

Equation A.1

$$g_z = \frac{3}{8} c$$

Equation A.2

$$I_{zz} = \frac{2\pi}{15} \rho abc (a^2 + b^2)$$

Equation A.3

$$I_{xx} = \frac{2\pi}{15} \rho abc (b^2 + c^2) - mg_z^2$$

Equation A.4

$$I_{yy} = \frac{2\pi}{15} \rho abc (a^2 + c^2) - mg_z^2$$

Equation A.5

### Elliptical Solid

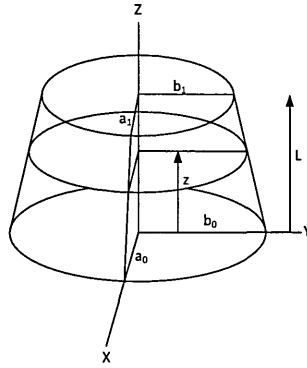


Figure 53 Elliptical solid geometric shape

$$m = \pi \rho L G_{20}(a, b)$$

Equation A.6

$$g_z = \frac{G_{21}(a, b)}{G_{20}(a, b)} L$$

Equation A.7

$$I_{zz} = \frac{\pi}{4} \rho L [G_{40}(a, a, a, b) + G_{40}(a, b, b, b)]$$

Equation A.8

$$I_{xx} = \frac{\pi}{4} \rho L G_{40}(a, b, b, b) + \pi \rho L^3 G_{22}(a, b) - m g_z^2$$

Equation A.9

$$I_{yy} = \frac{\pi}{4} \rho L G_{40}(a, a, a, b) + \pi \rho L^3 G_{22}(a, b) - m g_z^2$$

Equation A.10

### Stadium Solid

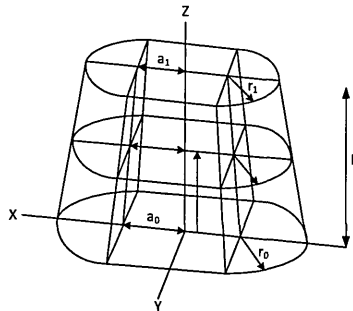


Figure 54 Stadium solid

$$m = 4\rho LG_{20}(a, r) + \pi\rho LG_{20}(r, r)$$

Equation A.11

$$g_z = \frac{4G_{21}(a, r) + \pi G_{21}(r, r)}{4G_{20}(a, r) + \pi G_{20}(r, r)} L$$

Equation A.12

$$I_{zz} = \frac{4}{3}\rho LG_{40}(a, a, a, r) + \pi\rho LG_{40}(a, a, r, r) + 4\rho LG_{40}(a, r, r, r) + \frac{\pi}{2}\rho LG_{40}(r, r, r, r)$$

Equation A.13

$$I_{xx} = \frac{4}{3}\rho LG_{40}(a, r, r, r) + \frac{\pi}{4}\rho LG_{40}(r, r, r, r) + 4\rho L^3 G_{22}(a, r) + \frac{\pi}{2}\rho L^3 G_{22}(r, r) - mg_z^2$$

Equation A.14

$$I_{yy} = \frac{4}{3}\rho LG_{40}(a, a, a, r) + \pi\rho LG_{40}(a, a, r, r) + \frac{8}{3}\rho LG_{40}(a, r, r, r) + \frac{\pi}{4}\rho LG_{40}(r, r, r, r) + 4\rho L^3 G_{22}(a, r) + \pi\rho L^3 G_{22}(r, r) - mg_z^2$$

Equation A.15

### Basic Integral functions

$$G_{20} = \frac{F_{22}(a, b)}{3} + \frac{F_{21}(a, b)}{2} + F_{20}(a, b)$$

Equation A.16

$$G_{21}(a, b) = \frac{F_{22}(a, b)}{4} + \frac{F_{21}(a, b)}{3} + \frac{F_{20}(a, b)}{2}$$

Equation A.17

$$G_{22}(a, b) = \frac{F_{22}(a, b)}{5} + \frac{F_{21}(a, b)}{4} + \frac{F_{20}(a, b)}{3}$$

Equation A.18

$$G_{40}(a, b, c, d) = \frac{F_{44}(a, b, c, d)}{5} + \frac{F_{43}(a, b, c, d)}{4} + \frac{F_{42}(a, b, c, d)}{3} + \frac{F_{41}(a, b, c, d)}{2} + F_{40}(a, b, c, d)$$

Equation A.19

where

$$F_{22}(a, b) = (a_1 - a_0)(b_1 - b_0)$$

Equation A.20

$$F_{21}(a, b) = a_0(b_1 - b_0) + (a_1 - a_0)b_0$$

Equation A.21

$$F_{20}(a, b) = a_0 b_0$$

Equation A.22

$$F_{44}(a, b, c, d) = (a_1 - a_0)(b_1 - b_0)(c_1 - c_0)(d_1 - d_0)$$

Equation A.23

$$F_{43}(a, b, c, d) = a_0(b_1 - b_0)(c_1 - c_0)(d_1 - d_0) + (a_1 - a_0)b_0(c_1 - c_0)(d_1 - d_0) \\ + (a_1 - a_0)(b_1 - b_0)c_0(d_1 - d_0) + (a_1 - a_0)(b_1 - b_0)(c_1 - c_0)d_0$$

Equation A.24

$$F_{42}(a, b, c, d) = a_0 b_0(c_1 - c_0)(d_1 - d_0) + a_0(b_1 - b_0)c_0(d_1 - d_0) + a_0(b_1 - b_0)(c_1 - c_0)d_0 \\ + (a_1 - a_0)b_0 c_0(d_1 - d_0) + (a_1 - a_0)b_0(c_1 - c_0)d_0 + (a_1 - a_0)(b_1 - b_0)c_0 d_0$$

Equation A.25

$$F_{41}(a, b, c, d) = (a_1 - a_0)b_0 c_0 d_0 + a_0(b_1 - b_0)c_0 d_0 + a_0 b_0(c_1 - c_0)d_0 + a_0 b_0 c_0(d_1 - d_0)$$

Equation A.26

$$F_{40}(a, b, c, d) = a_0 b_0 c_0 d_0$$

Equation A.27

## APPENDIX B: Force platform calculations

The following calculations relate to KISTLER plates, type 9128C (Kistler Instrumente AG, Winterthur, Switzerland). Data from the force plate was saved to an .ANC file. There were 8 channels of data for each plate and these corresponded to;

Channel number	Channel name
1	FX12
2	FX34
3	FY14
4	FY23
5	FZ1
6	FZ2
7	FZ3
8	FZ4

The following steps were used to convert the force channel raw,  $F_{raw}$ , output to Newtons;

Convert data in .anc files from digital units to mV;

$$F_{mV} = \frac{r}{u} \times F_{raw}$$

Equation B.1

where  $r = \text{range} = 10,000 \text{ mV}$ ;  $u = \text{number of digital units} = 12 \text{ bit} = 4096$ .

Divide each  $F_{mV}$  force by sensitivity values in table 50 to convert to Newtons;

Table 50 Calibrated sensitivity coefficients for each plate

N/mV	FX12	FX34	FY14	FY23	FZ1	FZ2	FZ3	FZ4
FP1	18.803	18.683	18.863	18.623	9.515	9.460	9.500	9.469
FP2	18.833	18.727	18.913	19.007	9.629	9.610	9.625	9.692

Force components  $F_x, F_y, F_z$  and centre of pressure coordinates  $a_x, a_y$ , were calculated using the formulae in table 51;

Table 51 Force parameter calculations

Parameter	Calculation	Description
$F_x$	$= FX12 + FX34$	Medio-lateral force
$F_y$	$= FY14 + FY23$	Anterior-posterior force
$F_z$	$= FZ1 + FZ2 + FZ3 + FZ4$	Vertical force
$ F_{resultant} $	$= \sqrt{(F_x^2 + F_y^2 + F_z^2)}$	Resultant force
$M_x$	$= b \times (FZ1 + FZ2 - FZ3 - FZ4)$	Plate moment about x-axis
$M_y$	$= a \times (-FZ1 + FZ2 + FZ3 - FZ4)$	Plate axis about y-axis
$a_x$	$= (F_x \times az0 - M_y) / F_z$	X-coordinate of force application point (COP)
$a_y$	$= (F_y \times az0 + M_x) / F_z$	Y-coordinate of force application point (COP)

where the plate dimensions were  $a = 0.12$ ,  $b = 0.2$ ,  $az_0 = -0.048$  as shown in figure 55;

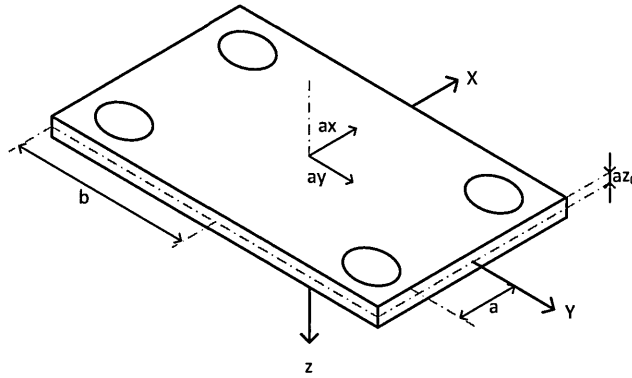


Figure 55 KISTLER coordinate system

## APPENDIX C: Force plate and force transducer calibration

### Static force plate calibration

For each plate (KISTLER type 9128C, Kistler Instrumente AG, Winterthur, Switzerland) masses of known load were placed approximately in the centre of each plate and using Bioware software (Kistler Instrumente AG, Winterthur, Switzerland) the vertical force output from the plates was measured during a 3 second trial. Table 52 shows the loads and corresponding KISTLER output;

Table 52 Static vertical force comparison: KISTLER plates vs. known static weights

Rear Plate			Front Plate		
Known force (N)	KISTLER (N)	Difference (N)	Known force	KISTLER	Difference (N)
96.5	97.4	1.0	96.5	96.7	0.3
191.4	191.5	0.1	191.4	192.4	1.0
286.7	287.2	0.5	286.7	287.6	0.9
383.0	381.9	-1.1	383.0	384.1	1.2
476.4	475.6	-0.9	476.4	478.6	2.2

Data from table 52 was used to plot graphs of known force vs. KISTLER measured force which was then used to convert force plate output to force using equation of straight line for each plate (figure 56). All subsequent data output from the force plates were adjusted according to equations E.1 and E.2;

$$F_{F\_cal} = 1.0042 \times F_{front} - 0.1109$$

Equation C.1

$$F_{B\_cal} = 0.9949 \times F_{back} - 1.3716$$

Equation C.2

where  $F_{F\_cal}$  and  $F_{B\_cal}$  are the calibrated forces from the front and back plates respectively, and  $F_{front}$ ,  $F_{back}$  are the force signals output from the plates.

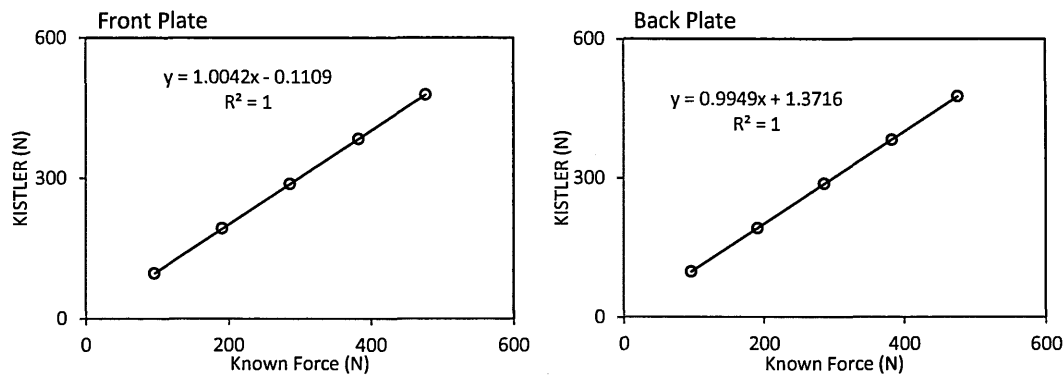


Figure 56 Force plate calibration data

### Transducer calibration

In the centre of plate, the transducer was dynamically loaded with a variable load for 5 seconds. Data from KISTLER plates measured through BioWare (Kistler Instrumente AG, Winterthur, Switzerland) and subject to calibration from previous testing (see above) was compared to output from transducer. This process was repeated three times in the centre of each plate (figure 57 & figure 58).

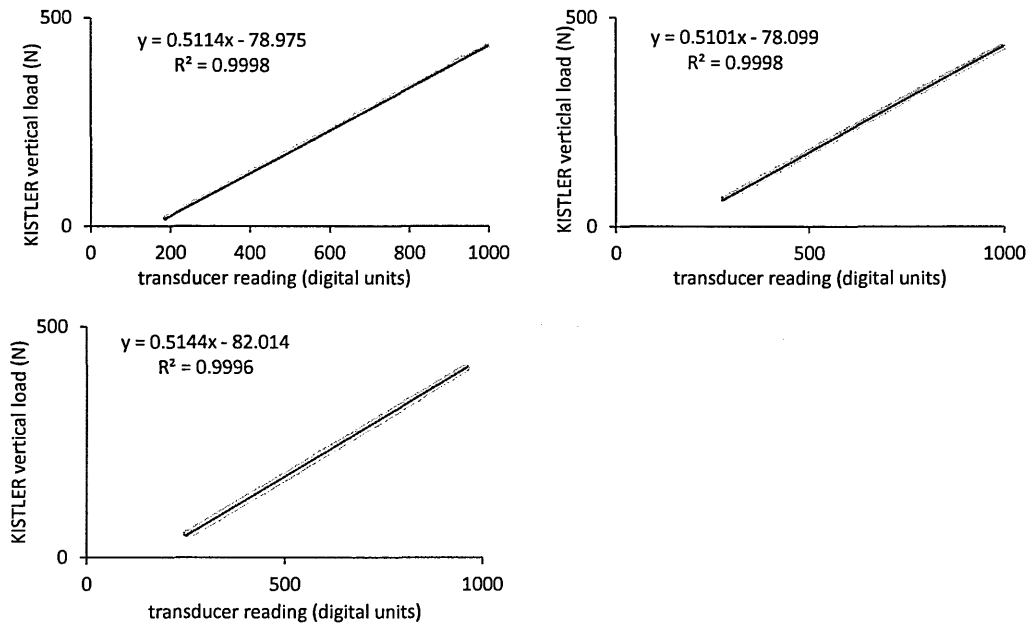


Figure 57 Front plate transducer calibration data

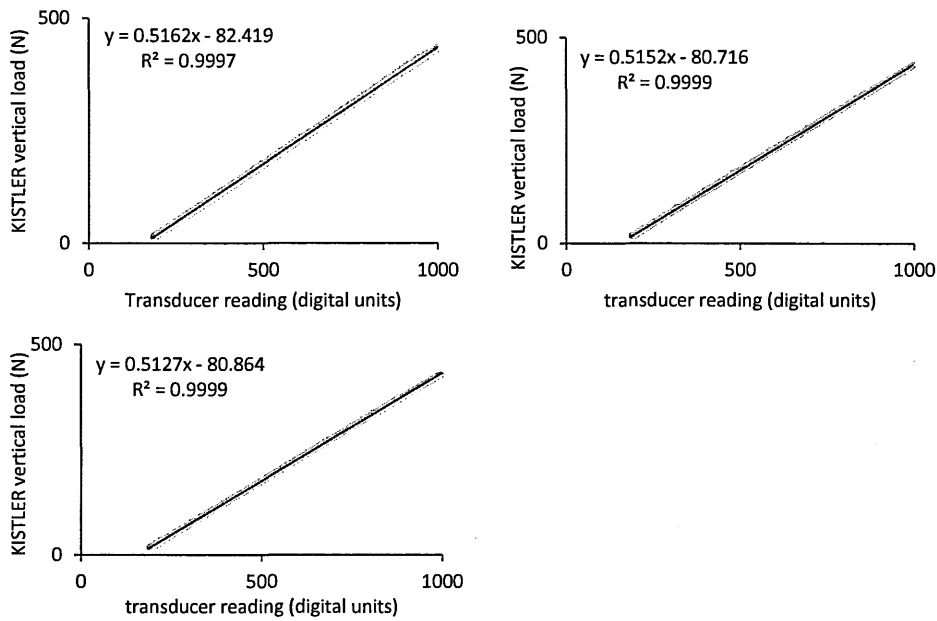


Figure 58 Back plate transducer calibration data

Calibration of the transducer was achieved by comparison of transducer output to KISTLER force, using the equations of line of best fit;

$$F_t = \bar{y} \times t + \bar{c}$$

Equation C.3

where  $F_t$  is the calibrated force output for the transducer in Newtons,  $t$  is the transducer reading in digital units,  $\bar{y}$  is the mean gradient of the line of best fit for the six tests and  $\bar{c}$  is the mean intercept value for the six tests.

Therefore, the calibrated force output  $F_t$  for the transducer was calculated using equation E.4;

$$F_t = 0.51 \times t + 80.7$$

Equation C.4

## APPENDIX D: Calculation of the combined standard uncertainty using numerical methods

In general, a measurand  $Y$  is not measured directly, but is determined from  $N$  other quantities or input parameters  $X_1, X_2, \dots, X_N$  through the functional relationship  $f$ :

$$Y = f(X_1, X_2, \dots, X_N)$$

Equation D.1

The combined standard uncertainty was determined using the methods recommended by The Guide to the Expression of Uncertainty in Measurement (GUM) (ISO, 1995), based on the law of propagation of uncertainty using a first order Taylor series approximation of  $Y = f(X_1, X_2, \dots, X_N)$  (Taylor, 1997). These equations assume that all input parameters are **independent**. The combined standard uncertainty  $u_c(y)$ , is given by

$$u_c(y) = \sqrt{\sum_{i=1}^N \left(\frac{\partial f}{\partial x_i}\right)^2 u^2(x_i)}$$

Equation D.2

where  $f$  is the function given in equation D.1. Each  $u(x_i)$  is the inaccuracy in each input parameter. The combined standard uncertainty is an estimated standard deviation that characterises the dispersion of values that could reasonably be attributed to the measurand  $Y$ .

The following example uses equation D.2 to determine the combined standard uncertainty associated with the calculation of the viscosity of a fluid.

Equation D.3 is a standard equation for calculating the viscosity of a fluid ( $\mu$ ) using falling sphere viscometry. Assuming stokes flow;

$$\mu = \frac{2gr^2(\rho_s - \rho_f)}{9V}$$

Equation D.3

where  $r$  is the radius of the sphere,  $g$  is acceleration due to gravity,  $V$  is the terminal velocity of the falling sphere,  $\rho_s$  is the density of the sphere and  $\rho_f$  is the density of the

fluid. The terminal velocity is calculated from the distance and time as shown in equation D.4;

$$V = \frac{d}{t}$$

Equation D.4

Where  $d$  is distance the bead travels over a certain amount of time  $t$ . The magnitude of the input parameters,  $x_i$ , and the inaccuracy associated with their measurement,  $u(x_i)$ , are;

$$r \pm u(r) = 2 \pm 0.05\text{cm}$$

Equation D.5

$$\rho_s \pm u(\rho_s) = 8.94 \pm 0.03\text{g/cm}^3$$

Equation D.6

$$\rho_f \pm u(\rho_f) = 1.32 \pm 0.02\text{g/cm}^3$$

Equation D.7

$$d \pm u(d) = 4 \pm 0.05\text{cm}$$

Equation D.7

$$t \pm u(t) = 5.0 \pm 0.25\text{s}$$

Equation D.8

Therefore, the viscosity,  $\mu$ , is calculated as;

$$\mu = \frac{2gr^2(\rho_s - \rho_f)}{9V} = 83.1\text{g/cm/s}$$

Equation D.9

From equation D.2, the partial derivatives  $\partial f/\partial x_i$  for each input parameter are calculated;

$$\frac{\partial \mu}{\partial r} = \frac{2g \times 2r \times (\rho_s - \rho_f)}{9V} = 83.1$$

Equation D.10

$$\frac{\partial \mu}{\partial \rho_s} = \frac{2gr^2}{9V} = 10.9$$

Equation D.11

$$\frac{\partial \mu}{\partial \rho_f} = \frac{-2gr^2}{9V} = -10.9$$

Equation D.12

$$\frac{\partial \mu}{\partial d} = \frac{2gr^2(\rho_s - \rho_f)}{9 \times d \times d/t} = 20.8$$

Equation D.13

$$\frac{\partial \mu}{\partial t} = \frac{2gr^2(\rho_s - \rho_f)}{9 \times d} = 16.6$$

Equation D.14

$$\left(\frac{\partial \mu}{\partial r} u(r)\right)^2 = 830.30 \times 0.05 = 17.2$$

Equation D.15

$$\left(\frac{\partial \mu}{\partial \rho_s} u(\rho_s)\right)^2 = 10.9 \times 0.03 = 0.1$$

Equation D.16

$$\left(\frac{\partial \mu}{\partial \rho_f} u(\rho_f)\right)^2 = -10.9 \times 0.02 = 0.05$$

Equation D.17

$$\left(\frac{\partial \mu}{\partial d} u(d)\right)^2 = 20.8 \times 0.05 = 1.1$$

Equation D.18

$$\left(\frac{\partial \mu}{\partial t} u(t)\right)^2 = 16.6 \times 0.25 = 17.2$$

Equation D.19

Summing each term and taking the square root, the combined standard uncertainty of the viscosity  $u_c(\mu)$  is;

$$u_c(\mu) = \sqrt{\left(\frac{\partial \mu}{\partial r} u(r)\right)^2 + \left(\frac{\partial \mu}{\partial \rho_s} u(\rho_s)\right)^2 + \left(\frac{\partial \mu}{\partial \rho_f} u(\rho_f)\right)^2 + \left(\frac{\partial \mu}{\partial d} u(d)\right)^2 + \left(\frac{\partial \mu}{\partial t} u(t)\right)^2}$$

$$= \sqrt{17.2 + 0.1 + 0.05 + 1.1 + 17.2} = 5.98$$

Equation D.20

Therefore

$$\mu = 83.1 \pm 5.98 \text{ g/cm/s}$$

Equation D.21

This method is useful when the function is simple, of which derivatives can easily be taken. The combined standard uncertainty may be calculated numerically. The numerical method involves an approximation to the function, but there is no need to take partial derivatives which can be useful in situations that are complex set of equations, and is a simpler to automate for general use (Coleman and Steele, 2009).

Equation D.2 can be written as;

$$u_c(y) = \sqrt{\sum_{i=1}^N [c_i u(x_i)]^2}$$

Equation D.22

where

$$c_i \equiv \frac{\partial f}{\partial x_i}$$

Equation D.23

The combined standard uncertainty  $u_c(y)$  may be calculated numerically by replacing  $c_i u(x_i)$  in equation D.22 with

$$Z_i = \frac{1}{2} \{f[x_1, \dots, x_i + u(x_i), \dots, x_N] - f[x_1, \dots, x_i - u(x_i), \dots, x_N]\}$$

Equation D.24

The following example uses the numerical method to determine the combined standard uncertainty associated with the calculation of the viscosity of a fluid.

$$Z_r = \frac{1}{2} \left\{ \left( \frac{2g(r + u(r))^2 (\rho_s - \rho_f)}{9V} \right) - \left( \frac{2g(r - u(r))^2 (\rho_s - \rho_f)}{9V} \right) \right\} = 4.15$$

Equation D.25

$$Z_{\rho_s} = \frac{1}{2} \left\{ \left( \frac{2gr^2 ((\rho_s + u(\rho_s)) - \rho_f)}{9V} \right) - \left( \frac{2gr^2 ((\rho_s - u(\rho_s)) - \rho_f)}{9V} \right) \right\} = 0.33$$

Equation D.26

$$Z_{\rho_f} = \frac{1}{2} \left\{ \left( \frac{2gr^2(\rho_s - (\rho_f + u(\rho_f)))}{9V} \right) - \left( \frac{2g(r - u(r))^2(\rho_s - (\rho_f - u(\rho_f)))}{9V} \right) \right\} = 0.22$$

Equation D.27

$$Z_d = \frac{1}{2} \left\{ \left( \frac{2gr^2(\rho_s - \rho_f)}{9(d + u(d))/t} \right) - \left( \frac{2gr^2(\rho_s - \rho_f)}{9(d - u(d))/t} \right) \right\} = 1.04$$

Equation D.28

$$Z_t = \frac{1}{2} \left\{ \left( \frac{2gr^2(\rho_s - \rho_f)}{9d/(t + u(t))} \right) - \left( \frac{2gr^2(\rho_s - \rho_f)}{9d/(t - u(t))} \right) \right\} = 4.15$$

Equation D.29

The combined standard uncertainty  $u_c(y)$  is;

$$u_c(y) = \sqrt{\sum_{i=1}^N Z_i^2 + Z_{\rho_s}^2 + Z_{\rho_f}^2 + Z_d^2 + Z_t^2}$$

$$= \sqrt{4.15^2 + 0.33^2 + 0.22^2 + 1.04^2 + 4.15^2} = 5.98$$

Equation D.30

Therefore, using numerical methods;

$$\mu = 83.1 \pm 5.98 \text{ g/cm/s}$$

Equation D.31

**APPENDIX E: Complete list of inaccuracy values for sets 1, 2 and 3**

Segment	Parameter	Operator	Set 1	Set 2	Set 3
RightFoot	SegmentMass	%	3.940	6.520	11.050
RightShank	SegmentMass	%	1.700	6.540	9.250
RightThigh	SegmentMass	%	3.450	5.050	10.740
LeftFoot	SegmentMass	%	3.940	6.520	11.050
LeftShank	SegmentMass	%	1.700	6.540	9.250
LeftThigh	SegmentMass	%	3.450	5.050	10.740
Pelvis	SegmentMass	%	2.340	2.480	6.230
Lumbar	SegmentMass	%	6.260	8.900	13.760
Thorax	SegmentMass	%	1.260	1.610	1.970
RightHand	SegmentMass	%	3.940	6.520	11.050
RightForeArm	SegmentMass	%	1.010	3.850	6.940
RightUpperArm	SegmentMass	%	9.980	18.790	28.470
LeftHand	SegmentMass	%	3.940	6.520	11.050
LeftForeArm	SegmentMass	%	1.010	3.850	6.940
LeftUpperArm	SegmentMass	%	9.980	18.790	28.470
Neck	SegmentMass	%	3.940	6.520	11.050
Head	SegmentMass	%	3.940	6.520	11.050
RightFoot	MOlap	%	4.040	7.560	12.930
RightShank	MOlap	%	8.870	15.500	19.260
RightThigh	MOlap	%	4.200	4.230	12.130
LeftFoot	MOlap	%	4.040	7.560	12.930
LeftShank	MOlap	%	8.870	15.500	19.260
LeftThigh	MOlap	%	4.200	4.230	12.130
Pelvis	MOlap	%	4.220	5.900	9.360
Lumbar	MOlap	%	3.280	12.800	14.070
Thorax	MOlap	%	3.400	6.410	9.150
RightHand	MOlap	%	4.040	7.560	12.930
RightForeArm	MOlap	%	4.000	4.050	10.610
RightUpperArm	MOlap	%	0.330	4.000	15.910
LeftHand	MOlap	%	4.040	7.560	12.930
LeftForeArm	MOlap	%	4.000	4.050	10.610
LeftUpperArm	MOlap	%	0.330	4.000	15.910
Neck	MOlap	%	4.040	7.560	12.930
Head	MOlap	%	4.040	7.560	12.930
RightFoot	MOlml	%	4.090	6.910	13.690
RightShank	MOlml	%	8.850	15.700	19.100
RightThigh	MOlml	%	4.200	4.320	13.000
LeftFoot	MOlml	%	4.090	6.910	13.690
LeftShank	MOlml	%	8.850	15.700	19.100
LeftThigh	MOlml	%	4.200	4.320	13.000
Pelvis	MOlml	%	2.700	5.760	16.700
Lumbar	MOlml	%	7.020	7.500	10.680
Thorax	MOlml	%	0.400	1.300	8.100
RightHand	MOlml	%	4.090	6.910	13.690
RightForeArm	MOlml	%	5.300	8.300	13.730
RightUpperArm	MOlml	%	0.130	5.500	14.510
LeftHand	MOlml	%	4.090	6.910	13.690
LeftForeArm	MOlml	%	5.300	8.300	13.730
LeftUpperArm	MOlml	%	0.130	5.500	14.510
Neck	MOlml	%	4.090	6.910	13.690
Head	MOlml	%	4.090	6.910	13.690
RightFoot	MOllong	%	2.600	7.660	13.440
RightShank	MOllong	%	2.040	5.600	11.130
RightThigh	MOllong	%	4.000	13.660	21.080
LeftFoot	MOllong	%	2.600	7.660	13.440
LeftShank	MOllong	%	2.040	5.600	11.130

APPENDIX E: Complete list of inaccuracy values for sets 1, 2 and 3

LeftThigh	MOIlong	%	4.000	13.660	21.080
Pelvis	MOIlong	%	1.970	2.200	5.180
Lumbar	MOIlong	%	3.500	8.160	12.890
Thorax	MOIlong	%	0.570	8.500	12.500
RightHand	MOIlong	%	2.600	7.660	13.440
RightForeArm	MOIlong	%	2.030	6.600	12.350
RightUpperArm	MOIlong	%	4.080	8.900	18.940
LeftHand	MOIlong	%	2.600	7.660	13.440
LeftForeArm	MOIlong	%	2.030	6.600	12.350
LeftUpperArm	MOIlong	%	4.080	8.900	18.940
Neck	MOIlong	%	2.600	7.660	13.440
Head	MOIlong	%	2.600	7.660	13.440
RightFoot	COMaccelx	+	0.058	3.209	4.065
RightShank	COMaccelx	+	0.058	3.209	4.065
RightThigh	COMaccelx	+	0.058	3.209	4.065
LeftFoot	COMaccelx	+	0.058	3.209	4.065
LeftShank	COMaccelx	+	0.058	3.209	4.065
LeftThigh	COMaccelx	+	0.058	3.209	4.065
Pelvis	COMaccelx	+	0.058	3.209	4.065
Lumbar	COMaccelx	+	0.058	3.209	4.065
Thorax	COMaccelx	+	0.058	3.209	4.065
RightHand	COMaccelx	+	0.058	3.209	4.065
RightForeArm	COMaccelx	+	0.058	3.209	4.065
RightUpperArm	COMaccelx	+	0.058	3.209	4.065
LeftHand	COMaccelx	+	0.058	3.209	4.065
LeftForeArm	COMaccelx	+	0.058	3.209	4.065
LeftUpperArm	COMaccelx	+	0.058	3.209	4.065
Neck	COMaccelx	+	0.058	3.209	4.065
Head	COMaccelx	+	0.058	3.209	4.065
RightFoot	COMaccely	+	0.058	3.209	4.065
RightShank	COMaccely	+	0.058	3.209	4.065
RightThigh	COMaccely	+	0.058	3.209	4.065
LeftFoot	COMaccely	+	0.058	3.209	4.065
LeftShank	COMaccely	+	0.058	3.209	4.065
LeftThigh	COMaccely	+	0.058	3.209	4.065
Pelvis	COMaccely	+	0.058	3.209	4.065
Lumbar	COMaccely	+	0.058	3.209	4.065
Thorax	COMaccely	+	0.058	3.209	4.065
RightHand	COMaccely	+	0.058	3.209	4.065
RightForeArm	COMaccely	+	0.058	3.209	4.065
RightUpperArm	COMaccely	+	0.058	3.209	4.065
LeftHand	COMaccely	+	0.058	3.209	4.065
LeftForeArm	COMaccely	+	0.058	3.209	4.065
LeftUpperArm	COMaccely	+	0.058	3.209	4.065
Neck	COMaccely	+	0.058	3.209	4.065
Head	COMaccely	+	0.058	3.209	4.065
RightFoot	COMaccelz	+	0.058	3.209	4.065
RightShank	COMaccelz	+	0.058	3.209	4.065
RightThigh	COMaccelz	+	0.058	3.209	4.065
LeftFoot	COMaccelz	+	0.058	3.209	4.065
LeftShank	COMaccelz	+	0.058	3.209	4.065
LeftThigh	COMaccelz	+	0.058	3.209	4.065
Pelvis	COMaccelz	+	0.058	3.209	4.065
Lumbar	COMaccelz	+	0.058	3.209	4.065
Thorax	COMaccelz	+	0.058	3.209	4.065
RightHand	COMaccelz	+	0.058	3.209	4.065
RightForeArm	COMaccelz	+	0.058	3.209	4.065
RightUpperArm	COMaccelz	+	0.058	3.209	4.065
LeftHand	COMaccelz	+	0.058	3.209	4.065

## APPENDIX E: Complete list of inaccuracy values for sets 1, 2 and 3

LeftForeArm	COMaccelz	+	0.058	3.209	4.065
LeftUpperArm	COMaccelz	+	0.058	3.209	4.065
Neck	COMaccelz	+	0.058	3.209	4.065
Head	COMaccelz	+	0.058	3.209	4.065
RightFoot	AngVelx	+	0.050	0.485	1.021
RightShank	AngVelx	+	0.050	0.485	1.021
RightThigh	AngVelx	+	0.050	0.485	1.021
LeftFoot	AngVelx	+	0.050	0.485	1.021
LeftShank	AngVelx	+	0.050	0.485	1.021
LeftThigh	AngVelx	+	0.050	0.485	1.021
Pelvis	AngVelx	+	0.050	0.485	1.021
Lumbar	AngVelx	+	0.050	0.485	1.021
Thorax	AngVelx	+	0.050	0.485	1.021
RightHand	AngVelx	+	0.050	0.485	1.021
RightForeArm	AngVelx	+	0.050	0.485	1.021
RightUpperArm	AngVelx	+	0.050	0.485	1.021
LeftHand	AngVelx	+	0.050	0.485	1.021
LeftForeArm	AngVelx	+	0.050	0.485	1.021
LeftUpperArm	AngVelx	+	0.050	0.485	1.021
Neck	AngVelx	+	0.050	0.485	1.021
Head	AngVelx	+	0.050	0.485	1.021
RightFoot	AngVely	+	0.050	0.485	1.021
RightShank	AngVely	+	0.050	0.485	1.021
RightThigh	AngVely	+	0.050	0.485	1.021
LeftFoot	AngVely	+	0.050	0.485	1.021
LeftShank	AngVely	+	0.050	0.485	1.021
LeftThigh	AngVely	+	0.050	0.485	1.021
Pelvis	AngVely	+	0.050	0.485	1.021
Lumbar	AngVely	+	0.050	0.485	1.021
Thorax	AngVely	+	0.050	0.485	1.021
RightHand	AngVely	+	0.050	0.485	1.021
RightForeArm	AngVely	+	0.050	0.485	1.021
RightUpperArm	AngVely	+	0.050	0.485	1.021
LeftHand	AngVely	+	0.050	0.485	1.021
LeftForeArm	AngVely	+	0.050	0.485	1.021
LeftUpperArm	AngVely	+	0.050	0.485	1.021
Neck	AngVely	+	0.050	0.485	1.021
Head	AngVely	+	0.050	0.485	1.021
RightFoot	AngVelz	+	0.050	0.485	1.021
RightShank	AngVelz	+	0.050	0.485	1.021
RightThigh	AngVelz	+	0.050	0.485	1.021
LeftFoot	AngVelz	+	0.050	0.485	1.021
LeftShank	AngVelz	+	0.050	0.485	1.021
LeftThigh	AngVelz	+	0.050	0.485	1.021
Pelvis	AngVelz	+	0.050	0.485	1.021
Lumbar	AngVelz	+	0.050	0.485	1.021
Thorax	AngVelz	+	0.050	0.485	1.021
RightHand	AngVelz	+	0.050	0.485	1.021
RightForeArm	AngVelz	+	0.050	0.485	1.021
RightUpperArm	AngVelz	+	0.050	0.485	1.021
LeftHand	AngVelz	+	0.050	0.485	1.021
LeftForeArm	AngVelz	+	0.050	0.485	1.021
LeftUpperArm	AngVelz	+	0.050	0.485	1.021
Neck	AngVelz	+	0.050	0.485	1.021
Head	AngVelz	+	0.050	0.485	1.021
RightFoot	AngAcelx	+	1.101	11.758	24.832
RightShank	AngAcelx	+	1.101	11.758	24.832
RightThigh	AngAcelx	+	1.101	11.758	24.832
LeftFoot	AngAcelx	+	1.101	11.758	24.832

LeftShank	AngAcelx	+	1.101	11.758	24.832
LeftThigh	AngAcelx	+	1.101	11.758	24.832
Pelvis	AngAcelx	+	1.101	11.758	24.832
Lumbar	AngAcelx	+	1.101	11.758	24.832
Thorax	AngAcelx	+	1.101	11.758	24.832
RightHand	AngAcelx	+	1.101	11.758	24.832
RightForeArm	AngAcelx	+	1.101	11.758	24.832
RightUpperArm	AngAcelx	+	1.101	11.758	24.832
LeftHand	AngAcelx	+	1.101	11.758	24.832
LeftForeArm	AngAcelx	+	1.101	11.758	24.832
LeftUpperArm	AngAcelx	+	1.101	11.758	24.832
Neck	AngAcelx	+	1.101	11.758	24.832
Head	AngAcelx	+	1.101	11.758	24.832
RightFoot	AngAcely	+	1.101	11.758	24.832
RightShank	AngAcely	+	1.101	11.758	24.832
RightThigh	AngAcely	+	1.101	11.758	24.832
LeftFoot	AngAcely	+	1.101	11.758	24.832
LeftShank	AngAcely	+	1.101	11.758	24.832
LeftThigh	AngAcely	+	1.101	11.758	24.832
Pelvis	AngAcely	+	1.101	11.758	24.832
Lumbar	AngAcely	+	1.101	11.758	24.832
Thorax	AngAcely	+	1.101	11.758	24.832
RightHand	AngAcely	+	1.101	11.758	24.832
RightForeArm	AngAcely	+	1.101	11.758	24.832
RightUpperArm	AngAcely	+	1.101	11.758	24.832
LeftHand	AngAcely	+	1.101	11.758	24.832
LeftForeArm	AngAcely	+	1.101	11.758	24.832
LeftUpperArm	AngAcely	+	1.101	11.758	24.832
Neck	AngAcely	+	1.101	11.758	24.832
Head	AngAcely	+	1.101	11.758	24.832
RightFoot	AngAcelz	+	1.101	11.758	24.832
RightShank	AngAcelz	+	1.101	11.758	24.832
RightThigh	AngAcelz	+	1.101	11.758	24.832
LeftFoot	AngAcelz	+	1.101	11.758	24.832
LeftShank	AngAcelz	+	1.101	11.758	24.832
LeftThigh	AngAcelz	+	1.101	11.758	24.832
Pelvis	AngAcelz	+	1.101	11.758	24.832
Lumbar	AngAcelz	+	1.101	11.758	24.832
Thorax	AngAcelz	+	1.101	11.758	24.832
RightHand	AngAcelz	+	1.101	11.758	24.832
RightForeArm	AngAcelz	+	1.101	11.758	24.832
RightUpperArm	AngAcelz	+	1.101	11.758	24.832
LeftHand	AngAcelz	+	1.101	11.758	24.832
LeftForeArm	AngAcelz	+	1.101	11.758	24.832
LeftUpperArm	AngAcelz	+	1.101	11.758	24.832
Neck	AngAcelz	+	1.101	11.758	24.832
Head	AngAcelz	+	1.101	11.758	24.832
RightFoot	ProxMomentArmx	+	0.010	0.020	0.043
RightShank	ProxMomentArmx	+	0.014	0.024	0.047
RightThigh	ProxMomentArmx	+	0.019	0.031	0.058
LeftFoot	ProxMomentArmx	+	0.010	0.020	0.043
LeftShank	ProxMomentArmx	+	0.014	0.024	0.047
LeftThigh	ProxMomentArmx	+	0.019	0.031	0.058
Pelvis	ProxMomentArmx	+	0.009	0.396	0.047
Lumbar	ProxMomentArmx	+	0.009	0.024	0.053
Thorax	ProxMomentArmx	+	0.008	0.017	0.041
RightHand	ProxMomentArmx	+	0.011	0.023	0.049
RightForeArm	ProxMomentArmx	+	0.009	0.022	0.052
RightUpperArm	ProxMomentArmx	+	0.031	0.040	0.064

LeftHand	ProxMomentArm	+	0.011	0.023	0.049
LeftForeArm	ProxMomentArm	+	0.009	0.022	0.052
LeftUpperArm	ProxMomentArm	+	0.031	0.040	0.064
Neck	ProxMomentArm	+	0.011	0.023	0.049
Head	ProxMomentArm	+	0.011	0.023	0.049
RightFoot	ProxMomentArm	+	0.009	0.020	0.046
RightShank	ProxMomentArm	+	0.003	0.013	0.043
RightThigh	ProxMomentArm	+	0.018	0.037	0.071
LeftFoot	ProxMomentArm	+	0.009	0.020	0.046
LeftShank	ProxMomentArm	+	0.003	0.013	0.043
LeftThigh	ProxMomentArm	+	0.018	0.037	0.071
Pelvis	ProxMomentArm	+	0.006	0.018	0.149
Lumbar	ProxMomentArm	+	0.018	0.057	0.213
Thorax	ProxMomentArm	+	0.011	0.037	0.183
RightHand	ProxMomentArm	+	0.010	0.031	0.184
RightForeArm	ProxMomentArm	+	0.013	0.028	0.109
RightUpperArm	ProxMomentArm	+	0.030	0.045	0.100
LeftHand	ProxMomentArm	+	0.010	0.031	0.184
LeftForeArm	ProxMomentArm	+	0.013	0.028	0.109
LeftUpperArm	ProxMomentArm	+	0.030	0.045	0.100
Neck	ProxMomentArm	+	0.010	0.031	0.184
Head	ProxMomentArm	+	0.010	0.031	0.184
RightFoot	ProxMomentArmz	+	0.009	0.015	0.040
RightShank	ProxMomentArmz	+	0.017	0.026	0.053
RightThigh	ProxMomentArmz	+	0.017	0.031	0.060
LeftFoot	ProxMomentArmz	+	0.009	0.015	0.040
LeftShank	ProxMomentArmz	+	0.017	0.026	0.053
LeftThigh	ProxMomentArmz	+	0.017	0.031	0.060
Pelvis	ProxMomentArmz	+	0.011	0.019	0.050
Lumbar	ProxMomentArmz	+	0.010	0.019	0.048
Thorax	ProxMomentArmz	+	0.010	0.017	0.048
RightHand	ProxMomentArmz	+	0.011	0.020	0.049
RightForeArm	ProxMomentArmz	+	0.009	0.017	0.044
RightUpperArm	ProxMomentArmz	+	0.031	0.044	0.071
LeftHand	ProxMomentArmz	+	0.011	0.020	0.049
LeftForeArm	ProxMomentArmz	+	0.009	0.017	0.044
LeftUpperArm	ProxMomentArmz	+	0.031	0.044	0.071
Neck	ProxMomentArmz	+	0.011	0.020	0.049
Head	ProxMomentArmz	+	0.011	0.020	0.049
RightFoot	DistMomentArm	+	0.004	0.015	0.041
RightShank	DistMomentArm	+	0.010	0.020	0.043
RightThigh	DistMomentArm	+	0.004	0.012	0.034
LeftFoot	DistMomentArm	+	0.004	0.015	0.041
LeftShank	DistMomentArm	+	0.010	0.020	0.043
LeftThigh	DistMomentArm	+	0.004	0.012	0.034
Pelvis	DistMomentArm	+	0.009	0.016	0.035
Lumbar	DistMomentArm	+	0.008	0.016	0.039
Thorax	DistMomentArm	+	0.008	0.016	0.039
RightHand	DistMomentArm	+	0.008	0.016	0.039
RightForeArm	DistMomentArm	+	0.008	0.016	0.039
RightUpperArm	DistMomentArm	+	0.008	0.020	0.047
LeftHand	DistMomentArm	+	0.008	0.016	0.039
LeftForeArm	DistMomentArm	+	0.008	0.016	0.039
LeftUpperArm	DistMomentArm	+	0.008	0.020	0.047
Neck	DistMomentArm	+	0.008	0.016	0.039
Head	DistMomentArm	+	0.008	0.016	0.039
RightFoot	DistMomentArm	+	0.001	0.008	0.030
RightShank	DistMomentArm	+	0.009	0.020	0.046
RightThigh	DistMomentArm	+	0.001	0.008	0.031

APPENDIX E: Complete list of inaccuracy values for sets 1, 2 and 3

LeftFoot	DistMomentArmy	+	0.001	0.008	0.030
LeftShank	DistMomentArmy	+	0.009	0.020	0.046
LeftThigh	DistMomentArmy	+	0.001	0.008	0.031
Pelvis	DistMomentArmy	+	0.008	0.021	0.049
Lumbar	DistMomentArmy	+	0.005	0.016	0.146
Thorax	DistMomentArmy	+	0.005	0.016	0.146
RightHand	DistMomentArmy	+	0.008	0.017	0.144
RightForeArm	DistMomentArmy	+	0.005	0.016	0.146
RightUpperArm	DistMomentArmy	+	0.003	0.015	0.042
LeftHand	DistMomentArmy	+	0.008	0.017	0.144
LeftForeArm	DistMomentArmy	+	0.005	0.016	0.146
LeftUpperArm	DistMomentArmy	+	0.003	0.015	0.042
Neck	DistMomentArmy	+	0.008	0.017	0.144
Head	DistMomentArmy	+	0.008	0.017	0.144
RightFoot	DistMomentArmz	+	0.002	0.017	0.051
RightShank	DistMomentArmz	+	0.009	0.015	0.040
RightThigh	DistMomentArmz	+	0.008	0.015	0.040
LeftFoot	DistMomentArmz	+	0.002	0.017	0.051
LeftShank	DistMomentArmz	+	0.009	0.015	0.040
LeftThigh	DistMomentArmz	+	0.008	0.015	0.040
Pelvis	DistMomentArmz	+	0.007	0.015	0.037
Lumbar	DistMomentArmz	+	0.008	0.015	0.040
Thorax	DistMomentArmz	+	0.008	0.015	0.040
RightHand	DistMomentArmz	+	0.010	0.015	0.037
RightForeArm	DistMomentArmz	+	0.008	0.015	0.040
RightUpperArm	DistMomentArmz	+	0.008	0.015	0.040
LeftHand	DistMomentArmz	+	0.010	0.015	0.037
LeftForeArm	DistMomentArmz	+	0.008	0.015	0.040
LeftUpperArm	DistMomentArmz	+	0.008	0.015	0.040
Neck	DistMomentArmz	+	0.010	0.015	0.037
Head	DistMomentArmz	+	0.010	0.015	0.037
LeftFoot	LeftGRFx	+	0.500	2.300	8.500
LeftFoot	LeftGRFy	+	0.400	2.500	9.100
LeftFoot	LeftGRFz	+	1.700	4.900	10.900
RightFoot	RightGRFx	+	0.500	2.300	8.500
RightFoot	RightGRFy	+	0.400	2.500	9.100
RightFoot	RightGRFz	+	1.700	4.900	10.900

Units were as follows; segment mass (%), segment moment of inertia (MOI) (%), COM linear acceleration ( $m/s^2$ ), angular velocity (rad/s), angular acceleration ( $rad/s^2$ ), proximal and distal moment arm (m), ground reaction force (GRF) (N).

## APPENDIX F: Uncertainty results tables for inaccuracy sets 2 and 3

Table 53 Mean joint moment estimates and uncertainty estimates for three sets of perturbations for top down model. Results represent the mean of all participants and swings. Moments have been normalised by body weight and height.

Segment	Backswing						Downswing															
	Mean JM±SD		Mean uncertainty ±SD		Set 3		Mean JM±SD		Mean uncertainty ±SD		Set 3											
	Set 1	Set 2	Set 1	Set 2	Set 1	Set 2	Set 1	Set 2	Set 1	Set 2	Set 1	Set 2										
<b>Left wrist</b>																						
lateral bending	0.06	0.016	0.01	±	0.002	0.02	±	0.003	0.07	±	0.012	-0.66	0.210	0.05	±	0.012	0.11	±	0.030	0.62	±	0.187
axial rotation	0.07	0.031	0.01	±	0.001	0.01	±	0.002	0.02	±	0.005	-0.05	0.100	0.04	±	0.011	0.07	±	0.022	0.17	±	0.050
flexion extension	-0.07	0.037	0.01	±	0.002	0.02	±	0.004	0.06	±	0.016	0.02	0.100	0.04	±	0.007	0.08	±	0.015	0.22	±	0.058
<b>Right wrist</b>																						
lateral bending	-0.04	0.019	0.01	±	0.002	0.02	±	0.003	0.06	±	0.011	0.51	0.200	0.05	±	0.016	0.09	±	0.032	0.46	±	0.170
axial rotation	0.06	0.017	0.01	±	0.001	0.01	±	0.001	0.02	±	0.003	0.07	0.130	0.04	±	0.007	0.07	±	0.013	0.17	±	0.031
flexion extension	0.06	0.015	0.01	±	0.002	0.02	±	0.004	0.07	±	0.014	-0.44	0.140	0.05	±	0.009	0.10	±	0.018	0.49	±	0.101
<b>Left elbow</b>																						
lateral bending	0.18	0.034	0.02	±	0.003	0.06	±	0.008	0.17	±	0.024	-1.15	0.370	0.09	±	0.024	0.19	±	0.049	0.78	±	0.222
axial rotation	0.02	0.02	0.01	±	0.002	0.03	±	0.004	0.07	±	0.010	-0.05	0.100	0.05	±	0.014	0.11	±	0.031	0.30	±	0.123
flexion extension	-0.08	0.053	0.02	±	0.003	0.06	±	0.009	0.12	±	0.018	-0.59	0.180	0.07	±	0.019	0.18	±	0.045	0.52	±	0.130
<b>Right elbow</b>																						
lateral bending	-0.12	0.027	0.02	±	0.003	0.05	±	0.008	0.13	±	0.017	0.12	0.380	0.05	±	0.012	0.11	±	0.026	0.43	±	0.111
axial rotation	0.01	0.023	0.01	±	0.001	0.02	±	0.003	0.06	±	0.006	0.3	0.100	0.08	±	0.018	0.16	±	0.034	0.47	±	0.113
flexion extension	-0.02	0.037	0.02	±	0.003	0.06	±	0.008	0.15	±	0.020	-1.85	0.470	0.09	±	0.021	0.21	±	0.044	0.98	±	0.190
<b>Left shoulder</b>																						
lateral bending	-0.05	0.105	0.08	±	0.017	0.18	±	0.032	0.28	±	0.051	0.87	0.510	0.27	±	0.090	0.46	±	0.146	0.87	±	0.274
axial rotation	0.08	0.034	0.05	±	0.010	0.08	±	0.013	0.15	±	0.021	-0.48	0.200	0.19	±	0.059	0.28	±	0.084	0.59	±	0.165
flexion extension	0.37	0.081	0.09	±	0.016	0.18	±	0.031	0.32	±	0.047	-1.57	0.500	0.27	±	0.095	0.44	±	0.141	1.06	±	0.320
<b>Right shoulder</b>																						
lateral bending	0.04	0.071	0.09	±	0.014	0.17	±	0.031	0.29	±	0.045	-1.88	0.550	0.26	±	0.063	0.43	±	0.099	0.99	±	0.227
axial rotation	-0.05	0.018	0.04	±	0.004	0.07	±	0.006	0.14	±	0.016	-1.85	0.470	0.26	±	0.057	0.40	±	0.083	1.11	±	0.223
flexion extension	0.02	0.054	0.09	±	0.013	0.17	±	0.029	0.29	±	0.040	0.18	0.260	0.17	±	0.038	0.27	±	0.056	0.62	±	0.099
<b>Upper trunk</b>																						
lateral bending	0.72	0.162	0.21	±	0.031	0.78	±	0.133	1.91	±	0.191	1.79	0.730	0.40	±	0.077	1.05	±	0.170	3.23	±	0.594
axial rotation	-0.38	0.176	0.20	±	0.042	0.46	±	0.073	1.02	±	0.170	5.81	1.340	0.49	±	0.119	0.86	±	0.176	2.14	±	0.436
flexion extension	2.45	0.667	0.25	±	0.044	0.90	±	0.171	2.96	±	0.694	1.39	0.890	0.42	±	0.101	1.12	±	0.208	3.73	±	0.828

Table 54 Mean joint moment estimates and uncertainty estimates for three sets of perturbations for bottom up model. Results represent the mean of all participants and swings. Moments have been normalised by body weight and height.

Segment	Mean uncertainty (normalised Nm/(BW x height) x 100%)																					
	Backswinging			Downswinging			Set 1			Set 2			Set 3									
	Mean JM	Set 1	Set 2	Set 1	Set 2	Set 3	Mean JM	Set 1	Set 2	Set 1	Set 2	Set 3	Mean JM	Set 1	Set 2	Set 3						
<b>Right ankle</b>																						
lateral bending	0.96	0.504	0.20	±	0.049	0.48	±	0.117	1.34	±	0.323	0.88	0.674	0.12	±	0.048	0.28	±	0.112	0.77	±	0.319
axial rotation	-0.22	0.750	0.34	±	0.069	0.80	±	0.162	2.28	±	0.448	0.04	0.594	0.26	±	0.076	0.62	±	0.181	1.75	±	0.512
flexion extension	-2.04	0.613	0.38	±	0.068	0.88	±	0.158	2.22	±	0.398	-3.88	0.793	0.26	±	0.078	0.61	±	0.183	1.57	±	0.465
<b>Left ankle</b>																						
lateral bending	0.07	0.299	0.10	±	0.019	0.23	±	0.043	0.64	±	0.121	0.23	1.145	0.32	±	0.079	0.76	±	0.187	2.14	±	0.527
axial rotation	-0.30	0.491	0.14	±	0.034	0.35	±	0.082	0.97	±	0.237	-2.12	1.080	0.26	±	0.093	0.61	±	0.220	1.68	±	0.611
flexion extension	-0.63	0.614	0.15	±	0.038	0.36	±	0.089	0.91	±	0.226	-2.01	0.980	0.39	±	0.105	0.90	±	0.241	2.22	±	0.596
<b>Right knee</b>																						
lateral bending	0.93	0.861	0.81	±	0.160	1.43	±	0.272	3.57	±	0.678	0.14	0.927	0.58	±	0.181	1.05	±	0.305	2.60	±	0.770
axial rotation	-0.31	0.410	0.21	±	0.068	0.38	±	0.119	0.93	±	0.295	0.19	0.561	0.13	±	0.045	0.24	±	0.082	0.57	±	0.202
flexion extension	1.33	1.754	0.75	±	0.147	1.49	±	0.284	3.35	±	0.645	-3.42	0.957	0.53	±	0.165	1.06	±	0.314	2.39	±	0.708
<b>Left knee</b>																						
lateral bending	-0.52	0.839	0.33	±	0.076	0.65	±	0.126	1.55	±	0.321	-3.40	0.979	0.69	±	0.211	1.24	±	0.350	3.06	±	0.893
axial rotation	-0.19	0.240	0.10	±	0.040	0.19	±	0.073	0.46	±	0.177	-0.40	0.922	0.49	±	0.127	0.86	±	0.218	2.14	±	0.536
flexion extension	0.75	0.676	0.30	±	0.071	0.65	±	0.136	1.46	±	0.305	6.45	2.470	0.71	±	0.207	1.48	±	0.401	3.41	±	0.933
<b>Right hip</b>																						
lateral bending	0.33	1.502	0.98	±	0.190	1.93	±	0.321	4.32	±	0.768	0.83	2.358	0.61	±	0.225	1.38	±	0.366	2.92	±	0.903
axial rotation	-0.14	0.650	0.30	±	0.175	0.55	±	0.310	1.30	±	0.740	0.10	0.608	0.36	±	0.098	0.65	±	0.176	1.51	±	0.405
flexion extension	-3.83	1.936	0.96	±	0.194	1.99	±	0.351	4.17	±	0.784	-9.17	1.826	0.65	±	0.197	1.50	±	0.364	3.06	±	0.805
<b>Left hip</b>																						
lateral bending	0.13	0.909	0.38	±	0.097	1.10	±	0.174	2.10	±	0.390	0.31	1.638	1.01	±	0.283	2.03	±	0.455	4.51	±	1.136
axial rotation	0.09	0.335	0.15	±	0.040	0.32	±	0.082	0.70	±	0.198	0.09	0.998	0.26	±	0.063	0.52	±	0.116	1.14	±	0.273
flexion extension	-1.14	0.498	0.37	±	0.091	1.09	±	0.182	2.05	±	0.361	4.71	1.166	0.93	±	0.266	2.00	±	0.469	4.27	±	1.084
<b>Pelvis</b>																						
lateral bending	0.76	0.385	1.12	±	0.219	2.56	±	0.422	5.40	±	0.952	-1.52	1.274	1.30	±	0.279	2.89	±	0.536	6.31	±	1.271
axial rotation	0.82	0.171	0.50	±	0.136	1.31	±	0.306	2.47	±	0.584	-4.15	1.401	0.64	±	0.200	1.53	±	0.513	2.96	±	0.858
flexion extension	-2.45	0.825	1.12	±	0.220	2.90	±	0.854	5.42	±	1.001	-2.21	0.547	1.25	±	0.241	3.21	±	1.113	5.98	±	1.161
<b>Mid trunk</b>																						
lateral bending	1.00	0.650	1.16	±	0.256	3.02	±	0.502	6.03	±	1.136	-1.38	1.003	1.35	±	0.327	3.39	±	0.677	7.21	±	1.554
axial rotation	0.66	0.386	0.54	±	0.084	1.38	±	0.220	2.68	±	0.401	-4.49	1.176	0.66	±	0.144	1.61	±	0.417	3.15	±	0.660
flexion extension	-1.35	0.923	1.16	±	0.228	3.30	±	0.850	6.29	±	1.075	-1.28	1.102	1.32	±	0.256	3.70	±	1.099	6.99	±	1.208

Table 55 Maximum joint moment estimates and uncertainty estimates for three sets of perturbations for top down model. Results represent the mean of all participants and swings. Moments have been normalised by body weight and height.

Segment	Max Uncertainty (normalised Nm/(BW x height) x 100%)																					
	Max JM	Backswing			Set 1			Set 2			Set 3			Downswing	Max JM							
		Set 1	Set 2	Set 3	Set 1	Set 2	Set 3	Set 1	Set 2	Set 3	Set 1	Set 2	Set 3									
<b>Left wrist</b>																						
lateral bending	0.57	0.135	0.02	±	0.003	0.03	±	0.006	0.15	±	0.038	1.19	0.542	0.18	±	0.047	0.37	±	0.116	1.93	±	0.731
axial rotation	0.27	0.088	0.01	±	0.002	0.02	±	0.005	0.04	±	0.010	0.61	0.302	0.11	±	0.043	0.22	±	0.086	0.51	±	0.193
flexion extension	0.25	0.093	0.01	±	0.003	0.03	±	0.006	0.10	±	0.030	0.53	0.242	0.14	±	0.030	0.29	±	0.059	0.80	±	0.179
<b>Right wrist</b>																						
lateral bending	0.45	0.149	0.02	±	0.003	0.03	±	0.006	0.16	±	0.037	0.93	0.431	0.17	±	0.060	0.32	±	0.119	1.39	±	0.641
axial rotation	0.28	0.049	0.01	±	0.002	0.02	±	0.004	0.05	±	0.009	0.97	0.370	0.13	±	0.031	0.23	±	0.056	0.55	±	0.133
flexion extension	0.31	0.071	0.01	±	0.003	0.03	±	0.005	0.12	±	0.025	1.20	0.401	0.17	±	0.040	0.39	±	0.085	1.73	±	0.472
<b>Left elbow</b>																						
lateral bending	0.79	0.140	0.03	±	0.004	0.08	±	0.009	0.24	±	0.038	1.93	0.579	0.25	±	0.060	0.50	±	0.133	2.01	±	0.671
axial rotation	0.18	0.039	0.02	±	0.003	0.04	±	0.007	0.10	±	0.019	0.70	0.316	0.12	±	0.036	0.24	±	0.075	0.79	±	0.430
flexion extension	0.45	0.103	0.03	±	0.004	0.07	±	0.011	0.17	±	0.034	1.07	0.344	0.24	±	0.056	0.52	±	0.123	1.54	±	0.352
<b>Right elbow</b>																						
lateral bending	0.36	0.067	0.03	±	0.004	0.07	±	0.010	0.19	±	0.030	1.37	0.701	0.16	±	0.042	0.32	±	0.086	1.18	±	0.426
axial rotation	0.4	0.033	0.02	±	0.002	0.04	±	0.005	0.13	±	0.022	1.05	0.496	0.25	±	0.059	0.47	±	0.109	1.57	±	0.490
flexion extension	0.57	0.161	0.03	±	0.004	0.08	±	0.011	0.24	±	0.032	5.18	1.308	0.29	±	0.066	0.65	±	0.142	3.00	±	0.665
<b>Left shoulder</b>																						
lateral bending	0.42	0.117	0.13	±	0.024	0.23	±	0.038	0.38	±	0.068	3.46	0.898	0.73	±	0.234	1.13	±	0.358	2.28	±	0.649
axial rotation	0.43	0.139	0.08	±	0.013	0.13	±	0.019	0.23	±	0.039	1.01	0.286	0.54	±	0.178	0.78	±	0.249	1.50	±	0.470
flexion extension	1.15	0.157	0.14	±	0.022	0.24	±	0.036	0.44	±	0.054	3.07	0.769	0.66	±	0.226	0.98	±	0.325	2.54	±	0.785
<b>Right shoulder</b>																						
lateral bending	0.56	0.239	0.13	±	0.020	0.23	±	0.037	0.38	±	0.057	5.11	1.596	0.69	±	0.110	1.12	±	0.180	3.04	±	0.619
axial rotation	0.55	0.179	0.09	±	0.022	0.14	±	0.033	0.28	±	0.059	4.82	1.255	0.60	±	0.113	0.95	±	0.194	2.86	±	0.641
flexion extension	0.48	0.104	0.13	±	0.020	0.22	±	0.034	0.41	±	0.051	2.73	0.827	0.45	±	0.112	0.68	±	0.164	1.63	±	0.349
<b>Upper trunk</b>																						
lateral bending	1.95	0.534	0.25	±	0.028	0.85	±	0.129	2.66	±	0.355	4.91	1.371	0.77	±	0.147	1.61	±	0.326	6.00	±	1.744
axial rotation	3.01	0.697	0.26	±	0.055	0.53	±	0.090	1.21	±	0.210	8.94	1.886	1.04	±	0.228	1.70	±	0.330	4.73	±	0.959
flexion extension	3.7	0.747	0.31	±	0.051	1.03	±	0.176	3.93	±	0.762	4.94	1.502	0.97	±	0.250	2.02	±	0.417	8.17	±	1.544



Table 57 Percentage contribution relative to peak JM for three sets of perturbations for top down model

Segment	% contribution								
	Backswing			Downswing					
	Set 1	Set 2	Set 3	Set 1	Set 2	Set 3	Set 1	Set 2	Set 3
<b>Left wrist</b>									
lateral bending	2.7 ± 0.31	5.1 ± 0.70	27.2 ± 3.84	16.6 ± 3.84	4.67 ± 33.5	9.61 ± 174.4	16.6 ± 3.84	4.67 ± 33.5	9.61 ± 174.4
axial rotation	3.8 ± 1.08	7.6 ± 2.21	16.7 ± 5.08	22.0 ± 5.08	9.28 ± 44.1	18.92 ± 103.0	22.0 ± 5.08	9.28 ± 44.1	18.92 ± 103.0
flexion extension	5.8 ± 0.99	12.1 ± 1.90	40.5 ± 5.80	33.8 ± 5.80	17.68 ± 69.6	35.95 ± 200.4	33.8 ± 5.80	17.68 ± 69.6	35.95 ± 200.4
<b>Right wrist</b>									
lateral bending	3.6 ± 0.98	6.7 ± 1.71	37.1 ± 9.54	20.3 ± 9.54	5.86 ± 37.7	10.98 ± 156.4	20.3 ± 9.54	5.86 ± 37.7	10.98 ± 156.4
axial rotation	3.8 ± 0.77	7.3 ± 1.72	16.7 ± 3.60	14.8 ± 3.60	5.12 ± 26.3	8.38 ± 63.4	14.8 ± 3.60	5.12 ± 26.3	8.38 ± 63.4
flexion extension	4.8 ± 0.45	10.0 ± 1.05	40.9 ± 9.90	15.2 ± 9.90	2.72 ± 34.2	6.08 ± 154.7	15.2 ± 9.90	2.72 ± 34.2	6.08 ± 154.7
<b>Left elbow</b>									
lateral bending	4.1 ± 0.47	9.7 ± 1.33	30.6 ± 3.47	13.4 ± 3.47	1.65 ± 26.2	3.03 ± 104.2	13.4 ± 3.47	1.65 ± 26.2	3.03 ± 104.2
axial rotation	10.7 ± 3.12	24.7 ± 6.86	60.8 ± 17.25	19.0 ± 17.25	5.44 ± 39.2	10.85 ± 119.9	19.0 ± 17.25	5.44 ± 39.2	10.85 ± 119.9
flexion extension	5.9 ± 0.79	16.9 ± 3.20	39.0 ± 5.96	23.7 ± 5.96	8.24 ± 53.0	18.50 ± 157.7	23.7 ± 5.96	8.24 ± 53.0	18.50 ± 157.7
<b>Right elbow</b>									
lateral bending	7.6 ± 1.02	18.6 ± 2.39	54.4 ± 5.02	13.9 ± 5.02	5.10 ± 26.8	8.97 ± 95.9	13.9 ± 5.02	5.10 ± 26.8	8.97 ± 95.9
axial rotation	5.3 ± 0.81	10.8 ± 1.58	31.7 ± 5.16	27.4 ± 5.16	8.83 ± 52.1	18.55 ± 181.2	27.4 ± 5.16	8.83 ± 52.1	18.55 ± 181.2
flexion extension	5.4 ± 1.08	14.7 ± 3.43	46.5 ± 10.81	5.7 ± 10.81	0.26 ± 12.7	0.57 ± 58.7	5.7 ± 10.81	0.26 ± 12.7	0.57 ± 58.7
<b>Left shoulder</b>									
lateral bending	32.2 ± 7.55	57.7 ± 13.37	95.3 ± 21.52	20.9 ± 21.52	3.19 ± 32.3	4.74 ± 66.0	20.9 ± 21.52	3.19 ± 32.3	4.74 ± 66.0
axial rotation	21.2 ± 6.08	31.5 ± 8.83	55.9 ± 13.35	54.7 ± 13.35	13.71 ± 80.1	19.44 ± 152.8	54.7 ± 13.35	13.71 ± 80.1	19.44 ± 152.8
flexion extension	12.5 ± 1.16	20.9 ± 2.20	39.0 ± 3.73	21.3 ± 3.73	4.32 ± 31.7	6.43 ± 82.3	21.3 ± 3.73	4.32 ± 31.7	6.43 ± 82.3
<b>Right shoulder</b>									
lateral bending	26.8 ± 8.80	46.2 ± 14.26	78.5 ± 24.57	14.3 ± 24.57	3.05 ± 23.2	4.50 ± 62.0	14.3 ± 24.57	3.05 ± 23.2	4.50 ± 62.0
axial rotation	19.1 ± 5.84	29.1 ± 8.50	57.5 ± 16.58	12.7 ± 16.58	1.38 ± 20.0	1.61 ± 60.4	12.7 ± 16.58	1.38 ± 20.0	1.61 ± 60.4
flexion extension	27.7 ± 6.96	46.7 ± 12.20	89.1 ± 21.58	17.0 ± 21.58	3.58 ± 25.7	5.22 ± 62.1	17.0 ± 21.58	3.58 ± 25.7	5.22 ± 62.1
<b>Upper trunk</b>									
lateral bending	13.3 ± 2.70	46.2 ± 10.14	145.5 ± 37.18	16.2 ± 37.18	3.04 ± 33.8	6.24 ± 125.0	16.2 ± 37.18	3.04 ± 33.8	6.24 ± 125.0
axial rotation	8.8 ± 1.77	18.1 ± 3.15	41.4 ± 7.56	11.7 ± 7.56	1.22 ± 19.2	2.09 ± 53.5	11.7 ± 7.56	1.22 ± 19.2	2.09 ± 53.5
flexion extension	8.5 ± 0.79	28.1 ± 1.73	106.9 ± 11.78	21.2 ± 11.78	5.29 ± 44.7	11.82 ± 181.6	21.2 ± 11.78	5.29 ± 44.7	11.82 ± 181.6



Table 59 Effect of uncertainty on the timing of peak joint moments for the top down model

Segment	Time differences to absolute peak joint moment (ms)								
	Backswing			Downswing					
	Set 1	Set 2	Set 3	Set 1	Set 2	Set 3	Set 1	Set 2	Set 3
<b>Left wrist</b>									
lateral bending	35.4 ±	65.6 ±	109.2 ±	159.0 ±	0.9 ±	15.0 ±	49.7 ±	70.3 ±	33.5 ±
axial rotation	-3.8 ±	10.8 ±	12.7 ±	12.7 ±	-7.6 ±	45.8 ±	46.3 ±	-3.1 ±	46.3 ±
flexion extension	0.0 ±	0.0 ±	17.7 ±	220.1 ±	0.5 ±	14.0 ±	14.5 ±	-5.4 ±	10.7 ±
<b>Right wrist</b>									
lateral bending	-17.5 ±	47.9 ±	47.9 ±	96.3 ±	4.7 ±	13.3 ±	3.9 ±	-29.2 ±	28.5 ±
axial rotation	0.0 ±	0.0 ±	0.0 ±	98.6 ±	-0.3 ±	0.6 ±	2.3 ±	50.2 ±	61.1 ±
flexion extension	0.0 ±	0.0 ±	73.2 ±	128.5 ±	5.7 ±	13.2 ±	15.3 ±	-6.8 ±	23.0 ±
<b>Left elbow</b>									
lateral bending	50.2 ±	92.9 ±	210.0 ±	246.0 ±	4.2 ±	11.2 ±	27.6 ±	-83.5 ±	35.6 ±
axial rotation	47.4 ±	113.2 ±	127.1 ±	195.5 ±	-1.4 ±	45.5 ±	42.5 ±	-4.9 ±	45.9 ±
flexion extension	-0.2 ±	0.5 ±	40.8 ±	207.7 ±	-6.4 ±	35.6 ±	59.2 ±	-59.0 ±	57.1 ±
<b>Right elbow</b>									
lateral bending	-76.6 ±	166.5 ±	225.6 ±	111.0 ±	-8.0 ±	21.0 ±	20.9 ±	-12.7 ±	32.1 ±
axial rotation	-0.9 ±	2.0 ±	12.1 ±	13.1 ±	12.2 ±	19.5 ±	49.8 ±	13.7 ±	76.0 ±
flexion extension	25.3 ±	86.6 ±	154.2 ±	234.8 ±	0.0 ±	0.0 ±	0.0 ±	0.5 ±	1.5 ±
<b>Left shoulder</b>									
lateral bending	51.0 ±	119.4 ±	282.9 ±	356.4 ±	0.2 ±	0.5 ±	0.5 ±	-0.5 ±	2.7 ±
axial rotation	120.5 ±	201.4 ±	223.6 ±	249.2 ±	7.5 ±	58.6 ±	52.9 ±	-47.2 ±	60.1 ±
flexion extension	83.5 ±	126.3 ±	160.5 ±	156.1 ±	-18.4 ±	43.5 ±	47.7 ±	-81.3 ±	38.1 ±
<b>Right shoulder</b>									
lateral bending	60.2 ±	131.6 ±	212.9 ±	183.1 ±	0.9 ±	2.0 ±	2.0 ±	8.7 ±	8.3 ±
axial rotation	174.0 ±	224.8 ±	217.2 ±	120.1 ±	0.0 ±	0.0 ±	0.0 ±	-0.3 ±	0.6 ±
flexion extension	-109.0 ±	156.9 ±	155.6 ±	171.2 ±	0.0 ±	0.0 ±	0.0 ±	0.2 ±	0.5 ±
<b>Upper trunk</b>									
lateral bending	-5.2 ±	9.9 ±	9.8 ±	73.0 ±	32.3 ±	55.8 ±	55.6 ±	38.4 ±	61.3 ±
axial rotation	-59.9 ±	119.7 ±	119.7 ±	119.7 ±	-10.6 ±	29.4 ±	29.4 ±	-15.8 ±	29.3 ±
flexion extension	-12.2 ±	27.0 ±	27.0 ±	53.1 ±	-7.8 ±	23.4 ±	23.6 ±	-8.0 ±	21.1 ±

Table 60 Effect of uncertainty on the timing of peak joint moments for the bottom up model

Segment	Time difference to absolute peak joint moment (ms)													
	Backswing				Downswing									
	Set 1	Set 2	Set 3		Set 1	Set 2	Set 3		Set 1	Set 2	Set 3			
<b>Right ankle</b>														
lateral bending	17.2	± 35.4	19.3	± 38.7	81.9	± 123.2	6.9	± 29.1	6.9	± 29.1	6.9	± 29.1	36.6	± 75.5
axial rotation	94.6	± 132.0	98.6	± 146.1	213.5	± 111.4	-24.0	± 70.4	-24.0	± 70.4	-24.0	± 70.4	-75.9	± 128.4
flexion extension	-26.0	± 163.5	-31.4	± 163.8	-40.5	± 338.1	2.6	± 6.4	2.6	± 6.4	2.6	± 6.4	-9.9	± 41.4
<b>Left ankle</b>														
lateral bending	-39.1	± 76.5	-128.8	± 251.7	-109.5	± 246.1	11.8	± 45.0	11.8	± 45.0	23.3	± 85.2	59.5	± 97.5
axial rotation	16.8	± 200.8	42.7	± 369.8	285.6	± 553.4	1.4	± 3.3	1.4	± 3.3	-1.0	± 18.8	-9.7	± 54.4
flexion extension	-41.5	± 66.0	-99.7	± 145.7	-162.0	± 322.5	-1.9	± 2.1	-1.9	± 2.1	9.7	± 37.7	-10.2	± 27.5
<b>Right knee</b>														
lateral bending	169.4	± 275.1	139.6	± 251.0	65.6	± 239.1	-22.2	± 44.0	-22.2	± 44.0	-28.0	± 63.7	-22.9	± 65.8
axial rotation	19.3	± 140.2	63.9	± 188.8	230.2	± 266.0	-13.2	± 36.8	-13.2	± 36.8	-16.7	± 37.3	-32.8	± 67.9
flexion extension	80.6	± 189.4	63.2	± 195.1	125.9	± 219.3	-5.7	± 14.6	-5.7	± 14.6	-10.4	± 18.1	-30.2	± 49.1
<b>Left knee</b>														
lateral bending	91.3	± 258.3	91.3	± 258.3	521.9	± 287.8	8.9	± 28.5	8.9	± 28.5	-12.0	± 65.9	-97.4	± 101.2
axial rotation	127.8	± 298.7	127.8	± 298.7	289.2	± 531.2	-26.2	± 51.6	-26.2	± 51.6	-58.9	± 66.2	-39.4	± 68.7
flexion extension	46.4	± 95.7	46.4	± 95.7	142.5	± 216.1	-1.0	± 1.2	-1.0	± 1.2	-3.1	± 4.0	-9.5	± 10.9
<b>Right hip</b>														
lateral bending	176.6	± 193.1	245.8	± 270.5	258.9	± 237.0	2.4	± 6.9	2.4	± 6.9	3.3	± 9.3	-15.1	± 65.0
axial rotation	-57.8	± 97.3	-80.2	± 132.6	-86.8	± 155.3	68.6	± 85.5	68.6	± 85.5	71.0	± 86.5	87.7	± 82.4
flexion extension	-17.4	± 34.2	9.0	± 61.8	295.1	± 304.7	1.2	± 2.6	1.2	± 2.6	1.2	± 2.6	3.6	± 10.2
<b>Left hip</b>														
lateral bending	64.8	± 183.8	234.2	± 374.7	284.4	± 405.2	-17.5	± 34.9	-17.5	± 34.9	-32.3	± 48.8	-31.1	± 80.5
axial rotation	90.6	± 181.9	210.6	± 236.3	240.3	± 242.2	-8.9	± 37.9	-8.9	± 37.9	-48.3	± 62.0	-71.4	± 88.8
flexion extension	-116.7	± 168.4	-195.8	± 298.8	-197.2	± 301.2	-1.6	± 2.6	-1.6	± 2.6	-1.9	± 2.5	-18.2	± 11.5
<b>Pelvis</b>														
lateral bending	182.1	± 173.3	172.9	± 208.9	150.9	± 164.7	-10.6	± 19.9	-10.6	± 19.9	-35.8	± 45.3	-24.5	± 50.3
axial rotation	114.4	± 166.5	139.1	± 216.7	131.3	± 200.3	-0.5	± 5.7	-0.5	± 5.7	-1.9	± 6.8	-18.1	± 26.3
flexion extension	-95.1	± 148.3	-296.9	± 153.2	-337.2	± 101.6	3.6	± 9.8	3.6	± 9.8	32.8	± 52.8	71.0	± 47.1
<b>Mid trunk</b>														
lateral bending	10.9	± 76.4	61.1	± 151.1	30.4	± 198.0	-19.1	± 25.9	-19.1	± 25.9	-32.6	± 58.7	-32.5	± 62.7
axial rotation	158.7	± 181.8	229.5	± 277.9	204.2	± 283.8	0.0	± 0.0	0.0	± 0.0	-0.2	± 0.5	-2.1	± 20.1
flexion extension	-184.5	± 164.5	-241.1	± 159.0	-93.6	± 249.6	25.9	± 54.8	25.9	± 54.8	47.2	± 54.0	47.4	± 54.0

APPENDIX G: Uncertainty figures for inaccuracy sets 2 and 3

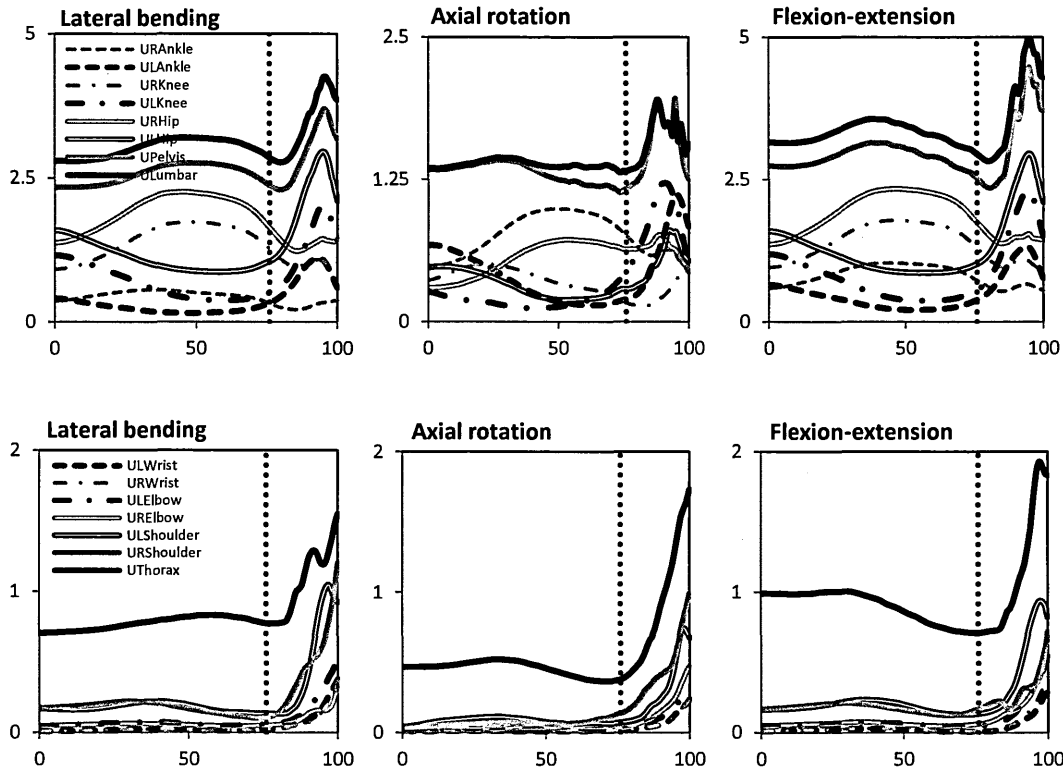


Figure 59 Set 2 uncertainty at each joint

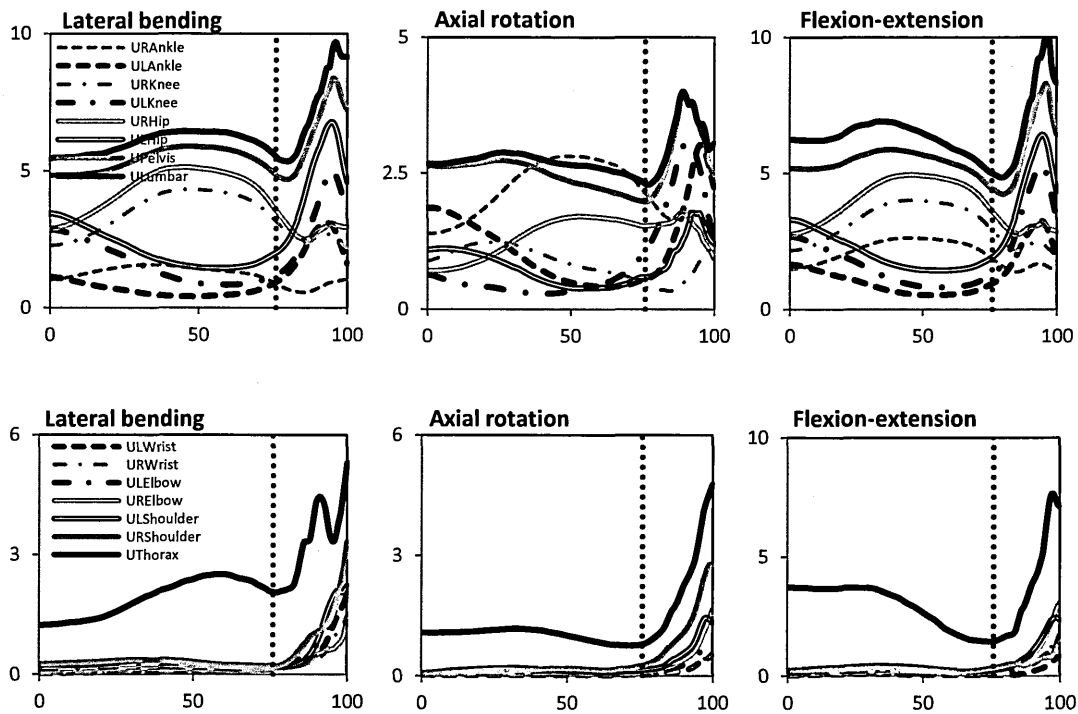


Figure 60 Set 3 uncertainty at each joint

## APPENDIX H: Top five most influential parameters tables

Table 61 Top five most influential parameters that contributed to the total uncertainty at the upper trunk joint

Upper trunk Uncertainties			Lateral bending			Axial rotation			Flexion-extension		
Segment	Parameter	Direction	Segment	Parameter	Direction	Segment	Parameter	Direction	Segment	Parameter	Direction
<b>Set 1</b>											
<b>Backswing</b>											
1	Upper trunk	Prox moment arm	z	Upper trunk	Prox moment arm	z	Upper trunk	ProxMomentArm	Upper trunk	ProxMomentArm	y
2	Upper trunk	Prox moment arm	y	Left shoulder	Prox moment arm	x	Upper trunk	ProxMomentArm	Upper trunk	ProxMomentArm	x
3	Upper trunk	Dist moment arm	z	Upper trunk	Prox moment arm	x	Left shoulder	ProxMomentArm	Left shoulder	ProxMomentArm	z
4	Left shoulder	Prox moment arm	x	Upper trunk	Dist moment arm	z	Right shoulder	ProxMomentArm	Right shoulder	ProxMomentArm	z
5	Right shoulder	Prox moment arm	x	Right shoulder	Prox moment arm	z	Upper trunk	DistMomentArm	Upper trunk	DistMomentArm	x
<b>Downswing</b>											
1	Right shoulder	ProxMomentArm	y	Left shoulder	ProxMomentArm	x	Left shoulder	ProxMomentArm	Left shoulder	ProxMomentArm	z
2	Upper trunk	ProxMomentArm	z	Right shoulder	ProxMomentArm	x	Upper trunk	ProxMomentArm	Upper trunk	ProxMomentArm	y
3	Left shoulder	ProxMomentArm	z	Upper trunk	ProxMomentArm	z	Right shoulder	ProxMomentArm	Right shoulder	ProxMomentArm	x
4	Upper trunk	ProxMomentArm	y	Right shoulder	ProxMomentArm	y	Left shoulder	ProxMomentArm	Left shoulder	ProxMomentArm	y
5	Right shoulder	ProxMomentArm	z	Left shoulder	ProxMomentArm	y	Upper trunk	ProxMomentArm	Upper trunk	ProxMomentArm	x
<b>Set 2</b>											
<b>Backswing</b>											
1	Upper trunk	COM acceleration	z	Upper trunk	ProxMomentArm	z	Upper trunk	ProxMomentArm	Upper trunk	ProxMomentArm	y
2	Upper trunk	Prox moment arm	z	Upper trunk	AngAcc	y	Upper trunk	COMacc	Upper trunk	COMacc	x
3	Upper trunk	Prox moment arm	y	Upper trunk	ProxMomentArm	x	Upper trunk	ProxMomentArm	Upper trunk	ProxMomentArm	x
4	Upper trunk	COM acceleration	y	Upper trunk	DistMomentArm	z	Left shoulder	COMacc	Left shoulder	COMacc	x
5	Upper trunk	Angular acc	x	Left shoulder	ProxMomentArm	x	Left shoulder	COMacc	Left shoulder	COMacc	z
<b>Downswing</b>											
1	Upper trunk	COM acc	z	Left shoulder	ProxMomentArm	x	Upper trunk	ProxMomentArm	Upper trunk	ProxMomentArm	y
2	Upper trunk	ProxMomentArm	y	Upper trunk	ProxMomentArm	z	Upper trunk	COMacc	Upper trunk	COMacc	x
3	Upper trunk	ProxMomentArm	z	Right shoulder	ProxMomentArm	x	Left shoulder	ProxMomentArm	Left shoulder	ProxMomentArm	z
4	Right shoulder	ProxMomentArm	y	Upper trunk	DistMomentArm	z	Upper trunk	ProxMomentArm	Upper trunk	ProxMomentArm	x
5	Upper trunk	AngAcc	x	Right shoulder	ProxMomentArm	y	Upper trunk	DistMomentArm	Upper trunk	DistMomentArm	y
<b>Set 3</b>											
<b>Backswing</b>											
1	Upper trunk	Prox moment arm	y	Upper trunk	ProxMomentArm	z	Upper trunk	ProxMomentArm	Upper trunk	ProxMomentArm	y
2	Upper trunk	Prox moment arm	z	Upper trunk	AngAcc	y	Upper trunk	DistMomentArm	Upper trunk	DistMomentArm	y
3	Upper trunk	COMacc	z	Upper trunk	ProxMomentArm	x	Left shoulder	ProxMomentArm	Left shoulder	ProxMomentArm	y
4	Upper trunk	Dist moment arm	y	Upper trunk	DistMomentArm	z	Upper trunk	ProxMomentArm	Upper trunk	ProxMomentArm	x
5	Upper trunk	Dist moment arm	z	Left shoulder	ProxMomentArm	z	Left shoulder	ProxMomentArm	Left shoulder	ProxMomentArm	x
<b>Downswing</b>											
1	Upper trunk	COM acc	z	Left shoulder	ProxMomentArm	z	Upper trunk	ProxMomentArm	Upper trunk	ProxMomentArm	x
2	Upper trunk	Prox moment arm	y	Upper trunk	AngAcc	y	Upper trunk	COMacc	Upper trunk	COMacc	x
3	Upper trunk	COMacc	z	Upper trunk	ProxMomentArm	x	Left shoulder	ProxMomentArm	Left shoulder	ProxMomentArm	y
4	Upper trunk	Dist moment arm	y	Upper trunk	DistMomentArm	z	Upper trunk	ProxMomentArm	Upper trunk	ProxMomentArm	x
5	Upper trunk	Dist moment arm	z	Left shoulder	ProxMomentArm	z	Left shoulder	ProxMomentArm	Left shoulder	ProxMomentArm	x

1	Upper trunk	ProxMomentArm	Y	Upper trunk	ProxMomentArm	Z	Upper trunk	ProxMomentArm	Y
2	Upper trunk	ProxMomentArm	Y	Left shoulder	ProxMomentArm	X	Upper trunk	DistMomentArm	Y
3	Upper trunk	DistMomentArm	Y	Right shoulder	DistMomentArm	Y	Upper trunk	ProxMomentArm	X
4	Right shoulder	ProxMomentArm	Z	Upper trunk	DistMomentArm	Z	Left shoulder	ProxMomentArm	Z
5	Right shoulder	ProxMomentArm	Y	Right wrist	ProxMomentArm	Y	Upper trunk	COMacc	X

Table 62 Top five most influential parameters that contributed to the total uncertainty at the mid trunk joint

Mid trunk Uncertainties			Lateral bending			Axial rotation			Flexion-extension			
	Segment	Parameter	Direction	Segment	Parameter	Direction	Segment	Parameter	Direction	Segment	Parameter	Direction
<b>Set 1</b>												
<b>Backswing</b>												
1	Right knee	ProxMomentArmz	Z	Right knee	ProxMomentArm	Z	Right hip	ProxMomentArm	X	Right hip	ProxMomentArm	X
2	Right hip	ProxMomentArmz	Z	Right hip	ProxMomentArm	Z	Right knee	ProxMomentArm	X	Right knee	ProxMomentArm	X
3	Right knee	DistMomentArmz	Z	Right ankle	ProxMomentArm	Z	Right knee	DistMomentArm	X	Right knee	DistMomentArm	X
4	Right ankle	ProxMomentArmz	Z	Right knee	DistMomentArm	Z	Pelvis	DistMomentArm	X	Pelvis	DistMomentArm	X
5	Pelvis	ProxMomentArmz	Z	Left knee	ProxMomentArm	Z	Right ankle	ProxMomentArm	Y	Right ankle	ProxMomentArm	Y
<b>Downswing</b>												
1	Left knee	ProxMomentArmz	Z	Left knee	ProxMomentArmz	Z	Left hip	ProxMomentArm	X	Left hip	ProxMomentArm	X
2	Left hip	ProxMomentArmz	Z	Left hip	ProxMomentArmz	Z	Left knee	ProxMomentArm	X	Left knee	ProxMomentArm	X
3	Right knee	ProxMomentArmz	Z	Left knee	DistMomentArmz	Z	Pelvis	DistMomentArm	X	Pelvis	DistMomentArm	X
4	Pelvis	ProxMomentArmz	Z	Left ankle	ProxMomentArmz	Z	Right knee	ProxMomentArm	X	Right knee	ProxMomentArm	X
5	Left knee	DistMomentArmz	Z	Left hip	ProxMomentArmz	X	Left knee	DistMomentArm	X	Left knee	DistMomentArm	X
<b>Set 2</b>												
<b>Backswing</b>												
1	Left hip	COMaccelz	Z	Left hip	COMaccel	X	Right hip	COMaccel	X	Right hip	COMaccel	X
2	Right hip	COMaccelz	Z	Right hip	ProxMomentArm	Z	Left hip	ProxMomentArm	X	Left hip	COMaccel	X
3	Right knee	ProxMomentArmz	Z	Left knee	COMaccel	Z	Right hip	ProxMomentArm	X	Right hip	ProxMomentArm	X
4	Right hip	ProxMomentArmz	Z	Right knee	ProxMomentArm	Z	Right knee	ProxMomentArm	X	Right knee	ProxMomentArm	X
5	Right knee	COMaccelz	Z	Left hip	COMaccel	X	Right knee	COMaccel	X	Right knee	COMaccel	X
<b>Downswing</b>												
1	Right hip	COMaccelz	Z	Left knee	ProxMomentArmz	Z	Right hip	COMaccel	X	Right hip	COMaccel	X
2	Left hip	COMaccelz	Z	Left hip	ProxMomentArmz	Z	Left hip	ProxMomentArm	X	Left hip	ProxMomentArm	X
3	Left hip	ProxMomentArmz	Z	Left hip	COMaccelz	X	Left hip	COMaccel	X	Left hip	COMaccel	X
4	Left knee	ProxMomentArmz	Z	Left ankle	DistMomentArmz	Z	Pelvis	ProxMomentArm	Y	Pelvis	ProxMomentArm	Y
5	Right knee	COMaccelz	Z	Left knee	DistMomentArmz	Z	Left knee	ProxMomentArm	X	Left knee	ProxMomentArm	X
<b>Set 3</b>												
<b>Backswing</b>												
1	Right ankle	DistMomentArmz	Z	Right ankle	DistMomentArm	Z	Mid trunk	ProxMomentArm	Y	Mid trunk	ProxMomentArm	Y
2	Right knee	ProxMomentArmz	Z	Right knee	ProxMomentArm	Z	Right knee	ProxMomentArm	X	Right knee	ProxMomentArm	X
3	Right hip	ProxMomentArmz	Z	Right hip	ProxMomentArm	Z	Right knee	DistMomentArm	X	Right knee	DistMomentArm	X
4	Right knee	DistMomentArmz	Z	Right ankle	ProxMomentArm	Z	Right hip	ProxMomentArm	X	Right hip	ProxMomentArm	X

5	Downswing	Right ankle	ProxMomentArmz	z	Right knee	DistMomentArm	z	Mid trunk	DistMomentArm	y
1		Mid trunk	ProxMomentArmz	y	Left ankle	DistMomentArmz	z	Mid trunk	ProxMomentArm	y
2		Left hip	ProxMomentArmz	z	Left knee	ProxMomentArmz	z	Left hip	ProxMomentArm	x
3		Left knee	ProxMomentArmz	z	Left hip	ProxMomentArmz	z	Mid trunk	DistMomentArm	y
4		Pelvis	ProxMomentArmz	z	Left knee	DistMomentArmz	z	Pelvis	ProxMomentArm	x
5		Pelvis	ProxMomentArm	y	Left ankle	ProxMomentArmz	z	Pelvis	DistMomentArm	x

## APPENDIX I: BSP Inaccuracy Study - Participant Information Sheet

	<p><i>Sheffield Hallam University</i></p> <p><b>Faculty of Health and Wellbeing Research Ethics Committee</b></p> <p><b>Sport and Exercise Research Ethics Review Group</b></p> <p><b>Participant Information Sheet</b></p>
---	---

<b>Project Title</b>	The accuracy of geometric modelling techniques for estimating full body inertial parameter
----------------------	--

<b>Supervisor/Director of Studies</b>	Dr Jon Wheat
---------------------------------------	--------------

<b>Principal Investigator</b>	Sarah Domone
-------------------------------	--------------

<b>Principal Investigator telephone/mobile number</b>	07872631986
---	-------------

<b>Purpose of Study and Brief Description of Procedures</b>
<i>(Not a legal explanation but a simple statement)</i>
<p>The purpose of this study is to investigate the accuracy body segment inertial parameter estimates made using a geometric modelling technique. Estimates of your body mass, trunk, head, arm and leg segment masses and segment inertial parameters will be made using five different measurement techniques (described below). Before the testing procedure begins direct measurements of height and mass will be obtained. Body fat percentage will also be estimated using skin fold callipers.</p> <p><b>1. Full body laser scan-</b> For this technique you will be required to wear a pair of tight fitting shorts. To enable segment boundaries to be identified markers will be attached directly on to the skin using double sided tape at various anatomical landmarks in preparation for the scan (this may require particularly hairy landmarks to be shaved). This process will involve palpation of bony landmarks in order to identify marker locations. Segments to be scanned</p>

include the head, thorax, lumbar, pelvis, one arm and one leg. The scan is expected to take 30 minutes.

**2.3.4.** The next three techniques will require you to wear a specially designed Golphysics jacket containing electromagnetic sensors held in place with Velcro straps. Once you have the jacket on and the sensors are attached you are required to remain standing a keep movement to a minimum, this will avoid/limit sensor movement. This section of the testing will take approximately 80 minutes.

**2.** This technique requires 79 anthropometric landmarks to be identified by palpation and recorded using a Polhemus stylus. Width and depth measurements of segments can then be calculated to enable the pre-defined variables to be calculated.

**3.** This technique will use the Polhemus stylus to measure the width and perimeter of segments to enable the pre-defined variables to be calculated.

**4.** The final model using the Golphysics suit will use the stylus as a scanner to build an estimate of segment volumes.

During these three techniques you will be asked to stand in the anatomical position (feet shoulder width apart, head up, arms at the side 20° to the body and palms facing forwards). Rest periods are allowed in between techniques.

**5.** A tape measure will be used to measure width and perimeter values of all the body segments.

All of the testing will take place in a single room. You will be given time to change in between each period of testing. The testing session in total will last approximately three hours. Please feel free to ask any questions you may have regarding this study.

You have the right to withdraw from the study at any time.

It has been made clear to me that, should I feel that these Regulations are being infringed or that my interests are otherwise being ignored, neglected or denied, I should inform Professor Edward Winter, Chair of the Faculty of Health and Wellbeing Research Ethics Committee (Tel: 0114 225 4333) who will undertake to investigate my complaint.

**APPENDIX J: BSP Inaccuracy Study - Ethics Form****CONFIDENTIAL**

*Sheffield Hallam University*

**Faculty of Health and Wellbeing**

**Research Ethics Committee**

**Sport & Exercise Research Ethics Review Group**

**APPLICATION FOR ETHICS APPROVAL OF RESEARCH**

In designing research involving humans, principal investigators should be able to demonstrate a clear intention of benefit to society and the research should be based on sound principles. These criteria will be considered by the Sport and Exercise Research Ethics Review Group before approving a project. **ALL** of the following details must be provided, either typewritten or word processed preferably at least in 11 point font.

Please either tick the appropriate box or provide the information required.

<b>1) Date of application</b>	10/11/2010
-------------------------------	------------

<b>2) Anticipated date of completion of project</b>	30/11/2010
---	------------

<b>3) Title of research</b>	The accuracy of geometric models for estimating full body inertial parameters
-----------------------------	---

<b>4) Subject area</b>	Sports Engineering/Biomechanics
------------------------	---------------------------------

<b>5) Principal Investigator</b>	
Name	Sarah Domone
Email address @ SHU	s.domone@shu.ac.uk
Telephone/Mobile number	07872631986
Student number (if applicable)	19046366

<b>6) State if this study is:</b>  (If the project is undergraduate or postgraduate please state module name and number)	<input type="checkbox"/> Research <input type="checkbox"/> Undergraduate <input checked="" type="checkbox"/> Postgraduate  Module name:  Module number:
--	---

<b>7) Director of Studies/Supervisor/Tutor name</b>	Dr Jon Wheat
---	--------------

<b>8) Intended duration and timing of project?</b>	17 <sup>th</sup> /18 <sup>th</sup> November 2010
--	--

<b>9) Location of project</b>  If external to SHU, provide evidence in support (see section 17)	Mundella House, Collegiate Crescent Campus Sheffield Hallam University
---	---

<b>10) State if this study is:</b>	<input checked="" type="checkbox"/> New  <input type="checkbox"/> Collaborative (please include appropriate agreements in section 17)  <input type="checkbox"/> Replication of :
------------------------------------	--

<b>11) Purpose and benefit of the research</b>
Statement of the research problem with any necessary background information (no more than 1 side of A4)
<b>Research Aims and Objectives</b>
The accuracy of geometric modelling techniques in estimating body segment inertial parameters will be determined. Three different methods of estimating segmental volumes will be investigated using three male participants who will represent each of the three somatotypes. Full body scans of the participants will provide accurate measured segment volumes that will allow the error in each estimation method to be calculated. The findings of this study will allow for the development of more accurate models which will afford more precise motion analysis outcomes.

**Research Context**

The estimation of accurate body segment inertial parameters (BSP) is essential for the biomechanical analysis of movement. The influence of inaccurate BSP values has been demonstrated to generate significant variations in joint kinematic estimates (Andrews and Mish, 1996; Kingma et al, 1996). BSP's can be derived from geometric modelling of segments which provide subject specific body segment data and hence overcome some of the drawbacks associated with other methods such as those that use predictive functions based on data from cadavers (Yeadon and Morlock, 1989).

Tuning body segment parameters for the individual is a trade off between accuracy of the estimates and the amount of work involved in making the anthropometric measurements. Geometric models of the human body of different complexity have been developed, the simplest of which suggested by Hanavan (1964) who divided the body into 15 simple uniform shapes. A more complex model by Yeadon (1990) segmented the body into 40 geometric solids that were specified by 95 anthropometric measurements and used 'stadium solids' to model the torso more accurately.

The errors associated with geometric modelling are due to both volume and density functions. Wicke and Dumas (2010) found that adopting a uniform density function produced only minor errors in the inertial estimates for the trunk and that, in fact, the greatest errors were due to inaccuracies in the volume function. The literature also suggests that some segments are more difficult to model than others. The trunk appears to be particularly difficult; in studies where segmentation is consistent and the sample is homogenous, the relative mass varies from 35.8% - 48.0% (Pearsall, Reed, Ross, 1994). Furthermore the abdominal region where body fat is most readily accumulated ranges in the literature from 10.4%-21.6% of relative body mass.

Pilot work used a geometric model adapted from Yeadon (1990) which split the body into 26 geometric solids defined by 79 separate anthropometric measurements. These measurements were made using a digital stylus, the output of which was recorded directly by the Polhemus system. Values for width and depth at segment boundaries and segment mid-points were taken in order to build up an accurate representation of each body segment. The results of this previous study indicated that the total predicted body mass was being underestimated in some cases by as much as 20%. Yeadon (1990) states that using the perimeter and width as input measurements as opposed to width and depth measurements reduces the error in estimation of the cross sectional area. Furthermore the palpation technique used to identify the marker positions depresses the soft tissue and thus may have the effect of reducing the width and depth measurements. This study will attempt to determine firstly in which specific segments the masses are being under estimated, the possible reasons for this, and an improved method for estimating segment volumes.

The three different methods of estimating segment volumes to be investigated are;

1. Full body model consisting of 26 geometric solids defined by 79 anthropometric measurements, width and depth measurements taken using a digital stylus.

2. Full body model consisting of 26 geometric solids defined by perimeter and width measurements. Perimeter measurements to be taken with a tape measure, width measurements to be taken with callipers.
3. Digital stylus used to build up a point cloud over the surface of each segment thus defining segment surface volume.

### References

Andrews, J. G., Mish, S. P. (1996). Methods for investigating the sensitivity of joint resultants to body segment parameter variations. *J. Biomech.* 29 (5): 651-54.

Kingma, I., Toussaint, H., Bruijnen, T. (1996) Validation of a full body 3D dynamic linked segment model. *Hum. Mov. Sci.* 15: 833-60.

Yeadon, M.R., and Morlock, M. (1989). The appropriate use of regression equations for the estimation of segmental properties. *J. Biomech.* 22: 683 - 89.

Hanavan, E.P. (1964) *A mathematical model of the human body*. Report no. AMRL-TR-64-102, AD-608-463. Ohio: Aerospace Medical Research Laboratories, Wright-Patterson Air Force Base.

Yeadon, M. R. (1990). The simulation of aerial movement II. A mathematical inertia model of the human body. *J. Biomech.* 23 (1): 67-74.

Wicke, J., Dumas, G. (2010). Influence of the volume and density functions within geometric models for estimating trunk inertial parameters. *J. App. Biomech.* 26 (1): 26-31.

Pearsall, D.J., Reid, J.G., Ross, R. (1994). Inertial properties of the human trunk of males determined from magnetic resonance imaging. *Ann. Biomed. Eng.* 22 (6): 692-706.

<b>12) Participants</b>	
<b>12.1 Number</b>	3
<b>12.2 Rationale for this number</b> (eg calculations of sample size, practical considerations)	It is important that the investigation considers all three somatotypes (ectomorph, mesomorph, and endomorph). The investigation requires full body scans of each participant which therefore dictates that, due to time and financial constraints, 3 is the maximum number of participants that can be used.
<b>12.3 Criteria for inclusion and exclusion</b> (eg age and sex)	Male participants which match the three somatotypes

<b>12.4 Procedures for recruitment</b> (eg location and methods)	Sheffield Tigers Rugby Club
<b>12.5 Does the study have *minors or ‡vulnerable adults as participants?</b>	<input type="checkbox"/> Yes <input checked="" type="checkbox"/> No
<b>12.6 Is CRB Disclosure required for the Principal Investigator?</b> (to be determined by Risk Assessment)	<input type="checkbox"/> Yes <input checked="" type="checkbox"/> No  If yes, is standard <input type="checkbox"/> or enhanced <input type="checkbox"/> disclosure required?
<b>12.7 If you ticked 'yes' in 12.5 and 'no' in 12.6 please explain why:</b>	

\*Minors are participants under the age of 18 years.

‡Vulnerable adults are participants over the age of 16 years who are likely to exhibit:

- a) learning difficulties
- b) physical illness/impairment
- c) mental illness/impairment
- d) advanced age
- e) any other condition that might render them vulnerable

### 13) Details of the research design

#### 13.1 Provide details of intended methodological procedures and data collection.

(For MSc students conducting a scientific support project please provide the following information: a. needs analysis; b. potential outcome; c proposed interventions).

Participants will be required to wear tight fitting shorts which will be provided for them. Prior to testing height and weight of each participant will be measured along with an estimate of body fat percentage. A single session will run as follows;

1. Full body laser scan  
 Markers will be placed directly to the skin at various anatomical landmarks in preparation for the scan. This process will require palpation of bony landmarks in order to identify marker locations. Segments to be scanned are the head, thorax, lumbar, pelvis, the dominant arm and leg. The scan is expected to take 30 minutes.

The next part of the data collection will require the participant to put on a specially designed

jacket which holds all the Polhemus sensors in place via Velcro straps. Once the jacket is put on and all the sensors have been attached the participant will not be able to sit down and movement should be kept to a minimum in order to prevent/limit sensor movement. Measurements will be made using a digital stylus, the output of which will be inputted directly into specially written software which relates the position and orientation of the Polhemus sensors to the coordinate data of the stylus marker positions.

2. Use Polhemus and digital stylus to build geometric models

The first model to be investigated requires 79 width and depth measurements to be taken using the stylus, marker locations are found by palpation. The second model will use the stylus to measure segment widths and perimeters. The third model will use the stylus as a scanner to build up segment surface volumes. Each model is expected to take up to 20minutes to build. Participants will be required to stand in the anatomical position whilst measurements are being taken, however rest periods will be offered between models.

3. Use a tape-measure to determine width and perimeter of body segments

All testing will take place in a single room with each participant being asked to attend a particular session lasting up to three hours.

**13.2 Are these "minor" procedures as defined in Appendix 1 of the ethics guidelines?**

Yes       No

**13.3 If you answered 'no' in section 13.2, list the procedures that are not minor**

**13.4 Provide details of the quantitative and qualitative analysis to be used**

The laser scanner will provide volumetric measures of the head, torso, one arm and one leg of each participant. The digital stylus linked to the Polhemus system will be used to mark the coordinates of a number of specific locations over the whole body. A tape measure will be used to measure the perimeter and width at various segment boundaries.

**14) Substances to be administered (refer to Appendix V of the ethics procedures)**

**14.1 The protocol does not involve the administration of pharmacologically active substances or nutritional supplements.**

Please tick box if this statement applies and go to section 15) [✓ ]

**14.2 Name and state the risk category for each substance. If a COSHH assessment is required state how the risks are to be managed.**

**15) Degree of discomfort that participants might experience**

Consider the degree of physical and psychological discomfort that will be experienced by the participants. State the details which must be included in the participant information sheet to ensure that the participants are fully informed about any discomfort that they may experience.

The participants will be required to stand for a prolonged period of time without being able to sit down. Whilst measurements are being taken they will be required to remain in the standard anatomical position (legs shoulder width apart, head up, arms abducted by 30°, palms facing forward). Rest periods have been included in the protocol however it is important that movement is kept to a minimum whilst in the Polhemus jacket to prevent sensor movement.

Participants will be required to wear minimal clothing throughout the testing process which may cause some level of psychological discomfort. It is important that all the participants are made aware of this prior to testing and the reasons for this explained. The number of investigators in the room during testing will be kept to a minimum (no more than 2 people).

**16) Outcomes of Risk Assessment**

Provide details of the risk and explain how the control measures will be implemented to manage the risk.

**LOW-** The testing procedures cause minor risks to the participant's wellbeing. However it is important for appropriate control measures to be identified and adhered to.

17) Attachments	Tick box
17.1 Risk assessment (including CRB risk assessment)	✓
17.2 COSHH assessment	
17.3 Participant information sheet (this should be addressed directly to the participant (ie you will etc) and in a language they will understand)	✓
17.4 Informed consent form	✓
17.5 Pre-screening questionnaire	✓
17.6 Collaboration evidence/support correspondence from the organisation consenting to the research (this must be on letterhead paper and signed) See sections 9 & 10.	
17.7 CRB Disclosure certificate <u>or</u> where not available CRB application form	
17.8 Clinical Trails form (FIN 12)	

**APPENDIX K: BSP Inaccuracy Study - Risk Assessment form**

*Sheffield Hallam University*

**Faculty of Health and Wellbeing Research Ethics Committee**

**Sport and Exercise Research Ethics Review Group**

**Risk Assessment Pro Forma**

<b>Title of research</b>	The accuracy of geometric modelling techniques for estimating full body inertial parameters
--------------------------	---

<b>Date Assessed</b>	9.11.2010
----------------------	-----------

<b>Assessed by (Principal Investigator)</b>	Sarah Domone
---	--------------

<b>Signed</b>	<b>Position</b>
	Principal Investigator

<b>Activity</b>	<b>Risks</b>	<b>Control Measures</b>
-----------------	--------------	-------------------------

<p>Testing procedure- Standing for long periods of time</p>	<p>1. Standing for long periods in the anatomical position may cause fatigue and a possible risk of fainting  (R1 = C1 x L1)</p>	<p><b>Low-</b> The risk of fainting is low.  Control measure: The participants will be provided with the opportunity to rest in between measurement techniques.</p>
<p>Body scanning with laser scanner</p>	<p>1. Lack of clothing causing the participant to feel uncomfortable  (R1 = C1 x L1)</p>	<p><b>Low-</b> Additional stress placed on the participant is low.  Control measure: The participant information sheet will clearly explain the scanning process and the number of examiners in the room whilst scanning will be kept to a minimum.</p>
	<p>2. Potential discomfort when removing markers attached by double sided tape  (R3 = C1 x L2)</p>	<p><b>Low -</b> Participant may feel slight discomfort when removing markers  Control Measure - Removal of hair before attaching markers will reduce discomfort</p>
	<p>3. Possible skin reaction to sticky labels used to attached markers  (R1 = C1 x L1)</p>	<p><b>Low -</b> Skin may become irritated by sticky labels  Control measure - Test small area of skin before application of all markers</p>

	<p>4. Shaving skin may cause irritation and could also cut the skin</p> <p>(R1 = C1 x L2)</p>	<p><b>Low</b> - There is a moderate risk of skin irritation after shaving however this may not be necessary for all participants</p> <p>Control measure - the size of the shaved area will be kept to minimum</p>
<p>Identification of anatomical landmarks using the Golphysics equipment</p>	<p>1. Tripping over cables</p> <p>(R1 = C1 x L1)</p>	<p><b>Low</b> - The risk of tripping is low as the majority of the wires are contained by the Golphysics equipment.</p> <p>Control measure: Extra care must be taken when using the steps to ensure the participant remains safe</p>

#### Risk Evaluation (Overall)

**LOW** - The testing procedures cause minor risks to the participant's wellbeing. However it is important for appropriate control measures to be identified and adhered to.

#### General Control Measures

Is a pre-screen medical questionnaire required? Yes [  ] No [  ]

Pre Screening medical questionnaire, participant Information sheet and informed consent form provided and agreed. Adherence to protocol including periods of rest for the participant.

### Emergency Procedures

Emergency first aid

### Monitoring Procedures

The experiment will be monitored at all times by at least two members of appropriately experienced staff.

## APPENDIX L: Golf Swing Data Collection - Participant Information Sheet

### Golphysics Participant Information Sheet

#### Study Purpose

The purpose of this study is to collect a large-scale normative database of golf swings.

#### Procedure

##### Step 1 – forms to complete

Unfortunately there are a number of forms to fill in before data collection can commence. On arrival you will be asked to complete an informed consent form, data ownership form and pre-screening questionnaires.

##### Step 2 – opportunity to ask questions

At the start of your data collection session you will have the chance to talk with the investigators and you will be invited to ask any questions about the project, procedures and testing. Please take as much time as you need to become familiar with what is expected of you.

##### Step 3 – preparation for data collection

The equipment we will be using to analyse your golf swing requires that small sensors are attached to your body. Several of these sensors are embedded in a jacket that you will be required to wear. To ensure that the jacket fits appropriately, you will be asked to wear only a t-shirt/polo-shirt on your upper body. Further sensors will be placed on your thigh and lower legs using straps that will be attached over your, preferably loose-fitting, trousers. Additional sensors will be secured to your head – via the cap with which you will be provided – and to your hands – via golf gloves that you will be required to wear on **both** your left and right hands.

At this stage, you need to be comfortable with the straps and sensors because they **cannot be moved** from this point on without invalidating all subsequent test results.

##### Step 4 – habituation

You will be given as much time as you need to become habituated to the data collection space and to warm-up. During this time you will have the opportunity to stretch as well as hit as many golf balls as you require.

#### **Step 5 – calibration**

A 'calibration trial' will be collected which will allow us to create a computer-generated model of your body. This will take approximately six minutes and will involve the investigator pointing to various points on your body using a stylus - a small pointer. You will be required to stand relatively still during the calibration trial but will be offered the opportunity to rest if required.

#### **Step 6 – golf shots**

You will then be asked to hit golf shots. We require that you hit ten shots with the Driver and five shots with the 5 and 9 irons. The order in which the clubs are presented to you will be randomised. You will be offered the opportunity to rest between shots and you should not feel rushed in any way to complete the required number of shots. During your golf swings, we will be collecting data from four different sources: 1) An electro-magnetic tracking system – this allows us to measure the movements of your body segments during your swings; 2) force platforms – these allow us to measure ground reaction forces in all directions during your swings; 3) Trackman – this will allow us to predict ball flight characteristics and club head characteristics during your swings; 4) a digital video camera – this is primarily used as a record of the data collection for quality control purposes.

#### **Step 7 - debrief**

After the shots are complete the sensors will be removed and you will have the chance to ask the investigators any further questions about the data collection.

All data will be kept confidential but summary data - in which you will **NOT** be identifiable - may be published in scientific journals and at scientific conferences and may be used in equipment or software related to golf coaching or other golf related activities. You are free to withdraw from the study at any point.

Thank you for participating.

**APPENDIX M: Golf Swing Data Collection - Ethics Form****CONFIDENTIAL****Sheffield  
Hallam  
University****Faculty of Health and Wellbeing****Research Ethics Committee****Sport & Exercise Research Ethics Review Group****APPLICATION FOR ETHICS APPROVAL OF RESEARCH**

In designing research involving humans, principal investigators should be able to demonstrate a clear intention of benefit to society and the research should be based on sound principles. These criteria will be considered by the Sport and Exercise Research Ethics Review Group before approving a project. **ALL** of the following details must be provided, either typewritten or word-processed preferably at least in 11 point font.

Please either tick the appropriate box or provide the information required.

<b>1) Date of application</b>	19/10/12
-------------------------------	----------

<b>2) Anticipated date of completion of project</b>	July 2013
---	-----------

<b>3) Title of research</b>	A Full Body Joint Kinetics Analysis of the Golf Swing
-----------------------------	---

<b>4) Subject area</b>	Biomechanics
------------------------	--------------

<b>5) Principal Investigator</b>	
Name	Sarah Domone
Email address @ SHU	s.domone@shu.ac.uk
Telephone/Mobile number	07872631986
Student number (if applicable)	

<b>6) State if this study is:</b> (If the project is undergraduate or postgraduate please state module name and number)	<input checked="" type="checkbox"/> Research <input type="checkbox"/> Undergraduate <input type="checkbox"/> Postgraduate Module name: Module number:
--	---

<b>7) Director of Studies/Supervisor/Tutor name</b>	Jon Wheat
---	-----------

<b>8) Intended duration and timing of project?</b>	6 months
--	----------

<b>9) Location of project</b> If external to SHU, provide evidence in support (see section 17)	Collegiate Hall
---	-----------------

<b>10) State if this study is:</b>	<input checked="" type="checkbox"/> New <input type="checkbox"/> Collaborative (please include appropriate agreements in section 17) <input type="checkbox"/> Replication of :
------------------------------------	--

**11) Purpose and benefit of the research**

Statement of the research problem with any necessary background information (no more than 1 side of A4)

A great number of biomechanical models of the golf swing have been developed in the past four decades which have aided in the understanding of one of one of the most complex motions in sport. In order to justify the degree of simplicity of many swing models more consideration needs to go into the validation techniques used. Three dimensional full body models go some way into overcoming some of the limitations of 2D analysis, however research into the validity of the kinetic output of these models is lacking. The indeterminacy caused by the arms forming a closed kinematic chain creates a fundamental problem in the application of inverse dynamics to the golf swing yet no studies have given this much consideration.

Some studies have been successful in establishing a validation technique for full body inverse dynamics models; comparing the estimated torques from a top down and bottom up analysis for example (Kingma, 1996), however this approach has yet to be applied to the specific case of the golf swing. Sensitivity analyses specific to the gait have reported uncertainties in torque estimates to range between 6-232% (Riemer et al, 2008). The main contributors to this uncertainty were the estimated segment angles and body segment parameters indicating that any inverse dynamics analysis should focus on minimising the error associated with these two factors. Therefore the first aim of this study is to establish a comprehensive and quantitative understanding of the uncertainties in inverse dynamics solutions specifically related to the golf swing.

**References**

Kingma, I. (1996). Validation of a full body 3-D dynamic linked segment model. *Human Movement Science*, 15(6), 833-860.

Riemer, R. et al. (2008). Uncertainties in inverse dynamics solutions: A comprehensive analysis and application to gait. *Gait and Posture*, 27 (4), 578 - 588.

**12) Participants****12.1 Number**

60

<p><b>12.2 Rationale for this number</b></p> <p>(eg calculations of sample size, practical considerations)</p>	<p>A large sample (25 - 30) of category 1 golfers as indicated by the CONGU Unified Handicapping System divisions will be recruited to replicate and progress the study of Anderson, Wright and Stefanyshn (2006).</p> <p>A large number (15 - 20) of category 2 and 3 golfers are also required to assess differences in the sequencing of kinetic energy between different playing standards.</p>
<p><b>12.3 Criteria for inclusion and exclusion</b> (eg age and sex)</p>	<p>Male golfers, at least 18 years old, Handicap from 0 - 20.</p>
<p><b>12.4 Procedures for recruitment</b></p> <p>(eg location and methods)</p>	<p>Local Golf Clubs, SHU golf society and golf contacts</p>
<p><b>12.5 Does the study have *minors or ‡vulnerable adults as participants?</b></p>	<p><input type="checkbox"/> Yes     <input checked="" type="checkbox"/> No</p>
<p><b>12.6 Is CRB Disclosure required for the Principal Investigator?</b> (to be determined by Risk Assessment)</p>	<p><input type="checkbox"/> Yes     <input checked="" type="checkbox"/> No</p> <p>If yes, is standard <input type="checkbox"/> or enhanced <input type="checkbox"/> disclosure required?</p>
<p><b>12.7 If you ticked 'yes' in 12.5 and 'no' in 12.6 please explain why:</b></p>	

\*Minors are participants under the age of 18 years.

‡Vulnerable adults are participants over the age of 16 years who are likely to exhibit:

a) learning difficulties

- b) physical illness/impairment
- c) mental illness/impairment
- d) advanced age
- e) any other condition that might render them vulnerable

### 13) Details of the research design

#### 13.1 Provide details of intended methodological procedures and data collection.

(For MSc students conducting a scientific support project please provide the following information: a. needs analysis; b. potential outcome; c proposed interventions).

Before the data collection commences golfers will be required to complete an informed consent form and pre-screening questionnaire. Height and mass will also be measured. Golfers will be given time to complete their usual warm-up routine before hitting 10 shots with a Driver and 5 shots with the 5 and 9 irons. To control the effect of fatigue the order in which clubs are presented will be randomly assigned. Sufficient practice trials will also be allowed to ensure golfers feel familiar with each club.

Prior to the data collection inertial properties of each golfers body segments will be estimated using a geometric model based on the Yeadon (1990) model. 12 electromagnetic sensors will be attached to each golfer using a specially designed suit comprising a baselayer jacket with adjustable straps, adjustable leg straps, two golf gloves and a cap. The locations of 79 palpable landmarks will be recorded using the Polhemus digital stylus, custom written software and the Polhemus LIBERTY electromagnetic tracing system.

During data collection kinematic data will be recorded using the Polhemus system and the 12 electromagnetic sensors contained in the specifically designed suit. The Polhemus system provides real time movement data at a rate of 240Hz with 6DOF and a static accuracy position of 0.03in and static accuracy orientation of 0.15° RMS. Ground reaction forces will also be collected using two forces plates, one for each foot. Impact will be measured using an accelerometer attached to the clubhead and ball flight characteristics will be measured using a Trackman radar unit.

#### 13.2 Are these "minor" procedures as defined in Appendix 1 of the ethics guidelines?

Yes       No

**13.3 If you answered 'no' in section 13.2, list the procedures that are not minor****13.4 Provide details of the quantitative and qualitative analysis to be used**

The data from this data collection will be used to establish a comprehensive and quantitative understanding of the uncertainties in inverse dynamics solutions specifically related to the golf swing. This analysis will consist of;

1. Comparison of the top down and bottom up calculation of joint torque at the L5/S1 joint
2. Prediction of Ground Reaction Forces (GRF) from the top down model compared to measured GRF
3. Taylor series uncertainty analysis to provide a upper bound error of joint torque profiles during the golf swing

**14) Substances to be administered (refer to Appendix VI of the ethics procedures)**

**14.1 The protocol does not involve the administration of pharmacologically active substances or nutritional supplements.**

Please tick box if this statement applies and go to section 15) [

**14.2 Name and state the risk category for each substance. If a COSHH assessment is required state how the risks are to be managed.**

**15) Degree of discomfort that participants might experience**

Consider the degree of physical and psychological discomfort that will be experienced by the participants. State the details which must be included in the participant information sheet to ensure that the participants are fully informed about any discomfort that they may experience.

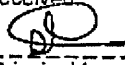
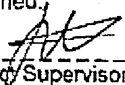
Participants will be required to stand for the duration of the data collection which could be up to an hour, the participant information sheet will state that this is necessary to minimise sensor movement. If a participant does not think they are capable of doing this they will be allowed to withdraw from the study.

The participants are only required to hit twenty shots however including warm-up shots they will hit approximately thirty - forty shots. Most of the players will be playing on a regular basis and therefore should not experience any discomfort hitting this amount of shots. However they will be given adequate time to rest between shots and between conditions.

#### **16) Outcomes of Risk Assessment**

Provide details of the risk and explain how the control measures will be implemented to manage the risk.

**Low** - The testing procedures cause minor risks to the participant's wellbeing. However it is important for the control measures to be adhered to. The golfers must be given adequate time to warm-up and rest periods should be allowed when required. Care should also be taken to ensure golf balls are contained within the hitting net or ball pyramid. The back of the hitting area should be kept free of wires and the wires of the Polhemus system should also be supported by a tripod behind the golfer.

<p><b>18. Signature Principal Investigator</b></p>	<p>Once this application is approved, I will undertake the research study as approved. If circumstances necessitate that changes are made to the approved protocol, I will discuss these with my Project Supervisor. If the supervisor advises that there should be a resubmission to the Sport and Exercise Research Ethics Review Group, I agree that no work will be carried out using the changed protocol until approval has been sought and formally received.</p> <p> Date <u>23/10/12</u></p> <p>Principal Investigator signature</p> <p>Name <u>SARAH DEMORE</u></p>
<p><b>19. Approval Project Supervisor to sign either box A or box B as applicable</b></p> <p>(refer to Appendix I and the flowchart in appendix VI of the ethics guidelines)</p>	<p><b>Box A:</b></p> <p>I confirm that the research proposed is based solely on 'minor' procedures, as outlined in Appendix 1 of the HWB Sport and Exercise Research Ethics Review Group 'Ethics Procedures for Research with Humans as Participants' document, and therefore does not need to be submitted to the HWB Sport and Exercise Research Ethics Review Group.</p> <p>In terms of ethics approval, I agree the 'minor' procedures proposed here and confirm that the Principal Investigator may proceed with the study as designed.</p> <p> Date <u>23/10/12</u></p> <p>Project Supervisor signature</p> <p>Name <u>JOW WHEAT</u></p>
	<p><b>Box B:</b></p> <p>I confirm that the research proposed is <u>not</u> based solely on 'minor' procedures, as outlined in Appendix 1 of the HWB Sport and Exercise Research Ethics Review Group 'Ethics Procedures for Research with Humans as Participants' document, and therefore <u>must</u> be submitted to the HWB Sport and Exercise Research Ethics Review Group for approval.</p> <p>I confirm that the appropriate preparatory work has been undertaken and that this document is in a fit state for submission to the HWB Sport and Exercise Research Ethics Review Group.</p> <p>_____ Date _____</p> <p>Project Supervisor signature</p> <p>Name _____</p>
<p><b>20. Signature Technician</b></p>	<p>I confirm that I have seen the full and approved application for ethics approval and technical support will be provided.</p> <p>_____ Date _____</p> <p>Technician signature</p> <p>Name _____</p>

## APPENDIX N: Golf Swing Data Collection - Risk Assessment Form

Valid until 31.12.10

	<i>Sheffield Hallam University</i>
<b>Faculty of Health and Wellbeing Research Ethics Committee Sport and Exercise Research Ethics Review Group</b>	
<b>Risk Assessment Pro Forma</b>	

<b>Title of research</b>	A Full Body Joint Kinetics Analysis of the Golf Swing
<b>Date Assessed</b>	19.10.2012
<b>Assessed by (Principal Investigator)</b>	Sarah Domone
<b>Signed</b> 	<b>Position</b> Principal Investigator

Activity	Risks	Control Measures
Hitting golf shots	<p>1. Muscular injury and fatigue caused by repetition of golf shots. (R1 = C1 + L1)</p> <p>2. Tripping over golf balls (R1 = C1 + L1)</p> <p>3. Lab users being hit by golf balls. (R1 = C1 + L1)</p> <p>4. Tripping when stepping onto the force platforms. (R1 = C1 + L1)</p> <p>5. Falling off force platforms when hitting shots. (R1 = C1 + L1)</p>	<p><b>Low-</b> The risk of muscular injury and fatigue is low as a maximum of 60 shots will be hit. The golfers will be playing regularly and this amount of shots should not cause fatigue. The risk of tripping is also low</p> <p>Control measure: Golfers will be given adequate time to warm up before testing and rest periods will be allowed when required.</p> <p>Care will be taken to ensure that golf balls are contained within the hitting net or ball pyramid.</p> <p>All lab users must be behind the golfer when they are hitting shots. Golfers will be advised to take care when stepping on and off the force platforms.</p>

Valid until 31.12.10

Hitting golf shots in the specifically designed suit.

1. Tripping over wires  
(R1 = C1 + I1)

Low - The risk of tripping is low as the majority of the wires are contained by the Golphysics equipment.  
Control measure: Ensure the wires are supported by a tripod behind the golfer.

**Risk Evaluation (Overall)**

LOW - The testing procedures cause minor risks to the participant's wellbeing. However it is important for appropriate control measures to be identified and adhered to.

**General Control Measures**

Is a pre-screen medical questionnaire required? Yes [  ] No [  ]

Pre Screening medical questionnaire, participant information sheet and informed consent form will be provided and agreed. Adherence to protocol including periods of rest for the participant will be ensured.

**Emergency Procedures**

Emergency first aid

**Monitoring Procedures**

The experiment will be monitored at all times by at least two members of appropriately experienced staff.

**Review Period**

Reviewed By (Supervisor)

Date



23/10/12

## APPENDIX O: Table of Assumptions

Assumptions	section, pg. no.
<b>Inverse Dynamics Assumptions</b>	2.4, pg.15
<ul style="list-style-type: none"> <li>• Segments are assumed to be rigid bodies with a fixed mass, centre of mass and inertia <ul style="list-style-type: none"> <li>◦ Inertial properties are estimated using regression equations, geometric models or scanning techniques. Rigid bodies have no moving parts and cannot be deformed, based on the idea that deformations that do take place within a body are small compared to the overall movement of a segment (Vaughan et al., 1982a).</li> </ul> </li> <li>• Net joint moment acting on a joint can be estimated from the linear acceleration and mass of the segment</li> <li>• Net joint moments can be calculated from the segment moments of inertia, angular acceleration, angular velocity and segment centre of mass position</li> <li>• From Newton's third law, the net reaction forces and moments acting at the distal end of a segment are equal in magnitude and opposite in sign to those acting on the proximal end of the adjacent segment</li> <li>• Joint constraints <ul style="list-style-type: none"> <li>◦ Segments are linked together into kinematic chain using joints with 1-6 degrees of freedom. Joints are ideal revolute joints that so do not dissipate energy due to friction or deformation which can be caused by passive resistance to motion (Zatsiorsky, 2002).</li> <li>◦ Pure rotation about a fixed joint axis is assumed, however movement can be more complex, for example the shoulder joint can translate significantly (Zatsiorsky, 2002).</li> </ul> </li> <li>• The body can be presented as a series of geometric solids <ul style="list-style-type: none"> <li>◦ The human body is continuous with muscles, ligaments and other soft tissues crossing over body parts making segmentation subject to judgement (Zatsiorsky, 2002).</li> </ul> </li> <li>• Body Segment Parameters are determined using scanning methods, geometric models or regression equations</li> <li>• The shape of a segment can be accurately modelled using a series of symmetric geometric shapes <ul style="list-style-type: none"> <li>◦ Some segments are more difficult to model than others, i.e. the trunk is particularly difficult (Pearsall and Reid, 1994).</li> <li>◦ Reliability and accuracy of palpation of anatomical landmarks also affects the accuracy of BSP estimates.</li> </ul> </li> <li>• The density of each segment is uniform throughout</li> <li>• Geometric joint centre is assumed for each joint. <ul style="list-style-type: none"> <li>◦ Assumes that the lines of action of joint reaction forces pass through joint centres.</li> <li>◦ There are a large number of methods which can be used to calculate joint centre locations</li> <li>◦ Assumes a fixed centre of rotation for each joint</li> </ul> </li> <li>• Kinematics can be measured with sufficient accuracy <ul style="list-style-type: none"> <li>◦ Soft tissue artefact can affect the accuracy of non-invasive measurement of skeletal kinematics. STA affects the calculation of segment angles, kinematic variables, joint centre location and segment centre of mass estimates</li> <li>◦ Dependant on the finite precision limits of the motion measurement system which can random or systematic in nature. These errors can propagate unpredictably to the estimation of segment kinematics.</li> <li>◦ Position and orientation data collected using motion capture systems are numerically differentiated to give the first and second order derivatives needed for calculation of forces and moments. the process of differentiation amplifies noise and will therefore affect the accuracy with which segment acceleration and velocity can be measured</li> </ul> </li> <li>• External forces can be measured with sufficient accuracy <ul style="list-style-type: none"> <li>◦ Can contain error in both the force magnitude and centre of pressure location (Lewis et al., 2007).</li> <li>◦ Discrepancy in the registration between the global coordinate system and the external measurement system also affects the accuracy with which external forces and COP can be calculated</li> </ul> </li> <li>• That there are sufficient independent equations to determine the unknown forces <ul style="list-style-type: none"> <li>◦ In the golf swing indeterminacy is caused by the club handle, arms and shoulders forming a closed kinematic chain. Nesbit (2005) considered the closed loop problem, choosing to distribute the load equally between the two arms.</li> </ul> </li> </ul>	
<b>Data Collection</b>	3, pg.44
<b>Mapping</b>	3.1.3.2, pg. 46
<ul style="list-style-type: none"> <li>• Distortion in the magnetic field caused by metal in the force plates and surrounding area can be corrected for using mapping techniques</li> </ul>	
<b>Club segment</b>	3.1.7.1, pg.60
<ul style="list-style-type: none"> <li>• The club segment was assumed to have fixed inertial parameters <ul style="list-style-type: none"> <li>◦ Mass, moments of inertia and centre of mass were calculated using a non-contact laser scanner (Model Maker D100, Metris, Leuven, Belgium) with a volumetric accuracy of +/- 0.051 mm (0.0020 in) and the density of the shaft and club head were provided by the manufacturer.</li> </ul> </li> <li>• It was assumed that the club was rigid, that the only forces acting on the hands were from the mass</li> </ul>	

<p>of the club and that the hands were placed 12cm from the top end of the club resulting in a fixed moment arm length from centre of mass of the club to the distal end of the hand.</p> <ul style="list-style-type: none"> <li>○ During the swing, the club has been shown to bend; the club head experiences maximum lag early in the downswing of 2-13cm before straightening up as the downswing progresses such that at impact the club head is leading the grip by 0-4.39cm (Butler and Winfield, 1994; Jorgensen, 1999; Milne and Davis, 1992c). It is likely that this club deformation has an effect on the forces at the hands and therefore would contribute to the uncertainty in joint moment estimates. To quantify this effect, a three dimensional flexible shaft model could be constructed (McGuan, 1996; Nesbit, 2005; Tsujiuchi et al., 2002b) or these forces could be measured directly using an instrumented club (Koike et al., 2006). The task of modelling a flexible shaft is not trivial since there is evidence that each golfer, regardless of skill level, has their own shaft loading signature with less skilled players demonstrating a greater degree of variability both within and between golfers (Cooper and Mather, 1994; Lee et al., 2002).</li> </ul>	
<b>Validation Study</b>	4, pg.73
<ul style="list-style-type: none"> <li>• Residual in the bottom up top down comparison of joint moments and forces was representative of modelling error <ul style="list-style-type: none"> <li>○ This makes the assumption that the error at each joint is cumulative when it is possible errors can compensate for each other as calculations proceed up the kinematic chain</li> </ul> </li> <li>• Residual in the measured vs. predicted GRF is representative of error <ul style="list-style-type: none"> <li>○ Makes the assumption that error at each joint is cumulative when it is possible errors compensate for each other</li> </ul> </li> <li>• Test statistics assumptions; <ul style="list-style-type: none"> <li>○ Paired samples t-test - differences between the means is normally distributed</li> <li>○ Degrees of freedom - trials were not averaged within participants</li> </ul> </li> </ul>	
<b>Quantification of inaccuracy magnitudes</b>	5, pg. 91
<b>Body Segment Parameter Inaccuracy</b>	5.2, pg. 95
<ul style="list-style-type: none"> <li>• Sample was representative of sample used in data collection/golfer population <ul style="list-style-type: none"> <li>○ Sample consisted of three body types, mesomorph-endomorph, balanced-mesomorph and a balanced-ectomorph, covering the extremes of body types likely to be used in the data collection therefore it was anticipated that using extreme body types would produce results which reflected the variability expected for larger sample sizes</li> </ul> </li> <li>• Non-contact laser scanner was accurate enough to measure volume of segments and be used as a 'gold standard' measurement method <ul style="list-style-type: none"> <li>○ Model Maker D100 non-contact laser scanner (Metris, Leuven, Belgium) has a volumetric measurement accuracy of +/- 0.051 mm (0.0020 in)</li> </ul> </li> <li>• Inaccuracy in BSP estimates for the hands, feet and head segments were sufficiently estimated from the means of other segments <ul style="list-style-type: none"> <li>○ These segments could not be scanned due to excessive movement and the data collection methods used which required that the feet and hands were in contact with a surface to reduce movement of the rest of the body.</li> <li>○ Segments that were scanned were used to provide information as to the expected overall performance of the geometric model</li> </ul> </li> <li>• Density only had a small influence on results compared to volume <ul style="list-style-type: none"> <li>○ Use of laser scanner meant measurements were limited to volumes and did not include density.</li> <li>○ It has been shown that BSP estimates are most sensitive to volume function with density having only a small secondary influence (Ackland et al., 1988; Wicke and Dumas, 2010)</li> </ul> </li> </ul>	
<b>Force Plate Measurement Inaccuracy</b>	5.3, pg. 108
<ul style="list-style-type: none"> <li>• Point load was representative of force application during a golf swing <ul style="list-style-type: none"> <li>○ Forces during the golf swing are applied over a finite area in the form of a distribution of pressure and shear force. The magnitude of the error is dependent on the load distribution; the error in COP for a point load has been shown to higher than a load distributed across the sole of the foot during the stance phase of git (Schmiedmayer and Kastner, 2000). Inaccuracies quantified were likely to be representative of the upper bound inaccuracies expected during the golf swing</li> </ul> </li> <li>• Alignment of MAC system and force plate coordinate system was accurate <ul style="list-style-type: none"> <li>○ Calibration between the two systems was performed carefully using three non-collinear markers placed at known locations on the force plate surface to reduce this error as much as possible</li> </ul> </li> <li>• MAC system was able to accurately measure the position and orientation of the pole <ul style="list-style-type: none"> <li>○ This will depend on the precision limits of the MAC system and also the number of markers on the pole used to define its position and orientation. The pole was fitted with 9 retro-reflective markers - seven markers were used to define orientation of the pole rather than the minimum requirement of three non-collinear markers to increase the accuracy of the estimation of the position of the virtual points (Challis, 1995).</li> </ul> </li> <li>• Dynamic loading was representative of loading during a golf swing <ul style="list-style-type: none"> <li>○ Forces reached 200, 100 and 400N in the x, y, z directions respectively</li> </ul> </li> </ul>	
<b>Kinematic Measurement Inaccuracy</b>	5.4, pg.116
<ul style="list-style-type: none"> <li>• Variance in relative position and orientation of two Polhemus sensors fixed to a rigid bracket was representative of the noise in kinematic measurements <ul style="list-style-type: none"> <li>○ Dynamic measurements were used as these better replicated the measurement</li> </ul> </li> </ul>	

<ul style="list-style-type: none"> <li>• conditions during golf swing data collection than static measurements</li> <li>• Kinematic measurement noise was random and white</li> <li>• Inaccuracies in kinematic measurements were random and not systematic <ul style="list-style-type: none"> <li>◦ Effects of systematic errors were not considered although they may have affected the results</li> </ul> </li> </ul>	
<b>Soft Tissue Artefact Quantification</b>	5.5.2, pg.131
<ul style="list-style-type: none"> <li>• Weighted average based on similarity scores was appropriate for quantification of mean effect of STA on moment arm and kinematic inaccuracies <ul style="list-style-type: none"> <li>◦ Similarity scores provided an objective measure of how similar a study was to the Golphysics data collection methods</li> <li>◦ Papers were scored out of 3 for each of the four questions, therefore total scores ranged from 0 - 12. This range was suitable considering the large differences in activities, segment velocities, location of marker attachment sites and fixation methods used between studies.</li> </ul> </li> </ul>	
<b>Noise In Derivatives Obtained From Kinematic Measurement Data</b>	5.6, pg.156
<ul style="list-style-type: none"> <li>• Measurement data assumed to be signals with added white noise <ul style="list-style-type: none"> <li>◦ White noise is not correlated between samples and has a mean value of zero</li> </ul> </li> <li>• Lanshammar's equation (1980) was used to estimate the noise remaining in the signal after differentiation <ul style="list-style-type: none"> <li>◦ Assumes that the signal is bandlimited, the noise contaminating the signal is white and the frequency response of the differentiator is ideal. These assumptions mean that the equation gives a minimum estimate of noise.</li> </ul> </li> <li>• Variance calculated during dynamic trials was representative of the random noise present throughout swing trials</li> <li>• Resultant distance and orientation measurement of the two sensors fixed to the bracket were normally distributed <ul style="list-style-type: none"> <li>◦ Shapiro-Wilk test for normality were conducted on the data to confirm that dynamic measurements were normally distributed</li> </ul> </li> <li>• Single sensor variance can be estimated as the variance of two sensors divided by two <ul style="list-style-type: none"> <li>◦ Assumes the two sensors have equal variance</li> <li>◦ Based on the theory that the distribution of the sum of two independent normally distributed variables is another normal distribution with variance <math>\sigma_{X+Y}^2 = \sigma_X^2 + \sigma_Y^2</math></li> </ul> </li> <li>• STA is normally distributed around the segment centre of gravity positions <ul style="list-style-type: none"> <li>◦ This was previously proposed to analytically estimate errors in joint kinematics (Oberhofer et al., 2009; Woltring, 1994; Woltring et al., 1985).</li> <li>◦ This did not allow for the observed relationship between STA magnitude and range of motion which has been reported for the knee (Manal et al., 2003), hip (Cappozzo et al., 1996), upper arm (Hamming et al., 2012) and the upper trunk (Heneghan and Balanos, 2010).</li> </ul> </li> </ul>	
<b>Taylor Series Method For Error Propagation</b>	6, pg.162
<ul style="list-style-type: none"> <li>• Input parameters are independent and uncorrelated <ul style="list-style-type: none"> <li>◦ The upper bound uncertainty was calculated as the relationship between parameters could not be assumed to be uncorrelated</li> </ul> </li> <li>• Inaccuracies in input parameters are random <ul style="list-style-type: none"> <li>◦ This assumption means that the results is often an over statement of the uncertainty because there may be partial cancellation of error in the input parameters (Taylor, 1997).</li> </ul> </li> <li>• Only approximate for non-linear models</li> <li>• Does not provide a complete description of the estimated uncertainty <ul style="list-style-type: none"> <li>◦ Perturbations are assumed to occur simultaneously in the worst possible combinations and based on this assumption the extreme condition or upper bound of uncertainty is output.</li> <li>◦ Re-running the uncertainty analysis three times with a minimum, mean and maximum set of inaccuracies provided a range of results to better characterise the uncertainty</li> </ul> </li> <li>• Some sources of inaccuracy not directly considered <ul style="list-style-type: none"> <li>◦ Rigid body assumption, effect of filtering on kinematic noise, error in anatomical landmark identification, anatomical coordinate system orientation</li> </ul> </li> </ul>	